

# Perioperative Structural Magnetic Resonance Imaging in Neurosurgery

by

Cameron Alistair Elliott

A thesis submitted in partial fulfillment of the requirements for the degree of

Doctor of Philosophy

in

Experimental Surgery

Department of Surgery  
University of Alberta

# Abstract

Magnetic resonance imaging (MRI) is a universally-used tool in clinical neurosurgery. It has revolutionized preoperative diagnosis, surgical planning, intraoperative targeting, and postoperative surveillance. Nevertheless, the idea that early, quantifiable perioperative structural changes of the brain relate meaningfully to the prediction of long-term structural consequences and functional outcomes remains underdeveloped.

The central hypothesis of this thesis is that the perioperative period provides a unique opportunity to examine brain structure using MRI, which may predict eventual clinical outcomes. The specific aims of this thesis were to determine (1) the predictive value of early, post-injury, perioperative clinical diffusion-weighted imaging (DWI) in the setting of pediatric traumatic brain injury (TBI) and suspected non-accidental trauma (NAT) to predict ultimate distribution of structural brain damage and functional outcome; (2) the relationship between structural characteristics of various components of the limbic system, measured using perioperative MRI, and seizure control or neuropsychological outcomes in patients with drug-resistant temporal lobe epilepsy (TLE); and (3) the feasibility of acquiring diffusion tensor imaging (DTI) intraoperatively, with an open cranium, during surgery for intraaxial brain lesions using a novel, readout-segmented DTI approach.

In study #1, we demonstrate that the pattern of restricted diffusion on early post-injury diffusion-weighted MRI is predictive of long-term structural

volume loss and corresponding clinical functional deficits in pediatric TBI due to suspected NAT. In study #2, we characterize the macrostructural and microstructural changes of limbic structures following resective surgery for drug-resistant TLE using a within-subjects longitudinal design with special focus on the early postoperative period. This work identified a novel structural biomarker of refractory postoperative seizures—contralateral hippocampal volume loss—significant within one-week of surgery and found to be more pronounced amongst those with postoperative seizures. Postoperative hippocampal DTI changes suggest that the mechanism of contralateral hippocampal atrophy is multifactorial, involving resolution of cytotoxic edema and deafferentation but not early postoperative fluid shifts. In study #3, we demonstrate the utility of readout-segmented DTI (compared to conventional, single-shot DTI) for open cranial intraoperative white matter reconstructions of surgically relevant tracts during resective neurosurgery by reducing the impact of susceptibility artifact-related image degradation and spatial distortion. Taken together, the studies presented in this thesis establish that structural brain changes can indeed be measured in the perioperative period and do relate meaningfully to patient outcome.

# Preface

This thesis, which was part of a larger collaborative effort of various coauthors, is an original work by Cameron Alistair Elliott. Ethical approval for all projects was provided by the Health Research Ethics Board at the University of Alberta. Chapter 3 of the thesis has been modified with permission from Cameron A. Elliott, Vijay Ramaswamy, Francois D. Jacob, Tejas Sankar and Vivek Mehta, “Early diffusion restriction of white matter in infants with small subdural hematomas is associated with delayed atrophy,” *Childs Nervous System* 2017, volume 33, pages 289 – 295. C. A. Elliott was responsible for study design, literature review, data collection, manuscript and figure composition, and manuscript revision. T. Sankar and V. Mehta were supervisory authors and contributed to the study design and manuscript revision.

Chapter 4 has been modified with permission from Cameron A. Elliott, Donald W. Gross, B. Matt Wheatley, Christian Beaulieu and Tejas Sankar, “c,” *Epilepsy Research* 2016, volume 125, pages 62 – 71. C. A. Elliott was responsible for study design, experimental methods, data collection, analysis, manuscript and figure composition, and manuscript revision. This project was funded by the Canadian Institutes of Health Research (principal investigator D. Gross). Some data collected by Min Liu and Lius Concha before the commencement of my graduate studies, including data on patients receiving pre- and post-operative TLE surgery scans as well as on healthy controls, were included. T. Sankar, D.

Gross and C. Beaulieu were supervisory authors and contributed to study design and manuscript revision.

Chapter 5 has been modified with permission from Cameron A. Elliott, Donald W. Gross, B. Matt Wheatley, Christian Beaulieu and Tejas Sankar, “Longitudinal hippocampal and extra-hippocampal microstructural and macrostructural changes following temporal lobe epilepsy surgery,” *Epilepsy Research* 2017, volume 140, pages 128 – 137. C. A. Elliott was responsible for study design, experimental methods, data collection, analysis, manuscript and figure composition, and manuscript revision. This project was funded by the Canadian Institutes of Health Research (principal investigator D. Gross). Data collection was also conducted by Min Liu and Lius Concha for a cohort of patients receiving pre- and post-operative TLE surgery scans and healthy controls prior to my graduate studies commencement. T. Sankar, D. Gross and C. Beaulieu were supervisory authors and contributed to study design and manuscript revision.

Chapter 6 of this thesis has not been published previously but is currently in preparation for submission as follows: Cameron A. Elliott, Hayden Danyluk, Keith E. Aronyk, Karolyn Au, B. Matt Wheatley, Donald W. Gross, Tejas Sankar and Christian Beaulieu, “Intraoperative acquisition of diffusion tensor imaging in cranial neurosurgery: readout-segmented versus standard single-shot DTI.” C. A. Elliott was responsible for study design, experimental methods, data collection, analysis, manuscript and figure composition, and manuscript revision. This

project was funded through a grant by the University Hospital Foundation Medical Research Competition (principal investigator T. Sankar). T. Sankar and C Beaulieu were supervisory authors and contributed to study design and manuscript revision.

Copyright permissions for all the above listed previously published manuscripts as well as for use of other original figures and tables (as specifically mentioned throughout this thesis) have been obtained by C. A. Elliott.

# Dedication

This thesis is dedicated to my wife, Chelsey, and our children, Alistair and Lydia.

# Acknowledgements

Many individuals at the University of Alberta have made this thesis possible. I would like to acknowledge the expert guidance and encouragement provided by my PhD supervisors, Dr. Tejas Sankar and Dr. Christian Beaulieu. I have benefited greatly from exposure to their unique research processes, which I hope to emulate in the not so distant future. Many thanks to them. My thanks also to Dr. Matt Wheatley, for his mentorship and encouragement throughout the surgeon-scientist training process; next, to the Division of Neurosurgery for allowing me to take time away from neurosurgery residency to pursue graduate studies; to my PhD committee members and examiners, Drs. Donald Gross, Thomas Churchill, Sanjay Kalra, Katheryn Todd and Paolo Federico, for their unique perspectives and thought provoking questions. I thank, Dr. Keith Aronyk for his persistence and optimism in seeing our intraoperative DTI project through to completion. I have learned a great deal from Dr. Aronyk on navigating inter-departmental undertakings and establishing enthusiasm for new endeavours that bridge the clinical-research gap. I thank Dr. Stephen Andrews, too, for his sage advice, friendship and reliable spotting in the Li Ka Shing weight room. I would also like to recognize the expert assistance of Kim Perry with iMRI scanning, Suad Taglipietra for assistance with recruitment, and the support staff at the Peter S. Allen MR Research Centre.

I am grateful to my family for their patience and love during this phase of my training—specifically to my wife, Chelsey; our children, Alistair and Lydia; and my parents, Gordon, Myrna, Della and Uday.

I specifically wish to acknowledge the generous salary support from the Clinician Investigator Program at the University of Alberta, the Division of Neurosurgery at the University of Alberta, the Killam Trusts, the Queen Elizabeth Doctoral Scholarship, the BMO Financial Group Graduate Scholarship, the Andrew Stewart Memorial Graduate Prize, the Marie Arnold Cancer Research Graduate Scholarship and the Ivy A Thomson and William A Thomson Graduate Scholarship. Research funding was provided through a grant by the University Hospital Foundation Medical Research Competition as well as by the Dr. Rowland and Muriel Haryett Fund.

# TABLE OF CONTENTS

<b>CHAPTER 1: Background and Literature Review .....</b>	<b>1</b>
<b>1.1 Thesis overview .....</b>	<b>1</b>
<b>1.2 Magnetic Resonance Imaging (MRI) .....</b>	<b>2</b>
1.2.1 Principles of MRI.....	2
1.2.2 T1-weighted MRI for quantitative structural imaging analysis.....	9
1.2.2.1 Background & Acquisition.....	9
1.2.2.2 Preprocessing.....	10
1.2.2.3 Analysis .....	12
1.2.2.3.1 Manual techniques.....	13
1.2.2.3.2 Automated techniques.....	18
1.2.2.4 Sources of error in structural MRI measures .....	20
1.2.2.5 Interpretation of Structural Measures.....	22
1.2.3 Diffusion Tensor Imaging (DTI) .....	24
1.2.3.1 Background & Acquisition.....	24
1.2.3.2 Preprocessing.....	32
1.2.3.3 Analysis .....	33
1.2.4 Perioperative applications of MRI in Neurosurgery .....	38
1.2.4.1 Unique Challenges of Post- and Intra-operative MRI .....	42
<b>1.3 Pediatric traumatic brain injury.....</b>	<b>45</b>
1.3.1 Introduction.....	45
1.3.2 Neuroimaging evaluation .....	46
1.3.3 Utility of diffusion MRI.....	47
1.3.4 Pathophysiology of diffusion abnormalities .....	49
1.3.5 Prognostic value of diffusion MRI.....	49
<b>1.4 Temporal Lobe Epilepsy .....</b>	<b>50</b>
1.4.1 Introduction.....	50
1.4.2 The epileptogenic hippocampus.....	53
1.4.2.1 Anatomy and nomenclature .....	53
1.4.2.2 Pathology of Hippocampal Sclerosis .....	59
1.4.3 Epilepsy Surgery .....	61
1.4.3.1 Historical Aspects.....	61
1.4.3.2 Temporal Lobe Epilepsy Surgery.....	62
1.4.4 Role of Imaging in TLE.....	67
1.4.4.1 Qualitative structural brain imaging in TLE.....	67
1.4.4.2 Quantitative structural brain imaging in TLE .....	69
1.4.4.2.1 Volumetry.....	69
1.4.4.2.2 T2 Relaxometry .....	75

1.4.4.2.3	Magnetic resonance spectroscopy.....	76
1.4.4.2.4	Diffusion tensor imaging .....	77
<b>1.5</b>	<b>Intraoperative DTI in Cranial Neurosurgery .....</b>	<b>79</b>
1.5.1	Introduction.....	79
1.5.2	Neuronavigation .....	82
1.5.3	DTI in neurosurgery: preoperative mapping .....	85
1.5.4	Surgically-induced brain deformation .....	87
1.5.5	Current utility of intraoperative MRI.....	89
1.5.6	Intraoperative DTI in cranial neurosurgery .....	90
1.5.7	Readout-segmented iDTI in 3-Tesla iMRI .....	93
 <b>CHAPTER 2: Aims and Hypotheses .....</b>		<b>96</b>
<b>2.1</b>	<b>General Aims .....</b>	<b>96</b>
<b>2.2</b>	<b>Specific studies within this thesis .....</b>	<b>97</b>
2.2.1	Study #1 (Chapter 3): Relationship between early diffusion restriction and delayed structural and clinical outcome in pediatric TBI.....	97
2.2.2	Study #2 (Chapter 4): Postoperative longitudinal hippocampal structural changes following surgery for drug resistant TLE.....	97
2.2.3	Study #2 (Chapter 5): Postoperative longitudinal limbic micro- and macro-structural changes following surgery for drug resistant TLE .....	98
2.2.4	Study #3 (Chapter 6): Evaluation of readout-segmented DTI open cranium white matter reconstruction in cranial intraaxial resections.....	99
 <b>CHAPTER 3: Early diffusion restriction of white matter in infants with small subdural hematomas is associated with delayed atrophy .....</b>		<b>101</b>
<b>3.1</b>	<b>Introduction.....</b>	<b>101</b>
<b>3.2</b>	<b>Methods .....</b>	<b>103</b>
<b>3.3</b>	<b>Cases .....</b>	<b>103</b>
3.3.1	Case 1: .....	103
3.3.2	Case 2: .....	104
3.3.3	Case 3: .....	106
3.3.4	Case 4: .....	107
<b>3.4</b>	<b>Discussion.....</b>	<b>111</b>
 <b>CHAPTER 4: Progressive contralateral hippocampal atrophy following surgery for medically refractory temporal lobe epilepsy .....</b>		<b>116</b>
<b>4.1</b>	<b>Introduction.....</b>	<b>116</b>
<b>4.2</b>	<b>Methods .....</b>	<b>118</b>
4.2.1	Participants.....	118
4.2.2	Image acquisition.....	119

4.2.3	Volumetric analysis.....	120
4.2.4	Defining a variability threshold for hippocampal volume .....	123
4.2.5	Seizure and neuropsychological outcome .....	123
<b>4.3</b>	<b>Results .....</b>	<b>126</b>
4.3.1	Descriptive patient data .....	126
4.3.2	Surgical outcome .....	129
4.3.3	Reliability of volumetric measures .....	129
4.3.4	Hippocampal volume: two scan group .....	130
4.3.5	Hippocampal volume: longitudinal group .....	132
4.3.6	Hippocampal atrophy differences by surgical approach and seizure outcome 137	
4.3.7	Caudate volumetry .....	140
4.3.8	Neuropsychological assessment.....	141
<b>4.4</b>	<b>Discussion .....</b>	<b>143</b>
<b>4.5</b>	<b>Conclusions.....</b>	<b>148</b>

## **CHAPTER 5: Longitudinal hippocampal and extra-hippocampal microstructural and macrostructural changes following temporal lobe epilepsy surgery .... 150**

<b>5.1</b>	<b>Introduction.....</b>	<b>150</b>
<b>5.2</b>	<b>Methods .....</b>	<b>153</b>
5.2.1	Participants.....	153
5.2.2	Image acquisition.....	155
5.2.3	DTI analysis of hippocampus .....	156
5.2.4	Volumetric analysis of fornix and mammillary bodies.....	157
5.2.5	Seizure and neuropsychological outcome .....	158
5.2.6	Statistical analysis.....	159
<b>5.3</b>	<b>Results .....</b>	<b>160</b>
5.3.1	Patient characteristics .....	160
5.3.2	Surgical outcome .....	163
5.3.3	Baseline hippocampal diffusion metrics.....	163
5.3.4	Postoperative contralateral hippocampal diffusion metrics .....	166
5.3.5	Relationship between hippocampal diffusion metrics and hippocampal volume 171	
5.3.6	Mammillary body volume loss.....	172
5.3.7	Fornix volume loss.....	179
5.3.8	Relationship to neuropsychological outcome .....	180
<b>5.4</b>	<b>Discussion .....</b>	<b>184</b>
<b>5.5</b>	<b>Conclusions.....</b>	<b>189</b>

## **CHAPTER 6: Intraoperative acquisition of diffusion tensor imaging in cranial intraaxial neurosurgery: readout-segmented versus standard single-shot DTI 191**

<b>6.1</b>	<b>Introduction.....</b>	<b>191</b>
<b>6.2</b>	<b>Methods .....</b>	<b>196</b>
6.2.1	Participants and ethical approval .....	196
6.2.2	Intraoperative MRI surgical suite .....	197
6.2.3	Image acquisition.....	197
6.2.4	Comparison of susceptibility artifact and grey-white delineation between RS-DTI and SS-DTI .....	199
6.2.5	DTI tractography.....	201
6.2.6	Analysis of tractographic data .....	203
6.2.7	Statistical analysis.....	204
<b>6.3</b>	<b>Results .....</b>	<b>205</b>
6.3.1	Patient characteristics .....	205
6.3.2	Impact of readout-segmentation iDTI on susceptibility artifact image degradation in presence of resection.....	208
6.3.3	Impact of readout-segmentation iDTI on gray-white matter delineation.....	212
6.3.4	Feasibility of intraoperative DTI tractography.....	213
6.3.5	Intraoperative tract shift analyses.....	216
<b>6.4</b>	<b>Discussion .....</b>	<b>220</b>
<b>6.5</b>	<b>Conclusions.....</b>	<b>224</b>
<b>Chapter 7: General discussion and Conclusions .....</b>		<b>225</b>
<b>7.1</b>	<b>General discussion .....</b>	<b>225</b>
<b>7.2</b>	<b>Thesis limitations.....</b>	<b>232</b>
7.2.1	Small sample size.....	232
7.2.2	Confounding factors .....	234
<b>7.3</b>	<b>Future directions.....</b>	<b>234</b>
<b>7.4</b>	<b>Conclusions.....</b>	<b>236</b>
<b>References.....</b>		<b>238</b>

# List of Figures

Figure 1.1: Concept of net magnetization in MRI .....	4
Figure 1.2: Relaxation time constants.....	6
Figure 1.3: Common tissue weights in MRI.....	9
Figure 1.4: Multiplanar viewing and manual segmentation in ITK-SNAP .....	14
Figure 1.5: Stejskal-Tanner diffusion pulsed gradient spin echo sequence.....	26
Figure 1.6: Diffusion-gradient parameters.....	27
Figure 1.7: The diffusion tensor matrix .....	29
Figure 1.8: The diffusion tensor ellipsoid.....	30
Figure 1.9: DTI maps.....	32
Figure 1.10: Trace and ADC-map images following a traumatic brain injury resulting in an acute subdural hematoma along the posterior falx cerebri. ....	34
Figure 1.11: Intraoperative MRI Theatre.....	41
Figure 1.12: Timing of MRI and potential utility in neurosurgery.....	42
Figure 1.13: Intraoperative MRI surface coil .....	44
Figure 1.14: The hippocampus and other limbic system components.....	55
Figure 1.15: Hippocampal subfields.....	56
Figure 1.16: The circuit of Papez.....	58
Figure 1.17: Photomicrographs of Nissl stained hippocampal slices .....	60
Figure 1.18: Anterior temporal lobectomy (ATL) versus selective amygdalohippampectomy (SAH).....	65
Figure 1.19: Distribution of structural volume loss in TLE.....	74
Figure 1.20: Neuronavigation components.....	83
Figure 1.21: Neuronavigational surgical display .....	85

Figure 3.1: Early areas of restricted diffusion predict ultimate structural consequences .....	110
Figure 4.1: Representative sub-regional hippocampal tracings.....	122
Figure 4.2: Postoperative two scan group hippocampal volumetry.....	131
Figure 4.3: Control subject hippocampal volumetry .....	132
Figure 4.4: Normalized individual longitudinal postoperative hippocampal volumetry .....	133
Figure 4.5: Raw longitudinal postoperative hippocampal volumetry.....	135
Figure 4.6: Control subject normalized longitudinal volumetry.....	137
Figure 4.7: Postoperative normalized hippocampal volume loss by seizure outcome .....	139
Figure 4.8: Receiver operating characteristics (ROC) curves for seizure freedom based on delayed hippocampal atrophy .....	140
Figure 4.9: Postoperative caudate volumetry.....	141
Figure 5.1: Preoperative diffusion parameters in TLE patients and controls .....	165
Figure 5.2: Postoperative changes in hippocampal diffusion compared to healthy controls.....	167
Figure 5.3: Mean early versus late postoperative contralateral hippocampal diffusion parameters compared with controls .....	169
Figure 5.4: Sub-regional hippocampal fractional anisotropy for before and after TLE surgery as well as in healthy controls .....	170
Figure 5.5: Correlation between preoperative contralateral hippocampal diffusion metrics and delayed postoperative hippocampal volume .....	172
Figure 5.6: Mammillary body and fornix volume before and after TLE surgery as well as in healthy controls .....	174
Figure 5.7: Ipsilateral versus contralateral mammillary body and fornix volume before and after TLE surgery as well as in healthy controls.....	176
Figure 5.8: Neuropsychological performance change plotted against diffusion parameter change for dominant resections .....	182

Figure 5.9: Neuropsychological performance change plotted against diffusion parameter change for non-dominant resections .....	183
Figure 6.1: Susceptibility artifact comparison of RS-DTI versus SS-DTI in three iMRI cases .....	209
Figure 6.2: Regional ratings of susceptibility artifact for RS-iDTI versus SS-iDTI	210
Figure 6.3: Average absolute anatomical deviation of RS-iDTI compared to SS-iDTI .....	211
Figure 6.4: Anatomical deviation of coregistered mean b1000 images for RS- and SS-iDTI relative to T1-reference .....	212
Figure 6.5: Global ratings of gray-white matter delineation on average b1000 diffusion images.....	213
Figure 6.6: Differences in intraoperative tractographic output and intraoperative shift in target-tract distance.....	218
Figure 6.7: Differences in intraoperative tractographic output and intraoperative tract shift in target-tract distance.....	219

# List of Tables

Table 1.1: Engel classification of postoperative seizure freedom .....	63
Table 1.2: ILAE classification of postoperative seizure freedom.....	63
Table 3.1: Summary of four cases of Non-Accidental Trauma (NAT) .....	109
Table 4.1: TLE surgery patient demographics.....	127
Table 4.2: Reliability data for hippocampal volumetry measurements .....	129
Table 4.3: Pre- and Post-operative average memory scores of patients following temporal lobe epilepsy surgery .....	142
Table 4.4: Pre- and Post-operative cognitive performance of patients following temporal lobe epilepsy surgery .....	143
Table 5.1: Characteristics of TLE surgery patients .....	161
Table 6.1: Susceptibility artifact and gray-white delineation rating scales .....	201
Table 6.2: Characteristics of 22 patients with intraaxial iMRI resections.....	207
Table 6.3: Tract reconstruction with intraoperative DTI in 22 iMRI patients.....	215
Table 6.4: Summary of tract analyses.....	217

# List of Abbreviations

2D: two-dimensional

3D: three-dimensional

AC-PC: bicommissural or anterior commissure-posterior commissural line

AD: axial diffusivity

ADC: apparent diffusion coefficient

AED: anti-epileptic drug

AHS: Ammon's horn sclerosis

ATL: anterior temporal lobectomy

ASDH: acute subdural hematoma

ATP: adenosine triphosphate

B<sub>0</sub>: main magnetic field

B<sub>1</sub>: radiofrequency field

CA: *cornu Ammonis*

CFT: Rey-Osterreith complex figure task

CPx: clinical presentation

Cr: creatine

CSF: cerebrospinal fluid

CSpT: corticospinal tract

CT: computerized tomography

CVMT: continuous visual memory test

D: diffusion coefficient (mm<sup>2</sup>/second)

DEC: directionally-encoded colour

DES: direct electrical stimulation

DICOM: Digital Imaging and Communications in Medicine

DKI: diffusion kurtosis imaging

DRE: drug-resistant epilepsy

DSI: diffusion spectral imaging

DTI: diffusion tensor imaging

DW: diffusion-weighted

DWI: diffusion-weighted imaging

Dx: diagnosis

EC: Engel class

EEG: electroencephalography

EMS: emergency medical services

EOR: extent of resection

FA: fractional anisotropy

FACT: fiber assignment by continuous tracking

FAIS: focal awareness impairing seizure

FAST: FMRIB's Automated Segmentation Tool

FCD: focal cortical dysplasia

FIRST: FMRIB's Integrated Registration and Segmentation Tool

FLAIR: fluid-attenuation inversion recovery

fMRI: functional magnetic resonance imaging

FM: figural memory aggregate score

FMS: focal motor seizure

FOV: field-of-view

FS: febrile seizure

FSL: FMRIB Software Library

Fx: functional

GCS: Glasgow coma scale

GM: grey matter

GTR: gross total resection

$^1\text{H}$ : hydrogen

HARDI: high angular resolution diffusion imaging

HBV: hippocampal body volume

HGG: high-grade glioma

HHV: hippocampal head volume

HS: hippocampal sclerosis

HTV: hippocampal tail volume

ICC: intraclass correlation coefficient

ICP: intracranial pressure

ICV: intracranial volume

iDTI: intraoperative diffusion tensor imaging

ILAE: International League Against Epilepsy

IQ: intelligence quotient

iMRI: intraoperative magnetic resonance imaging

LGG: low-grade gliomas

LHD: left-hand dominant

LM: logical memory

IPI: initial precipitating injury

M: months

$M_0$ : equilibrium value of  $M_z$

MD: mean diffusivity

MEP: motor evoked potential

MNI: Montreal Neurologic Institute Space

MPRAGE: Magnetization-Prepared Rapid Gradient Echo

MR: magnetic resonance

MRA: magnetic resonance angiography

MRI: magnetic resonance imaging

MRS: magnetic resonance spectroscopy

MSR: maximal safe resection

MTS: mesial temporal sclerosis

$M_0$ : equilibrium value of  $M_z$

$M_{xy}$ : net transverse magnetization

$M_z$ : net longitudinal magnetization

NAA: N-acetylaspartate

NAT: non-accidental trauma

NIfTI: Neuroimaging Informatics Technology Initiative

PD: proton (spin) density

PHG: parahippocampal gyrus

PRI: perceptual reasoning index

RD: radial diffusivity

QOL: quality of life

RAVLT: Rey auditory verbal learning test

RESOLVE: REadout Segmentation Of Long Variable Echo trains

RF: radiofrequency

RHD: right-hand dominant

RMF: recognition memory for faces

RMW: recognition memory for words

ROI: region of interest

RS-DTI: readout-segmented diffusion tensor imaging

SEEG: stereoelectroencephalography

SAH: selective amygdalohippocampectomy

SNR: signal-to-noise ratio

SPM: statistical parametric mapping, software package

SS-DTI: single-shot diffusion tensor imaging

SUDEP: sudden unexplained death in epilepsy

Sz: seizure

T1: longitudinal relaxation time

T2: transverse relaxation time

T2\*: effective T2

TBI: traumatic brain injury

TE: echo time

TLE: temporal lobe epilepsy

TR: repetition time

Tx: treatment

VBM: voxel-based morphometry

VCI: verbal comprehension index

VM: verbal memory aggregate score

VPA: verbal paired associates

$\omega_0$ : Larmour precessional frequency

WAIS: Weschsler adult intelligence scale

WHO: World Health Organization

WHV: whole hippocampal volume

WM: white matter

WMI: working memory index

$\gamma$ : gyromagnetic ratio

# **CHAPTER 1: Background and Literature Review**

**Cameron A. Elliott**

## **1.1 Thesis overview**

Magnetic resonance imaging (MRI) is a universally-used tool in clinical neurosurgery. It has revolutionized preoperative diagnosis, surgical planning, intraoperative targeting, and postoperative surveillance. However, the relationship between quantitative, MRI-based perioperative structural measures of the brain and clinical outcomes has been underexplored.

The aim of this thesis is to characterize brain structural changes in the perioperative period, including both the intraoperative and postoperative period, and their relationship to clinically relevant surgical outcome variables. The thesis will begin with an introduction to MRI along with background specific to pediatric traumatic brain injury (TBI), temporal lobe epilepsy (TLE) surgery and finally intraoperative diffusion tensor imaging (iDTI) in the intraoperative MRI surgical theatre. In chapter 2, the overarching hypotheses and specific aims of each of the three studies that make up this thesis are summarized. Chapter 3 examines the relationship between early, perioperative post-injury diffusion-weighted imaging (DWI) changes and long-term structural and functional outcomes in the setting of pediatric TBI attributable to suspected non-accidental

trauma (NAT). In chapters 4 and 5, the nature and time course of postoperative macrostructural and microstructural changes of structures in the limbic system (hippocampus, mammillary bodies and fornix) following resective surgery for drug-resistant TLE are discussed. In particular, the relationship between these MRI measures and clinically relevant neuropsychological and seizure control outcomes are discussed. Chapter 6 describes the relative utility of readout-segmented DTI in comparison to standard single shot DTI for susceptibility artifact-resistant open cranial DTI tractography in the intraoperative setting to identify surgically-relevant white matter tracts during supratentorial intraaxial surgery. Following these four chapters (chapters 3 through 6) containing original data, a brief discussion highlighting the key findings and impact of this work is presented, along with general limitations and future directions.

## **1.2 Magnetic Resonance Imaging (MRI)**

### **1.2.1 Principles of MRI**

MRI capitalizes on the behavior of specific atomic nuclei placed in a powerful static external magnetic field ( $B_0$ ) and exposed to a perpendicular oscillating magnetic field generated by a radiofrequency coil to create an image sensitive to the local tissue environment. The typical MRI signal is derived largely from the human body's hydrogen ( $^1\text{H}$ ) nuclei, which are principally associated with water and fat molecules—although other elements such as  $^{19}\text{F}$ ,  $^{23}\text{Na}$  or  $^{31}\text{P}$  can also be used in MRI (Pooley, 2005). Each individual hydrogen nucleus

(indeed every atomic and subatomic particle) has an intrinsic spin angular momentum ('spin') in which the positively-charged proton spins about an axis and has a slight polarity or net magnetic dipole moment. At baseline the vector sum of all the individual dipoles will be zero because of their random orientation. However, once in  $B_0$ , individual dipoles will align either in the same direction (parallel; lower energy state) or exact opposite (anti-parallel; higher energy state) direction, with slight preponderance of the former, resulting in a net longitudinal magnetization (termed  $M_z$  for its alignment with  $B_0$  along the z-axis which has a maximal value, at equilibrium, of  $M_0$ ). In addition, protons precess at a frequency ( $\omega_0$ ) according to the Larmor equation, where  $\omega_0$  is the precessional frequency,  $\gamma$  is the gyromagnetic ratio of the MRI-active nucleus (42.6 MHz/Tesla for  $H^1$ ) and  $B_0$  is the main magnetic field.

$$\text{Equation 1.1} \quad \omega_0 = \gamma B_0 \text{ (Larmor Equation)}$$

The application of a radiofrequency (RF) pulse—a time varying excitation ( $B_1$ ) field with components oscillating at the Larmor frequency and oriented perpendicular to  $B_0$ —perturbs or 'tips' the net alignment away from  $M_z$ . Although at baseline, prior to the RF pulse, individual nuclei are precessing, their vector sum (net magnetization,  $M_z$ ) is not yet precessing about the axis of  $B_0$  (Figure 1.1, A/B)(Elster, 2015). Precession of net magnetization begins after the energy input from the RF pulse tips  $M_z$  away from its equilibrium alignment (Figure 1.1, C/D).

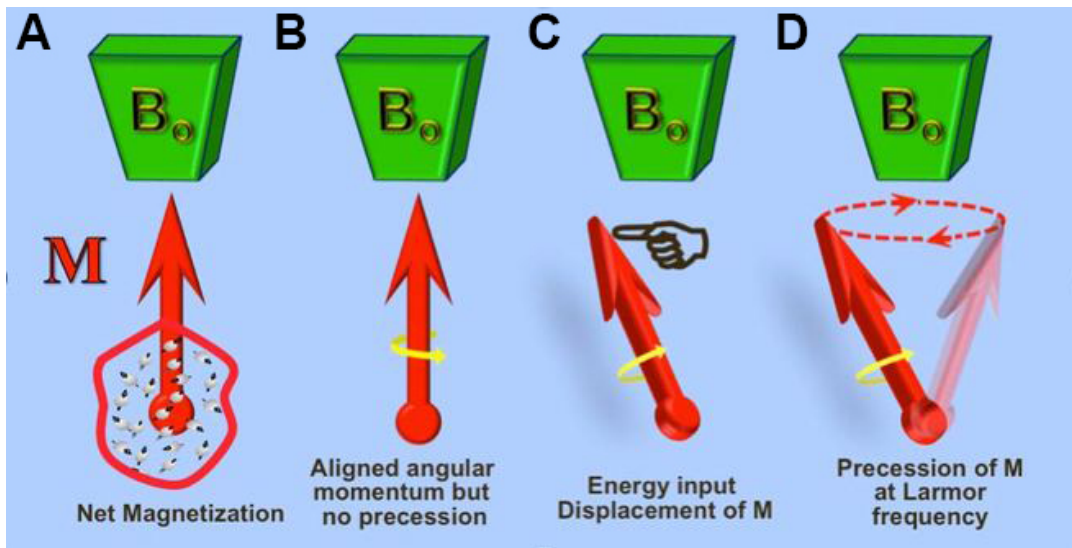


**Figure 1.1: Concept of net magnetization in MRI**

(A) Net magnetization ( $M$ ) is the vector sum of all individual nuclei included in a sample, which are all individually precessing, but at baseline the net magnetization is not (B). Once subjected to the main magnetic field,  $B_0$ ,  $M$  will develop over time; however, net magnetization does not precess until perturbed by the energy input from an RF pulse (C) that induces precession of  $M$  at the Larmor frequency (D). Adapted with permission from Elster, 2015.

The exchange of energy between RF pulse and protons causes some spins to adopt a higher energy state and align to precess in a different orientation, resulting in a progressive tipping of the net magnetization away from  $M_z$  such as into the transverse plane (in which case,  $B_1$  is labeled a  $90^\circ$  RF pulse). A longer RF pulse can achieve further tipping of net magnetization to any orientation such as  $180^\circ$  or in the  $-z$  direction, in which case  $B_1$  is called a  $180^\circ$  RF pulse. It is only after the injection of energy from the RF pulse that an MR signal can be recorded—a manifestation of Faraday's law of induction—such that an induced

current is generated in the receive coil, a set of electromagnetic coils which detects each sweep of the precessing M.

After the RF pulse, relaxation of the excited (higher energy state) group of spins is stimulated by interaction with its external environment and results in a release of absorbed energy (Pooley, 2005). In terms of net magnetization this can be described by two independent relaxation processes called longitudinal relaxation (T1) and transverse relaxation (T2) (Bloch, 1946). Longitudinal relaxation describes the recovery of the longitudinal component of net magnetization as higher energy state protons stimulated by interactions with their environment begin to fall back to lower energy states, thereby emitting absorbed energy into the local environment (spin-lattice). The longitudinal relaxation time (T1) is defined as the time required for  $M_z$  to recover from 0 to 63% of its equilibrium value ( $M_0$ ; Figure 1.2A). Transverse relaxation describes the decay of the transverse component ( $M_{xy}$ ) after an RF pulse as spins dephase (lose phase coherence) because of static magnetic field inhomogeneities and interactions with adjacent nuclei (spin-spin interactions). The transverse relaxation time (T2) is defined as the time required for  $M_{xy}$  to decay to 37% of its initial value (Figure 1.2B).

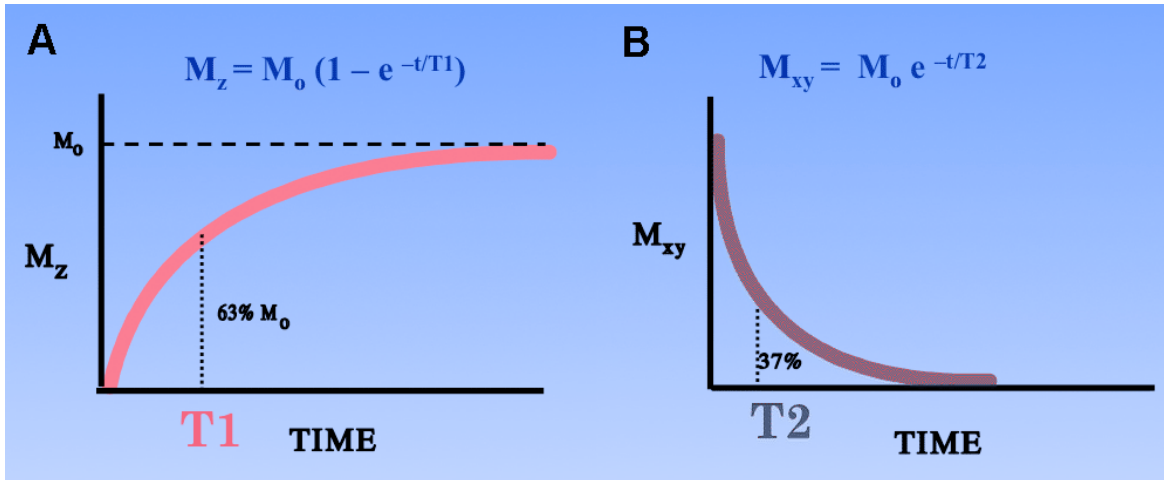


**Figure 1.2: Relaxation time constants**

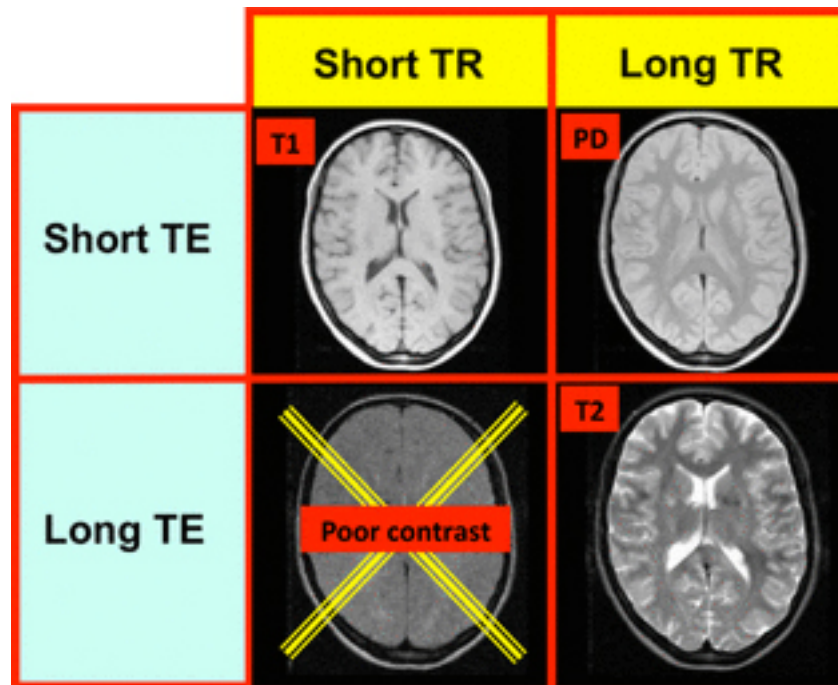
Graphical representations of relaxation time constants: (A) longitudinal relaxation time (T1) and (B) transverse relaxation time (T2). Adapted with permission from Elster, 2015.

Image contrast in MRI is based on different values for T1 and T2 in different tissues or pathological processes. The value of T1 and T2 is largely dependent on the size and motion of molecules within which hydrogen resides such that small mobile molecules (e.g., water) will have long T1 and T2. In the brain, for example, cerebrospinal fluid (CSF) has very long T1 while white matter has very short T1 (rapid relaxation), with grey matter (GM) having an intermediate value. Finally, it is important to mention that in practice  $M_{xy}$  decay proceeds faster than expected based on molecular interactions alone at a rate noted as T2\*. This faster-than-expected dephasing occurs as the result of inhomogeneities in the main magnetic field, which arise from  $B_0$  inhomogeneity or magnetic susceptibility distortions (e.g., resulting from superparamagnetic blood products such as hemosiderin).

However, to take advantage of differences in signal of different tissue types throughout the volume of interest (e.g., the brain), the problem of spatial localization of signal from a variety of locations must be solved. Various methods are used to achieve this, including differences in frequency, phase, signal timing, and distance from receive coils (Elster, 2015). Frequency encoding using supplemental magnetic fields called gradients (generated by gradient coils) alters the  $B_0$  predictably as a function of position such that the local resonance frequency will vary as a function of position (e.g., x-axis). This principle can also be used to excite selectively (select) a particular slice of spins along the axis perpendicular to the applied linearly varying gradient (e.g., z-axis) by applying an RF pulse tuned to the particular Larmor frequency of that slab. Within this slice, the application of gradients in the x- and y-direction (frequency- and phase-encoding directions, respectively) generates voxels within a particular slice. For each voxel, ultimate signal intensity is dependent on local T1 and T2 as well as on proton density (PD). The raw data output is represented in k-space in which values corresponding to the spatial frequencies of the MR image are represented, which can be transformed into image space by a Fourier transform.

Ultimately, MR image contrast is determined by varying operator-selected sequence parameters, including time between successive RF pulses (repetition time, TR) and the time between an RF pulse and measurement of signal (echo time, TE). The extent to which image contrast is influenced by tissue, T1, T2, PD, susceptibility, or diffusion is determined largely by these parameters, which are often communicated by the parameter 'weighting' (Figure

1.3). Images that are primarily influenced by T1 are called '*T1-weighted*' and will have short TR and TE (Figure 1.3). Specifically, in T1-weighted images the short TR allows tissue contrast between areas with long T1 (e.g., CSF) and short T1 (e.g., GM), such that CSF would have low signal (i.e., recovered  $M_z$ ) compared to GM. Images that are primarily influenced by T2 are called '*T2-weighted*' and will have long TR and TE (Figure 1.3) such that tissues with substantially different T2 will be contrasted based on the extent of  $M_{xy}$  decay. Images that are primarily influenced by PD have long TR but short TE (Figure 1.3). Although T1- and T2-weighted images are the most commonly used, several other contrasts, such as susceptibility or diffusion, can be used.



**Figure 1.3: Common tissue weights in MRI**

Common parameter weightings (T1, T2, PD) and their relative repetition time (TR) and echo time (TE). Used with permission from Elster, 2015.

## 1.2.2 T1-weighted MRI for quantitative structural imaging analysis

T1-weighted images with high spatial resolution—such as are acquired using the Magnetization-Prepared Rapid Gradient Echo (MPRAGE)—are commonly used for the types of quantitative analyses discussed below.

### 1.2.2.1 Background & Acquisition

MPRAGE, a workhorse sequence of cranial neuroimaging, is a fast 3D gradient echo sequence preceded by the application of magnetization-prepared 180° RF pulse (to invert the net magnetization vector to the -z plane). High-

resolution ( $1 \times 1 \times 1 \text{mm}^3$ ) MPRAGE provides high signal, grey-white matter tissue differentiation (e.g., at the cortical ribbon) and visualization of smaller structures owing to high spatial resolution with a reasonable acquisition time (Brant-Zawadzki et al., 1992; Keller and Roberts, 2009). Spatial resolution in MRI is defined by the size of voxels, which in turn depends on operator-selected factors including matrix size (number of steps in frequency encoding and phase encoding direction), field-of-view (FOV) and slice thickness. Specifically, dividing the FOV by the matrix size will provide in-plane resolution or voxel size, whereas slice thickness determines depth (z-axis) of the voxel. Most quantitative structural analyses are carried out on sequences with isotropic voxels, i.e., the same size in all directions, most commonly  $1 \times 1 \times 1 \text{mm}$ . The optimal orientation of the acquisition is dependent on the planned structural analysis (see section 1.2.2.3.1 on manual volumetry for further details) but generally occurs along the bicommissural (AC-PC) line. At the time of acquisition, MRI data is routinely inspected for gross acquisition problems such as motion artifact, inadequate coverage of the structure of interest, or missing slices.

### **1.2.2.2      *Preprocessing***

After acquisition, MRI data is transferred to a computer workstation where gross visual inspection of the raw data is repeated (particularly if the observer was not present at the time of the initial quality assurance step during acquisition). Malrotation or malalignment not recognized at the time of

acquisition can be corrected or realigned using internal points of reference such as the AC-PC plane (Boccardi et al., 2014). Raw scan data in DICOM (Digital Imaging and Communications in Medicine) format is converted to NIFTI (Neuroimaging Informatics Technology Initiative) a common input file format for a wide variety of software packages. Next, a correction for intensity non-uniformity (or inhomogeneity) is applied using one of several widely-available algorithms (Brinkmann et al., 1998; Sled et al., 1998). Intensity non-uniformity is a non-anatomic variation of signal within a structure made of the same tissue. The cause of this distortion may be multifactorial but generally results from inhomogeneity in the RF or static field or patient motion and has been described to be more prominent in acquisitions involving surface coils (which are common in MR neuroimaging) (Ganzetti et al., 2016; Hou, 2006; Sled et al., 1998). Intensity non-uniformity can significantly affect attempts to segment brain tissue by tissue type (e.g., grey versus white matter) or by common patterns of tissue contrast in specific brain regions, owing to low-frequency alterations of MR signal at edges or contours (Hou, 2006). Finally, certain structural analyses that require comparison between MR data from different subjects, or acquired in different orientations, may require image registration. Registration is defined as spatially aligning multiple MR data sets. Registration can occur either between scans directly or between scan data and a common template, such as the MNI ICBM 152 brain (Montreal Neurological Institute), a template space generated from scans of 152 normal adult brains (Chau and McIntosh, 2005). Registration requires the application of a transformation of the input image to the reference

space; this can be accomplished by either a linear or non-linear approach. Linear registration can be accomplished either by using a 6-parameter rigid or 12-parameter affine method, with the latter allowing for scaling and shearing transformations in addition to the translocation and rotational transformations allowed in the 6-parameter rigid method (Despotović et al., 2015; Viergever et al., 2001). In contrast, non-linear registration is commonly used to pool results across subjects in a common reference space for which linear methods may not achieve satisfactory registration. Specifically, non-linear registration also allows deformations or ‘warps’ executed by computer algorithms to create improved registration across subjects (Andersson et al., 2007; D’Agostino et al., 2003; Van Hecke et al., 2007).

### **1.2.2.3      *Analysis***

As mentioned above, quantitative analysis of structural MRI data is commonly carried out using T1-weighted images (e.g., high-resolution MPRAGE) that offer excellent tissue-type differentiation (e.g., between GM, white matter and CSF). However, quantitative analysis of other sequences yields complementary data such as proton-density sequences (for manual measurement of intracranial volume—for instance, see Nordenskjold et al., 2013), T2-weighted images (for T2-relaxometry, see section 1.4.4.2.2) or diffusion tensor images (DTI, see sections 1.2.3, 1.3.3-1.3.5 and 1.4.4.2.4).

Structural MRI analysis can be categorized as manual or automated techniques, which are described in detail below.

#### *1.2.2.3.1 Manual techniques*

There are two manual techniques for in vivo MRI-based measurement of a structure of interest: stereology and volumetry (Keller and Roberts, 2009). In stereological methods, volume or surface area is estimated by first randomly choosing a set of parallel and equidistant MR images through the structure of interest and then superimposing a grid of points and counting the total number of points that fall within the boundaries of the structure (Garcia-Finana et al., 2009, 2003; Keller and Roberts, 2009; Roberts et al., 2000). In contrast, manual volumetry (also called segmentation or tracing), as used in chapters 4 and 5, involves the slice-by-slice delineation using a mouse or stylus-driven cursor of an entire brain structure or region by an expert observer based on an in-depth knowledge of neuroanatomy. Volumetry is generally performed based on an established protocol which defines the specific procedure by which the observer traces or fills in the anatomical structure of interest on synchronized 2D orthogonal MR-images (i.e., axial, coronal and sagittal). Based on the tracings on each slice, the structure of interest can be extracted as a 3D object and verified for expected shape/contours; its total volume can be computed (voxels within label multiplied by the number of  $\text{mm}^3$  per voxel, based on image resolution)

and then used as a scalar metric in subsequent analyses. Various software packages exist to facilitate multi-planar viewing. These include, e.g., MNI Display (McConnell Brain Imaging Centre) or ITK-SNAP (Figure 1.4)(Yushkevich et al., 2006), among others.

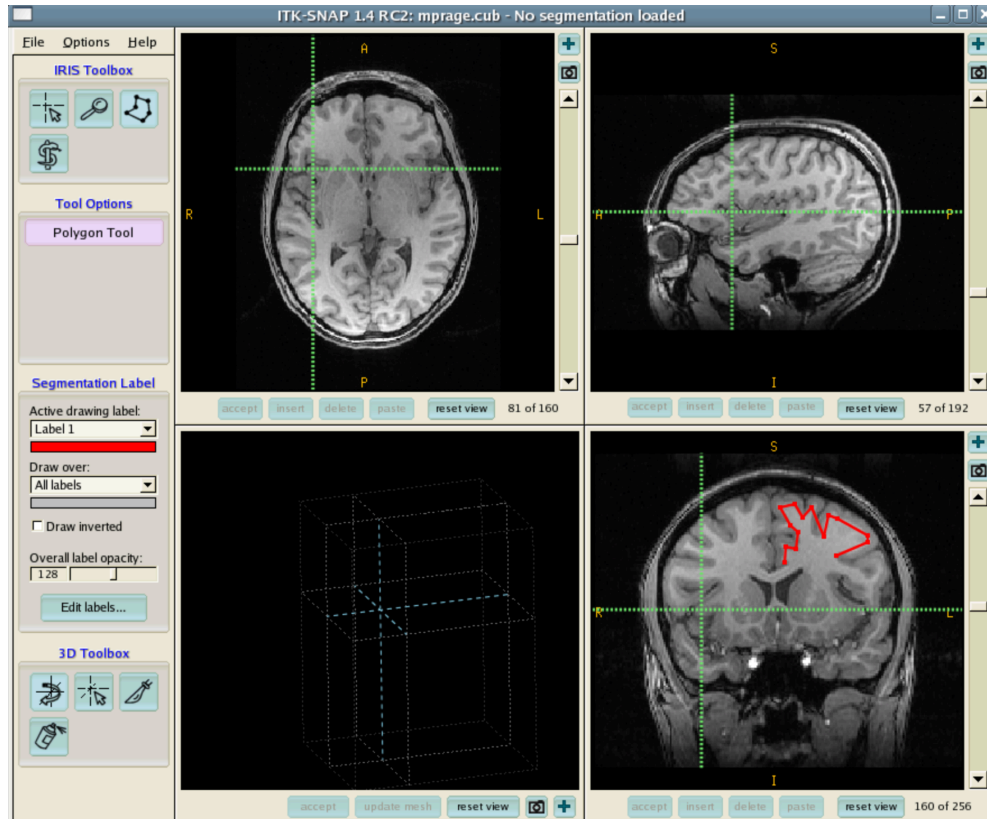


**Figure 1.4: Multiplanar viewing and manual segmentation in ITK-SNAP**

Used with permission from Prof. P. Yushkevich, ITK-SNAP ([www.itksnap.org](http://www.itksnap.org)).

Manual volumetry protocols exist for a variety of distinct structures or regions including the hippocampus, amygdala, thalamus, fornix, mammillary bodies and temporopolar, entorhinal, and perirhinal cortices (Cendes et al., 1993a; Copenhaver et al., 2006; Frisoni et al., 2014; G Gong et al., 2008; Insausti

et al., 1998; Malykhin et al., 2007; Watson et al., 1997). Volumetry data has contributed to our understanding of the natural history, structural-functional correlation (e.g., neuropsychological performance) and structural consequences of medical or surgical interventions in Alzheimer disease, schizophrenia, depression and TLE (Bonilha and Keller, 2015; C. A. Elliott et al., 2016; Elliott et al., 2018; Fernandes et al., 2014; Frisoni et al., 2010; Heckers, 2001; Mueller et al., 2010; Noulhiane et al., 2006; Sheline et al., 2003, 1996; Yasuda et al., 2010).

Manual volumetry is the most commonly used and most accurate method for in vivo structural interrogation using MRI data (Morey et al., 2008; Pardoe et al., 2011). Moreover, when evaluating volumetric output from any automated method of segmentation, due diligence requires some level of quality assurance that is still best conducted by an expert observer with not only the prerequisite knowledge of the relevant regional neuroanatomy but also the experience with the appearance of structures of interest on an MRI. For this reason, it remains critical that investigators using automated techniques are well-versed in manual volumetry techniques for their structure of interest. In fact, manual volumetry has been used for the generation of probabilistic brain atlases upon which atlas-based automated segmentation approaches are designed (see 1.2.2.3.2 below) and is generally used as the gold standard against which automated algorithms are evaluated (Frisoni and Jack, 2011). Finally, manual volumetry is best able to handle distorted anatomy that may produce abnormal MR signal, accompany certain disease states, or pertain following neurosurgical interventions or

resection, after which large portions of the brain may be missing or have abnormal MR signal.

Nonetheless, manual volumetry does have important drawbacks. Foremost is the investment of time required to train 'expert' tracers, validate their performance, and perform tracings of the structure of interest (a typical hippocampal tracing takes 30 – 40 minutes). The validation phase of training requires blinded intra-rater reliability assessment of tracings separated in time as well as inter-rater reliability assessment with expert tracings. Manuscripts using manual segmentation should provide measures of intra- and inter-observer reliability (e.g., intraclass correlation coefficient, ICC) (Koo and Li, 2016; Nugent et al., 2013; Shrout and Fleiss, 1979). Manual volumetry is therefore largely not feasible in larger datasets, nor has it been adopted clinically. The labor-intensive nature of manual volumetry may result in errors resulting from observer fatigue (Morey et al., 2008). Second, unique to manual volumetry, there is a theoretical risk of 'hand wobble' resulting in inadvertent inclusion of non-target tissue or exclusion of true target tissue (Keller and Roberts, 2009). In practice, this can largely be mitigated by adjusting the sensitivity of the mouse or stylus driving the cursor and by carefully toggling 'on' and 'off' of tracings (to facilitate visualization of underlying anatomy) to verify that target tissue is filled in satisfactorily. Third, the tracing output of observers may be systematically biased by a priori knowledge of clinical variables, scan date, patient identity, or treatment group. In many cases (see methods, chapter 3), such sources of bias can be minimized by anonymization, coning down to the

structure to be segmented (e.g., the non-resected, contralateral hippocampus to avoid the observer viewing the ipsilateral resection cavity, thereby identifying the subject as a patient who has undergone surgery for TLE and not a control), and finally random order presentation with respect to relevant patient variables (e.g., patient versus control or scan date). Similarly, other sources of bias have been described—such as left-right perceptual asymmetry bias—which may impact results if scans are not flipped such that all tracings occur on the same side of the screen (Guo et al., 2009; Jewell and McCourt, 2000; Maltbie et al., 2012; Rogers et al., 2012). However, certain qualitative abnormalities (e.g., T1 hypointensity or alterations of normal hippocampal architecture) are not possible to conceal from the observer. Next, considerable differences may exist in local protocols used by different laboratories, the impact of which may vary based on the anatomical complexity or indistinctness of boundaries on MRI (e.g., anterior boundaries of hippocampal head and amygdala; posterior boundaries of hippocampal tail and isthmus or thalamus; lateral boundaries of thalamus with internal capsule) (Frisoni et al., 2014; G Gong et al., 2008; Pruessner et al., 2000). For example, there are currently more than 12 unique local protocols for manual hippocampal volumetry, resulting in widely ranging estimates of normal hippocampal volume differing by as much as 2.5-fold (Boccardi et al., 2011; Geuze et al., 2005). Recently, this issue was partially addressed by an international Delphi panel, leading to the creation of the “EADC-ANDI Harmonized Hippocampal Protocol,” which the panel found to have superior measurement stability (intra- and inter-rater reliability) compared to local

protocols (Boccardi et al., 2015). As an illustrative example, this process found enhanced stability of segmentations performed with an AC-PC orientation, rather than the traditional acquisition along the long axis of the hippocampus (Frisoni et al., 2014). However, this protocol has not yet been widely adapted, nor do similar protocols exist for other brain structures (Wisse et al., 2017).

#### *1.2.2.3.2 Automated techniques*

An exhaustive overview of various automated MRI segmentation techniques is outside of the scope of this thesis, except specifically to highlight the basics of two key techniques which are treated later in this chapter, discussing the diffuse nature of structural change in TLE. Automated techniques obtain regional or global brain measures without substantial direct user input. Such measures are obtained by matching geometric and tissue signal intensity patterns to a probabilistic neuroanatomic atlas by spatial normalization or differences in signal intensity alone (Keller and Roberts, 2009; Toga and Mazziotta, 2002). For example, in the FMRIB Software Library (FSL), the intensity-based segmentation FMRIB of the Automated Segmentation Tool (FAST; <https://fsl.fmrib.ox.ac.uk/fsl/fslwiki/FAST>) assigns each scanned voxel to a tissue type (GM; WM; CSF) on the basis of fitting a Gaussian probability to a histogram of the intensity of all voxels (Despotović et al., 2015; Zhang et al., 2001). Output tissue type metrics can be used directly or the GM segmentation can be used to perform voxel-based morphometry (VBM) in which local

differences in cortical or subcortical GM density (a surrogate marker of volume) or cortical thickness (regional or global combined thickness of all cortical layers perpendicular to the cortical surface) can be performed (MacDonald et al., 2000). Finally, in atlas-based automated segmentation, the image to be segmented is coregistered to a probabilistic atlas generated by multiple prior expert manual segmentations (Dale et al., 1999; Patenaude et al., 2011). Next, voxels are assigned to be part of a particular brain structure or region on the basis of signal intensity and spatial position (e.g., FreeSurfer—<https://surfer.nmr.mgh.harvard.edu/>)(Dale et al., 1999). Alternatively, in the FSL-FIRST algorithm (<http://fsl.fmrib.ox.ac.uk/fsl/fslwiki>), a shape/appearance model is generated (from a probabilistic atlas generated by manual segmentation) for a subcortical structure (e.g., left hippocampus). This model is expressed as a deformable surface mesh that is represented mathematically by a set of connected vertices (point distribution model). Each model is determined by mean vertex position for a structure of interest from the manual volumetry training set. To segment a structure, its model is first fit to the input image by transforming it into target space and then searching for the most probable shape given the local signal intensities (Patenaude et al., 2011).

Automated segmentation is much less labor-intensive than manual techniques, allowing application to large imaging datasets without the direct need for expert neuroanatomical knowledge (Morey et al., 2008). Automated segmentation algorithms are not subject to potential biases that may affect manual segmentation as direct user input is limited. Finally, automated output is

highly reproducible on the same scan data (Gronenschild et al., 2012). However, automated segmentation results still require thorough slice-by-slice interrogation by neuroanatomical experts to ensure validity. Moreover, automated tools may produce erroneous segmentations if spatial registration fails, which is especially problematic when used in cases of advanced disease, brain malformations, or following resective cranial neurosurgery (Despotović et al., 2015). Outside of problems with registration, automated segmentation algorithms may also produce segmentation errors when subject data differs significantly from the population upon which the atlas reference was built, in terms of age, sex, or neuropathology (Despotović et al., 2015).

#### **1.2.2.4 Sources of error in structural MRI measures**

To interpret observed changes in structural measures at the individual or group level, it is necessary to understand factors that may cause fluctuations of the measurement of interest. Potential sources of variance have been categorized previously as scanner-related, acquisition-related, physiologic, or measurement-related (Biberacher et al., 2016). A full treatment of measurement-related factors influencing variance has been provided above (section 1.2.2.3.1). Scanner-related factors may include intrascanner variability (scanner drift) or interscanner variability. Scanner drift is generally not a major issue in structural MRI studies, though it has been demonstrated to be an important factor to correct for in diffusion MRI analyses (Vos et al., 2017). To

minimize intrascanner variability, it is important that MRI scanners (in particular those used for quantitative research) undergo routine quality assurance (Firbank et al., 2000). Interscanner variability, in contrast, may be responsible for significant differences in automated global and regional brain volume measurements in healthy controls scanned over time on different scanners and at different field strengths (Biberacher et al., 2016; Droby et al., 2015; Huppertz et al., 2010; Jovicich et al., 2009; Moorhead et al., 2009; Schnack et al., 2010; Shokouhi et al., 2011; Suckling et al., 2012; Takao et al., 2011; Whitwell et al., 2001). The impact of inter-scanner variability (including different field strengths) in manual volumetry is less clear. For example, one study found no significant difference in measurement error of healthy controls scanned at 1.5-Tesla versus 3-Tesla (Briellmann et al., 2001) while another found significant volume differences at 1.5-Tesla versus 4-Tesla (Levy-Reis et al., 2000). Acquisition-related factors such as subject motion (Reuter et al., 2015) and position with respect to scanner isocentre (to minimize static field inhomogeneity) and gravity (particularly relevant when the cranium is open during surgery) are also important considerations (Caramanos et al., 2010; Romano et al., 2011). It is also important to consider the effect of physiologic factors on structural measures, including hydration levels (Duning, Heindel and Knecht, 2005; Kempton et al., 2011), time of day (Nakamura et al., 2015), stress (Cho, 2001; Fink, 2011), or day of menstrual cycle (Hagemann et al., 2011).

Given the multitude of factors that may affect experimental variance of MR-based brain volume measurements, one group took a unique approach to

assess the sample size needed to detect a patient-control volume difference of 5% (with 80% statistical power) in a 2-sample cross-sectional versus longitudinal study design using a scan-rescan paradigm of 52 healthy controls assumed to have stable volume over time (Steen et al., 2007). Given this effect size and the measured variability between individuals in this study, they reported a required sample size of 73 patients and 73 controls for a cross-sectional study versus 5 patients and 5 controls for a longitudinal design. Such longitudinal designs are attractive in that each subject's brain volumes are compared within subject over time, thus limiting the variance associated with the above factors, which cannot be easily controlled (Morey et al., 2008, 2010).

#### **1.2.2.5 Interpretation of Structural Measures**

Individual or group-wide MRI-based structural measures can be reported either as absolute or relative values (Watson et al., 1997). Reporting relative values requires a comparison either as a ratio or a difference (i.e., between left and right sides in the same individual or for the same structure in the same subject over time; see chapter 3). Absolute values, on the other hand, are complicated by the potential impact of variables that may affect regional volume of interest such as brain size, head size, age, gender and side (Barnes et al., 2010; Davis and Wright, 1977; Nordenskjold et al., 2013; Scahill et al., 2003; Watson et al., 1997; Whitwell et al., 2001). An optimal approach would normalize the volume of the structure of interest by comparing patients to age and gender

matched control subjects for a particular side, which can then be corrected by head or brain size (Watson et al., 1997). Head size correction is performed by presenting a ratio of the target volume to an estimation of head size (or brain size, which is usually estimated by a measure of intracranial volume, ICV) or by using head size as a covariate in the analysis (Bengtson et al., 2000; Bilir et al., 1998; Kuzniecky et al., 1996; Watson et al., 1997). However, estimating intracranial volume is in and of itself a technical challenge as several different methods exist to accomplish it, ranging from slice-by-slice manual volumetry (gold standard, requires 25 minutes), to every  $n^{\text{th}}$  slice manual volumetry, to automated techniques (e.g., as available in Statistical Parametric Mapping (SPM) or FreeSurfer) (Eritaia et al., 2000; Nordenskjold et al., 2013). Nonetheless, as Nordenskjold et al., explain "...normalizing a structure by dividing it by an estimated ICV containing error, the normalized volume will contain an error proportional to the error in the ICV estimation" (p. 360, 2013). Moreover, in comparison to manual volumetry measures of ICV, commonly used automated measures tend to overestimate ICV by 5 – 21% and vary in association with factors such as gender or degree of atrophy such that the selected ICV method may influence study conclusions (Nordenskjold et al., 2013). Unanswered questions regarding ICV estimation include the impact of cranial neurosurgical procedures on measures of ICV itself or whether postoperative surrogates for brain size should account for resected areas or not.

## 1.2.3 Diffusion Tensor Imaging (DTI)

### 1.2.3.1 Background & Acquisition

The process of diffusion, or Brownian motion, describes the random movement of molecules due to thermal collisions (Brown, 1887). The net flux of particles down their concentration gradient, as described by Fick's first law, is dependent on the concentration gradient and the diffusion coefficient,  $D$ , expressed in  $\text{mm}^2/\text{second}$  (Fick, 1855). However, diffusion continues even in the absence of a concentration gradient (i.e. at equilibrium) such that molecules will travel a distance ( $r$ ), in time ( $t$ ) based on the diffusion coefficient ( $D$ ) of the medium (Einstein, 1905):

$$\text{Equation 1.2: } r = \sqrt{2Dt}$$

The diffusion coefficient ( $D$ ) was subsequently described to be proportional to the Boltzmann constant ( $k$ ) and absolute temperature ( $T$ ) yet inversely proportional to the particle size ( $r$ ) and medium viscosity ( $n$ ) according to the Stokes-Einstein equation:

$$\text{Equation 1.3: } D = \frac{kT}{6\pi r n}$$

Diffusion is also influenced by the presence or absence of physical barriers, at the microstructural level, which limit random molecular movement in certain directions more than in others. For example, in the absence of any physical

barriers (e.g., in a homogeneous fluid), diffusion is observed to occur similarly in all directions and is said to be isotropic. In this case, diffusion can be described by a single diffusion coefficient ( $D$ ). However, in biological tissues, diffusion varies with direction and is said to be anisotropic. Cerebral white matter, for example, has a high degree of diffusion anisotropy on account of myelin in axon sheaths, cellular membranes and various microstructural elements, which tend to restrict diffusion to a direction perpendicular, rather than parallel, to the long axis of such structural elements. Anisotropic diffusion cannot be characterized by a single diffusion coefficient, but rather by a diffusion tensor which is a  $3 \times 3$  matrix of diffusion in different orientations. Specifically, each part of the diffusion tensor is estimated by measuring the extent to which protons dephase when placed in diffusion-weighting gradients of particular directions (Winston, 2012), which will be more pronounced in protons that move during and in between diffusion gradient application.

Diffusion MRI is sensitized to molecular movement with the application of two equal diffusion-sensitizing gradients applied on either side of a refocusing  $180^\circ$  RF pulse, as first performed by Stejskal and Tanner using a pulsed spin echo sequence (Figure 1.5)(Stejskal and Tanner, 1965).

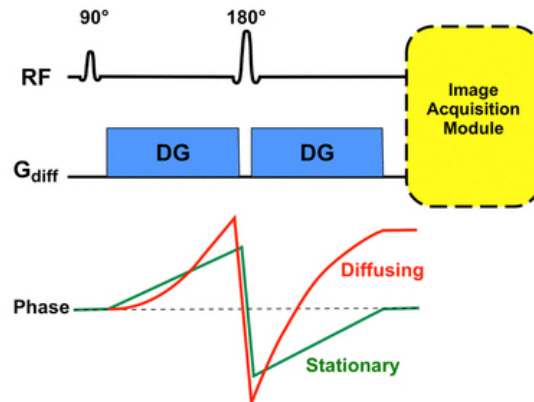


**Figure 1.5: Stejskal-Tanner diffusion pulsed gradient spin echo sequence**

**Strong symmetric diffusion gradients on either side of a 180° refocusing RF pulse results in net dephasing of mobile spins but not stationary spins (slice and phase imaging gradients not shown)(adapted with permission from Elster, 2015).**

Following application of the 90° RF pulse, net magnetization is rotated horizontally ( $M_{xy}$ ). Then the diffusion-sensitizing gradients are turned on, causing the spins to dephase. Next, a refocusing 180° RF pulse flips the direction of precession such that with the application of the second lobe of the diffusion-sensitizing gradient, the direction is effectively reversed, resulting in rephasing of the dephased spins. Stationary (non-diffusing) spins experience equal dephasing and rephasing effects, do not develop any net phase shift, and therefore generate relatively hyperintense signal. Mobile (diffusing) spins experience unequal rephasing compared to the dephasing experienced during initial diffusion-sensitizing gradient application owing to proton movement in the direction of this gradient such that they experience a different gradient strength in the second lobe of the diffusion-sensitizing gradient, developing net phase shift and therefore net signal loss. The extent of this signal loss is

measured in multiple unique directions from which a tensor can be calculated. The extent of diffusion-weighting of an image (i.e., the sensitivity to molecular motion) is determined by the b-value (Equation 1.4), which is dependent on the gyromagnetic ratio ( $\gamma$ ) as well as diffusion gradient pulse features including strength ( $G$ ), time interval ( $\Delta$ ), and duration ( $\delta$ ) of the diffusion-sensitizing gradient (Figure 1.6) (Elster, 2015).

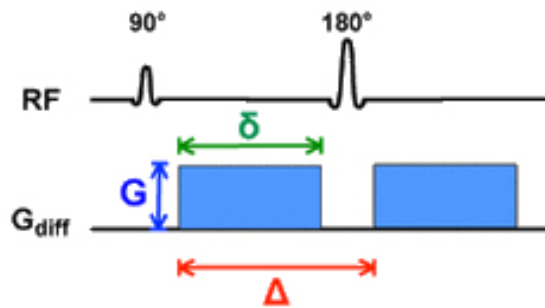


**Figure 1.6: Diffusion-gradient parameters**

The b-value of Stejskal and Tanner diffusion sequence is related to the magnitude ( $G$ ), duration ( $\delta$ ), and time interval ( $\Delta$ ) of the diffusion-sensitizing gradients.

Equation 1.4: 
$$b = \gamma^2 G^2 \delta^2 \left( \Delta - \frac{\delta}{3} \right)$$

Signal in DWI ( $S$ ) after application of diffusion-sensitizing gradients is related to signal at baseline in the  $b_0$  image ( $S_0$ ), b-value ( $b$ , in  $s/mm^2$ ) and the diffusion coefficient ( $D$ , in  $mm^2/s$ ) according to equation 1.5:

Equation 1.5:  $S = S_0 e^{-bD}$

Therefore, greater signal loss will occur when diffusion-sensitizing gradients are applied in an orientation with a high tissue diffusion coefficient or when scanning using higher b-values. The larger the b-value, the stronger the diffusion effects observed; however, the lower overall signal in the image due to increased signal loss due to increased T2 relaxation.

In DWI as is commonly used clinically, diffusion is interrogated using gradients applied in three mutually orthogonal directions and with multiple b-values to calculate the apparent diffusion coefficient (ADC) simplified for each voxel as an average value. In contrast, when diffusion is interrogated with at least six unique gradient directions, more sophisticated models can be used to represent the diffusion in a voxel—such as in DTI. Specifically, in DTI, diffusion-weighting gradients are used to estimate diffusion in six or more dimensions as well as one at baseline ( $b_0$ ), which is mathematically described by a [3 x 3] array or matrix of numbers describing diffusion rates in different orientations (Figure 1.7, Elster 2015).

$$\mathcal{D} = \begin{bmatrix} D_{xx} & D_{xy} & D_{xz} \\ D_{yx} & D_{yy} & D_{yz} \\ D_{zx} & D_{zy} & D_{zz} \end{bmatrix}$$

**Figure 1.7: The diffusion tensor matrix**

The diffusion tensor matrix describes diffusion rates in three principal (x, y and z) directions of the scanner (corresponding to  $D_{xx}$ ,  $D_{yy}$  and  $D_{zz}$ ) as well as 6 other terms that represent diffusion occurring in orientations in-between these. In the case of completely isotropic diffusion, a single diffusion coefficient,  $D$ , can completely describe diffusion in a voxel such that  $D = D_{xx} = D_{yy} = D_{zz}$  and the other terms all are zero.

The calculated tensor for each voxel can then be modelled as a diffusion ellipsoid using a different frame of reference than at scan acquisition, with the main axis of this ellipsoid shifted to lie along the axis of the principal diffusion direction as well as two mutually perpendicular minor axes. Each axis of the ellipsoid can be described by orthogonal eigenvectors ( $\varepsilon_1, \varepsilon_2, \varepsilon_3$ ), with length specified by a designated eigenvalue ( $\lambda_1, \lambda_2, \lambda_3$ ), that are proportional to diffusion in that direction (Figure 1.8).

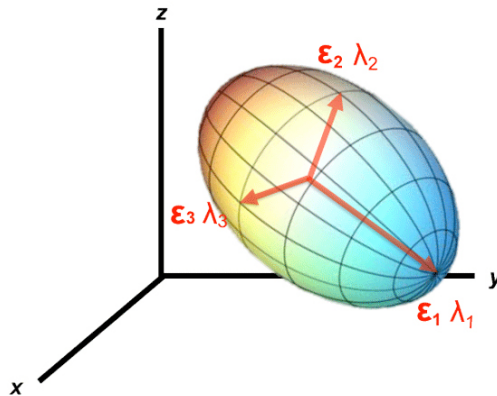


**Figure 1.8: The diffusion tensor ellipsoid**

Diffusion can be modelled by shifting the frame of reference to a coordinate system parallel to the principal direction of diffusion expressed as eigenvectors ( $\epsilon_1, \epsilon_2, \epsilon_3$ ) and eigenvalues ( $\lambda_1, \lambda_2, \lambda_3$ ) (adapted with permission from Elster, 2015).

Whereas both DWI and DTI provide information on interrogated tissue microstructure, DWI outputs are limited to added eigenvalues (trace) or averaged (mean diffusivity, MD or apparent diffusion coefficient, ADC which is equal to trace/3). In contrast, in DTI, the eigenvalues can also be used to create images or maps that provide information about the directionality of tissue microstructure. The main diffusion metrics include axial diffusivity (AD), radial diffusivity (RD), mean diffusivity (MD), and fractional anisotropy (FA). Axial diffusivity is the first eigenvalue (equation 1.6). Radial diffusivity is the average of the second and third eigenvalues, describing diffusion perpendicular to the principal diffusion direction (equation 1.7).

Equation 1.6       $AD = \lambda_1$

Equation 1.7  $RD = \frac{(\lambda_2 + \lambda_3)}{2}$

Mean diffusivity is a scalar measure of the average diffusion in a voxel or the mean of three eigenvalues, such that lower values mean less molecular diffusion.

Equation 1.8:  $MD = \frac{\lambda_1 + \lambda_2 + \lambda_3}{3}$

Fractional anisotropy describes the extent of diffusion anisotropy in a voxel by relating the relative difference between the first eigenvalue and the others (ranging from 0 - 1). It is rotationally invariant, containing no particular information about the principal orientation of diffusion.

Equation 1.9:  $FA = \sqrt{\frac{(\lambda_1 - \lambda_2)^2 + (\lambda_2 - \lambda_3)^2 + (\lambda_1 - \lambda_3)^2}{2(\lambda_1^2 + \lambda_2^2 + \lambda_3^2)}}$

Each of these scalar diffusion metrics can be plotted as grey scale image where voxel intensity corresponds to metric value. For example, in an FA map, voxel intensity would relate to FA value such that relatively dark voxels would have lower FA (lower anisotropy) than bright voxels (higher anisotropy)(Figure 1.9, A). By combining the rotationally invariant information regarding FA with orientation of the ellipsoid in each voxel (as indicated by the eigenvector,  $\epsilon_1$ ), a directionally encoded color (DEC) or colored FA map can be constructed in which the principal diffusion direction is described relative to the patient such that red indicates mediolateral, green indicates anteroposterior and blue indicates superoinferior (Figure 1.9, B). Finally, virtual white matter dissection can be achieved in vivo using the deterministic approach of fiber assignment by

continuous tracking (FACT) or white matter tractography (Catani et al., 2002; Mori et al., 1999). In this approach, fiber tracks are assigned in user-specified region(s) of interest (ROI) assuming one single diffusion tensor is adequate to represent diffusion in that voxel based on the principal direction (eigenvector) of diffusion in each voxel (Figure 1.9, C). DTI analysis methods are detailed further in section 1.2.3.3 below.

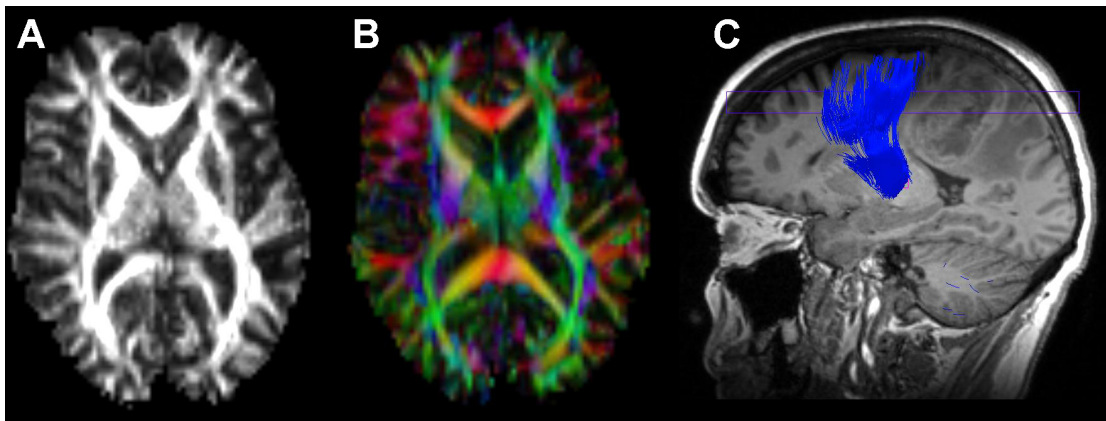


**Figure 1.9: DTI maps**

Examples of an FA map (A), directionally-encoded colour map (B) and tractography of the corticospinal tract (C).

### **1.2.3.2 Preprocessing**

After acquisition, diffusion MRI datasets are transferred to a computer workstation where gross visual inspection of raw data diffusion data is performed including comparison to co-acquired structural MRI data to look for evidence of image degradation resulting from artifacts or flips of diffusion data in image space (Soares et al., 2013). Numerous DTI-analysis software packages are available for data preprocessing steps and DTI analysis—a full discussion of

which is beyond the scope of this thesis. DTI analyses in this thesis have been carried out using ExploreDTI (version 4, Utrecht, The Netherlands)(Leemans et al., 2009) as well as StealthViz (Medtronic Inc., Louisville, CO, 2013). For example, in ExploreDTI, data preprocessing may include correction of signal drift (Vos et al., 2017), Gibbs ringing, subject motion, eddy current induced distortions (Leemans et al., 2009), and geometric distortions caused by B0-inhomogeneity (Huang et al., 2008; Irfanoglu et al., 2012; Tournier et al., 2011).

### **1.2.3.3      *Analysis***

Diffusion MRI data can be analyzed in several different ways, ranging from largely qualitative assessment of trace and ADC maps (e.g., chapter 3), to quantitative regional analysis of DTI metrics (e.g., chapter 5), to quantitative and reconstructive modeling of particular tracts, or white matter tractography (e.g., chapter 6). For example, clinically, trace or average DW images that display the geometric mean diffusion of diffusion-weighted images along three orthogonal directions (i.e., x-, y-, and z-axes) are compared qualitatively to ADC maps, which are created by dividing the signal in each voxel of the mean DW images ( $S_{DWI}$ ) by the signal of a corresponding location in the B0 image ( $S_0$ ) and then taking the logarithm (Equation 1.10 and Figure 1.10).

Equation 1.10:  $S_{DWI} = S_o e^{-b \cdot ADC} \Rightarrow ADC = -\frac{1}{b} \ln\left(\frac{S_{DWI}}{S_o}\right)$

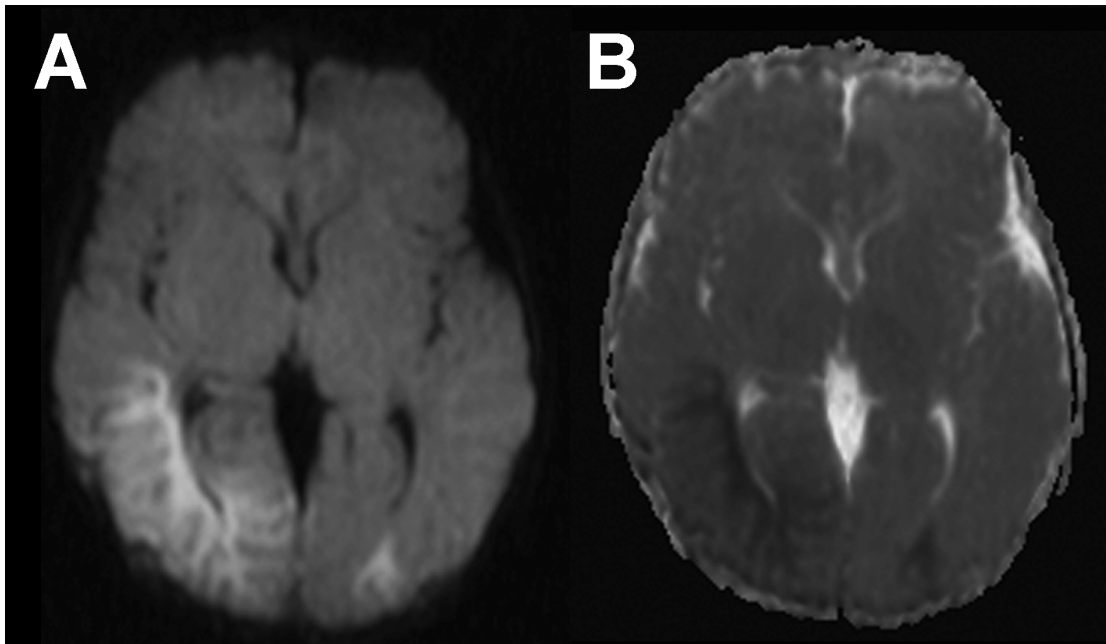


**Figure 1.10: Trace and ADC-map images following a traumatic brain injury resulting in an acute subdural hematoma along the posterior falx cerebri.**

Trace diffusion-weighted images provide the average diffusion of three orthogonal directions (A) during application of diffusion-sensitizing gradients to which the signal in corresponding points of an apparent-diffusion coefficient (ADC) map (B) will be inversely related, as in this example of a patient with an acute subdural hematoma along the posterior falx cerebri. See also equation 1.10. Adapted with permission from Elliott et al., 2017.

Signal intensity on trace DWI relates to how much diffusion occurs during application of diffusion-sensitizing gradients such that hyperintensity (e.g., acute stroke, or cerebral abscesses) indicates less mobile spins (i.e. restricted) which

rephase more completely than freely diffusing spins (i.e., unrestricted), which experience unequal rephasing and therefore decreased signal. The ADC-map, voxel-by-voxel, is inversely related to the trace DW image and by convention displays voxels with higher ADC (diffusion) as hyperintense (white) and voxels with lower ADC as hypointense (dark). However, because the trace DW images are in fact somewhat diffusion- and T2-weighted, it becomes necessary to compare trace DW images to ADC image maps to detect cases where DW images are falsely hyperintense or “contaminated” by lesions which have very long T2 (e.g., cerebral gliomas). This situation has been termed “T2-shine-through,” wherein which case bright areas on DW images would not correspond to dark areas on the ADC-map images. Conversely, lesions with very short T2 (e.g., subacute intracerebral hematoma) may cause false signal loss on DW images (enhanced T2\*-decay caused by paramagnetic effects of deoxyhemoglobin) with scattered areas of bright and dark voxels on the ADC-map (Elster, 2015).

Alternatively, quantitative analysis of diffusion metrics can be extracted and averaged for regions or structures of interest from parametric maps (e.g., MD, FA) to provide information regarding tissue microstructure. In this approach, particular attention must be paid to selecting an ROI, which for complex anatomical structures may not necessarily be best carried out on the relatively low spatial resolution diffusion images or corresponding maps (for more thorough handling of this issue please refer to further discussion found in chapter 5, sections 5.2.3 and 5.4). Selection of ROIs on non-anatomical DW images may falsely include adjacent non-target structures or CSF, or may index

only a small portion of the anatomical structure of interest. These sources of error may substantially change the output diffusion metric result and make comparisons across studies more challenging.

Finally, the directional information provided by diffusion data may be used to create reconstructions of white matter tracts, termed white matter tractography (Basser and Jones, 2002; D K Jones et al., 1999; Mori et al., 1999). White matter tractography is a burgeoning field in neuroimaging, with numerous strategies available that vary considerably in acquisition technique, applied method of tract modeling, and fiber tracking (Essayed et al., 2017). The DTI model alone will be briefly reviewed here, although several other more sophisticated models exist, including diffusion kurtosis imaging (DKI), high angular resolution diffusion imaging (HARDI) and diffusion spectral imaging (DSI) (Alexander et al., 2007; Tuch et al., 2002; Wedeen et al., 2008). In the DTI model, as employed in this thesis (chapters 5 & 6), diffusion in each voxel is represented by a single tensor, which is most accurate when a voxel is dominated by one major population of fibers transiting in a single orientation. When this is not the case, as is common for mixed populations of crossing fibers, kissing fibers, or rapidly bending fibers, the DTI model may no longer completely describe diffusion, and fiber tractography techniques (described below) may struggle as FA will fall, causing fiber tracking to cease (Duffau, 2014).

White matter tract reconstruction is carried out by either deterministic or probabilistic fiber tracking algorithms (Essayed et al., 2017). Both methods aim

to describe likely fiber tracks emanating from a start or 'seed' ROI but differ in that deterministic tractography generates a *single* track or streamline from the seed ROI while probabilistic tractography, in contrast, describes *all possible* connections along with their probabilities (Basser et al., 2000; Behrens et al., 2007; Winston, 2012). For example, in this thesis (chapter 6), the deterministic method FACT is used to generate tract reconstructions based on user selected tract initiation (seeding) ROIs. From these ROIs, the algorithm will attempt to follow the primary diffusion orientation eigenvector from voxel-to-voxel based on inputted values of FA for track initiation (typically 0.2 to 0.3) and termination, turning angle (usually 30-45°), and minimum or maximum track length. Additional ROI constraints may be applied to further limit reconstructed tracks including 'and' ROI (requiring reconstructed tracks to pass through both 'seed' as well as 'and' gates) or 'not' ROI (removing reconstructed tracks that pass through 'not' regions).

It is important to recognize that the extensive user input required for deterministic tractography may significantly affect resulting white matter reconstructions. For example, although more permissive FA thresholds (e.g., 0.10-0.15) may permit tracking near brain tumours associated with vasogenic edema, they may also introduce spurious tracks (Akai et al., 2005). Similarly, the selection of ROIs, which is prone to variability, bias, and presupposed user knowledge of complex neuroanatomy, has been shown to significantly affect tractography results (Colon-Perez et al., 2016; Essayed et al., 2017; Golby et al., 2011). Numerous atlases exist which may help guide ROI selection in both

normal and disease states, and limit ROI-related variability in tractography; however, considerable disagreement between sources still exists limiting universal application (Catani and Thiebaut de Schotten, 2008; Holodny et al., 2001; Lawes et al., 2008; Munnich et al., 2018; Niu et al., 2016; Radmanesh et al., 2015; Wassermann et al., 2016). Although it is possible (albeit computationally expensive) to create whole-brain DTI tractography maps seeding from the entire brain instead of from user selected ROIs, practically this method requires some form of parcellation to facilitate human interpretation for comparisons across subjects or to interpret output in individual patients and often is not used clinically thanks to its prolonged computing time (Wakana et al., 2007). Similarly, although probabilistic tractography may more accurately reconstruct tracts which are difficult to model by deterministic method (e.g., the optic radiation), wide scale clinical application is limited by the computational requirements (Winston et al., 2012). Therefore, deterministic DTI tractography, as employed in chapter 6 of this thesis, despite its recognized limitations, remains the most commonly used tool for white matter reconstruction in clinical neurosurgery.

#### **1.2.4 Perioperative applications of MRI in Neurosurgery**

Following its development by Lauterbur, Mansfield, Damadian and others in the 1970s and its rapid uptake in the neurological sciences in the subsequent

decades, MRI has become a ubiquitous component of preoperative evaluation, surgical planning and postoperative surveillance for many cranial neurosurgical pathologies (Damadian, 1971; Damadian et al., 1977; Lauterbur, 1973; Macchia et al., 2007). However, modern cranial neurosurgery is also dependent on preoperative MRI data for accurate intraoperative targeting and complication avoidance. Specifically, cranial neurosurgery is exclusively performed using neuronavigation (discussed in detail in section 1.5.2) to display the position of a navigated instrument on preoperative cross-sectional MRI data create tailored craniotomies and avoid adjacent non-target tissues (e.g. cortical veins, dural venous sinuses, functional cortex or subcortical white matter tracts). However, in the case of gliomas or epileptogenic lesions—which may lack distinct boundaries with adjacent non-target tissue—neuronavigation is also used throughout the operation to inform the extent of resection. The accuracy of preoperatively acquired MRI data during surgery is decreased by unpredictable brain deformation, or ‘brain shift’ (see also section 1.5.4), which accompanies all cranial neurosurgery (Mislow et al., 2009).

One approach to overcoming the problem of brain shift is to update neuronavigation patient space with intraoperatively acquired MRI data. Pioneering work at the Brigham and Women’s Hospital in Boston led by Dr. Peter Black culminated in the first, 0.5-Tesla, open-configuration, double-donut intraoperative MRI system in 1994 (Gering et al., 2001; Mislow et al., 2009). Although several other low field open-configuration iMRI systems were subsequently developed (e.g. PoleStar 0.12-Tesla developed by Moshe Hadani

with Medtronic, Louisville, USA) it was not until the advent of higher-field closed-bore iMRI solutions that higher SNR and spatial resolution images could be acquired. For example, the 1.5-Tesla ceiling-mounted, mobile Siemens iMRI developed by Dr. Garnette Sutherland and IMRIS in 1999 which allowed high quality intraoperative MRI acquisition in surgical position by moving the scanner in and out of the surgical field (Sutherland et al., 1999). More recently, 3-Tesla ceiling-mounted iMRI designs are available (Figure 1.11), which have been shown to enhance surgical targeting and allow intraoperative verification of lesion resection for cerebral gliomas, pituitary and skull base lesions, pediatric tumors and drug-resistant epilepsy (DRE) (Choudhri et al., 2014b; Coburger et al., 2017, 2016, 2014; Ginat et al., 2014; Hatiboglu et al., 2010, 2009; Mohammadi et al., 2014; Napolitano et al., 2014; Senft et al., 2011; Shah et al., 2012; Sylvester et al., 2015; Wu et al., 2014).



**Figure 1.11: Intraoperative MRI Theatre**

The Dan and Bunny Widney Intraoperative MRI Surgical Suite at the University of Alberta Hospital. Image used with permission, courtesy of IMRIS.

Despite the unquestioned utility of MRI to improve the safety and quality of neurosurgical procedures, there have, to date, been relatively few attempts to use perioperative MRI (especially intra- and early post-operative MRI) to predict clinically meaningful outcomes or provide pathophysiological insights into neurosurgical illness. This concept is a key theme of the work presented in this thesis. Figure 1.12 outlines the potential utility of perioperative MRI in three disease entities that will be covered in chapters 3-6. Sections 1.3 – 1.5 of this chapter provide a literature review related to these three entities.

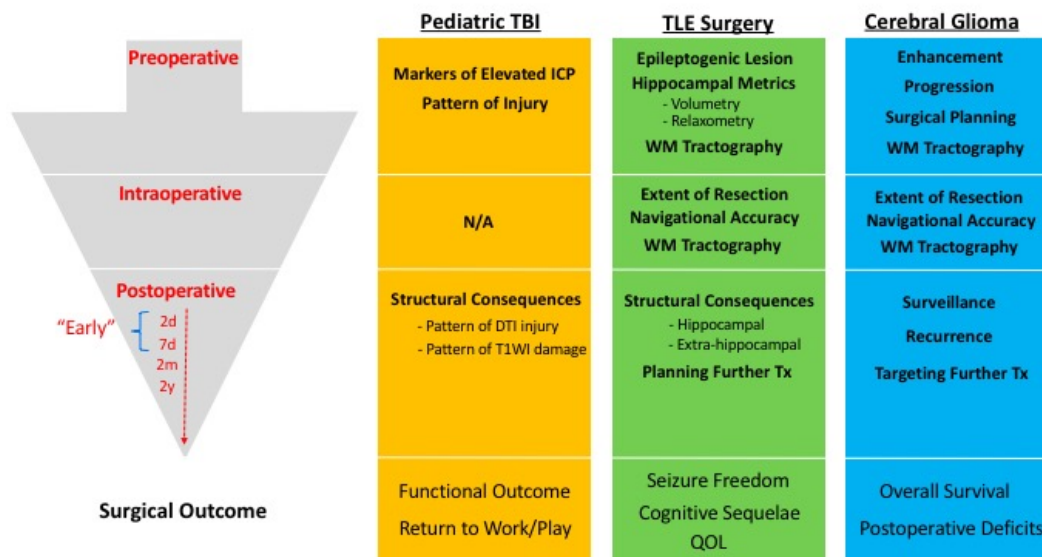


**Figure 1.12: Timing of MRI and potential utility in neurosurgery**

Examples of specific utility of MRI with respect to the time of surgical intervention in the three neurosurgical diseases discussed in this thesis. WM: white matter; ICP: intracranial pressure; Tx: treatment, QOL: quality of life.

#### **1.2.4.1 Unique Challenges of Post- and Intra-operative MRI**

There are several unique challenges specific to MRI acquisition in the early postoperative period (arbitrarily defined as within seven days of cranial neurosurgery). Postoperative pain, nausea, emesis, confusion or seizures, among others, can limit patient tolerance to often lengthy research scans, which can increase motion artifact or require abbreviated MRI acquisition protocols. Anticipation and aggressive symptomatic treatment may help in certain circumstances to mitigate the impact on data acquisition and quality. Next, invasive monitoring equipment which may remain in-situ temporarily—

particularly on the first postoperative day—including Foley catheters, external ventricular drains, endotracheal tubes, and arterial or central venous catheters although not contraindicated for research MRI acquisition, increase the logistical challenges of ultra-early postoperative scans owing to the added difficulty of patient transfer from unit to MRI machine and from bed to MRI table as well as by occasionally requiring the presence of specific healthcare professionals at the time of scan (e.g., medical doctor and/or registered nurse, based on MRI-unit regulations). Clinical MRI in the pediatric age group or in patients with altered levels of consciousness often requires sedation to prevent substantial motion artifact. Finally, skin should be closed with sutures rather than standard stainless steel surgical staples which may impart ferromagnetic artifact. Although magnetic field interactions and heating are generally not problematic, they may require special safety clearance when present, particularly for 3-Tesla scanners (Gill and Shellock, 2012).

The iMRI environment also presents a host of challenges which may affect data quality. First, typical iMRI installations—such as the IMRIS 3-Tesla surgical suite (Figure 1.11)—are limited to 8-channel, two-piece, flexible receive surface coils (Figure 1.13) which typically provide inferior signal-to-noise (SNR) compared to typical 32- or 64-channel research scanner receive coils.



**Figure 1.13: Intraoperative MRI surface coil**

Eight-element flexible, surface receive coil affixed to IMRIS-adapted Mayfield cranial fixation device and surgical table (image used with permission and courtesy of IMRIS)

In addition, many neurosurgical procedures require a non-supine, non-neutral head position which, depending on patient body habitus, may result in scanning away from isocentre, which in turn may affect static field homogeneity or gradient linearity (Choudhri et al., 2014a). Non-neutral head positions can make registration of intraoperatively acquired structural or diffusion images to preoperative reference images more challenging or impossible; they also can affect the diffusion-sensitizing gradient direction in diffusion scans, making directionally-encoded colour (DEC) FA maps more difficult to interpret (C Nimsky et al., 2005b).

## **1.3 Pediatric traumatic brain injury**

### **1.3.1 Introduction**

Trauma is the most common cause of death in children (CDC, 1990). Among infants ( $\leq 2$  years of age), inflicted head injury is the most common cause of traumatic death (Duhaime et al., 1992) and a leading etiology of NAT. Inflicted head injury in infants is associated with 31-45% morbidity and 6-26% mortality (Duhaime et al., 1998, 1992; Ghahreman et al., 2005; Holloway et al., 1994; Jayawant et al., 1998; Kemp et al., 2009; King et al., 2003). Clinical evaluation and management of infantile TBI should always include consideration of the possibility of NAT. Infants are more vulnerable to catastrophic injury secondary to TBI or NAT for a variety of reasons including immature musculoskeletal structure (e.g., cranial bones remain thin, pliable, and largely unfused at sutures), increased vulnerability of the developing brain to excitotoxic injury, relatively large skull to body ratio, more pronounced impact of repeated injury, and potential for cascading impact of disruption of myelination and arborization early in life (Figaji, 2017; Sarioglu et al., 2017). “Shaken-baby syndrome” is one common type of NAT which is thought to involve an abrupt angular deceleration force on the cranium when an infant is shaken while held by the trunk, leading to an impact of the skull on a nearby hard surface (Duhaime et al., 1998). This syndrome is commonly accompanied by a pattern of injury including subdural and subarachnoid hematoma, long bone fractures, and retinal hemorrhages.

Evaluation and management of pediatric TBI is a complex, multidisciplinary process which will not be described in this thesis. Rather the remainder of this section will describe the expanding role of neuroimaging—particularly DWI—in pediatric TBI.

### **1.3.2 Neuroimaging evaluation**

Initial neuroimaging evaluation of pediatric TBI is carried out by computerized tomography (CT) which rapidly identifies cranial vault fractures, intracranial bleeding (e.g., epidural, subdural, intraparenchymal, intraventricular or subarachnoid hemorrhage), intracranial hypertension (i.e., elevated intracranial pressure), or established infarct. Modern multiplanar CT is fast, often obviating the need for sedation or anesthesia to facilitate motion-artifact free scanning, in contrast to MRI scanning, which almost always requires sedation in this age group. However, one CT scan of the head exposes the patient to approximately 4 milli-Sieverts, which is equivalent to approximately 200 chest x-rays or a 10-month dose of background irradiation, unlike MRI (Brody et al., 2007; The Royal College of Radiologists and The Royal College of Paediatrics and Child Health, 2008). Also, CT imaging has limited utility in accurate characterization of the extent and pattern of intracranial injury (Kemp et al., 2009).

MRI, in contrast, particularly when accompanied by DWI, provides superior characterization of the patterns of injury that commonly accompany

TBI/NAT, such as focal or diffuse hypoxia/ischemia, intraparenchymal shearing injury (diffuse axonal injury), subtle post-traumatic cortical injury, or microhemorrhages (Barnes, 2011; Biousse et al., 2002; Duhaime et al., 1998; Ichord et al., 2007; Imagawa et al., 2014; Parizel et al., 2005; Vazquez et al., 2014). For example, a recent meta-analysis of the relative utility of cranial MRI following CT amongst children with suspected NAT brain injury provided additional findings in 25% of a total of 367 cases (across 18 included studies), including subdural hematoma, subarachnoid hemorrhage, ischemia and diffuse axonal injury, not identified on initial CT (Kemp et al., 2009). Moreover, the signal of blood products on various T1- and T2-weighted sequences provides additional information as to the timing of injury and may identify hemorrhages of different ages. Therefore, these authors suggest that early MRI with DWI be performed in all cases of pediatric TBI for which potential for NAT exists and in which either the CT head is abnormal or there are ongoing clinical concerns (Kemp et al., 2009). Finally, MRI in TBI secondary to NAT is predictive of subsequent functional outcome in cases found to have intraparenchymal lesions—however, the relative utility of CT versus MRI was not assessed (Bonnier et al., 2003).

### **1.3.3 Utility of diffusion MRI**

The extent of DWI abnormalities in pediatric TBI and suspected NAT provides the most accurate early estimate of the true extent of microstructural

injury, which may help to inform ultimate clinical outcome (Ashwal et al., 2011; Elliott et al., 2017; Geddes et al., 2001b; Suh et al., 2001). DWI can demonstrate abnormalities within minutes to hours of injury before the diffuse nature of insult may be visualized on conventional MRI or CT (Suh et al., 2001). For example, DWI commonly reveals more widespread abnormalities than other non-DWI MRI sequences or CT alone in 50-89% of cases (Biousse et al., 2002; Kemp et al., 2009; Suh et al., 2001; Zimmerman et al., 2007). This finding is largely based on DWI being sensitive to the presence of cytotoxic edema—a final common pathway that accompanies a variety of cerebral insults that compromise cellular membrane ionic balance—unlike T1- and T2-weighted sequences. Specifically, in cytotoxic edema, there is impaired ATP-dependent sodium/potassium pump function resulting in a relative increase in the fraction of intracellular water (due to increased intracellular sodium) characterized by high signal on DWI with corresponding areas of low signal on ADC (restricted diffusion; as well as reduced MD) (Ebisu et al., 1993; Hergan et al., 2002; Schaefer et al., 2000). The most familiar clinical scenario in which this occurs is, of course, ischemic stroke, in which within minutes of arterial occlusion, restricted diffusion becomes readily apparent and predictive of the infarct core. However, in the setting of brain injury secondary to NAT, DWI is useful to identify other non-ischemic causes of restricted diffusion. Zimmerman et al., for example, described five distinct patterns of altered DWI signal associated in 33 patients with NAT head trauma including (1) diffuse, supratentorial hypoxic ischemic injury (39%), (2) watershed-type supratentorial ischemia (42%), (3)

venous infarction (12%), (4) diffuse axonal injury (6%) and (5) contusion (6%) (Zimmerman et al., 2007). Other patterns of injury have been described in older patients with subdural hematoma secondary to NAT, such as unilateral white matter DWI restriction (McKinney et al., 2008).

### **1.3.4 Pathophysiology of diffusion abnormalities**

The observed pattern of diffusion injury has been interpreted to reflect the presumed pathophysiology of the injury and has been dichotomized as either (1) hypoxic-ischemic type injury typified by confluent diffusion abnormalities approximating known vascular territories, or (2) directly traumatic type, which tends to be more focal in nature (Ichord et al., 2007). Many of the described mechanisms of injury in head injury secondary to NAT (e.g., transient or persistent cardiorespiratory compromise, vasospasm adjacent to subarachnoid hemorrhage, or primary direct injury) fit with this dichotomy, except for excitotoxic injury secondary to seizures or status epilepticus (Goldstein et al., 2011; Kemp et al., 2003; Moritani et al., 2005; Pierce et al., 2002; Zimmerman et al., 2007).

### **1.3.5 Prognostic value of diffusion MRI**

The extent of early post-injury diffusion MRI abnormalities in head injury secondary to suspected NAT provides potentially useful information about

clinical outcome. Suh et al., for example, found a significant correlation between the extent of DWI injury (categorized as (1) focal, unilateral; (2) multifocal but unilateral; (3) multifocal, bilateral but not diffuse or (4) diffuse) in 20 children with presumed or suspected head injury secondary to NAT with Children's Outcome Scale at the time of discharge from hospital (Suh et al., 2001). However, in this study, long-term functional outcome or follow-up MRI imaging was unavailable and outcome was assessed at the time of discharge (mean length of stay was 13 days). It remains unclear how early DWI abnormalities relate to outcome at more clinically meaningful follow-up intervals in the months and years after injury. Specifically, the long-term structural and functional consequences of early DWI abnormalities are poorly understood. In chapter 3 of this thesis, we attempt to address this question by examining the relationship of extensive, unilateral white-matter areas of restricted diffusion in infants with subdural hematomas suspected to be secondary to NAT.

## **1.4 Temporal Lobe Epilepsy**

### **1.4.1 Introduction**

Epilepsy is a highly disabling disease characterized by an enduring predisposition to recurrent unprovoked seizures thought to affect over 70 million people globally (Ngugi et al., 2010). A seizure is defined as a transient abnormal excessive or synchronous neuronal discharge accompanied by signs or symptoms (Fisher et al., 2017, 2014, 2005). Epilepsy is the fourth most common

neurologic condition accounting for 1% of the global burden of disease (Engel et al., 2012; Hirtz et al., 2007). In the United States alone approximately 3.4 million people have active epilepsy conveying a total direct and indirect societal cost of over \$15 billion per year (England et al., 2012; Zack and Kobau, 2017). Epilepsy is associated with increased mortality and morbidity as well as marked stigmatization (Bandstra et al., 2008; Tedrus et al., 2017). Individuals with epilepsy, compared to the general population, have higher rates of premature death secondary to status epilepticus, accidents or sudden unexplained death in epilepsy (SUDEP) with standardized mortality ratios ranging from 1.6 to 19.8 deaths per 1000 people with epilepsy in high-income countries and low- and -middle-income countries respectively (Levira et al., 2017; Thurman et al., 2017). In addition, individuals with epilepsy experience substantial morbidity and decreased quality of life secondary to higher rates of bodily injury, progressive cognitive impairment, psychiatric illness, and unemployment (Devinsky et al., 2016).

Approximately 30 - 40% of patients with epilepsy experience ongoing seizures despite optimized anti-epileptic drug (AED) therapy (Engel, 2016). Operationally, the International League Against Epilepsy (ILAE) categorizes such patients as DRE based on failure of adequate trials of two tolerated, appropriately chosen and used antiepileptic drugs to achieve seizure freedom (Kwan et al., 2011, 2010; Kwan and Brodie, 2000). Patients with DRE are at highest risk of epilepsy-related morbidity and mortality (5 -10x higher than general population) and account for up to 80% of the cost of epilepsy (Engel,

2016). Of the surgical epilepsies, TLE is the most common, representing approximately 60% of all focal epilepsies—so named for their origin in one hemisphere or, as often, in one lobe (Engel, 2001; Fisher et al., 2017). Typical patients with TLE presents in their third to fourth decade with DRE, classically following an initial precipitating injury (IPI), early in life, which may include febrile seizures (FS), birth trauma, TBI or meningitis/encephalitis (Thom et al., 2009). Patients classically experience seizure onset in the second decade of life following a seizure-free interval (latency period) followed by a period of inadequately controlled seizures with mean duration of 22 years (Berg, 2004; MacRae et al., 2002). The classic semiology (signs and symptoms of seizures) of TLE is a focal awareness impairing seizure (FAIS) that classically involves a focal aware seizure (or aura), most commonly an epigastric rising sensation followed by a blank, motionless stare, oral or manual automatisms (purposeless, stereotyped and repetitive movements such as lip smacking or picking at things), or contralateral dystonic posturing (Fisher et al., 2017).

Based on seizure semiology, electroencephalographic findings, neurocognitive assessment, and MRI findings, TLE can be subdivided into mesial versus lateral (neocortical) TLE (Engel, 2001). Mesial TLE is the most common subtype, named for seizures arising from the infero-mesial temporal lobe structures of the hippocampus, parahippocampal gyrus (PHG), and amygdala. The most common etiology of mesial TLE is a focal loss of hippocampal neurons accompanied by gliosis termed hippocampal sclerosis (HS), Ammon's horn sclerosis (AHS), or mesial temporal sclerosis (MTS) which accounts for 50 – 60%

of cases (Blümcke et al., 2007; Gates and Cruz-rodriguez, 1990; Thom, 2014). Low grade neoplasms and focal cortical malformations (dysplasia) are two other common causes of mesial TLE (Blümcke, 2009). In approximately 5% of cases HS will co-occur in the presence of an additional extrahippocampal abnormality such as a neocortical focal cortical dysplasia (FCD), low grade tumours, vascular malformations, or gliotic cortex (Blumcke and Spreafico, 2012).

## **1.4.2 The epileptogenic hippocampus**

### **1.4.2.1 *Anatomy and nomenclature***

The hippocampal formation is a paired, inferomedially located temporal lobe structure which consists of both the hippocampus proper (cornu Ammonis) and the dentate gyrus (Figure 1.14)(Duvernoy et al., 2005). It is an integral part of the limbic system, a group of structures implicated broadly in declarative memory and emotion (Duvernoy, 2005). The dominant and non-dominant hippocampi (relative to laterality of language, i.e., dominant, indicating on the same side of language representation) is thought to be involved with verbal and figural memory, respectively (Corkin, 1965; Kimura, 1963; Milner, 1971, 1968). Phylogenetically, the hippocampus and the adjacent PHG are 3-layered archicortex, with the latter including several cortical parts called the entorhinal cortex, perirhinal cortex, and posterior parahippocampal cortex (Scharfman et al., 2000).

The limbic system, so-named by Paul Broca for its location at the *limbus* (Latin for border) of the cerebral hemispheres and the brainstem (Broca, 1878), consists of both cortical and subcortical components (Figure 1.14). Limbic cortical areas include the hippocampus and PHG as well as neocortical areas including the insular, cingulate, orbitofrontal, and subcallosal cortices (Chan et al., 1997; Rajohan and Mohandas, 2007; Swenson, 2006). Subcortical structures include the amygdala, hypothalamus, mamillary body septal nuclei, olfactory bulb, and parts of the thalamus (Swenson, 2006).

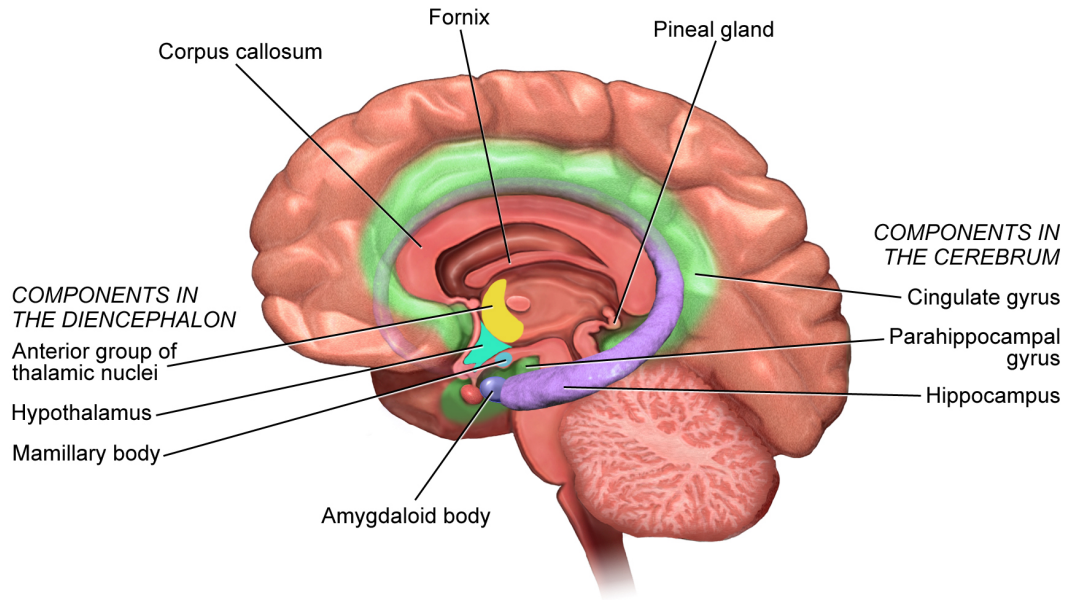


**Figure 1.14: The hippocampus and other limbic system components**

The hippocampus is a paired inferomedially located temporal lobe structure shown here in relation to limbic cortical components including the parahippocampal gyrus and cingulate gyrus as well as subcortical structures including the amygdala (amygdaloid body), anterior nucleus of the thalamus, hypothalamus and mamillary body. The mamillary body receives hippocampal output via the limbic white matter tract, the fornix. Modified and used with permission from Blausen.com staff 2014 (Blaus, 2014).

The hippocampus is a curved, tubular structure likened to a seahorse or a ram's horn (the latter being the basis for which hippocampal subfields—shown in Figure 1.15; see CA1 - CA4—were named *cornu Ammonii*) (Duvernoy, 2005). Microscopically, hippocampal subfield distinctions are made based on architectonic variations of both cellular morphology and connectivity, according to the seminal work of Lorente de No (Lorente de No R, 1928) and these subfields are differently affected in HS. For example, CA1 (so-called Sommer sector or the vulnerable sector), which is continuous with the subiculum, is the area most commonly involved in HS while CA3 (so-called Spielmeyer sector or

the “resistant sector”) is commonly spared (Sommer, 1980; Spielmeyer, 1927). The relative relationship of the cornu Ammonis and the dentate gyrus is preserved along the anterior-posterior extent of the hippocampus, consisting of two interlocking U-shaped laminae each with distinct cellular composition. Macroscopically, the hippocampus is divided, along its anterior-posterior extent, into three subregions: the head, body, and tail. The entire adult human hippocampus generally spans 4 – 4.5 cm (Duvernoy, 2005).

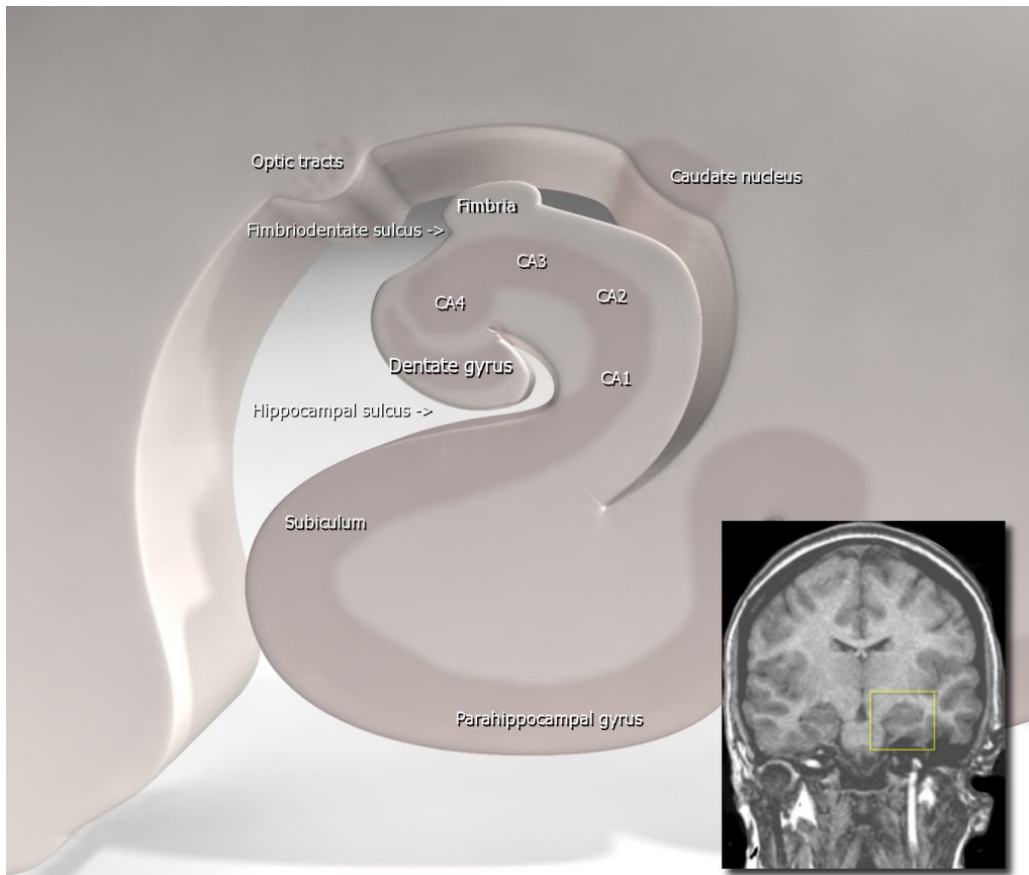


**Figure 1.15: Hippocampal subfields**

Coronal illustration with inset coronal MRI (bottom right) through body of hippocampus demonstrating the relative position of cornu Ammoni 1 – 4, dentate gyrus, subiculum and parahippocampal gyrus. Used with permission from Wikimedia commons under the GNU\_Free\_Documentation\_License.

Input to the hippocampus arises largely from the entorhinal cortex (layers II and III) as well as via the fornix from septal, diencephalon, basal forebrain and commissural fibers from the contralateral hippocampus (Mark et al., 1995; Rajohan and Mohandas, 2007). The dentate gyrus, which is made up of granule cells, receives most of the excitatory input from the entorhinal cortex passing through the subiculum (termed the perforant pathway). Axons of granule neurons called mossy fibers (so named by Ramon y Cajal for numerous varicosities along their length (Cajal S, 1894)) project to CA4/CA3 pyramidal cells. Thereafter CA3/CA4 axons leave the hippocampus as the alveus, eventually coalescing as the fimbria of the fornix. In addition, exiting axons from CA3/CA4 may also emit collateral projections back to CA1 as so-called Schaeffer collaterals. CA1 axons may subsequently project back to the entorhinal cortex, closing a trisynaptic loop, or go on to enter the alveus and then the fimbria, accompanied by fibers from CA3/CA4 (as well as by substantial projections from the subiculum) to provide the main output from the hippocampus (Chan et al., 1997; Duvernoy, 2005). In addition, there are direct alvear pathway projections from entorhinal cortex neurons to CA1 pyramidal cells which then either project via the alveus to the fimbria-fornix or innervate the subiculum, which ultimately projects back to the deeper layers of the entorhinal cortex (Duvernoy, 2005). Accumulated axons of the alveus assemble on the ventricular surface of the hippocampus, forming the crus of the fornix at the level of the splenium of the corpus callosum, which projects anteriorly as the body then columns of the fornix innervating the anterior nucleus of the thalamus directly (or indirectly via

the mammillary bodies, as the mammillothalamic tract). Thalamic output thereafter innervates either the retrosplenial area or the cingulate cortex, and from the latter the cingulum ultimately projects back to the entorhinal cortex, completing the circuit of Papez (Figure 1.16)(Nakano, 1998; Oikawa et al., 2001; Papez, 1937; Thomas et al., 2011).

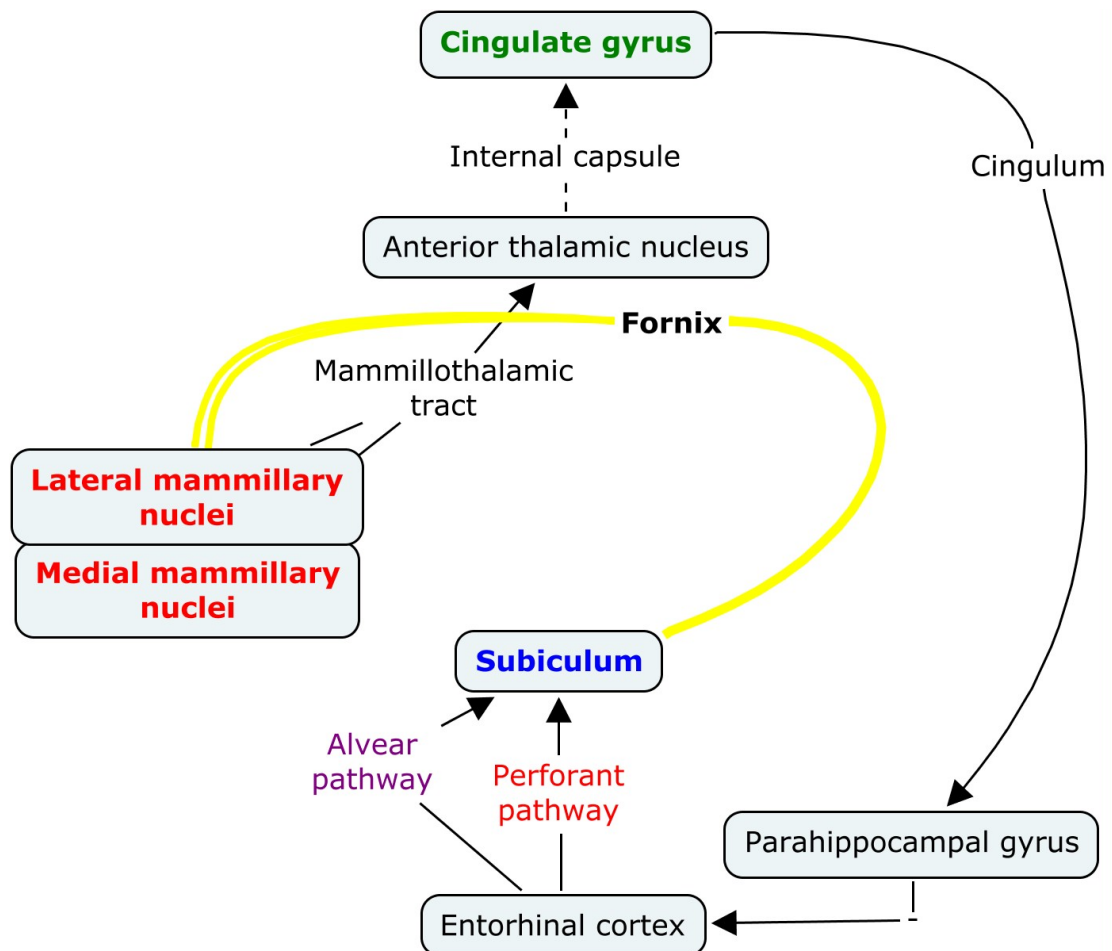


**Figure 1.16: The circuit of Papez**

The circuit of Papez begins in the subiculum of the hippocampus from which postcommissural fornix fibers largely project to the mammillary body. The mamillothalamic tract projects from mammillary bodies to the anterior nucleus of the thalamus, which in turn projects via the cingulum from the cingulate cortex to the entorhinal cortex where via either direct (alvear) or perforant pathway, the circuit concludes back in the subiculum. Modified with permission from WikimediaCommons (public domain).

#### **1.4.2.2 Pathology of Hippocampal Sclerosis**

Hippocampal sclerosis was first reported in 1825 (Bouchet and Cazauvieilh, 1825). In 1980, Sommer described the observation of subfield specific loss of hippocampal pyramidal cells (Sommer, 1980). Although HS may accompany any epilepsy syndrome, it is the classic and most commonly identified etiology of mesial TLE, making up 56% of surgical cases (Malmgren and Thom, 2012; Novy et al., 2013; Thom, 2014). The term HS, or its eponym Ammon's horn sclerosis (AHS), specifically refers to focal neuronal loss restricted to the hippocampus proper (cornu Ammonis); in some cases sclerosis and neuronal loss occurs extrahippocampally in the adjacent mesial temporal structures of the amygdala and uncus, in which case, the term "MTS" is more aptly used (Mitchell et al., 1999). Histopathological characteristics of HS include segmental hippocampal cell loss, granule cell dispersion within the dentate gyrus, and reactive gliosis. The classic pattern (MTS type I) of selective subfield hippocampal pyramidal cell death occurs predominantly in CA1 and to a lesser extent in CA3 and CA4 (hilar region) with relative sparing of CA2 and dentate gyrus granule cells (Figure 1.17)(Blumcke, 2009; Thom et al., 2009; Thom et al., 2010).

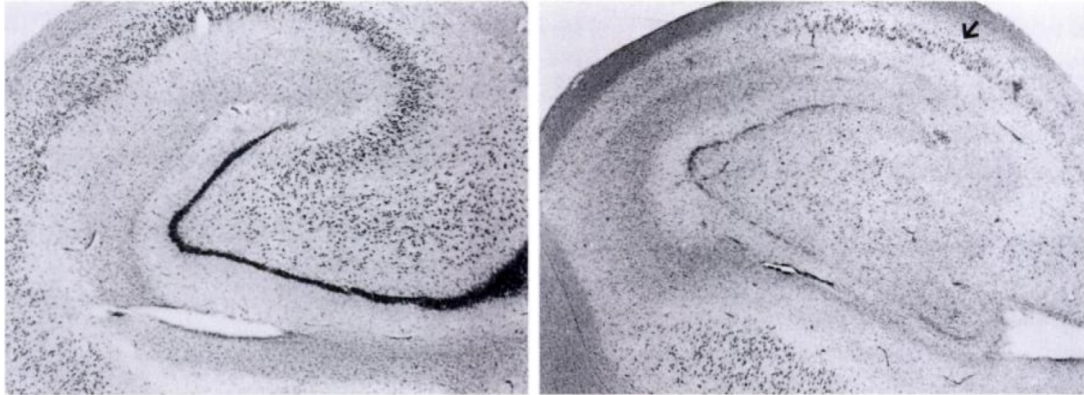


**Figure 1.17: Photomicrographs of Nissl stained hippocampal slices**

Shown in a normal subject (left) and (right) in a patient with mesial temporal sclerosis showing marked CA1/3/4 pyramidal cell loss with relative sparing of CA2 (arrow). Adapted with permission from Chan et al., 1997.

Other less common subtypes of MTS include (1) MTS type 2, characterized by cell loss restricted to CA1 alone, or (2) MTS type 3 (or end folium sclerosis) which involves cell loss mostly in the CA4/hilar region (Thom et al., 2010). Although the atypical subtypes of MTS account for up to only 10% of cases they may be more difficult to visualize on preoperative imaging and have been reported to be associated with a worse surgical outcome with seizure-free rates as low as 25% for MTS type 3 (Blumcke et al., 2007; Thom et al., 2010; Thom et al., 2002; VanPaesschen et al., 1997).

### **1.4.3 Epilepsy Surgery**

#### **1.4.3.1 *Historical Aspects***

The concept of surgical treatment of medically refractory epilepsy began in the early 1900s with surgical pioneers including Victor Horsley, Fedor Krause and Harvey Cushing; each who independently carried out successful focal brain resections while avoiding eloquent regions identified by mapping using direct cortical stimulation (Feindel et al., 2009). Subsequently in 1928, Wilder Penfield carried out the first staged, anterior temporal lobectomy (ATL) for drug-resistant post-traumatic TLE (Feindel, 1991). Over the next two decades, Herbert Jasper and Penfield were largely responsible for a shift in focus to the role of mesial temporal structures in epileptogenesis, the iterative development of the ability to record intraoperatively from these regions, and the surgical technique required to safely resect this tissue. Penfield and Baldwin published the first technical description of a subtotal, ATL (or the “Montreal Procedure”) in 1952; this involved inferomesial temporal resection including the amygdala, uncus, and hippocampus (Feindel et al., 2009; Preul and Feindel, 1991). The widespread uptake of this approach and its subsequent modification to include en bloc resection by Falconer facilitated the discovery of the histopathological characteristics of mesial TLE (Falconer, 1953). The advent of cross-sectional imaging such as CT and subsequently MRI allowed accurate detection of pathologic tissue preoperatively and also ensured satisfactory surgical resection (Feindel, 1991; Kuzniecky et al., 1987, 1996).

### **1.4.3.2      *Temporal Lobe Epilepsy Surgery***

Ultimately, approximately one third of patients with epilepsy and up to 90% of those with HS will develop DRE and may present for epilepsy surgical evaluation (Kwan et al., 2011; Schuele and Lüders, 2008; Semah et al., 1998). In these cases the surgical treatment has been demonstrated to convey superior rates of seizure freedom relative to ongoing medical management in well-designed, randomized, controlled studies (Dwivedi et al., 2017; Engel et al., 2012; Wiebe et al., 2001). In their landmark randomized-controlled trial involving 80 TLE patients, Wiebe et al., (2001) found significantly higher rates of freedom from disabling seizures in patients randomized to ATL versus ongoing maximal medical therapy (58% versus 8%), as well as improved quality of life scores. Similarly, in the Early Randomized Surgical Epilepsy Trial (ERSET), patients randomized to ATL and continued AED treatment were found to have a significantly higher rate of freedom from disabling seizures (73%) compared to ongoing AED treatment alone (0%) at 2 years follow-up (Engel et al., 2012). Most recently, Dwivedi et al. randomized a group of pediatric patients with DRE not limited to TLE, finding that surgery along with ongoing medical treatment resulted in substantially higher seizure freedom (77%) at 1 year after surgery compared with ongoing medical treatment alone (7%). Seizure control after surgery is commonly categorized using one of two clinical scales, the Engel or ILAE classification of epilepsy surgery seizure outcome (Table 1.1 and 1.2) (Durnford et al., 2011; Engel et al., 1993b; Wieser et al., 2001).

**Table 1.3: Engel classification of postoperative seizure freedom**

---

Class I: Free of disabling seizures<sup>a</sup>

- A: Completely seizure free since surgery
- B. Nondisabling simple partial seizures only since surgery
- C. Some disabling seizures after surgery, but free of disabling seizures for at least 2 years
- D. Generalized convulsions with AED discontinuation only

Class II: Rare disabling seizures (“almost seizure free”)

- A. Initially free of disabling seizures but has rare seizures now
- B. Rare disabling seizures since surgery
- C. More than rare disabling seizures since surgery, but rare seizures for the last 2 years
- D. Nocturnal seizures only

Class III: Worthwhile improvement<sup>b</sup>

- A. Worthwhile seizure reduction
- B. Prolonged seizure-free intervals amounting to greater than half the followed-up period, but not <2 years

Class IV: No worthwhile improvement

- A. Significant seizure reduction
- B. No appreciable change
- C. Seizures worse

---

<sup>a</sup> Excludes early postoperative seizures (first few weeks).

<sup>b</sup> Determination of “worthwhile improvement” will require quantitative analysis of additional data such as percentage seizure reduction, cognitive function, and quality of life.

(Adapted with permission from Engel, 1993).

**Table 1.2: ILAE classification of postoperative seizure freedom**

Outcome classification	Definition
1	Completely seizure free; no auras
2	Only auras; no other seizures
3	One to three seizure days per year; ± auras
4	Four seizure days per year to 50% reduction of baseline seizure days; ± auras
5	Less than 50% reduction of baseline seizure days to 100% increase of baseline seizure days; ± auras
6	More than 100% increase of baseline seizure days; ± auras

---

(Adapted with permission from Wieder et al., 2001).

Several surgical approaches exist for the treatment of drug-resistant mesial TLE. Although it was the traditional en bloc ATL (Falconer and Taylor, 1968; Morris, 1956; Penfield and Baldwin, 1952; Walker, 1967) that was formally compared to medical management in the above mentioned randomized controlled trials (Engel et al., 2012; Wiebe et al., 2001), a number of other available surgical options include lesionectomy, selective amygdalohippocampectomy (SAH), and the Spencer anteriomesial lobectomy (Spender et al., 1984). As well, minimally invasive options such as radiosurgery (Régis et al., 1999) and MRI-guided laser thermal ablation (LaRiviere and Gross, 2016) (Figure 1.18) also exist.

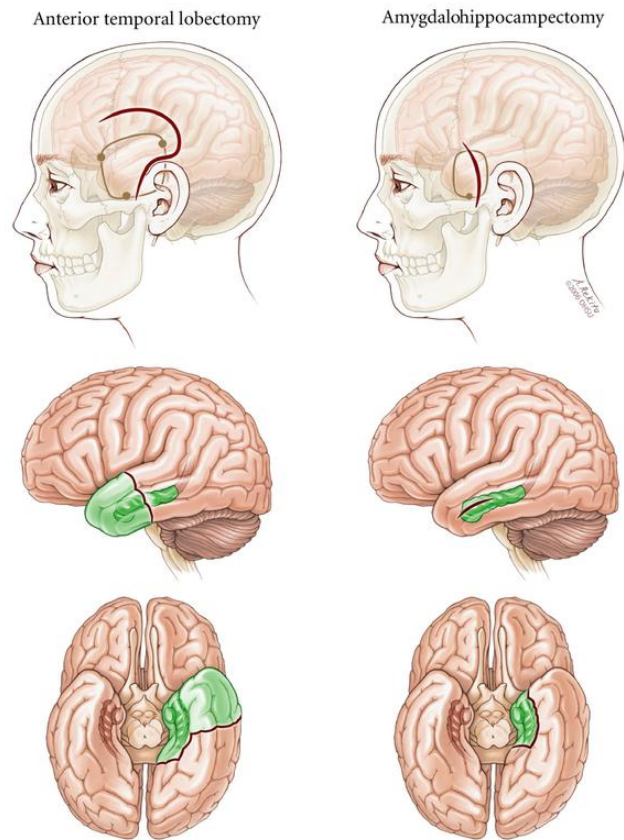


**Figure 1.18: Anterior temporal lobectomy (ATL) versus selective amygdalohippocampectomy (SAH)**

Diagrammatic representation of the differences in resected tissue (green shading) between ATL (left column) and SAH via a transcortical approach (right column). Adapted with permission from (Spencer and Burchiel, 2012).

The en bloc ATL involves resection of anterolateral temporal neocortex (6 – 6.5 cm for the non-dominant hemisphere, 4 – 4.5 cm for the dominant hemisphere measured from the temporal tip) with mesial resection of the amygdala and anterior 3 – 4 cm of the hippocampus (Wiebe et al., 2001). In contrast, in SAH, an equivalent mesial temporal resection is performed either via

a subtemporal, transsylvian, or transcortical (trans-middle temporal gyrus) route to spare the lateral temporal neocortex (Niemeyer, 1958; Olivier, 2000; Wheatley, 2008). Initially developed by Brazilian neurosurgeon Paulo Niemeyer in 1958, the rationale for this procedure is to achieve equivalent seizure control with better neuropsychiatric outcomes. Indeed, numerous retrospective studies have found similar rates of postoperative seizure control to ATL (Arruda et al., 1996; Clusmann et al., 2002; Helmstaedter et al., 2008; Paglioli et al., 2004; Sindou et al., 2006; Tanriverdi et al., 2008; Tanriverdi and Olivier, 2007) with improvement in neurocognitive outcome. Finally, in the Spencer procedure greater posterior resection of the hippocampus is permitted via an en bloc anterolateral resection 4.5 cm from the temporal tip, sparing the lateral temporal neocortex (Spender et al., 1984). Although randomized controlled trial data comparing these surgical approaches is lacking, there is a meta-analysis of 1200 mesial TLE patients treated in a non-randomized fashion with either ATL or SAH revealing an 8% higher rate of seizure freedom amongst those who underwent an ATL (Josephson et al., 2013). Notably, in this study robust comparison of neuropsychological outcomes was not feasible because of heterogeneity.

As the postoperative surveillance period is lengthened, rates of seizure freedom after TLE surgery decline to 47% at 5-years postoperatively and to 41% at 10 years (McIntosh et al., 2004; Paglioli et al., 2004). Similarly, in another prospective series with long-term postoperative follow-up of 615 patients (of whom 497 underwent ATL), rates of freedom from disabling seizures decayed to

52% at 5 years after surgery, 47% at 10 years and only 37% at 10 years (de Tisi et al., 2011). It remains difficult to predict which patients will experience durable seizure freedom following TLE surgery such that only 28% of patients will have stopped AED by ten years after surgery (de Tisi et al., 2011). Although certain factors—such as identifying a lesion on preoperative MRI, the absence of simple partial seizure within 2 years following surgery, or complete mesial resection on postoperative MRI—may portend better long-term rates of seizure freedom, none of these are particularly useful at the individual patient level (de Tisi et al., 2011; Stefan et al., 2009).

#### **1.4.4 Role of Imaging in TLE**

##### **1.4.4.1 *Qualitative structural brain imaging in TLE***

While MRI is central to epilepsy evaluation in terms of lesion detection and characterization, it is also critical in surgical cases to define planned resection areas and to plan invasive recordings (Malmgren and Thom, 2012). The diagnostic yield of MRI in patients with DRE ranges from 50-80% based on technical factors (e.g., sequence selection and orientation of acquisition; field strength; receiver coil characteristics), patient factors (e.g., motion artifact) and assessor factors (e.g., epilepsy radiologist versus general non-cranial radiologist) (von Oertzen et al., 2002). On the basis of MRI findings, TLE can be classified as mesial TLE with HS, lesional TLE (temporal lesions other than HS or HS associated with additional lesions) or non-lesional (MRI-negative) TLE. Lesional

TLE may include either solitary temporal lesions other than HS or HS associated with additional temporal or extratemporal lesions—termed dual pathology—such as FCD or low-grade tumors, which occur in up to 35% of TLE cases (Ingmar Blümcke, 2009). Overall, however, the most common neuropathological finding in surgical epilepsy series in adults is HS (Ingmar Blümcke, 2009). Qualitative visually-detectable abnormalities of HS seen on high quality clinical MRI include increased hippocampal signal on T2-weighted or FLAIR images (in 80 – 85%), hippocampal volume loss (in 90 – 95%), decreased signal intensity on T1-weighted images (in 10 – 95%), and loss of normal hippocampal architecture (60 – 95%) (Berkovic et al., 1991; Jackson et al., 1993, 1990; Kuzniecky et al., 1987; Woermann et al., 1998). Based on these findings, experienced neuroradiologists will identify HS in 80 – 90% of histologically confirmed cases, although quantitative adjuncts such as hippocampal volumetry, morphometry or T2-Relaxometry increase this sensitivity to 90-95% (Bronen et al., 1997; Jack et al., 1990; Jackson et al., 1993; Koepp & Woermann, 2005; Woermann et al., 1998). The preoperative identification of HS is one of the most important predictors of postoperative seizure freedom in many surgical series (Arruda et al., 1996; Berkovic et al., 1995; McIntosh et al., 2001, 2004; Spencer et al., 2005; Spencer and Huh, 2008).

However, in many cases the epileptogenic zone, as approximated by surrogate markers including the epileptogenic lesion and symptomatogenic zone, may extend beyond the mesial temporal lobe or even extratemporally (Bartolomei et al., 2008; Berkovic et al., 1995; Kahane and Bartolomei, 2010;

Ozkara and Aronica, 2012; Wieser, 2004). Structural and functional abnormalities in TLE, therefore, are best conceptualized to fall along a spectrum ranging from focal-mesial temporal lobe subtype to a network extending beyond the temporal lobe (so-called temporal plus subtype) (Kahane and Bartolomei, 2010). Mounting evidence indicates that the spatial extent of the TLE epileptogenic network relates to the duration of a patient's epilepsy, implying that the disease is progressive and that early, successful resective surgery may halt this process (Bartolomei et al., 2008).

#### **1.4.4.2      *Quantitative structural brain imaging in TLE***

Advanced imaging techniques and a variety of post-processing tools have not only improved the sensitivity of MRI-based diagnosis of epileptogenic lesions but have also revealed further evidence of brain-wide structural abnormalities, in TLE, that may extend beyond the hippocampus and temporal lobe—extending even into the contralateral hemisphere. Quantitative MRI analysis tools, including hippocampal volumetry, T2-relaxometry, magnetic resonance spectroscopy (MRS), DTI, and VBM may improve preoperative identification of epileptogenic lesions as well as of diffuse structural abnormalities in TLE.

##### **1.4.4.2.1      *Volumetry***

Hippocampal volumetry (as used in chapters 3 and 4) is a quantitative technique wherein hippocampal tissue is segmented or traced on contiguous T1-

weighted MR images acquired perpendicular to the long axis of the hippocampus or along the AC-PC line (Cendes et al., 1993a; Cook et al., 1992; Jack et al., 1990b; Watson et al., 1997). The basic principles of manual volumetry are covered in detail above, in section 1.2.2.3.1. Reduced MRI hippocampal volumes have been demonstrated to correlate with reduced subfield pyramidal cell density (Bronen et al., 1989, 1991; Lencz et al., 1992). Hippocampal volumetry is performed in either an automated (computed software-based algorithm) or a manual fashion by a trained observer. Manual hippocampal volumetry is more sensitive than automated methods, but it is much more time consuming and requires an expert tracer given the complex anatomy involved (Pardoe et al., 2011). Considerable variability in manual hippocampal volumetry protocol exists resulting in poor inter-observer agreement between protocols (Frisoni et al., 2014) although there is relatively high agreement between rates when using the same protocol (Malykhin et al., 2007).

Manual hippocampal volumetry has been consistently demonstrated to be superior to visual identification of the qualitative abnormalities associated with HS (Cendes et al., 1993a; Coan et al., 2014; Coan and Kobayashi, 2004; Jack et al., 1990b), particularly in cases of bilateral HS, mild unilateral disease, or in cases where no detectable atrophy is apparent (Jackson et al., 1994). A direct comparison of hippocampal volumetry to visual analysis showed only slightly superior sensitivity (76% versus 71%, respectively) for pathological HS (Jack et al., 1990b); however, there was a significant relationship between volume loss of the operated hippocampus and postoperative seizure freedom (Jack et al., 1992).

In blinded manual volumetry for TLE, the superiority of manual hippocampal volumetry to visual assessment was even clearer (sensitivity 92% versus 56%, respectively) (Cendes et al., 1993b). In a recent assessment of 203 patients clinically diagnosed with mesial TLE and having undergone 3-Tesla MRI scanning, visual analysis identified 125 (62%) as having radiographic signs of HS. The automated FreeSurfer hippocampal volumetry agreed in 95% of the cases; however, it mistakenly identified an additional 10 (13%) as having HS when in fact they were visually judged to be normal (Coan et al., 2014). When combined with T2-relaxometry analysis, automated analysis resulted in an increase in detection of HS by 28%, which was corroborated by histopathological analysis in all but one of the patients who went on to have TLE resective surgery.

Volumetric abnormalities in mesial TLE are not limited to the mesial temporal structures ipsilateral to the seizure focus. The concept of TLE as a brain-wide disease emerged in Margerison and Corsellis's neuropathological autopsy study (1966) in which they systematically examined and identified abnormalities in extrahippocampal structures such as the thalamus, cerebellum, and cerebral cortex in patients with TLE (Margerison and Corsellis, 1966). Subsequent analysis of structural MRI data using automated techniques (introduced above, section 1.2.2.3.2) have largely supported this idea. Volume loss in patients with mesial TLE is consistently reported to be most severe in the ipsilateral (adjacent) extrahippocampal structures including the amygdala, temporopolar, parahippocampal, and lateral temporal cortices (Bernasconi,

2003; Bernasconi et al., 2004, 2003; Bernhardt et al., 2010; Cendes et al., 1993a; Kalviainen et al., 1997; Keller and Roberts, 2008; Lee et al., 1998; Salmenperä et al., 2001; Sankar et al., 2008)(Figure 1.19). Left-sided TLE with HS typically has a more pronounced, bilateral pattern of atrophy as well as more severe neuropsychological deficits compared to right-sided TLE (Ahmadi et al., 2009; Bernhardt et al., 2008; Bonilha et al., 2007, 2004b; S S Keller et al., 2002; S. S. Keller et al., 2012; Simon S. Keller et al., 2002; Keller and Roberts, 2008; Kemmotsu et al., 2011; Riederer et al., 2008). Entorhinal cortex atrophy often accompanies mesial TLE—with or without HS—correctly lateralizing the seizure focus in cases of mesial TLE without HS in 64% of cases and being largely absent in cases of extratemporal epilepsy (Bernasconi et al., 2003, 2001). Mesial TLE is consistently accompanied by lateral temporal and frontal lobe decreases in cortical thickness irrespective of the presence of HS; however, mesiotemporal volume loss is considerably more severe amongst patients with HS (Bernhardt et al., 2010).

Contralateral atrophy has also been demonstrated in unilateral HS (Figure 1.19) involving the contralateral temporal pole, hippocampus, and PHG as well as global temporal atrophy (Araújo et al., 2006; Lee et al., 1998). However, hippocampal atrophy contralateral to the epileptogenic focus may be less common than once thought, as a recent review of VBM analyses found it to be present in only 17% of reports (Keller and Roberts, 2008). This may, in part, be due to some studies including and analysing patients with both left and right HS together. For instance, Bernasconi and colleagues found that bilateral

hippocampal head and entorhinal cortex atrophy was present only in left-sided mesial TLE (Bernasconi, 2003; Bernasconi et al., 2003). In addition, areas of bilateral extratemporal GM loss in mesial TLE include frontal and prefrontal cortices (DeCarli et al., 1998; Keller et al., 2009) and the cerebellum (Lawson et al., 2000; Sandok et al., 2000). Atrophy is worse ipsilateral to the epileptogenic area and is usually more diffuse in left-sided mesial TLE. Bilateral atrophy in the dorsal prefrontal cortex in these cases correlates with impaired performance on tests of executive function (Keller et al., 2009; S S Keller et al., 2002; Simon S. Keller et al., 2002; Keller and Roberts, 2008).

These diffuse cortical changes are accompanied by bilateral subcortical atrophy of the thalamus, globus pallidus, and mammillary bodies (Figure 1.19)(Alex et al., 1995; G Gong et al., 2008; Keller and Roberts, 2008; Kim et al., 1995; Nagasaka et al., 2002; Natsume et al., 2003; Scanlon et al., 2013). Thalamic atrophy is most pronounced ipsilateral to the epileptogenic focus and correlates with the duration of epilepsy (G Gong et al., 2008; Nagasaka et al., 2002; Natsume et al., 2003; Scanlon et al., 2013). Similar to findings in entorhinal cortex, thalamic atrophy may help with clinical lateralization of epilepsy by including patients with mesial TLE but normal hippocampal volumes (Bernasconi et al., 2001; Natsume et al., 2003).

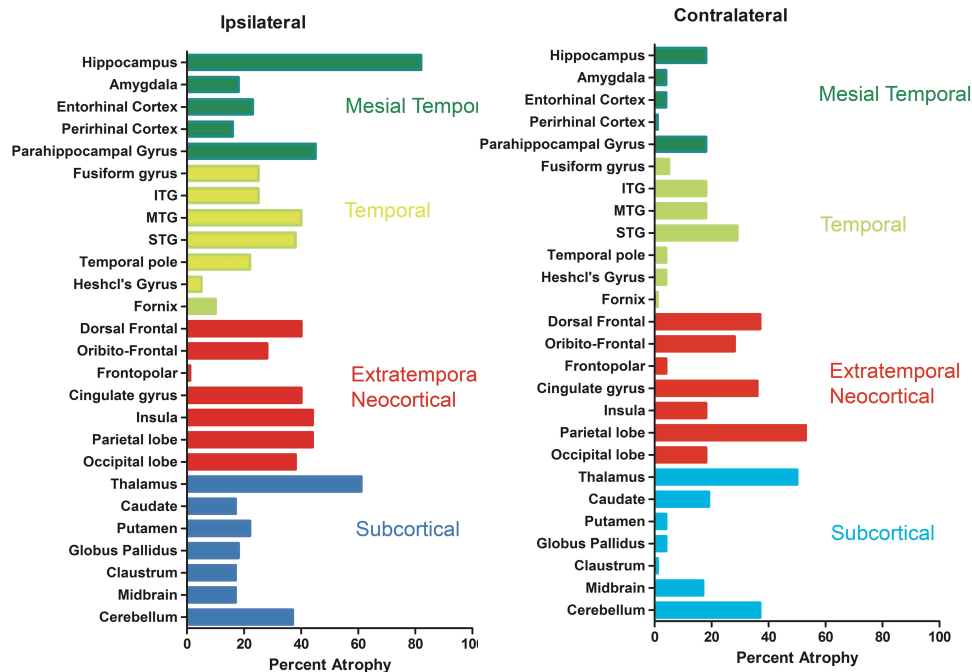


**Figure 1.19: Distribution of structural volume loss in TLE**

Brain regions in TLE patients found to have significantly reduced volume relative to healthy controls. Ipsilateral (left) and contralateral (right) are relative to the epileptogenic focus. Adapted with permission from Keller and Roberts, 2008.

There is mounting evidence that hippocampal, extrahippocampal temporal, and even extratemporal volume loss may represent an ongoing and progressive pattern of injury correlating significantly with duration and severity of seizures, further emphasizing the need for definitive surgical intervention in drug resistant TLE (Bernasconi et al., 2005; Caciagli et al., 2017). Moreover, the extent of preoperative temporal and extratemporal volume loss may relate to ongoing seizures following TLE surgery. For example, in a VBM analysis of preoperative imaging in patients who underwent TLE surgery, those with refractory post-operative seizures were found to have more pronounced and widespread gray matter atrophy in the temporal and extratemporal regions,

bilaterally (Keller et al., 2007). In a similar study following TLE surgery, Yasuda et al. found the surgical failure group to have significantly more preoperative gray matter atrophy in bilateral temporal lobes as well as extratemporal atrophy in the thalamus, caudate, and insula; and in frontal, occipital, and parietal lobes (Yasuda et al., 2010). Although atrophy was more extensive in the temporal lobe ipsilateral to the epileptogenic focus, the finding of extratemporal as well as bilateral areas of gray matter atrophy was thought to be at least partially responsible for continued epileptogenesis. Preoperative contralateral entorhinal cortical atrophy (Bernhardt et al., 2013) as well as ipsilateral posterior medial temporal and contralateral medial temporal atrophy (Keller et al., 2007) in patients with mesial TLE have also been identified to correlate with worse post-surgical epilepsy outcomes. Other studies, however, find no relation between preoperative extrahippocampal (Urbach et al., 2005) or extratemporal (Gross et al., 2006) atrophy and worse surgical outcomes. Thus it remains unclear whether these extratemporal or contralateral hippocampal abnormalities are predictive of refractory seizures following temporal resection or are simply collateral damage (Arfanakis et al., 2002; Cendes et al., 1997; Gross et al., 2006; Seidenberg et al., 2005).

#### *1.4.4.2.2 T2 Relaxometry*

MRI relaxometry is the measurement of relaxation times (T1, T2, T2\*) on appropriate MRI sequences. T2 relaxometry, specifically, is a quantitative technique whereby the signal intensity on T2-weighted images can be measured in an ROI (Berkovic et al., 1991; Jackson et al., 1993, 1990). T2 relaxometry may

improve detection of hippocampal abnormalities, including cases of mild unilateral HS, bilateral HS, mesial TLE but no hippocampal volume loss (Bernasconi et al., 2000; Sato et al., 2016), and neocortical abnormalities (Rugg-Gunn et al., 2005). For example, drug resistant TLE patients with HS will show marked increases (>10 ms) in hippocampal T2 relaxation times relative to healthy controls, ipsilateral to the seizure focus (Jackson et al., 1993; Namer et al., 1998; Van Paesschen et al., 2001; Woermann et al., 1998). T2-relaxometry may also be elevated (albeit to a lesser degree) and can assist in preoperative lateralization of the seizure focus amongst drug resistant TLE patients with normal MRI (i.e., no HS) (Bernasconi et al., 2000).

#### *1.4.4.2.3 Magnetic resonance spectroscopy*

MR spectroscopy allows in vivo measurement of the chemical composition of an ROI in terms of the presence and concentration of metabolites (Duncan, 1996). Proton MRS studies in TLE, for example, reveal reduction in the metabolite N-acetylaspartate (NAA) relative to creatine (Cr) in one or both temporal lobes, which is thought to relate to neuronal loss or mitochondrial injury (Cendes et al., 1997, 1994; Hugg et al., 1993). Although the current clinical utility of MRS in lateralization of TLE is limited, it may have potential as a biomarker that relates to multi-focal epileptogenesis in patients who fail to respond to resective surgery or as a marker of postoperative recovery of NAA level when seizures control is achieved with an ATL (Cendes et al., 2002, 1997; Hugg et al., 1996; Serles et al., 2001).

#### 1.4.4.2.4 *Diffusion tensor imaging*

DTI is a quantitative imaging technique that can mathematically model characteristics of diffusion in each voxel of diffusion data as a tensor and can provide information regarding tissue microarchitecture (Winston, 2012). The basic principles of diffusion MRI are discussed above (section 1.2.3). Although DTI analysis is most commonly used to provide information about white matter tract integrity, so too can it provide information about gray matter structures, such as the hippocampus (Fellgiebel et al., 2004; Förster et al., 2012; Hong et al., 2010; Müller et al., 2005; Ostojic et al., 2015; Pereira et al., 2014; Pfeuty et al., 2011; Sagi et al., 2012). To date, hippocampal DTI in TLE has been performed using an ROI type approach drawn on non-anatomical diffusion images (Assaf et al., 2003; Bernhardt et al., 2016; Ercan et al., 2016; Hugg et al., 1999; Pereira et al., 2006; Salmenpera et al., 2006). Characteristically, these reports find that hippocampal DTI in TLE is associated with elevated mean MD and reduced FA ipsilateral to the seizure focus and may assist in clinical disease lateralization in preoperative evaluation. The hippocampus contralateral to the seizure focus may have diffusion properties similar to healthy controls (Assaf et al., 2003; Düzel et al., 2004; Ercan et al., 2016; Hugg et al., 1999; Kantarci et al., 2002; U. C. Wieshmann et al., 1999), or it may be abnormal with isolated decrease in FA (Ercan et al., 2016; Kimiwada et al., 2006; Liacu et al., 2010) or MD (Londono et al., 2003; Thivard et al., 2005). However, hippocampal DTI measures provide microstructural data that is complementary to volumetry data without clear correlation between the degree of diffusion data abnormality (relative to healthy

controls) and either the severity of hippocampal atrophy (Düzel et al., 2004; Londono et al., 2003; U. Wieshmann et al., 1999) or duration of disease (Thivard et al., 2005). Diffusion abnormalities of the contralateral hippocampus may be partially reversible following TLE surgery (e.g., recovery of depressed hippocampal MD) which may correlate with postoperative improvement in some measures of verbal and non-verbal (i.e., hippocampally-mediated) memory (Pfeuty et al., 2011; Thivard et al., 2007, 2005).

The variability of hippocampal diffusion data in TLE may be, in part, a result of sampling errors when an ROI approach is applied on non-anatomical (i.e., poor spatial resolution) raw diffusion images to interrogate a variable portion of the hippocampus with variable placement along the anterior-posterior axis of the structure. Given the complexities of hippocampal anatomy, described above, inaccuracies of ROI placement may be a key source of sampling error. For example, Assaf et al. report a 4 x 8 mm ROI drawn on diffusion images amongst 12 non-lesional TLE patients while Hugg et al. elected to measure DTI on a single coronal slice which also included the amygdala (Assaf et al., 2003; Hugg et al., 1999). Moreover, hippocampal diffusion has been shown to vary significantly along the anterior-posterior axis (Elliott et al., 2018; Hong et al., 2010). In chapter 3 of this thesis, we present a means to measure hippocampal DTI using an ROI that encompasses the whole hippocampus created using manual hippocampal tracings, which mitigates some of these technical concerns.

DTI has also been used to demonstrate diffuse, brain-wide white matter abnormalities in TLE which vary slightly based on the presence or absence of HS and the side of the seizure focus. For example, patients with TLE and HS have been reported to have reduced FA in the fornix (bilaterally), cingulum, external capsule, corpus callosum, temporal lobe white matter, arcuate fasciculus, and uncinate fasciculus (Arfanakis et al., 2002; Concha et al., 2009, 2005a; Focke et al., 2008; Gross et al., 2006; Kim et al., 2008; Lin et al., 2008; Nilsson et al., 2008; Thivard et al., 2005). Notably, reported white matter tract abnormalities vary from study to study and amongst TLE patients without HS are generally reported to be less severe (Concha et al., 2009). The distribution and extent of white matter DTI abnormalities may also differ depending on the side of HS, with left-sided lesions typically associated with greater extrahippocampal and extratemporal abnormalities (Focke et al., 2008; S. Keller et al., 2012). Moreover, bilateral white matter changes in the temporal lobe white matter, thalamus, putamen, and corpus callosum are accompanied by corresponding reductions in volume (albeit only in patients with left-sided HS)(S. S. Keller et al., 2012).

## **1.5 Intraoperative DTI in Cranial Neurosurgery**

### **1.5.1 Introduction**

The concept of maximal safe surgical removal underlies the neurosurgical treatment for a wide variety of cranial pathologies originating from within the brain itself (so-called intraaxial lesions). This requires a delicate balance between

removing the greatest amount of target tissue possible while minimizing damage to adjacent functional tissue. Clinical assessment of the former—also called extent of resection (EOR)—may be defined radiographically (e.g., T1- or T2- abnormality in the case of low-grade gliomas, LGG) or conceptually (e.g., epileptogenic zone in the case of DRE). In many cases, achieving a gross total resection (GTR) does not necessarily imply that the pathological tissue is completely removed; for example, in high-grade glioma (HGG), tumour cells are known to invade well beyond the borders of the lesion on imaging, or in FCD, neuronal migrational abnormalities may extend broadly. Interestingly, the concept of minimizing damage to perilesional functional brain tissue depends largely on how one defines “functional brain”. One possible way to define functional brain tissue would be based on the extent of clear radiographic abnormality such that all normal appearing perilesional tissue would be presumed to be functional and endeavored to be preserved. Alternatively, one might define functional brain as “eloquent cortex,” or tissue which has a “readily identifiable neurological function and, if injured, [may] result in a disabling neurological deficit.” (p. 477.) (Spetzler and Martin, 1986)

Intraoperatively, functional brain tissue can be assessed using direct electrical stimulation (DES) either to produce a stereotypical motor response or to interrupt the conscious performance of a higher-order task during awake craniotomy. In the former, the DES current required to elicit a motor evoked potential (MEP) recorded from an intramuscular electrode can be used as a surrogate marker of proximity to primary motor cortices or corticospinal tract

(CSpT). In the latter, DES-related interruption of language tasks such as naming pictures of common objects or spontaneous speech can provide information regarding the proximity of the stimulation site to cortical or subcortical structures involved in these tasks. Electrophysiological monitoring, although it is the gold standard for defining and preserving eloquent tissue, is not without limitations and cannot be applied universally. For example, while electrophysiological monitoring of motor or sensory systems is possible under general anesthesia, it requires expert neurophysiological interpretation and can be limited by stimulation-provoked seizures. By contrast, electrophysiological monitoring of language-related tasks is considerably more complex to interpret and requires the patient to be awake during surgery such that various components of language (e.g., productive speech or naming) can be assessed often using the intraoperative presentation of visual stimuli. However, there are several potential patient factors, such as claustrophobia, pediatric or geriatric patients, intraoperative patient fatigue, sensory limitations (e.g., poor hearing), low pain tolerance, the presence of lesion-related symptoms such as altered level of consciousness or preexisting motor impairment, and medical factors, such as anesthesia concerns that limit the broad application of this technique. Moreover, electrophysiological monitoring paradigms are not described for all eloquent regions of the brain, and institutional experience is highly variable. Preoperative localization of perilesional areas of functional importance is also possible using MRI techniques such as DTI (see section 1.2.3) to create white matter tract reconstructions or functional MRI (fMRI) statistical maps of brain function

secondary to increases in regional blood flow. Regardless of how surgical targets or functional limits are defined, the more formidable challenge is to translate these definitions into the intraoperative environment.

### **1.5.2 Neuronavigation**

Modern cranial neurosurgical intraoperative identification of target and non-target tissue relies heavily on frameless stereotaxy or “neuronavigation,” which allows the real-time visualization of the tip of a pointer or navigated instrument on a reference cross-sectional imaging data set (most commonly an MRI dataset)(Roberts et al., 1986). Stereotaxy (from the Greek word *stereo* meaning “solid” (thus three dimensional) and *taxis* meaning “touch”) is the concept that relates any intracerebral point to signed distances from three mutually orthogonal planes (Cartesian coordinate system) when touched by an intracranial probe contacting a rigid extracranial frame mounted to the calvarium (Gildenberg, 1997). In the most commonly used form of neuronavigation, called optical neuronavigation, a cranial surface (‘skin’) model generated from a preoperative T1-weighted image is registered in three-dimensional space to the unique contours of sincipital and nasal anatomy or to the unique position of fiducial skin references (placed prior to preoperative scan) traced or touched by a navigational probe with known tip geometry relative to four infrared-reflective spheres (Figure 1.20). Thereafter, once the relationship between craniofacial contours and the model of these contours is

established and because the calvarium is rigidly affixed to the surgical table using a skull clamp, to which in turn a navigation reference arm is attached, the reference arm when visualized will have a known localization in this registered space as the arm itself is tracked by four additional reflective spheres. In other words, patient space is linked to image space through the process of registration, whereby the rigid geometrical transformation that is required to achieve this link is determined (Fitzpatrick, 2010; Mert et al., 2013). Accuracy of such neuronavigational systems has been shown to range from 0.9 to 3.2 millimeters when compared intraoperatively to anatomical landmarks (Mascott, 2005; Wolfsberger et al., 2002).

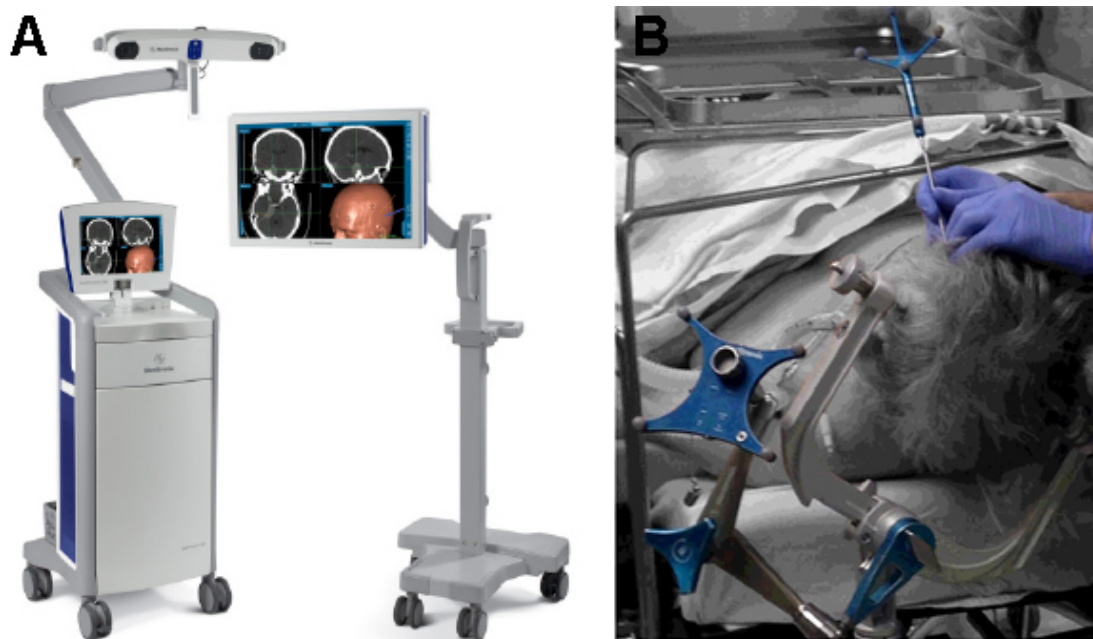


**Figure 1.20: Neuronavigation components**

(A) Medtronic neuronavigational components including base station (far left) with infrared emitter and detector “eyes”, and surgeon’s monitor (larger screen, right). (B) Navigational reference arm affixed to Mayfield cranial fixation device topped with four reflective spheres and navigational probe (held in gloved hand) with known geometry and localized in navigational reference space with four additional reflective spheres. Panel A adapted with permission from Springer:

The history, current status, and future of StealthStation treatment guidance system by R. Bucholz and L McDermont (2009)(Bucholz and McDermont, 2009). Panel B adapted with permission from Elsevier: Brain shift in neuronavigation of brain tumors: a review by Gerald, IJ et al., 2017(Gerard et al., 2017).

Once registration is established, neuronavigation provides real time spatial location of the navigational probe or any navigated instrument such as a suction catheter or ultrasonic aspirator relative to the navigation reference arm-skull clamp-patient head construct, and relative to intracranial target tissue superimposed on anatomical MRI images (Figure 1.21). Neuronavigation use in clinical neurosurgery is commonplace, particularly so for intraaxial lesions, and is used at all stages of the operation including preoperative planning (i.e., skin incision, determining craniotomy location and size) as well as iteratively during the operation itself (i.e., prior to opening dura or performing corticectomy, and during and after target lesion removal). In circumstances where the target tissue is difficult to distinguish from non-target tissue intraoperatively by texture or appearance—as may commonly be the case in MRI-negative resections for DRE or in some diffusely infiltrating, low grade gliomas—neuronavigation also helps to define the limits of resection. In many cases, input data from different MRI sequences or even imaging modalities may be combined (or “merged”) in neuronavigational systems in reference space (commonly defined with a T1-weighted MRI). For example, in a calcified LGG, the reference exam might be a T1-weighted image with both brain and forehead/nasal coverage merged with a T2-weighted image to better define the intended EOR.

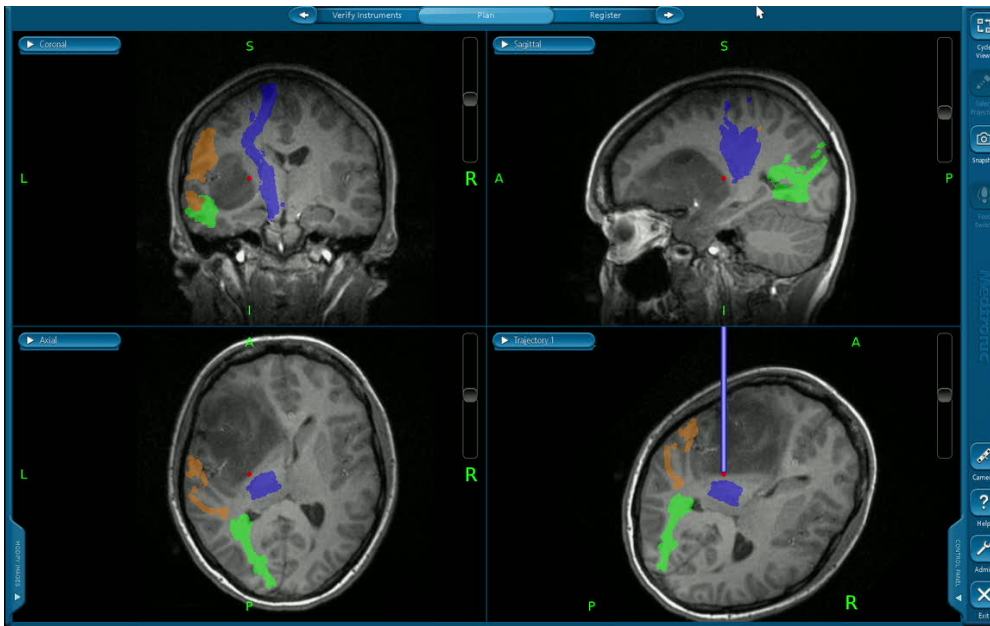


**Figure 1.21: Neuronavigational surgical display**

Surgeon's neuronavigational monitor displaying the position of probe (purple wand, bottom right panel) and tip (red dot, posteromedial to lesion on axial slice, bottom left panel) superimposed on non-enhancing left frontotemporal glioma (T1-weighted image) and transiting tracts (corticospinal, blue; inferior frontooccipital fasciculus, green; superior longitudinal fasciculus, orange). Images generated with i7 StealthStation manufactured by Medtronic and used with permission.

### 1.5.3 DTI in neurosurgery: preoperative mapping

A wide variety of other spatial data may be integrated into neuronavigational systems following registration to anatomical reference space, including cortical surface maps, vessel reconstructions, DTI-based tract models, fMRI-based statistical maps, or perfusion weighted images (Mert et al., 2013; Salama et al., 2017). In current neurosurgical practice, white matter reconstructions are commonly obtained using deterministic FACT methods, user selected ROIs and the diffusion tensor model (introduced above, section 1.2.3) on

preoperatively acquired diffusion data. Fiber reconstructions or DEC maps may either be interpreted offline or following merging into anatomical reference space—a practice first described in 2001 (Coenen et al., 2001)—providing a glimpse into true white matter tract morphology, which is not readily apparent on standard anatomical MR images. DTI-based tract reconstructions may help confirm the location of tracts relative to target tissue or suspected anatomical structures (e.g., central sulcus), may inform preoperative risk stratification and patient counseling, and may guide intraoperative direct electrophysiological mapping (Hendler et al., 2003; Mori et al., 2002). The anatomic accuracy of DTI tractography-based track reconstructions can be indexed, in the case of the CSpT, by relating the required current (in milliamperes, mA) applied via direct cortical or subcortical stimulation to elicit a stereotyped peripheral motor response (Kamada et al., 2007, 2005; Zhu et al., 2012). For example, Zhu et al., 2012, interrogated the accuracy of CSpT tractography using DES, identifying a significantly greater distance to modelled tract location for subcortical stimulation sites that did not elicit a motor response (negative sites) versus those that did (positive sites;  $12.4 \pm 2.9$  versus  $5.2 \pm 2.2$ , mean  $\pm$  SD, respectively). Moreover, the concordance between DTI corticospinal models and stimulation sites was high with reported sensitivity of 92.6% and specificity of 93.2% (Zhu et al., 2012). Bello et al. (2008) identified a similarly high correspondence between DTI-tractography (not limited to the CSpT obtained at 3-Tesla) and DES sites with reported sensitivities for CSpT of 95% and for language tracts of 97% (Bello et al., 2008).

The utility of DTI-tractography was formally evaluated in a randomized-controlled trial by Wu et al., (2007) for patients with cerebral gliomas who underwent microsurgical resection using neuronavigation either with merging of DTI-based CSpT reconstructions (n = 118) or without (n = 120). Interestingly, although no difference in EOR was identified overall (or when stratified by LGG and HGG), DTI-based neuronavigation was found to significantly reduce the occurrence of postoperative motor deficits, to improve the 6-month Karnofsky Performance Scale as well as to increase the overall survival of HGG patients (Wu et al., 2007). By contrast, other large (n = 190) non-randomized series have demonstrated significant improvements in EOR in LGG in favor of DTI when combined with overlay of functional MRI and intraoperative stimulation versus intraoperative-stimulation resections alone (EOR 90% versus 77%, respectively) (Ius et al., 2012).

#### **1.5.4 Surgically-induced brain deformation**

A major problem with neuronavigational data based on preoperatively acquired images is that the correspondence between intracranial and extracranial anatomy (the latter, of course, upon which neuronavigational registration is established) deteriorates once the skull is opened due to surgically-induced brain deformation (“brain shift”), which may significantly decrease navigational accuracy. Although brain shift has long been appreciated in intraaxial cranial neurosurgery (Dorward et al., 1998; Nauta and Bonnen,

1998), it was not objectively quantified until widespread adoption of neuronavigation (Nabavi et al., 2001). It was not until the advent of intraoperative MRI—initially as low-field (<0.5-Tesla) (Black et al., 1997) and subsequently as high-field systems (1.5-Tesla or greater)(Sutherland et al., 1999)—which allowed intraoperative anatomical MRI with sufficient soft tissue detail to be acquired that the complexity and extent of brain shift was fully realized (Dorward et al., 1998; Hartkens et al., 2003; Hill et al., 1998; Jacobsohn and Roberts, 1999; Maurer et al., 1998; Nabavi et al., 2001). Initial neuronavigational studies identified inward shift (“sinking”) in glioma patients undergoing resection with more than one-third having marked shifts of greater than 1 cm (Dorward et al., 1998; Hill et al., 1998). By contrast, subsequent iMRI-based studies where patients were scanned at a variety of stages during surgery—for example (as categorized by Nabavi et al., (2001)), immediately after dural opening, after resection, and finally after dural closure but prior to closure of skull cap and skin—revealed a more complicated picture of brain shift as a continuous, unpredictable, bidirectional process that occurs diffusely throughout the entire brain (Maesawa et al., 2010; Nabavi et al., 2001; C Nimsky et al., 2005a).

It is relevant to note that a variety of other non-iMRI-based methods have also been applied to compensate for brain shift including intraoperative ultrasound (Reid, 1978), computed tomography (Shalit et al., 1979), or optical brain surface scanning (Roberts et al., 1999). These so-called sparse-data

solutions, which have inherent limitations in surgical field coverage, resolution, and soft tissue contrast, are beyond the scope of this thesis.

### **1.5.5 Current utility of intraoperative MRI**

Intraoperative MRI (iMRI) neurosurgical theatres allow acquisition of updated anatomical MR images which when merged with neuronavigational reference images account for brain shift by updating the intraoperative position of target tissue relative to adjacent non-target tissue. Although several configurations exist, high-field applications (e.g., IMRIS 3-Tesla iMRI surgical suite similar to the Dan and Bunny Widney 3-Tesla Intraoperative Surgical Suite at the University of Alberta Hospital, Figure 1.11) seamlessly move the magnet in and out of the operating theatre on ceiling-mounted rails to mate with a specifically designed surgical table and head clamp to scan the patient in surgical position while covered by a sterile drape (Sutherland et al., 1999).

Overall iMRI has been found to enhance EOR in enhancing (Hatiboglu et al., 2009; Napolitano et al., 2014; Senft et al., 2011) and non-enhancing gliomas (Coburger et al., 2016; Mohammadi et al., 2014; Wu et al., 2014), pituitary/skull base lesions (Coburger et al., 2014; Sylvester et al., 2015), pediatric lesions (Choudhri et al., 2014b; Shah et al., 2012) and DRE (Nowell et al., 2017). For example, Senft et al. (2001) studied iMRI utility in contrast enhancing gliomas, identifying a significant increase in EOR of contrast enhancing tumor tissue among patients randomized to the iMRI group versus conventional microsurgery

(96% vs 68%, respectively), which was associated with a significantly longer progression-free survival (226 days versus 98 days). More recently, in a triple-blinded study including patients with both LGG and HGG, Wu et al. (2014) postponed patient randomization until after the treating surgeon was satisfied with the EOR (using conventional tools alone), at which point patients who were randomized to further iMRI-interrogation were scanned and reoperated if residual target tissue was identified and felt to be resectable. In patients with HGG, randomization to the iMRI group led to further resective efforts in 8/22 (36%) but did not result in a group-wide difference compared to the non-iMRI group in terms of the rate of GTR (91% versus 73%, respectively). By contrast, in patients with LGG, randomization to the iMRI group led to further resective efforts in 9/22 (41%), which did increase the rate of GTR compared to the non-iMRI group (82% versus 43%, respectively).

### **1.5.6 Intraoperative DTI in cranial neurosurgery**

Given the benefit of DTI and iMRI in achieving more complete intraaxial resections, and faced with the complex and unpredictable nature of brain shift, a logical next step would be to extend iMRI acquisitions to include DTI (hereafter iDTI). A major technological barrier which currently limits iDTI acquisition, particularly in 3-Tesla iMRI units, is the image degradation encountered due to susceptibility artifact (Potgieser et al., 2014). For example, current iDTI acquisition strategies at high-field employing standard single-shot echo-planar

imaging are rendered unusable for DTI-tractography due to susceptibility artifact in 36% of cases (Ostrý et al., 2013). Moreover, in most published iDTI reports tract reconstructions are largely limited to the CSpT. Susceptibility artifact describes image degradation because of spatial mismapping of the MR signal and signal loss occurring as the result of local inhomogeneities in the static magnetic field caused by diamagnetic, paramagnetic or ferromagnetic materials which accelerate spin dephasing (Elster, 2015). Susceptibility artifact is particularly problematic at tissue boundaries such as air-tissue interfaces which occur at baseline (prior to any surgical intervention) in the orbitofrontal cortex and anterior temporal poles due to proximity to the frontal and paranasal air sinuses. This spatial distortion of the MR signal can significantly impact tract reconstructions such that modeled tracts terminate in different sulci entirely (Jones and Cercignani, 2010). For example, Treiber et al. recently identified preoperative spatial distortions due to susceptibility artifact in 250 patients with brain tumours which produced spatial inaccuracies ranging from 1.2 – 5.9 mm (median 2.1mm) (Treiber et al., 2016). The impact of such artifact within the iMRI environment as well as when collecting DTI data while the cranium is open is less clear.

Ostry et al. (2013) investigated single-shot echo-planar iDTI (SS-DTI) in a 3-Tesla iMRI suite in 25 patients with supratentorial intraaxial lesions adjacent to the CSpT (Ostrý et al., 2013). They interrogated CSpT reconstructions based on pre- and post-iMRI DTI data using monopolar subcortical DES for motor mapping by recording the minimal current required to provoke an MEP and

relating this to the measured distance from this stimulation site to the tract position. Significant current-distance correlations were identified for both pre-iMRI ( $R = 0.47$ ,  $p < 0.001$ ) and post-iMRI ( $R = 0.34$ ,  $p < 0.001$ ). However, 9 of 25 (36%) iDTI scans were rated as unusable for tractography due to poor SNR and image distortion. Moreover, in this work quantitative analyses regarding tract shift are not provided. By contrast, image degradation due to susceptibility artifact has not been reported as a significant problem for iDTI at lower field (0.3 – 1.5T), although tractographic analyses in these studies have largely been limited to the CSpT (Maesawa et al., 2010; Christopher Nimsky et al., 2005; Ozawa et al., 2009; Prabhu et al., 2011; Romano et al., 2011; Shahar et al., 2014). For example, Nimsky et al. (2005) first described intraoperative DTI acquisition using single-shot echo-planar imaging at 1.5-Tesla during supratentorial glioma resection in 37 patients (mostly with HGG) and without the use of DES (Nimsky et al., 2005). Using registered colour FA maps in neuronavigation, they reported unpredictable and bidirectional shift white matter with maximal shift relative to preoperative location ranging from -8 to 15 mm (negative indicating inward shift), although mean tract shift was found to be  $2.7 \pm 6$  mm (Nimsky et al., 2005). More recently, Maesawa et al., performing iDTI at 1.5-Tesla in 28 patients with pericentral gliomas, described a marked intraoperative CSpT shift ranging from -23 to +12 mm (Maesawa et al., 2010). In contrast to the findings of Ostry (2013), Maesawa et al. reported a significant correlation between the distance from stimulation sites to the modeled intraoperative tract position and subcortical DES intensity ( $R = 0.757$ ,  $p < 0.01$ ), which was not found when using

CSpT reconstructions obtained from preoperatively acquired data ( $R = 0.154$ ) (Maesawa et al., 2010). Subsequent work by Prabhu et al. (2011) confirmed the finding of a significant correlation between tumor-to-CSpT distance and subcortical direct electrical stimulus intensity for intraoperative DTI but not preoperative DTI (Prabhu et al., 2011). They identified similar tumor-to-CSpT differences in comparing pre- to intra-operative DTI with a mean of  $5.4 \pm 5.4$  mm (range 0 – 18 mm). Shahar et al. identified mean intraoperative tumor-to-CSpT shift of  $2.95 \pm 4.18$  mm (range -8.8 to 19.2 mm); however, they found it to be significantly greater in enhancing gliomas (mean tract shift  $3.93 \pm 3.64$  mm) versus non-enhancing gliomas (mean tract shift  $0.18 \pm 0.18$  mm;  $p < 0.001$ ) (Shahar et al., 2014). Other iDTI studies have reported other factors to be important predictors of subcortical shift, including the presence of peritumoral vasogenic edema or craniotomy size (Romano et al., 2011) or entry into the ventricular system during surgery (Nimsky et al., 2000).

### **1.5.7 Readout-segmented iDTI in 3-Tesla iMRI**

Intraoperative 3-Tesla MRI generally provides superior image quality with higher SNR and more rapid acquisition and permits higher resolution imaging compared to lower field (0.3 – 1.5-Tesla) iMRI systems (Ginat et al., 2014; Jissendi et al., 2008; Vargas et al., 2009). However, these advantages may be offset by image degradation due to artifacts which are more pronounced at higher field strength, especially susceptibility artifact. Image degradation due to

susceptibility artifact is particularly problematic for sequences such as conventional DTI employing a single-shot echo-planar imaging (SS-DTI)(Elster, 2015; Vargas et al., 2009) and currently presents a technical limitation for open cranial, 3-Tesla iDTI as discussed above (section 1.5.6). In SS-DTI, data from an entire slice is rapidly acquired in a ‘single-shot’ (TR, approximately 100ms) following a 90° RF and 180° refocusing pulse by applying an oscillating readout gradient along the frequency-encode axis (x-axis) accompanied by a brief orthogonal phase-encoding gradient (y-axis) filling k-space line by line (Cohen-Adad, 2012). Although this method allows fast whole brain DTI, minimizing motion-related artifact, it results in geometric distortions owing to susceptibility artifact. This geometric distortion is more pronounced at tissue boundaries (e.g., air-tissue, calvaria-muscle) where differences in susceptibility result in local  $B_0$ -inhomogeneities that cause accelerated spin dephasing and the accumulation of phase-encoding errors in the phase-encode direction (Cohen-Adad, 2012; Elster, 2015). In addition, the prolonged TE of SS-DTI results in  $T_2^*$ -blurring (compounded in areas of local  $B_0$ -inhomogeneity) and decreased signal amplitude in white matter which has  $T_2$  of approximately 70 ms at 3-Tesla (Cohen-Adad, 2012; Porter and Heidemann, 2009).

These SS-DTI problems can be mitigated by minimizing sampling time either by decreasing echo spacing, increasing receiver bandwidth or using parallel imaging techniques (Porter and Heidemann, 2009). Alternatively, in so-called Readout-Segmented DTI (RS-DTI), sampling time can be abbreviated at the cost of longer imaging time by limiting the portion of k-space filled in the readout

direction (with full coverage in the phase encoding direction) for each of a number of shots which when combined provide complete slice coverage (Frost et al., 2012; Porter and Heidemann, 2009; Robson et al., 1997). Porter and Heidemann have described reduced image degradation due to susceptibility artifact with improved SNR and spatial resolution using RS-DTI compared with standard SS-DTI research high-field (3-Tesla) applications, commonly with 32 – 64 channel receive coils. However, the utility of RS-DTI for both preoperative and intraoperative DTI in the 3-Tesla iMRI setting is unknown; it is the focus of chapter 6 of this thesis.

# **CHAPTER 2: Aims and Hypotheses**

**Cameron A. Elliott**

## **2.1 General Aims**

The general aim of this thesis is to improve the clinical utility of MRI acquired in the perioperative period in neurosurgery. The original manuscripts which are presented in the following chapters are centered on the following three questions: (1) whether early-post injury DWI predicts long-term structural and functional consequences in pediatric TBI and suspected NAT; (2) whether immediate and longitudinally-acquired postoperative anatomical and diffusion MRI measures of the hippocampus and extrahippocampal limbic structures relate to, or predict, seizure outcome in TLE surgery; and (3) whether intraoperative readout-segmented DTI (RS-DTI) permits susceptibility-artifact resistant intraoperative DTI which can be employed during cranial intraaxial resections for the purposes of brain-shift resistant neuronavigation.

## **2.2 Specific studies within this thesis**

### **2.2.1 Study #1 (Chapter 3): Relationship between early diffusion restriction and delayed structural and clinical outcome in pediatric TBI**

**Rationale/Aim:** MRI with DWI sequences is the imaging modality of choice to identify the extent of cerebral injury in the acute evaluation of pediatric TBI thought to be secondary to NAT. This study aimed at identifying the association between areas of diffusion restriction identified on early clinical MRI scans and delayed follow-up structural MRI.

**Hypothesis:** Areas of restricted diffusion identified on early post-injury DWI will be associated with delayed T1-weighted MRI atrophy and functional deficits among patients with pediatric TBI suspected to be secondary to NAT.

### **2.2.2 Study #2 (Chapter 4): Postoperative longitudinal hippocampal structural changes following surgery for drug resistant TLE.**

**Rationale/Aim:** Resective surgery has been demonstrated to be an effective treatment for drug-resistant TLE. However, it remains difficult in these patients to predict long-term seizure freedom (i.e., durable surgical cure of epilepsy). The

structural consequences of TLE surgery as detected by longitudinal postoperative MRI and their potential relationship to relevant patient outcome variables such as postoperative seizure freedom or neuropsychological outcome are inadequately characterized. This study aimed at identifying the extent and time course of postoperative volumetric changes of the non-resected or contralateral hippocampus following resective surgery for drug resistant TLE.

**Hypothesis:** Longitudinal structural MRI will identify changes in the volume of the contralateral (i.e., not resected) hippocampus that are associated with eventual postoperative seizure and neuropsychological outcome following surgery for drug-resistant TLE.

### **2.2.3 Study #2 (Chapter 5): Postoperative longitudinal limbic micro- and macro-structural changes following surgery for drug resistant TLE**

**Rationale/Aim:** Resective surgery has been demonstrated to be an effective treatment for drug-resistant TLE. However, it remains difficult in these patients to predict long-term seizure freedom (i.e., durable surgical cure of epilepsy). This study aimed at characterizing the course of postoperative microstructural changes in the contralateral, non-resected hippocampus using longitudinal DTI, as well as extrahippocampal structural changes of the fornix and mammillary

bodies (i.e., key components of the limbic circuit). Structural changes were correlated with postoperative seizure and neuropsychological outcome.

**Hypothesis:** Longitudinal structural and diffusion metrics of the limbic system are associated with postoperative seizure and neuropsychological outcome following surgery for drug-resistant TLE. Longitudinal postoperative hippocampal diffusion metrics will provide insight as to potential mechanisms of observed postoperative hippocampal volume change.

#### **2.2.4 Study #3 (Chapter 6): Evaluation of readout-segmented DTI open cranium white matter reconstruction in cranial intraaxial resections**

**Rationale/Aim:** Intraoperative acquisition of DTI data in 3-Tesla intraoperative MRI installations for white matter tractography is currently limited by image degradation due to susceptibility artifact. A novel readout-segmented DTI (RS-DTI), REadout Segmentation Of Long Variable Echo trains (RESOLVE)(Frost et al., 2012; Porter and Heidemann, 2009), shows promise for minimizing susceptibility artifact and increasing SNR relative to standard single-shot DTI (SS-DTI); however, its utility has not yet been demonstrated in 3-Tesla iMRI. This study aimed to compare RS-DTI to SS-DTI for open cranium iMRI DTI acquisition to measure anatomical deviation relative to artifact-resistant T1-

weighted reference images, image contrast for delineation of gray-white junction and the feasibility of clinical deterministic tractographic analysis.

**Hypothesis:** RS-DTI will decrease susceptibility-artifact related anatomical distortion, improve gray-white junction delineation and facilitate white matter tract reconstructions relative to standard SS-DTI.

# **CHAPTER 3: Early diffusion restriction of white matter in infants with small subdural hematomas is associated with delayed atrophy**

**Cameron A. Elliott, Vijay Ramaswamy, Francois D Jacob, Tejas Sankar and Vivek Mehta**

This chapter has been published in part as:

Elliott CA, Ramaswamy V, Jacob FD, Sankar T and Mehta V. **Early diffusion restriction of white matter in infants with small subdural hematomas is associated with delayed atrophy.** *Childs Nerv Syst* 2017, 33: 289-295.

## **3.1 Introduction**

Traumatic Brain Injury (TBI) is a major cause of infant morbidity and mortality. In children less than two, evaluation of pediatric TBI should include consideration of NAT which is a common cause of brain injury leading to death or significant long-term disability (Duhaime et al., 1998, 1992). The most common cranial manifestations of NAT in infancy are subdural hematomas and retinal hemorrhages. Infants have poorer outcomes after TBI than older children and adults (Anderson et al., 2005, 2000), which may relate to a combination of: increased vulnerability of the developing brain to excitotoxic injury; immature physical structure of the brain, skull and neck musculature; synergistic impact of possible repeated injury; and cascading impact of early disruption of normal

developmental processes such as myelination and arborization (Anderson et al., 2005; Durkin et al., 1998; Jagannathan and Jagannathan, 2008; Moritani et al., 2005). The initial neuroimaging modality of choice in evaluating pediatric head trauma is CT which rapidly identifies intracranial hemorrhage, but has limited utility in identifying the extent and pattern of microstructural brain injury (Kemp et al., 2009). Characterizing the pattern of injury has value in prognostication of outcome and documentation of the extent of injury, and may eventually guide neuroprotective strategies (Bonnier et al., 2004, 2003). MRI, specifically DWI, is superior to CT in documenting the pattern of brain injury in children, especially in those with suspected NAT which is more commonly accompanied by diffuse hypoxia/ischemia (Barnes, 2011; Biousse et al., 2002; Duhaime et al., 1998; Ichord et al., 2007; Imagawa et al., 2014; Parizel et al., 2005; Vazquez et al., 2014). MRI may also be superior in demonstrating subtle intraparenchymal injury such as diffuse axonal injury, microhemorrhages and cortical injury (Parizel et al., 2005).

In this case series, we describe novel acute and chronic MRI findings in four infants with subdural hematomas secondary to suspected NAT. Specifically, these cases highlight that restricted diffusion of the white matter on early DWI obtained in the acute post-injury setting may be associated with long-term structural and functional consequences.

## **3.2 Methods**

The Institutional Review Board of the University of Alberta approved this retrospective review (Pro00066737).

## **3.3 Cases**

Relevant details for all cases are summarized in table 3.1; specific case descriptions are found in the text below.

### **3.3.1 Case 1:**

This patient was a 16-month-old male with mild language delay, who presented to the Emergency Department for irritability after he fell out of his toddler bed. There was no associated loss of consciousness and GCS on admission two hours post-injury was 14/15. His head circumference on admission was at the 98<sup>th</sup> percentile. A CT scan of the head revealed an acute left sided subdural hematoma and bilateral extra-axial fluid collections with associated midline shift (Figure 3.1, Patient 1, A). A repeat CT scan, 12 hours later, showed an increase in midline shift which prompted burrhole evacuation of the subdural collection and placement of a left subdural drain. On post-injury day 3 he had a cluster of focal seizures of the right arm and leg lasting 2 minutes each treated successfully with an intravenous dose of 20mg/kg of Phenobarbital. A daily prophylactic dose of Phenobarbital was then initiated. DWI MRI of the

brain 5 days post-injury showed restricted diffusion with corresponding reduction in ADC limited to the left hemisphere cerebral white matter (Figure 3.1, Patient 1, B-C). Time of flight MR angiography (MRA) and bilateral duplex doppler carotid ultrasound were normal. T2 gradient echo imaging did not reveal intraparenchymal hemorrhage. A bone scan showed possible increased uptake in the left distal tibia and right humerus however a full body MRI failed to confirm these findings. Ophthalmological assessment revealed bilateral multilayered retinal hemorrhages. A full metabolic and hematological workup was negative. The child protection medical team was consulted. At three weeks post admission, a persistent left subdural collection was drained via subdural-peritoneal shunt insertion. At 18 months post-injury, his language development was reported to be delayed and had persistent distal right hand weakness but was ambulatory. At 9 years post-injury he has persistent right spastic hemiparesis treated with an ankle-foot orthosis and botulinum toxin injections. MRI at 9 years post-injury revealed obvious left sided cortical and subcortical atrophy (Figure 3.1, Patient 1, D-E), corresponding to the original area of restricted diffusion on DWI.

### **3.3.2 Case 2:**

This patient was an 18-month-old developmentally normal and previously healthy male who fell backwards from a height of 6 feet from an elevated high chair with immediate loss of consciousness. His GCS was 8/15

upon arrival of EMS and he was intubated and brought to the Pediatric Intensive Care Unit. Head circumference on admission was well above the 98<sup>th</sup> percentile. An initial CT scan of the head showed a small right frontal subdural hematoma (Figure 3.1, Patient 2, A) which was drained through a burrhole with placement of an intraparenchymal pressure monitor. On post-injury day 3 the patient was noted to have three brief left arm and leg motor seizures treated with an intravenous infusion of 20mg/kg of Phenobarbital with initiation of a daily prophylactic dose without subsequent events. DWI MRI, on post-injury day 4, revealed restricted diffusion of the white matter bilaterally (Figure 3.1, Patient 2, B-C). Time of flight MRA of the intracranial vasculature was normal and T2 gradient echo imaging did not reveal intraparenchymal hemorrhage. Ophthalmological examination revealed multi-layered retinal hemorrhages. A bone scan and skeletal survey were negative. A metabolic workup consisting of serum quantitative amino acids and urine organic acids and a full hematological workup were negative. The child protection medical team was consulted. Upon discharge to the rehabilitation hospital approximately one month post-injury the patient was visually impaired, aphasic and non-ambulatory. Over the next few months he continued to have accumulation of bilateral subdural collections requiring repeat burrhole drainage. At 10 months post-injury, he had regained some language function, however, remained delayed for age, has reduced visual acuity but ambulates independently with obvious bilateral spasticity and weakness. At 9 years post-injury he has persistent left sided hemiparesis, peripheral visual field constriction and has broad developmental disability. MRI

at 9 years post-injury revealed right parieto-occipital atrophy and ex vacuo dilatation of the occipital horn of the right lateral ventricle (Figure 3.1, Patient 2, D-E).

### **3.3.3 Case 3:**

A 6-month-old male, previously well and developmentally normal, presented with a 10-minute clonic seizure of the left face, arm and leg. The patient was described to be irritable with periods of emesis in the preceding 24 hours. His head circumference on admission was at the 50<sup>th</sup> percentile. A CT scan of the head at admission revealed a small subdural hematoma along the posterior falx cerebri and a hypodensity in the right medial occipital lobe (Figure 3.1, Patient 3, A). DWI MRI, on post-admission day 3, revealed restricted diffusion in the right parietal and occipital lobe in the territory of the posterior cerebral artery limited to the white matter (Figure 3.1, Patient 3, B-C). A duplex doppler ultrasound of the carotid arteries was normal. He had two subsequent two-minute left-sided focal seizures on post-admission day 1 which were controlled with intravenous Phenobarbital. Urine organic acids and hematological workup were negative. Ophthalmological assessment revealed bilateral multilayered retinal hemorrhages. A bone scan and skeletal survey were both normal. The child protection medical team was consulted. Eight months post injury the patient remained paretic in the left arm, was non-ambulatory and had delayed language and gross motor skills. MRI 8-years post-

injury revealed atrophy of the right occipital and parietal lobe, corresponding to the original area of restricted diffusion on DWI (Figure 3.1, Patient 3, D-E). At 8-years post-injury, the child has persistent left spastic hemiparesis, is ambulatory with an ankle-foot orthosis (AFO) and attends a school for the developmentally disabled.

#### **3.3.4 Case 4:**

A 19-month-old previously well and developmentally normal female, presented with an altered level of consciousness, recurrent apneas and a GCS of 12/15. Multiple bruises and an area of swelling in the left parietal scalp were noted. A CT scan of the head revealed a subdural hematoma along the left posterior falx cerebri (Figure 3.1, Patient 4, A). Her head circumference was at the 50<sup>th</sup> percentile at admission. Ophthalmological assessment revealed bilateral multilayered retinal hemorrhages and a bone scan revealed increased uptake in the left fibula. On post-injury day 4 the patient had multiple right face, arm and leg clonic seizures. The seizures were initially controlled with intravenous Phenobarbital. A repeat CT scan of the head revealed a midline shift to the right and loss of grey-white differentiation in the entire left hemisphere. She subsequently went into partial status epilepticus lasting one hour and deteriorating to a GCS of 7 prompting an urgent decompressive left hemicraniectomy. Post-operatively the patient had five right focal motor seizures over 2 days eventually controlled with intravenous phenobarbital,

phenytoin and a midazolam infusion. MRI of the brain and contrast enhanced MRA of the neck was done on day 6 post-injury; DWI revealed extensive restricted diffusion of the left hemisphere white matter (Figure 3.1, Patient 4, B-C), while MRA did not show arterial dissection. T2 gradient echo MRI did not reveal any micro-hemorrhages. A full metabolic and hematological workup was negative. The patient regained antigravity strength of the right leg and regained movement with gravity distally in the right upper extremity. The child protection medical team was consulted. Six months post-injury the patient started saying a few words, was able to ambulate independently, had antigravity movement in the full range of movement of the right upper extremity with a right homonymous hemianopsia. MRI at 6 years post-injury revealed marked left parietal and frontal lobe atrophy (Figure 3.1, Patient 4, D-E). Currently, the child is ambulatory, attends school for the developmentally disabled and remains on Phenobarbital for seizures.

**Table 3.1: Summary of four cases of Non-Accidental Trauma (NAT)**

Number	Age	Mechanism	CT Head	Seizure Type (Post-injury interval; days)	MRI Restricted Diffusion (Post-injury interval; days)	Surgical Tx	Delayed MRI (Post-injury interval; years)	Clinical Outcome (Post-injury interval; years)
1	16M	Fall from toddler bed	Lt. 6mm ASDH	FMS Rt. arm/leg* (3)	Lt. hemispheric WM (5)	Burrhole evacuation with drain Burrhole evacuation with intraparenchymal ICP monitor	Lt. hemispheric cortical/subcortical atrophy (9)	Rt. Spastic hemiparesis (9)
2	18M	Fall from high chair	Rt. 3mm ASDH	FMS Lt. arm/leg* (3)	Bilateral hemispheric WM (4)	Burrhole evacuation with intraparenchymal ICP monitor	Rt. Parieto-occipital cortical/subcortical atrophy and ex-vacuo dilation of occipital horn right lateral ventricle (9)	Lt. hemiparesis, peripheral visual loss & broad developmental delay (9)
3	6M	Unknown	Small falcine ASDH	FMS Lt. arm/leg* (1)	Rt. Parieto-occipital WM (3)	None	Rt. Cortical/subcortical parieto-occipital atrophy (8)	Lt. Spastic hemiparesis and developmental delay (8)
4	19M	Unknown	Small falcine ASDH	FMS Rt. Face/arm/leg followed by partial status epilepticus* (5)	Lt. hemispheric WM (6)	Decompressive Lt. hemicraniectomy	Lt. cortical/subcortical fronto-parietal (6)	Developmental delay (6)

Abbreviations: M, Months; ASDH, Acute Subdural Hematoma; FMS, Focal Motor Seizures; WM, White matter; \*Phenobarbital initiated after seizure; ICP, Intracranial Pressure.

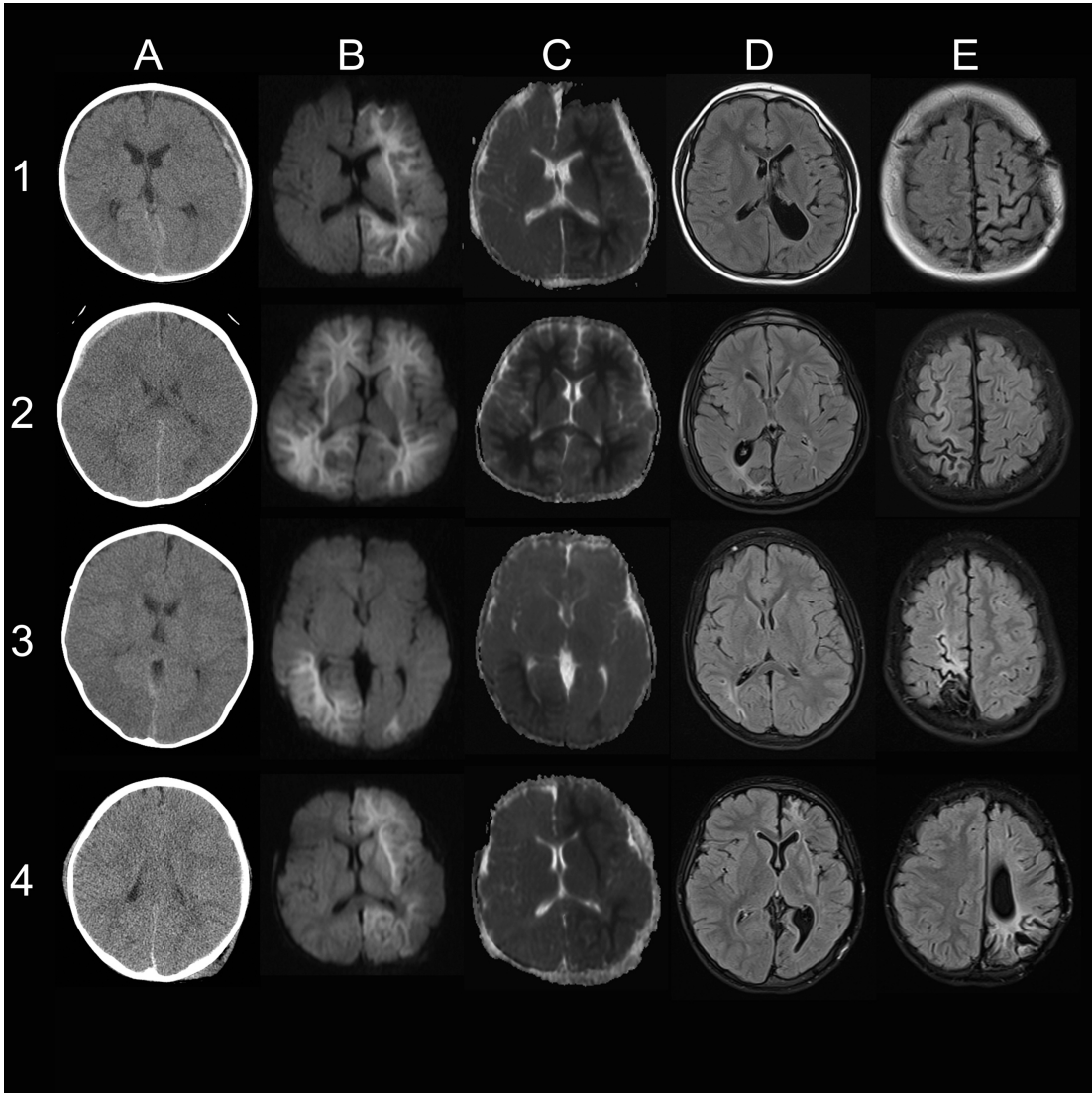


**Figure 3.1: Early areas of restricted diffusion predict ultimate structural consequences**

Patient 1: a) Axial CT scan four hours post injury showing a left sided acute subdural hematoma, b) Axial B1000 image and c) Axial ADC map at the level of the extreme capsule at 5 days post-injury revealing restricted diffusion in the left sided cerebral white matter, d - e) Delayed axial T1 weighted images at the level of the globus pallidus and higher showing cortical and subcortical atrophy of the left hemisphere at 9 years post-injury.

Patient 2: a) Axial CT at presentation showing a right frontal subdural hematoma, b) Axial B1000 image and c) Axial ADC map at 4 days post-injury at the level of the posterior limb of the internal capsule showing restricted diffusion bilaterally and symmetrically in the cerebral white matter, d - e) Delayed axial T1 weighted images showing right parietal and occipital atrophy and ex-vacuo dilatation of the occipital horn of the right lateral ventricle.

Patient 3: a) Axial CT scan at presentation showing an acute subdural hematoma along the posterior falx cerebri, b) Axial B1000 at the level of the posterior limb of the internal capsule and b - c) Axial B1000 and ADC map at the level of the centrum semiovale 3 days post-injury showing restricted diffusion of the right posterior white matter, some restricted diffusion in the right occipital and parietal lobe, d - e) Delayed axial T1 weighted images at 8-years post-injury showing atrophy of the right occipital and parietal lobe.

Patient 4: a) Axial CT scan at presentation showing an acute subdural hematoma along the posterior falx cerebri, b) Axial B1000 and c) Axial ADC map 6 days post-injury at the level of the posterior limb of the internal capsule showing restricted diffusion in the left cerebral white matter and d - e) Delayed axial T1 weighted images at 6-years post-injury showing marked left parietal and frontal atrophy.

### **3.4 Discussion**

In this case series, we highlight that relatively small traumatic subdural hematomas in very young children with TBI can manifest with extensive, predominantly unilateral white matter injury as detected by early DWI. We also demonstrate for the first time the long-term structural and functional consequences to this pattern of injury, demonstrated respectively by delayed atrophy on structural MRI in regions initially showing restricted diffusion, and by the presence of long-term neurological deficits and developmental delay.

Our finding of restricted diffusion in the post-TBI setting is in and of itself not unprecedented. Indeed, DWI is frequently obtained in the evaluation of suspected NAT in infants and often (in up to 89% of cases) reveals more extensive injury than is evident with CT or conventional, non-DWI, MR sequences alone (Biousse et al., 2002; Kemp et al., 2009; Suh et al., 2001; Zimmerman et al., 2007). The severity of DWI abnormality has been

demonstrated to correlate well with ultimate clinical outcome (Ashwal et al., 2011; Geddes et al., 2001a; Suh et al., 2001). Previous reports have described DWI restriction in NAT as occurring in five different radiographic patterns, including: 1) hypoxic-ischemic injury presenting with diffuse supratentorial swelling (39%); 2) watershed type infarction (42%); 3) venous infarction secondary to bridging vein disruption (12%); 4) diffuse axonal injury (6%); or 5) contusion (6%) (Zimmerman et al., 2007). None of these, however, are consistent with the observed patterns of injury in our case series.

McKinney et al. (McKinney et al., 2008) do describe a pattern of unilateral white matter DWI restriction on subacute MRI in a subset of children with suspected NAT (2 of 11 patients over 5 years, both of whom had SDH, albeit without post traumatic seizures) which they proposed might be secondary to transient cervical compression. However, their patients were older than in our series, and they did not report long term clinical and radiographic follow up. In this paper, we demonstrate for the first time the association between areas with early diffusion restriction and long term structural and clinical outcomes.

Restricted diffusion is thought to be largely due to cytotoxic edema secondary to disruption of normal cellular metabolism resulting in net movement of water molecules into cells where diffusion is relatively restricted compared to an extracellular location (Hergan et al., 2002). The pathophysiology of diffusion restriction in TBI falls along a spectrum that can be dichotomized as either hypoxic-ischemic (tending to be more diffuse) or directly traumatic (focal)

in nature (Ichord et al., 2007). The etiology of restricted diffusion in suspected NAT is multifactorial and may include transient cardiorespiratory compromise (e.g. apnea, strangulation), direct primary traumatic injury, reactive vasospasm of cerebral arteries in the vicinity of hemorrhagic lesions, excitotoxic injury, seizures or damage from convulsive or non-convulsive status epilepticus all occurring in the context of an inherently greater vulnerability of the developing brain to injury regardless of cause (Goldstein et al., 2011; Kemp et al., 2003; Moritani et al., 2005; Pierce et al., 2002; Zimmerman et al., 2007).

It is unclear why the predominantly unilateral areas of restricted diffusion we observed were limited to white matter, largely sparing the metabolically much more active overlying cerebral cortex which is considered more vulnerable to ischemia (Bastin et al., 2000; Brierley and Excell, 1966; Marcoux et al., 1982). Global hypoxic-ischemic encephalopathy has been shown to cause extensive white matter injury while sparing the cortex, but it tends to occur in a bilaterally symmetric pattern (Chalela et al., 2001; Hirano and Zimmerman, 1971; Schwedemberg, 1957). That being said, one potential explanation accounting for unilateral restricted diffusion of the subcortical white matter may be that it might represent a subacute (3 - 7 days) phase of hypoxic-ischemic encephalopathy secondary to transient cervical compression due to Wallerian degeneration following initial cortical injury (Chalela et al., 2001; McKinney et al., 2008; Pantoni et al., 1999). We believe this is less likely in our case series as the pattern of white matter injury on DWI in all patients involves both anterior and posterior circulations, and in no cases was there external

evidence of trauma to the neck. Furthermore, the M1 territory of the middle cerebral artery was spared in all four patients, arguing against proximal carotid occlusion as a mechanism for this pattern of injury.

Unilateral peri-ictal diffusion abnormalities have been reported following seizures and/or status epilepticus, though these also tend to involve the cortex and tend to be transient (although may result in delayed cortical atrophy) (Chatzikonstantinou et al., 2011; Cole, 2004; Donaire et al., 2006; Lansberg et al., 1999; Rennebaum et al., 2016; Senn et al., 2003; Szabo et al., 2005). These changes are thought to be secondary to peri-ictal increases in regional energy metabolism, hyperperfusion and cytotoxic edema due to net movement of water into cells following failure of Na/K ATPase pumps (Heiniger et al., 2002; Lansberg et al., 1999). In the current case series, we suspect that seizure activity, which was present in all subjects (including one patient with focal status epilepticus, as described), likely contributed to the extent of brain injury and eventual outcome. However, the atypical pattern of restricted diffusion leads us to speculate that there may have been a potentially synergistic effect of seizure activity following SDH. This would be consistent with the observed concordance between the laterality of focal seizures, the SDH, and the most confluent area of restricted diffusion observed in all patients. Future imaging studies in which additional MRI sequences, such as MR spectroscopy and perfusion imaging, are obtained in the early post-traumatic setting, may help to further elucidate other mechanisms at play in patients such as those we describe.

This case series has limitations which are important to highlight. Admittedly, our study population only includes 4 patients, though this is similar to previously published case series<sup>30</sup>. Second, although long-term follow-up MRI was available in all patients, there was some variability in the timing of its acquisition (6 – 9 years). Third, electroencephalographic data were not available in these cases so we cannot conclusively exclude the possibility of non-convulsive seizures or non-convulsive status epilepticus as contributors to the observed pattern of restricted diffusion. Finally, in these four cases anticonvulsants were not instituted prophylactically but rather only reactively once focal motor seizures occurred.

In summary, the four cases presented here highlight that relatively small subdural hematomas in the setting of suspected NAT—complicated by post-traumatic seizures—may produce in a unique pattern of predominantly unilateral, early white matter injury evident on DWI. This pattern of injury may in turn be associated with delayed brain atrophy of affected brain regions, and further may result in clinically significant, long-term functional consequences.

# **CHAPTER 4: Progressive contralateral hippocampal atrophy following surgery for medically refractory temporal lobe epilepsy**

**Cameron A. Elliott, Donald W. Gross, B. Matt Wheatley, Christian Beaulieu and Tejas Sankar**

This chapter has been published in part as:

Elliott CA, Gross DW, Wheatley BM, Beaulieu C, Sankar T. **Progressive contralateral hippocampal atrophy following surgery for medically refractory temporal lobe epilepsy.** *Epilepsy Research* 2016, 125: 62 – 71.

## **4.1 Introduction**

Surgical treatment of medically refractory, TLE with MTS is associated with a high rate of seizure control, with rates of seizure freedom ranging between 41-72% depending on the length of follow-up (Cohen-Gadol et al., 2006; de Tisi et al., 2011; McIntosh et al., 2004; Wiebe et al., 2001). Despite effective seizure control, it remains difficult to predict which patients will continue to experience seizures post-operatively. Moreover, post-operative neuropsychological consequences (e.g. verbal or non-verbal memory deficits) need to be balanced against long-term seizure benefit.

High resolution, structural MRI demonstrates diffuse pre-operative gray matter atrophy in TLE relative to healthy controls, which may be associated with cognitive dysfunction (Keller and Roberts, 2008). Though present throughout the brain, atrophy is most pronounced in the temporal lobe ipsilateral to the epileptic focus (S S Keller et al., 2002; Keller and Roberts, 2008), and quantitative, MRI-based, pre-surgical manual volumetry has consistently shown that hippocampal atrophy—sometimes undetectable visually—correlates well with the epileptogenic focus (Cendes et al., 1993a, 1993b; Jack et al., 1990a; Watson et al., 1997). Gray matter changes following TLE surgery, however, are much less thoroughly described with largely inconsistent results based exclusively on comparisons between a single pre-operative and a single post-operative scan (Fernandes et al., 2014; Noulhiane et al., 2006). For example, one recent longitudinal study identified mild post-operative contralateral hippocampal atrophy in 47 TLE surgery patients imaged post-operatively at a single delayed time point (mean 4-years, range 0.5-9.6 years)(Fernandes et al., 2014). In contrast, an earlier report which compared contralateral hippocampal volumes at 6-months following TLE surgery in 24 patients with unilateral MTS to those in 16 healthy controls did not find any significant difference in hippocampal volumes (Noulhiane et al., 2006). Both of these reports studied the hippocampus as a whole and did not look at hippocampal subcomponents.

Understanding the specific structural consequences of TLE surgery may ultimately be clinically useful, as they may help to predict the likelihood of poor post-operative seizure control or neuropsychological deterioration on the basis

of early post-operative imaging findings. In this study, the first objective was to characterize the extent and time course of changes found in the contralateral hippocampus, including its subcomponents of head, body, and tail, following TLE surgery in patients scanned longitudinally at short intervals within the first post-operative week and beyond. The second objective was to investigate the relationship between post-operative contralateral hippocampal volume and neurocognitive outcomes, surgical approach, resected side and seizure control.

## **4.2 Methods**

This study was approved by the University of Alberta Health Research Ethics Board and informed consent was obtained from all participants.

### **4.2.1 Participants**

Our study included 26 patients with medically refractory TLE who underwent surgery at the University of Alberta Hospital from 2005 – 2014 and group of 12 control subjects of similar age with no history of epilepsy or any other neurologic or psychiatric disease. Participants were referred through the comprehensive epilepsy program. Each patient had a standard preoperative assessment including MRI, ictal and inter-ictal long-term video electroencephalography (EEG) and neuropsychological evaluation. On the basis of this evaluation participants either underwent an ATL or SAH by a single

neurosurgeon (author B.M.W.). In our institution, only patients with clear cut MRI evidence of MTS accompanied by corroborative clinical and EEG findings are offered SAH as an option. The majority of cases had subjective evidence of unilateral MTS on MRI (visually detectable hippocampal atrophy, or abnormal hippocampal shape/internal architecture with or without increased signal on T2/FLAIR sequences) (n=23) with concordant evidence from surface EEG-video telemetry and neuropsychiatric evaluation. The remaining three cases included one participant with imaging evidence of bilateral MTS (surgical side with more severe visible atrophy than non-surgical side), one with an isolated right inferior frontal lesion and one with no detectable lesion. In seven cases, surgery was preceded by bitemporal stereoelectroencephalography (SEEG) evaluation when recommended by the comprehensive epilepsy team on the basis of ambiguous surface telemetry. In all seven cases SEEG demonstrated unilateral temporal ictal onset.

#### **4.2.2 Image acquisition**

Patients were imaged in two distinct groups, either: i) as part of a two-scan group (N = 16) having a single preoperative and a single delayed postoperative scan (average inter-scan interval  $5.4 \pm 3.2$  years, range 0.4 – 8.6); or ii) as part of an intensively imaged longitudinal group (N = 10) scanned on postoperative days 1, 2, 3, 6, 60, 120 and a delayed time point (average  $2.4 \pm 1.5$  years, range 1.0 - 5.7) in order to better characterize the early time course of

postoperative hippocampal volume change. Sutures were used to close skin in the longitudinal group instead of staples for high quality MRI scanning in the immediate post-operative period. To investigate variability of hippocampal volumes in the non-operated, non-epileptic brain, nine healthy subjects (average age  $33.3 \pm 13.1$  years old; range 23 – 58; all but one right-hand dominant) were scanned on two separate occasions (average inter-scan interval  $6.9 \pm 2.1$  years; range 3.6 – 9.1) as controls for the two-scan group, while three healthy subjects (20, 22, and 33-years of age, all right-hand dominant) were imaged longitudinally (i.e., at baseline and then in a delayed fashion on days 1, 2, 3, 6 and 60) as controls for the longitudinal group.

Images for all patients and controls were acquired on a Siemens Sonata 1.5T scanner (Siemens Healthcare, Erlangen, Germany) using an eight-element head coil. Whole brain, axial, T1-weighted, 3D-MPRAGE images were obtained aligned to anterior-posterior commissural line with voxel size 1 mm x 1 mm x 1 mm, TR 1890 ms, TE 4.38 ms, and scan time 6:03 min.

### **4.2.3 Volumetric analysis**

Volumetric analysis was performed using manual segmentation by a single trained observer (author C.E.). DISPLAY software (Montreal Neurological Institute, Montreal, Canada) was used to delineate anatomical boundaries of the structures of interest in three orthogonal planes simultaneously on 3D-MPRAGE images (Bonilha et al., 2004a). The observer was blinded to surgical status (i.e.,

pre-resection, post-resection or control) and time point (i.e., post-operative day) by ensuring that anonymized images of patients were interspersed with controls in random order. Images were zoomed in to the structure of interest such that the resection cavity (or lack thereof) was not visible. The hippocampal formation was traced using a protocol described by Malykhin and colleagues with previously demonstrated robust inter- and intra-rater reliability (Malykhin et al., 2007). Segmentation yielded whole hippocampal volume (WHV), as well as hippocampal head (HHV), body (HBV) and tail (HTV) volumes for each subject (Figure 4.1). To evaluate the possibility of mechanical deformation causing spurious atrophy of periventricular structures—say, due to dural opening and/or CSF egress during resection—the volume of the caudate nucleus was measured using a manual protocol described by Looi and coworkers (Looi et al., 2008). The caudate nucleus is not directly connected to the mesial temporal lobe and would not be expected to change in volume by way of disconnection following temporal resection.

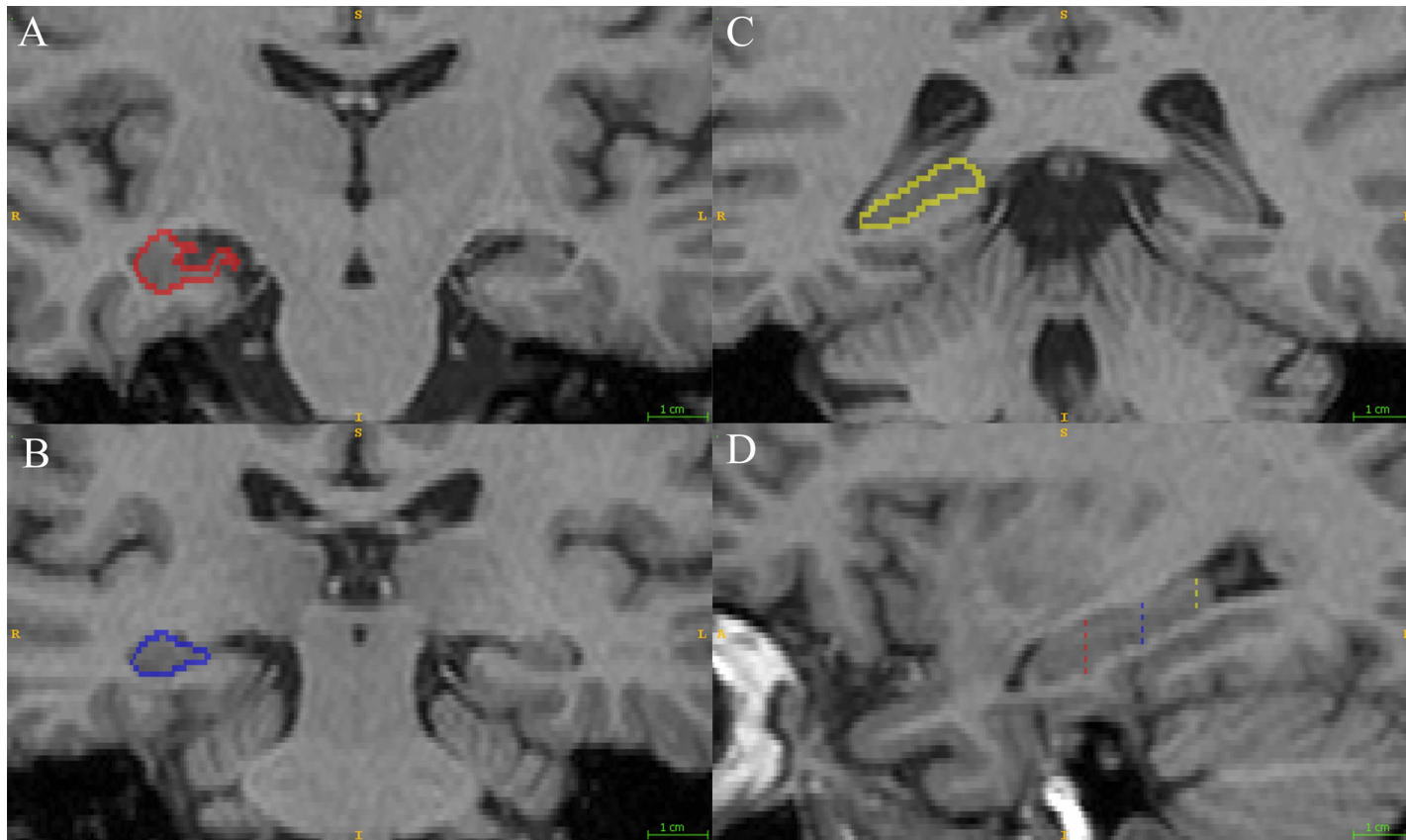


**Figure 4.1: Representative sub-regional hippocampal tracings**

Examples of sub-regional hippocampal tracings on a pre-operative study patient according to protocol by Malykhin et al., 2007 showing first coronal slice of the hippocampal head (A), middle coronal slice of the hippocampal body (B) and first coronal slice of the hippocampal tail (C) as well as. Lateral sagittal slice of the hippocampus (D) showing location of three previous tracings, respectively

#### **4.2.4 Defining a variability threshold for hippocampal volume**

To identify a conservative threshold beyond which changes from baseline in the longitudinal surgical group would represent a real change (attributable to a surgical effect rather than measurement error), a normal variation range for hippocampal (and sub-regional) measurements was calculated in our longitudinal control group (not expected to undergo significant changes over time apart from scanner-related effects such as scanner drift). Similar to previous longitudinal studies, the normal variation range for hippocampal (and sub-regional) measures were defined arbitrarily as twice the average absolute deviation from baseline for both hippocampi in each of three healthy controls scanned longitudinally (index scan and four subsequent scans at day 1, 3, 6 and 60) (Liu et al., 2013). In the longitudinal surgical arm, the absolute difference of each post-operative measure relative to each patient's pre-operative baseline was calculated and considered significant if it exceeded the normal variation range.

#### **4.2.5 Seizure and neuropsychological outcome**

Seizure outcome was categorized based on the modified Engel classification (Engel et al., 1993a). Accordingly, seizure outcome was dichotomized as either free from disabling seizures (Engel I; including nondisabling simple partial seizures or auras) or not (Engel >I). Each patient

underwent pre- and post-operative tests of verbal and figural memory as well as the Wechsler Adult Intelligence Scale (WAIS; standard scores) with full-scale IQ (IQ), verbal comprehension index (VCI), perceptual reasoning index (PRI) and working memory index being recorded. Verbal memory was summarized using an average (VM) of t-scores (population mean = 50, SD = 10) for recognition memory test for words (immediate recall), verbal paired associates II (delayed), logical memory II (delayed) and Rey auditory verbal learning test (RAVLT; delayed). Figural memory was summarized as an average (FM) of t-scores (population mean = 50, SD = 10) for recognition memory for faces, continuous visual memory test (CVMT; delayed) and Rey-Osterreith complex figure (CFT; delayed). Pre- and post-operative group means were compared for each of these six scores (IQ, VCI, PRI, WMI, VM and FM) separately for dominant and non-dominant hemisphere surgery. Hemispheric dominance was established based on handedness alone 9/17 (53%), fused dichotic listening test 6/17 (35%), fMRI for language lateralization 1/17 (6%) and/or intracarotid amygdal procedure 3/17 (18%).

#### **4.2.6 Statistical analysis**

To assess intra-rater reliability for hippocampal volume, the same observer (C.E.) traced the hippocampus in 20 subjects (10 patients and 10 controls) on the same scan on two separate occasions within two weeks of the original tracing. Inter-rater reliability was assessed using an in-house training

data set of normal and diseased hippocampi traced by Malykhin and colleagues to which tracings of a single observer (C.E) were compared (Malykhin et al., 2007). Intra- and inter-rater reliability were assessed using the two-way random effects ICC for absolute agreement between measures.

A paired t-test was used to compare pre- to post-operative volumes in the two scan group. For the longitudinal group, hippocampal volumes were normalized to pre-operative baseline and expressed as a percentage of the same. A linear regression between normalized hippocampal volumes obtained during the first post-operative week relative to baseline was performed to estimate the rate of daily hippocampal atrophy during this time. A non-parametric Wilcoxon Signed-Rank Test with Holm-Bonferroni corrections for multiple comparisons (3) was used to compare pre-operative, day 6-7 and year 1 – 3 post-operative means in the longitudinal group. An unpaired t-test was used to compare atrophy across surgical approach, side and based on seizure outcome (dichotomized as free of disabling seizures—Engel class I—or continued disabling seizures—Engel class > I). A non-parametric Wilcoxon Signed-Rank Test was used to compare mean pre- and post-operative neuropsychological testing scores due to the smaller number of patients in whom scores were measured. A non-parametric Mann-Whitney U-test was used to compare median post-operative hippocampal volumes stratified for seizure outcome (seizure free versus continued seizures) due to small sample size in the continued seizure group. A linear regression between normalized hippocampal volumes obtained during the first post-operative week relative to baseline was performed to

estimate the rate of daily hippocampal atrophy during this time.  $P < 0.05$  was used as the threshold for statistical significance throughout; Bonferroni correction was used to correct for multiple comparisons where appropriate. SPSS version 21 (IBM) was used for all statistical analyses.

## **4.3 Results**

### **4.3.1 Descriptive patient data**

Detailed patient ( $n = 26$ ) demographic data is displayed in Table 4.1. In summary, the mean age was  $39.9 \pm 10.8$  years (range 19 - 59 years) with 42% (11/26) patients being male. The control group consisted of 12 subjects of similar age ( $p = 0.24$ , unpaired t-test; average age  $35 \pm 13$  years old; range 20 - 58) with no history of epilepsy or any other neurologic or psychiatric disease. Fourteen patients (55%) underwent an ATL. Left-sided surgery occurred in 12/26 (46%). Surgical pathology was consistent with MTS in 23 patients. Surgical pathology in the remaining three patients was reported as normal, FCD type 1C and gliosis respectively (see Table 4.1).

**Table 4.1: TLE surgery patient demographics**

Demographics for TLE surgery patients with 1-16 from two scan group and 17-26 from more frequent longitudinally scanned groups.

Pt	MRI Lesion	Sex/Age(yrs)/Handedness	IPIs	SEEG	Surgery	Disease Duration (yrs)	Pathology	Outcome (EC)
1	MTS	F/38/RHD	FS	No	Left SAH	37	MTS	IIa
2	MTS	M/33/RHD	None	No	Left SAH	15	MTS	Ia
3	MTS	F/21/RHD	FS	No	Left SAH	10	MTS	IIb
4	MTS	M/31/RHD	None	No	Left SAH	23	MTS	Ia
5	NL <sup>†</sup>	M/55/RHD	None	No	Left SAH	15	MTS	Ia
6	MTS	F/41/RHD	TBI	No	Right SAH	27	MTS	Ia
7	MTS	F/37/RHD	None	No	Right SAH	36	MTS	IIc
8	MTS	F/37/RHD	FS	No	Right SAH	29	MTS	Ia
9	MTS	F/46/RHD	FS, TBI	No	Right SAH	32	MTS	IIa
10	MTS	M/19/RHD	FS	No	Left ATL	16	MTS	Ia
11	NL <sup>†</sup>	F/44/RHD	None	No	Left ATL	6	MTS	Ia
12	MTS	F/41/RHD	None	Yes	Left ATL	18	MTS	Ia
13	MTS	F/52/RHD	FS, TBI	No	Left SAH	13	MTS	Ia
14	MTS	M/44/RHD	M	Yes	Left ATL	43	MTS	Ic
15	MTS	F/58/RHD	None	No	Left ATL	47	MTS	IIa
16	MTS	F/36/LHD	FS, TBI	No	Right ATL	16	MTS	Ia
17	MTS	M/34/RHD	None	No	Left SAH	6	MTS	Ia
18	MTS	M/45/RHD	FS	No	Right SAH	28	MTS	Ia
19	MTS	F/54/RHD	None	Yes	Left ATL	26	MTS	Ia
20	MTS	M/24/LHD	FS, M	No	Left ATL	12	MTS	Ia
21	MTS*	F/39/RHD	None	No	Right ATL	20	Normal	Ia
22	MTS	M/29/RHD	None	No	Right ATL	11	MTS	Ia
23	Bilat MTS	M/59/RHD	TBI	Yes	Right ATL	29	MTS	Ia
24	R. Fr T2 AbN	F/50/RHD	None	Yes	Right ATL	8	Gliosis	Ia
25	MTS	M/31/RHD	TBI	Yes	Right ATL	7	FCD type 1C	IIa
26	MTS	F/36/RHD	TBI	Yes	Right ATL	24	MTS	Ia

AbN: Abnormality; ATL: Anterior Temporal Lobectomy; EC: Engel Class; FCD: Focal Cortical Dysplasia; FS: febrile seizure; IPI: Initial Precipitating Incident; LHD: Left-Hand Dominant; M: Meningitis; NL: non-lesional; RHD: Right-Hand Dominant; SAH: Selective Amygdalohippocampectomy; TBI: traumatic brain injury. \*Although patient 21 had MRI evidence of MTS, pathology was reported as normal. † Two patients reported as non-lesional on MRI were found to have evidence of MTS on final pathology

### 4.3.2 Surgical outcome

Seizure control across all patients, determined at an average of  $5.2 \pm 3.6$  years following surgery, was as follows: Engel I—77% (IA - 73%, IC - 4%) IIA - 15%, IIB - 4%, IIC - 4%. There was no significant difference between seizure freedom rates by surgical approach (SAH - 67%; ATL - 79%;  $p = 0.47$ ).

### 4.3.3 Reliability of volumetric measures

Intra-rater reliability for the whole hippocampus (WHV) was high with an average measures ICC of 0.97 (95% confidence interval 0.93 - 0.99;  $F(19,19) = 40.19$ ,  $p < 0.001$ ). Inter-rater reliability for WHV was also high with an average measures ICC of 0.93 (95% confidence interval 0.71 - 0.98;  $F(9,9) = 13.97$ ,  $p < 0.001$ ). Intra- and inter-rater reliability data for the hippocampal head (HHV), body (HBV) and tail (HTV) demonstrated ICC ranging from 0.89 - 0.99 with the highest ICCs observed for HBV (Table 4.2).

**Table 4.2: Reliability data for hippocampal volumetry measurements**

Inter- and intra-rater reliability as measured by average measure ICC (with 95% confidence interval) for hippocampal volumes and sub-regions (head, body and tail).

	HHV	HBV	HTV	WHV
Inter-Rater Reliability (ICC)	0.92 (0.69 - 0.98)	0.99 (0.96 - 0.99)	0.89 (0.56 - 0.97)	0.93 (0.71 - 0.98)
Intra-Rater Reliability (ICC)	0.91 (0.78 - 0.97)	0.99 (0.98 - 0.97)	0.98 (0.96 - 0.99)	0.97 (0.93 - 0.99)

#### 4.3.4 Hippocampal volume: two scan group

In the two scan group (n = 16: ATL = 6; SAH = 10; Figure 4.2), with a mean interval between surgery and post-operative scan of  $5.4 \pm 3.2$  years (range 150 days - 8.6 years), there was statistically significant post-operative atrophy of contralateral whole hippocampus volume (WHV) (preoperative mean WHV  $3462 \pm 379$  mm<sup>3</sup> versus post-operative mean WHV  $3054 \pm 471$  mm<sup>3</sup>;  $p < 0.001$ , paired t-test) with 12% mean volume loss relative to baseline. When analyzed separately, there was significant atrophy of hippocampal body volume (HBV) with 27% mean volume loss relative to baseline (pre-operative mean HBV  $1066 \pm 158$  mm<sup>3</sup> versus post-operative mean HBV  $780 \pm 150$  mm<sup>3</sup>;  $p < 0.001$ , paired t-test). There was more modest atrophy of hippocampal tail volume (HTV) with 9% mean volume loss relative to baseline (pre-operative mean HTV  $558 \pm 144$  mm<sup>3</sup> versus post-operative mean HTV  $509 \pm 115$  mm<sup>3</sup>;  $p = 0.041$ , paired t-test), which did not survive Bonferroni correction for multiple comparisons (i.e.,  $p > 0.05/3$  or 0.017). There was no significant post-operative atrophy of contralateral hippocampal head volume (HHV) (pre-operative mean HHV  $1838 \pm 324$  mm<sup>3</sup> versus post-operative mean HHV  $1766 \pm 329$  mm<sup>3</sup>;  $p = 0.063$ , paired t-test). In contrast, hippocampal volumes were not significantly different over time in the two-scan healthy control group (n = 9) with similar inter-scan interval (WHV: scan 1 mean  $4075 \pm 350$  mm<sup>3</sup> versus scan 2 mean  $4020 \pm 339$  mm<sup>3</sup>;  $p = 0.099$ , paired t-test; HBV: scan 1 mean  $1356 \pm 164$  mm<sup>3</sup> versus scan 2 mean  $1335 \pm 134$  mm<sup>3</sup>;  $p = 0.213$ , paired t-test) (Figure 4.3).

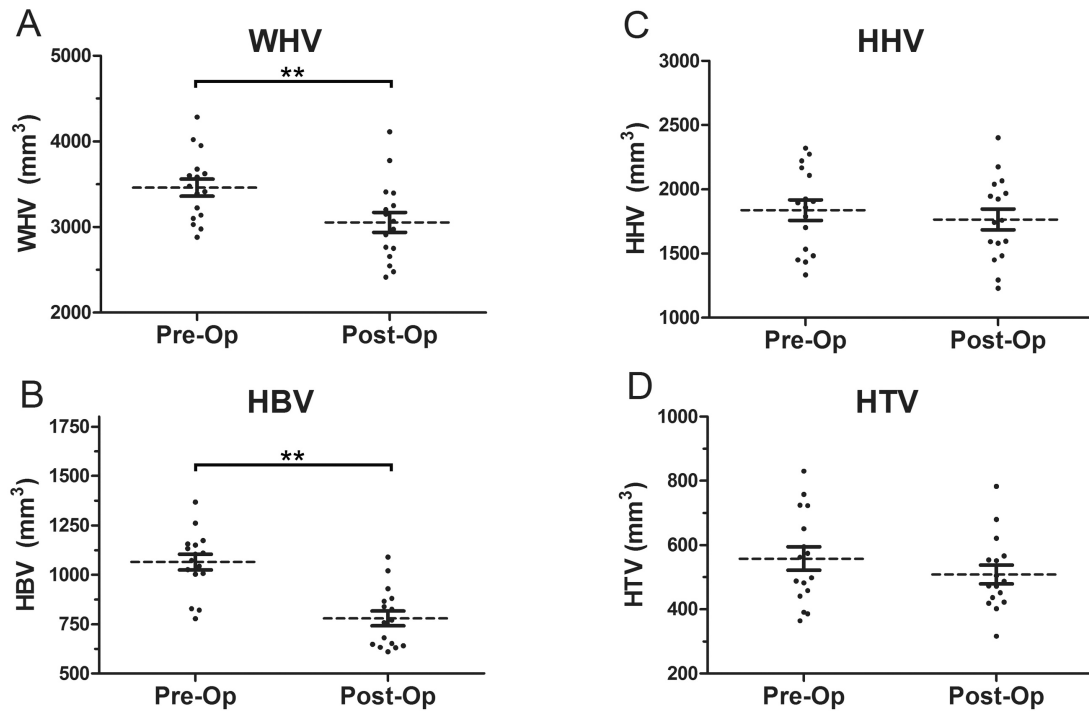


**Figure 4.2: Postoperative two scan group hippocampal volumetry**

Mean contralateral hippocampal volume (mm<sup>3</sup>) pre- and post-operatively in the two scan group (n = 16; ATL - 6; SAH - 10). There was statistically significant post-operative atrophy (mean of 5.4 ± 3.2 years after surgery) for (A) whole hippocampus (WHV) by 12%, (B) hippocampal body (HBV) by 28%, but not (C) hippocampal head (HHV) or (D) tail (HTV). \* denotes p<0.05, \*\*denotes p<0.01. Error bars denote SEM.

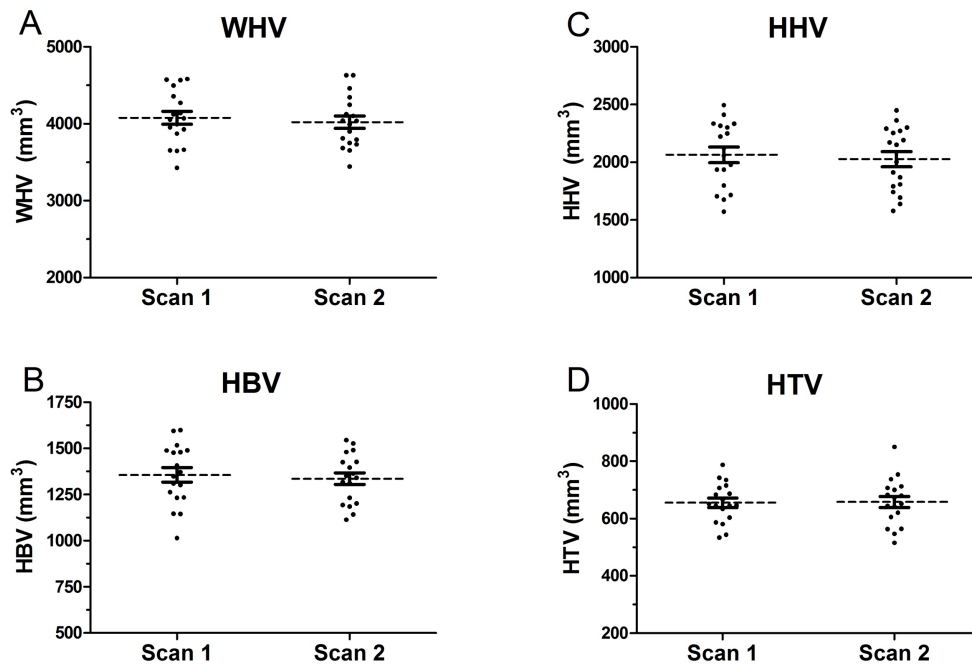


**Figure 4.3: Control subject hippocampal volumetry**

Mean hippocampal volume ( $\text{mm}^3$ ) in the healthy control group ( $n = 9$ ) scanned twice over time (mean inter-scan interval  $6.9 \pm 2.1$  years). There was no significant difference over time amongst healthy controls in mean (A) whole hippocampus, hippocampal (C) head, (B) body or (D) tail. Error bars denote SEM.

#### 4.3.5 Hippocampal volume: longitudinal group

In the longitudinal group ( $n = 10$ ; ATL = 8; SAH = 2) post-operative hippocampal atrophy progressed rapidly over the first week (Figure 4.4A) with an average volume loss of 1.3%/day (best-fit regression line first post-operative week revealed a slope significantly different from zero;  $y = -1.3x + 97.2$ ,  $t = -3.1$ ,  $p = 0.005$ ). All ten subjects had major reductions in WHV by the end of the first post-operative week (mean  $12 \pm 4.8\%$ ).

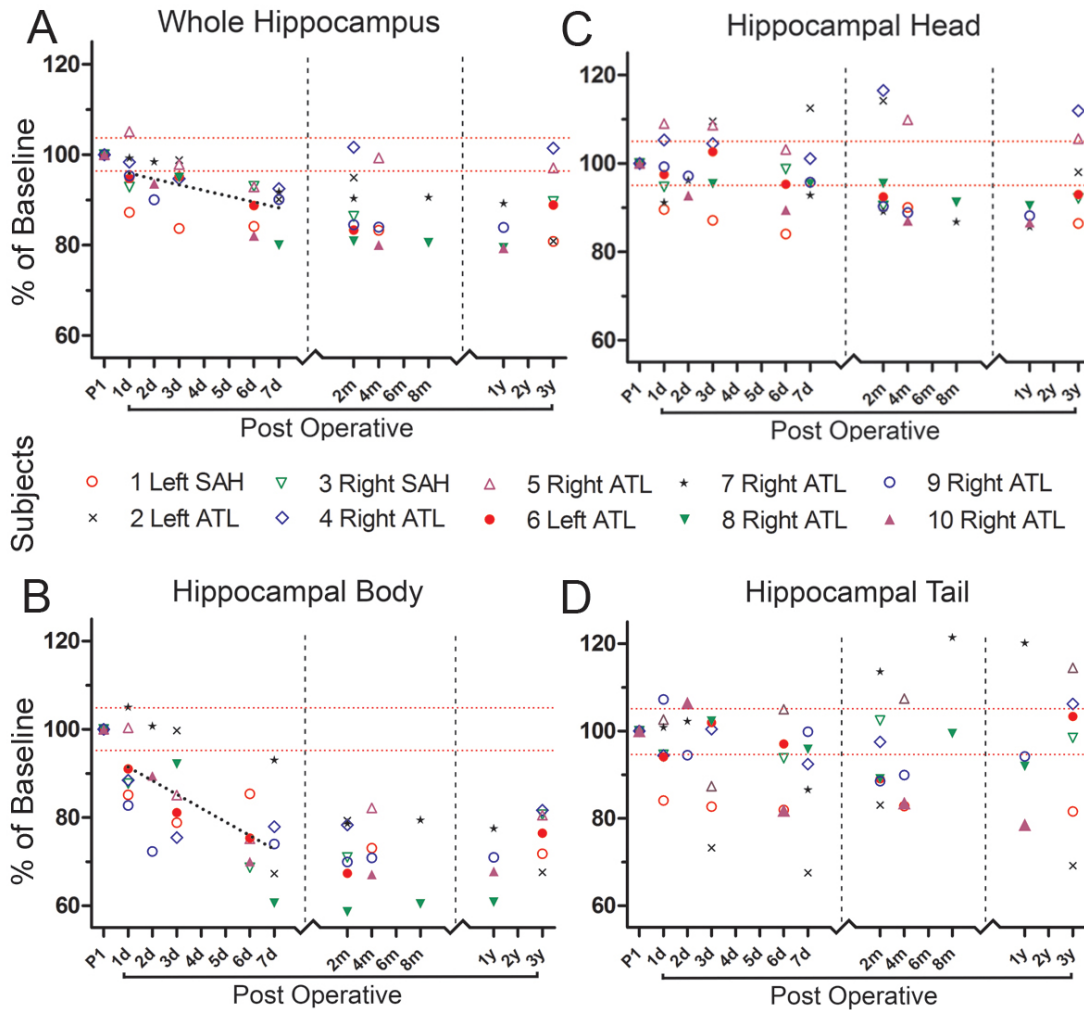


**Figure 4.4: Normalized individual longitudinal postoperative hippocampal volumetry**

Longitudinal normalized volume of the contralateral (non-resected) hippocampus in ten patients prior to (P1) and following (days, d; months, m and years, y) temporal lobe epilepsy surgery (ATL – 8; SAH – 2) for medically refractory epilepsy. Post-operative measures were normalized to each subject's pre-operative baseline. The dashed red lines show the normal variation range defined from repeated measures of both hippocampi in three healthy controls using the same scanner, protocol and time period. (A) WHV loss occurred rapidly over the first week (-1.3%/day) such that all ten subjects had significant reductions from baseline by the end of the first post-operative week which subsequently recovered in two subjects but remained significantly depressed in all others at long-term follow up. (B) HBV loss accounted for the majority of hippocampal atrophy occurring drastically over the first post-operative week (-3.0%/day) in all subjects and remained significantly depressed in all subjects at long-term follow up. (C) HHV was more scattered and less severe although significant volume loss occurred over the first week in three subjects and

ultimately in 7 subjects at delayed follow up. (D) HTV was considerably heterogeneous with long-term significant volume loss relative to baseline occurring in 5 subjects. SAH, selective amygdalohippocampectomy; ATL, anterior temporal lobectomy.

The majority of the observed post-operative hippocampal atrophy was largely complete by day 7 ( $p < 0.001$ ) without any further significant decline at the group wide level thereafter relative to the most delayed scan point ( $> 3$  years; Figure 4.5A, whole hippocampal volume, WHV).

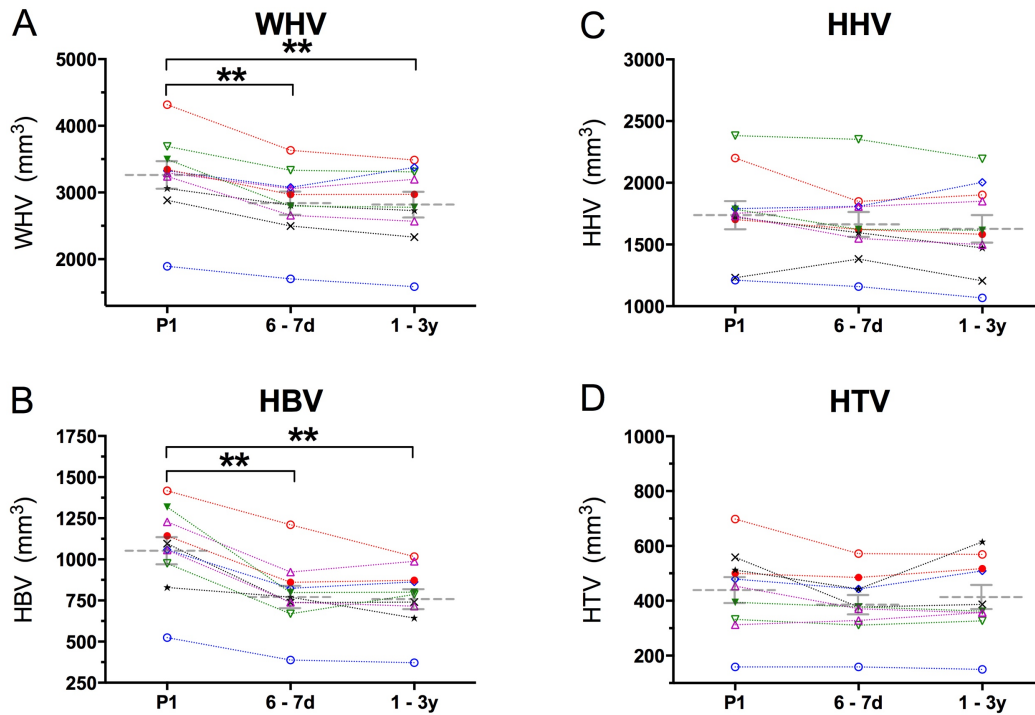


**Figure 4.5: Raw longitudinal postoperative hippocampal volumetry**

Early (6 - 7 days, 6 - 7d) and delayed (1 - 3 years, 1 - 3y) post-operative contralateral hippocampal and sub-regional absolute volume (in mm<sup>3</sup>) changes following surgery for medically refractory TLE in the longitudinal group (n = 10; ATL - 8; SAH - 2). Despite the factor of 2-3 variability in the absolute volumes across subjects, there is statistically significant and consistent early atrophy of the whole hippocampus (WHV, A) and the hippocampal body (HBV, B), followed by volumetric stabilization without any further atrophy or recovery at the group-wide level. The hippocampal head (HHV) and tail (HTV) do not undergo similar group-wide changes over the same time period. \*\*denotes p<0.01 relative to baseline. Error bars denote SEM. Individual subject labels are the same as in figure 4.4.

That being said, at the individual level there was considerably more variability in WHV beyond the first post-operative week (Figure 4.4A). For example, six subjects (1, 2, 3, 7, 9 and 10) had further hippocampal atrophy ( $-4.6 \pm 2.6\%$ , mean  $\pm$  SD) from the end of the first post-operative week until the most delayed

scan. Two subjects (6 and 8) had no further hippocampal atrophy outside of the first week while two subjects (4 and 5) had hippocampal volumes that returned to or near preoperative baseline

Sub-regional analysis revealed that the WHV change is accounted for by volume loss specific to the hippocampal body (Figure 4.4B). Hippocampal body atrophy occurred rapidly over the first week following surgery with an average volume loss of 3.0%/day (best fit regression line plotted over the first post-operative week revealed a slope significantly different from zero;  $y = -3.0x + 94.1$ ,  $F_{1,24} = 15.05$ ,  $p = 0.007$ ). As a group there was no further significant atrophy or recovery in HBV after the first post-operative week (Figures 4.4B and 4.5B). For the HHV and HTV, no significant early or delayed longitudinal changes were observed given the inter-subject variability (Figures 4.4C/D and 4.5C/D).

As predicted, longitudinal hippocampal and sub-regional volumes in healthy control group scanned at similar time intervals as the longitudinal surgical arm did not show significant change over time (Figure 4.6). Left and right hippocampal measurements had similar longitudinal variability for each measure. The normal variation range was 3.0% for WHV, 5.6% for HHV, 3.4% for HBV and 6.3% for HTV.

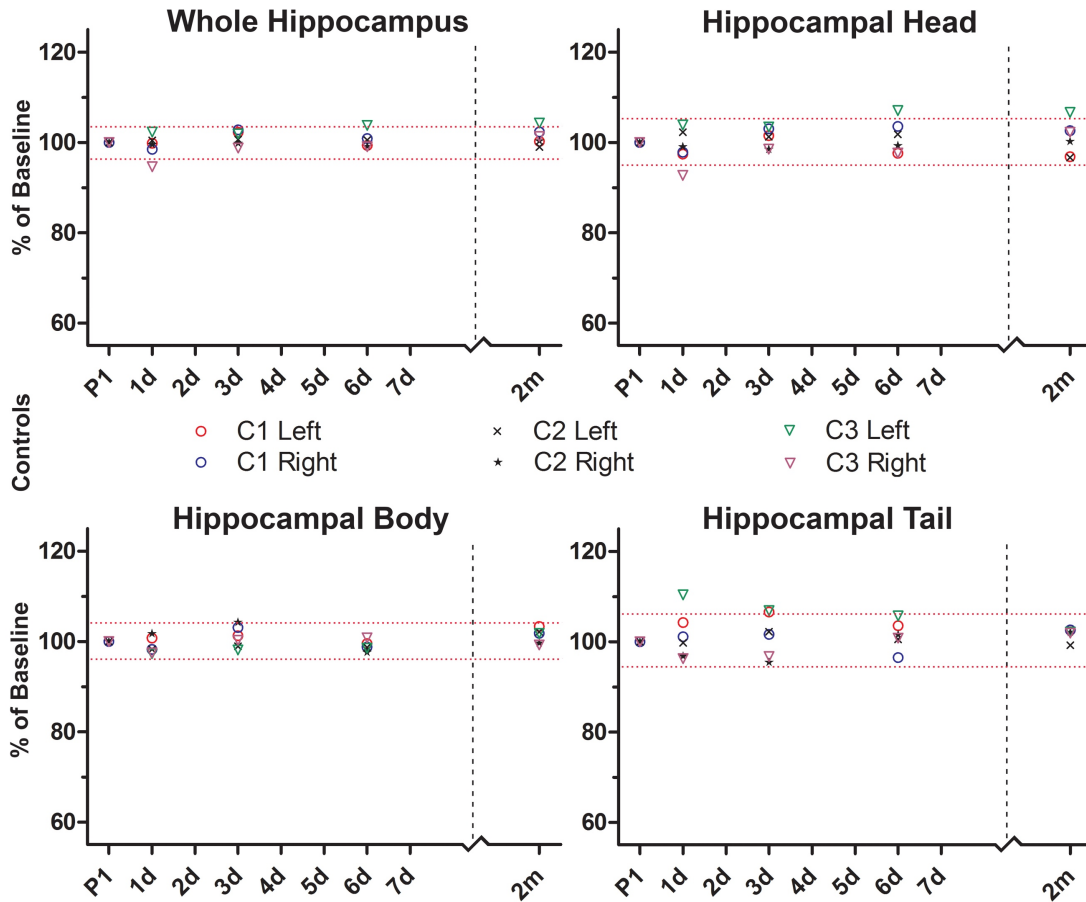


**Figure 4.6: Control subject normalized longitudinal volumetry**

Time course of normalized hippocampal and sub-regional volume from three controls (C1, C2, C3) imaged longitudinally over a similar time span as the longitudinal surgical group. Measurements are normalized to each subject's baseline for each structure. The normal variation range (two red dashed lines) was defined as twice the average absolute deviation from the initial scan baseline of the six hippocampi.

#### 4.3.6 Hippocampal atrophy differences by surgical approach and seizure outcome

Combining the data from the post-operative scan from the two-scan group with the most delayed post-operative scan of the longitudinal group (i.e. all 26 TLE patients together), baseline hippocampal volumes contralateral to the

identified surgical target (seizure focus) were significantly smaller in TLE patients than in healthy controls (TLE WHV  $3381 \pm 493 \text{ mm}^3$  versus control WHV  $3992 \pm 486 \text{ mm}^3$ ;  $p < 0.001$ , unpaired t-test).

Overall the average volume loss at  $4.3 \pm 3.0$  years was  $12 \pm 6\%$  for the WHV and  $27 \pm 8\%$  for the HBV. There was no significant difference in mean atrophy of either WHV or HBV by surgical approach (WHV:  $12 \pm 7\%$  vs.  $12 \pm 5\%$ , ATL vs. SAH,  $p = 0.94$ ; HBV:  $26 \pm 8\%$  vs.  $27 \pm 8\%$ , ATL vs SAH,  $p = 0.66$ ) or side of resection (WHV:  $14 \pm 5\%$  vs.  $11 \pm 7\%$ , Left vs. Right,  $p = 0.31$ ; HBV:  $26 \pm 8\%$  vs.  $27 \pm 9\%$ , Left vs. Right,  $p = 0.89$ ). However, when post-operative hippocampal atrophy was analyzed by seizure outcome, there was significantly less atrophy of the WHV in patients free of disabling seizures (Engel I) ( $11 \pm 6\%$ , median  $\pm$  SD,  $n = 20$ ) versus those with continued post-operative disabling seizures ( $18 \pm 5\%$ ,  $n = 6$ ; Mann-Whitney U = 27.0,  $p = 0.048$ ); results were similar for HBV ( $23 \pm 7\%$ ;  $n = 20$  Engel I, versus  $36 \pm 8\%$ ;  $n = 6$  with ongoing seizures; Mann-Whitney U = 21.0;  $p = 0.019$ , Figure 4.7). There was no significant difference in pre-operative contralateral hippocampal volume when analyzed by seizure outcome (WHV stratified by Engel 1 vs Engel  $>1$ , Mann Whitney U-Test,  $p = 0.61$ ; HBV stratified by Engel 1 vs Engel  $>1$ , Mann Whitney U-Test,  $p = 0.38$ ).

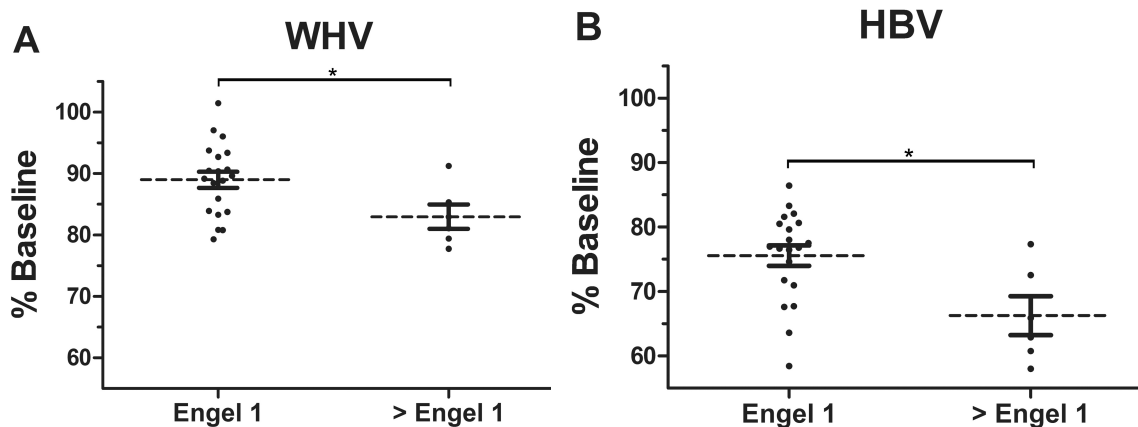


**Figure 4.7: Postoperative normalized hippocampal volume loss by seizure outcome**

Post-operative contralateral whole hippocampal (WHV; A) and hippocampal body (HBV; B) atrophy expressed as a percentage of baseline at most delayed time point ( $4.3 \pm 3.0$  years post-surgery) combined across both single-scan group and longitudinal group ( $n=26$ ). There was a statistically significant difference between subjects who were seizure free (Engel I,  $n=20$ ) versus those with continued post-operative seizures (Engel  $> 1$ ,  $n=6$ ) who had a greater reduction of hippocampal volume. \* denotes  $p < 0.05$ . Error bars denote SEM.

The performance of delayed WHV or HBV alone as a predictor of seizure outcome (Engel 1 versus Engel  $> 1$ ) was evaluated with ROC curves which revealed an area under the curve (AUC) of  $0.775 \pm 0.117$  ( $0.57 - 0.914$ ;  $p = 0.019$ ) and  $0.825 \pm 0.099$  ( $0.626 - 0.945$ ;  $p = 0.001$ ), respectively (Figure 4.8). The optimal cutoff value was WHV atrophy of greater than 17% (sensitivity = 67%; specificity = 85%) or HBV atrophy of greater than 32% (sensitivity = 67%; specificity of 90%) with no significant difference between ROC curves.

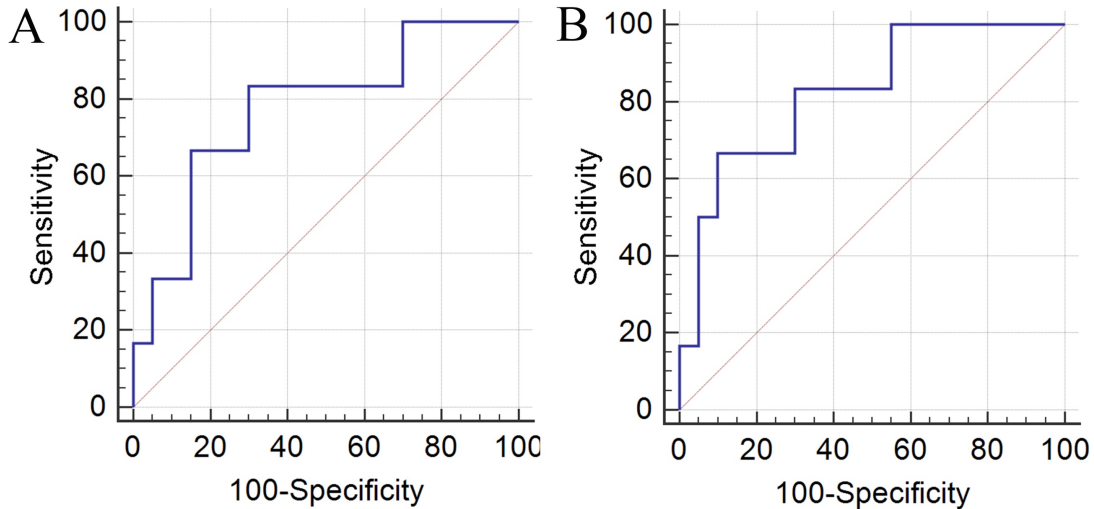


**Figure 4.8: Receiver operating characteristics (ROC) curves for seizure freedom based on delayed hippocampal atrophy**

ROC curves showing discrimination between subjects who are free of disabling seizures (Engel 1) versus those with disabling post-operative seizures (Engel >1) on the basis of atrophy at the most delayed scan time across two-scan and longitudinal group: left, whole hippocampal volume and right, hippocampal body volume. For whole hippocampal volume the area under the ROC curve (AUC) was 0.775 (SE = 0.117, 95% Confidence interval 0.57 – 0.914; p-value = 0.019) with the optimal criterion being atrophy of greater than 14% relative to baseline with a sensitivity of 67% and specificity of 85%. For hippocampal body volume alone the area under the ROC curve (AUC) was 0.825 (SE = 0.099, 95% confidence interval 0.626 – 0.945; p-value = 0.001) with the optimal criterion being atrophy of greater than 32% relative to baseline with a sensitivity of 67% and specificity of 90%. Pairwise comparison of ROC curves did not reveal a statistically significant difference between whole hippocampal versus hippocampal body volume alone as a predictor of seizure outcome (p = 0.732).

#### 4.3.7 Caudate volumetry

The caudate nucleus contralateral to the side of resection was used as a control region since it would not be expected to undergo atrophy due to disconnection caused by temporal lobe resection but might experience

mechanical deformation following surgery. Caudate volume in the longitudinal surgical group revealed no significant atrophy following surgery (Figure 4.9).

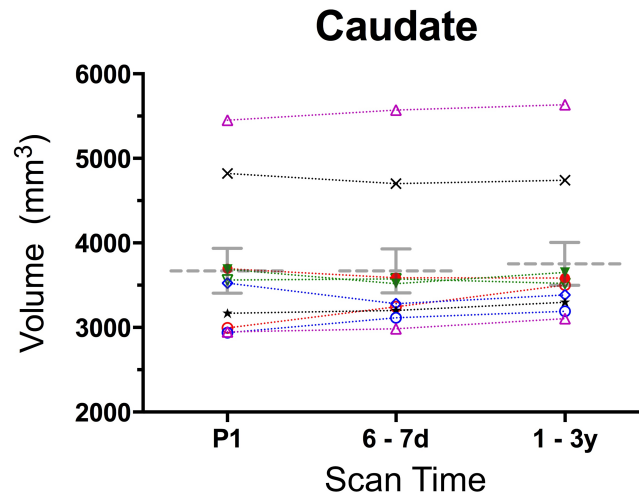


**Figure 4.9: Postoperative caudate volumetry**

Post-operative contralateral caudate volume following surgery for medically refractory TLE in the longitudinal group (n = 10; ATL - 8; SAH - 2) at 6 - 7 days (6 - 7d) and at the most delayed scan time (1 - 3 years) compared to pre-operative baseline (P1). Caudate volume did not change significantly following surgery. Dashed grey lines indicate mean and error bars indicate SEM.

#### 4.3.8 Neuropsychological assessment

Neuropsychological testing was performed at an average of  $1.7 \pm 2.0$  years post-operatively in 17 of 26 patients. Our principal goal was to assess pre- and post-operative verbal and figural memory function, since these are widely believed to be hippocampally-mediated (Corkin, 1965; Kimura, 1963; Milner, 1971, 1968). These results are summarized for dominant (n = 8) and non-dominant (n = 9) hemisphere resections in Table 4.3. There was no significant change in verbal memory or figural memory average t-scores for non-dominant

resections or verbal memory average score following dominant resections. There was a statistically significant improvement in figural memory average t-scores following dominant resection (from  $26 \pm 7$  pre-surgery to  $30 \pm 8$ ,  $p = 0.02$ ) which did survive Bonferroni correction for multiple comparisons (i.e.,  $p < 0.05/2$  or  $0.025$ ). There was no significant correlation between any memory score and the delayed contralateral hippocampal volumes. The pre- and post-operative full-scale IQ, verbal comprehension index, perceptual reasoning index and working memory index did not show any statistically significant post-operative changes (Table 4.4).

**Table 4.3: Pre- and Post-operative average memory scores of patients following temporal lobe epilepsy surgery**

Displayed scores are average T-scores  $\pm$  standard deviation.

Score	Dominant Resection (n = 8)			Non-dominant Resection (n = 9)		
	PreOp	PostOp	p-value	PreOp	PostOp	p-value
VM	$38 \pm 8$	$38 \pm 7$	0.84	$41 \pm 9$	$44 \pm 8$	0.16
FM	$26 \pm 7$	$30 \pm 8$	0.02*	$26 \pm 6$	$27 \pm 5$	0.74

VM: verbal memory average score; FM: figural memory average score.

**Table 4.4: Pre- and Post-operative cognitive performance of patients following temporal lobe epilepsy surgery**

Displayed score are average standard scores  $\pm$  standard deviation.

Score	Dominant Resection (n = 8)			Non-dominant Resection (n = 9)		
	PreOp	PostOp	p-value	PreOp	PostOp	p-value
IQ	87 $\pm$ 10	88 $\pm$ 8	0.73	80 $\pm$ 11	83 $\pm$ 10	0.20
VCI	87 $\pm$ 10	84 $\pm$ 9	0.69	81 $\pm$ 9	82 $\pm$ 8	0.60
PRI	96 $\pm$ 9	99 $\pm$ 11	0.45	90 $\pm$ 16	92 $\pm$ 14	0.21
WMI	91 $\pm$ 17	91 $\pm$ 15	0.73	83 $\pm$ 16	83 $\pm$ 17	0.87

IQ: intelligence quotient; VCI: verbal comprehension index; PRI: perceptual reasoning index; WMI: working memory index.

## 4.4 Discussion

Following TLE surgery, we report atrophy of the contralateral, non-resected hippocampus, occurring largely in the hippocampal body with this finding being demonstrated independently in two separate groups (two scan and longitudinal groups). Based on the longitudinal study, atrophy begins immediately post-operatively and continues during the first post-operative week where it then levels off after a sizeable drop of  $\sim$ 12% for whole hippocampus and  $\sim$ 27% for the body. Delayed atrophy was significantly more severe amongst patients who continued to have disabling seizures following surgery, but no significant differences were observed based on surgical approach or side of surgery.

To our knowledge there have been no previous reports examining gray matter changes following TLE surgery with the same degree of temporal resolution, nor have hippocampal sub-regions been specifically studied in the postoperative period. The design of the longitudinal arm of our study did limit

recruitment due to a host of challenges associated with scanning in the immediate post-operative period (e.g. tolerating transfer or scan, inability to perform in-patient research scans on weekends at our institution), which have been described in other studies of this type (Fuerst et al., 2003; Liu et al., 2013). Nevertheless, our study design with imaging at short intervals in the immediate post-operative period allowed us to show, for the first time, that post-operative contralateral hippocampal volume decreases at an estimated rate of 1.3%/day over the first post-operative week (2.9%/day for HBV), stabilizing thereafter but remaining significantly reduced relative to baseline years later.

The earliest published study examining contralateral hippocampal structural changes after TLE surgery did not detect a significant reduction in contralateral hippocampal volumes, though these authors actually compared post-operative 6-month hippocampal volumes from patients to those of healthy controls (rather than to pre-operative volumes in the same patients) (Noulhiane et al., 2006). A more recent study reported the presence of mild contralateral hippocampal atrophy after TLE surgery (n=47 with unilateral MTS) at approximately 4 years of follow-up (Fernandes et al., 2014). Their reported mean post-operative hippocampal atrophy of 3.9% at 4 years post-surgery relative to pre-operative baseline was much smaller than the 12% drop observed in our study. Methodological differences in manual hippocampal volumetry may account for this difference in the degree of reported atrophy at similar post-operative times. Supporting this possibility is the fact that their study reports very large baseline mean hippocampal volumes of 5437 mm<sup>3</sup> 14,

certainly much larger than both the mean hippocampal volume we report (approximately 3400 mm<sup>3</sup>) and typically reported normative data in other studies of hippocampal volume in healthy adults (~3000 - 4000 mm<sup>3</sup>) (Frisoni et al., 2014).

It is not immediately obvious why we observed dramatic, early, and sustained post-operative contralateral hippocampal atrophy. One possible underlying explanation may be deafferentation, which has been suggested to contribute to pre-operative contralesional atrophy in TLE relative to healthy controls (which we also find in this study), because ipsilateral MTS-related cell loss may result in decreased input to contralateral temporal structures (Bonilha et al., 2010). Similarly, in the post-operative state, the removal of tonic commissural excitatory input originating from the resected epileptogenic focus and projecting to contralesional structures may contribute to atrophy. Furthermore, the consequences of deafferentation can be rapid: brain insults such as ischemic stroke or TBI have been demonstrated to induce a robust contralesional plasticity response as early as four days after injury (Andersson et al., 2013; Buga et al., 2008; Kim et al., 2005; Pekna et al., 2012). For example, stereotactic entorhinal cortex injury in mice elicits a rapid, contralateral, glial cell mediated genetic response which is at least partially triggered by deafferentation (Andersson et al., 2013). Longitudinal DTI following TLE surgery also supports our observation that post-operative brain changes occur soon after surgery, with limited progression seen beyond 2-4 months (McDonald et al., 2010; Winston et al., 2014). One DTI study showed changes in FA of the

fornix as early as post-operative day 2 after TLE surgery(Liu et al., 2013). Early decreases in FA are consistent with deafferentation experiments in animal models describing dendritic atrophy within 2 hours of axotomy followed shortly after by cell body atrophy at 48 hours (Deitch and Rubel, 1989). Finally, deafferentation is further supported by our finding of similar atrophy in patients who had ATL or SAH suggesting that specific removal of hippocampal-hippocampal connections may mediate contralateral volume loss.

It is possible that glucocorticoid-mediated hippocampal atrophy—as seen in Major Depressive Disorder (Fink, 2011; Kanner, 2011; Sheline et al., 1996; Vachon-Preseu et al., 2013)—may at least partial contribute to our findings, given the expected cortisol rise due to the post-operative stress response. Unfortunately, we did not routinely measure serum cortisol levels during this study in order to establish a correlation with hippocampal volume. Another potential contributor to early post-operative atrophy may be generalized mechanical deformation following craniotomy or local periventricular atrophy due to egress of CSF. Our finding that the volume of the contralateral caudate nucleus—a periventricular structure—did not change post-surgery, suggests that neither of these explanations is likely.

It is unclear why atrophy in this study is most pronounced in the hippocampal body. Subdivision of the hippocampus into head, body, and tail as in our segmentation protocol is classically based on differences in anatomical connectivity (Duvernoy, 1998). Previous MRI studies examining regional

hippocampal atrophy in preoperative TLE have reached disparate conclusions as to the sub-region most severely affected by the disease, with some showing greater atrophy of the head (Bernasconi, 2003), others favouring volume loss in the body (Bronen et al., 1995) and still others suggesting atrophy is distributed across the entire structure (Quigg et al., 1997). It is certainly possible that different sub-regions may also be differentially affected by TLE surgery, and we speculate that surgery likely results in a greater disconnection of commissural fibers of the hippocampal body compared to those of the head or tail. It is also possible that the chance of outlier measurements for the hippocampal head and tail was greater due to inherent greater measurement error and variability (inter and intra rater reliability was better for the HBV than HHV and HTV- Table 4.2). This combined with the fact that the HHV and HTV together make up more than twice the volume contribution to the whole hippocampus as the hippocampal body may have contributed to less clear trends than for the hippocampal body alone.

Our neuropsychological analysis did not reveal cognitive deficits attributable to the shrinking, non-resected hippocampus. This may have been the result of the positive impact on cognition of post-operative seizure control and/or cessation of AED. In fact, for dominant temporal lobe surgery, there was a significant improvement in figural memory aggregate score. For other tests including IQ, verbal comprehension, perceptual reasoning, working memory and verbal memory aggregate score there was no significant change from preoperative baseline.

This is the first study of patients who have undergone TLE surgery with intensive longitudinal post-operative imaging including a healthy control group with imaging at similar time points. It would have been ideal to include an age-matched, medically-refractory, non-surgical TLE group serially at identical intervals, however this was not feasible as essentially all medically intractable TLE patients with MTS proceeded to surgery. Previous studies have demonstrated that the contralateral hippocampus in unilateral TLE (without surgery) is atrophic relative to healthy controls (Keller and Roberts, 2008) which we confirm with this study. However, longitudinal hippocampal volumetry in this population does not reveal progressive atrophy contralateral to the epileptogenic focus in patients with ongoing disabling seizures in contrast to the ipsilateral hippocampus which does shrink over time (Fuerst et al., 2003).

## **4.5 Conclusions**

In conclusion, we describe the degree and time-course of atrophy of the contralateral hippocampus following TLE surgery for medically refractory epilepsy. Post-operative contralateral hippocampal atrophy begins immediately and progresses significantly over the first post-operative week. Atrophy does not significantly differ by surgical approach or surgical side, but is significantly worse in patients with ongoing post-operative seizures. Neuropsychological testing reveals no significant post-operative deficit attributable to this post-

operative hippocampal atrophy. The observation that patients with ongoing disabling post-operative seizures experience greater hippocampal atrophy, combined with the observation that most of the significant atrophy occurs within the first week after surgery, may in the future allow for predictions of treatment failure based on early post-operative MR-based hippocampal volumetry. Future work will be necessary to describe the influence of TLE surgery on extra-hippocampal and extra-temporal neuroanatomy, and associated downstream effects on seizure and neurocognitive outcome.

# **CHAPTER 5: Longitudinal hippocampal and extra-hippocampal microstructural and macrostructural changes following temporal lobe epilepsy surgery**

**Cameron A. Elliott, Donald W. Gross, B. Matt Wheatley, Christian Beaulieu and Tejas Sankar**

This chapter has been published in part as:

Elliott CA, Gross DW, Wheatley BM, Beaulieu C, Sankar T. **Longitudinal hippocampal and extra-hippocampal microstructural and macrostructural changes following temporal lobe epilepsy surgery.** *Epilepsy Research* 2017.

<https://doi.org/10.1016/j.epilepsyres.2018.01.008>

## **5.1 Introduction**

Surgical treatment of medically refractory TLE with MTS is associated with excellent short term seizure control compared to non-operative treatment (Wiebe et al., 2001). However, seizure control decays over time, such that by 10 years after surgery less than half of patients remain seizure free (de Tisi et al., 2011; McIntosh et al., 2004). Reliable prediction of post-operative seizure outcome remains challenging. Recently, using longitudinally-obtained structural MRI scans in patients undergoing surgery for TLE, early and progressive post-

operative volume loss of the non-resected (i.e., contralateral) hippocampus was identified (C. A. Elliott et al., 2016). This post-operative contralateral hippocampal volume loss was significantly more pronounced amongst patients with seizure recurrence at two years after surgery but was uncorrelated with surgical approach or neurocognitive outcome. At present, the mechanisms underlying this phenomenon of contralateral hippocampal volume loss are not yet known. Whether post-operative atrophy extends beyond the contralateral hippocampus, especially within structures having direct hippocampal connections, is also an open question.

DTI is a quantitative MRI approach which can be used to assess microstructural changes within brain regions of interest. In the hippocampus, DTI is a sensitive measure of microstructure which may provide information which is both complementary and partially overlapping to volumetry. Hippocampal DTI measures depend on the disease process in question and in the case of TLE are related to seizure lateralization (Bernhardt et al., 2016; Ercan et al., 2016; Fellgiebel et al., 2004; Fellgiebel and Yakushev, 2011; Förster et al., 2012; Gaolang Gong et al., 2008; Kantarci, 2014; Kimiwada et al., 2006; Londono et al., 2003; Nazem-Zadeh et al., 2014; Szabo et al., 2014; U. Wiesmann et al., 1999; Yuce et al., 2016). Specifically, the hippocampus ipsilateral to seizure focus is generally found to have increased MD and reduced FA relative to healthy controls (Bernhardt et al., 2016; Salmenpera et al., 2006). TLE DTI findings in the hippocampus contralateral to the seizure focus are more disparate, with some reports showing no difference from healthy controls (Assaf et al., 2003), and

others showing reduced FA alone (Kimiwada et al., 2006; Liacu et al., 2010) or reduced MD alone (Thivard et al., 2005). In one prior study, contralateral hippocampal diffusivity changes were found to be at least partially reversible following either SAH or ATL in 23 patients, based on a single post-operative scan (mean delay 8 months post-operatively) using a coarse region-of-interest drawn on native MD maps (Pfeuty et al., 2011). Interestingly, recovery of hippocampal diffusivity was suggested to correlate with postoperative improvement in measures of verbal and non-verbal memory—thought to be largely hippocampally mediated.

Previous investigations have used DTI extensively to examine longitudinal postoperative microstructural changes in TLE including extrahippocampal structures such as the fornix, cingulum, external capsule, and uncinate fasciculus among others (Concha et al., 2007; Liu et al., 2013; McDonald et al., 2010; Schoene-Bake et al., 2009; Winston et al., 2014; Yogarajah et al., 2010). Although early postoperative scans (within 1-2 months of surgery) are uncommonly acquired, when available, changes in diffusion parameters including in the fornix are evident within this time frame or earlier (Liu et al., 2013; McDonald et al., 2010). However, such postoperative longitudinal analyses have not been extended to include volumetric analysis of the interconnected structures that form part of the circuit of Papez, such as the fornix and mammillary bodies—an important next step given the more direct relationship between MRI-evident volume loss and histologic cell loss (Fuerst et al., 2003;

Watson et al., 1997). It also remains unclear to what extent surgery affects the fornix and mammillary bodies ipsilateral and contralateral to the side of surgery.

The first goal of this study was to characterize the evolution of the microstructural properties of the contralateral, non-operated hippocampus using DTI metrics over time following TLE surgery. The second aim was to characterize the downstream extra-hippocampal changes of volume in the mammillary bodies and fornix. The final objective was to examine the relationship between these measures and clinically relevant outcome variables of seizure and neurocognitive outcome, as well as hippocampal volume.

## **5.2 Methods**

### **5.2.1 Participants**

Our study included 25 patients with medically refractory TLE who underwent surgery at the University of Alberta Hospital from 2005 – 2014 and a group of 12 control subjects of similar age with no history of epilepsy or any other neurologic or psychiatric disease. These subjects make up a subgroup of patients who also had longitudinal DTI taken from a previously published article on hippocampal volumetric change after TLE surgery (C. A. Elliott et al., 2016) and include some of the same TLE subjects investigated using DTI changes of the fornix after surgery (Concha et al., 2010, 2009, 2007, 2005b; Liu et al., 2013). This study was approved by the University of Alberta Health Research Ethics

Board and informed consent was obtained from all subjects. Participants were referred through the comprehensive epilepsy program. Each patient had a standard preoperative assessment including MRI, ictal and inter-ictal long-term video electroencephalography (EEG) and neuropsychological evaluation. On the basis of this evaluation, participants either underwent an ATL (n = 13) or SAH (n = 12) by a single neurosurgeon (author B.M.W.). In our institution, only patients with clear cut MRI evidence of MTS accompanied by corroborative clinical and EEG findings were offered SAH as an option. Subjects had evidence of MTS on MRI (visually detectable hippocampal atrophy, or abnormal hippocampal shape/internal architecture with or without increased signal on T2/FLAIR sequences) (n = 23) and/or surgical pathology (n = 23) with concordant evidence from surface EEG-video telemetry and neuropsychiatric evaluation. One participant had imaging evidence of bilateral MTS (surgical side having more severe visible atrophy than the non-surgical side). Two subjects were reported as non-lesional on MRI but surgical pathology was consistent with MTS. In seven cases, surgery was preceded by bitemporal SEEG evaluation when recommended by the comprehensive epilepsy team on the basis of ambiguous surface telemetry. In all seven cases SEEG demonstrated unilateral temporal ictal onset.

## 5.2.2 Image acquisition

All patients were imaged preoperatively (within 3 months prior to surgery) and postoperatively (mean post-operative interval  $4.3 \pm 3.0$  years, range 0.4 – 8.6). A subset of patients ( $n = 10$ ) were also imaged at frequent intervals on postoperative days 1, 2, 3, 6, 60 and 120 in order to better characterize early postoperative structural brain changes. Sutures were used to close skin instead of staples for high quality MRI scanning in the immediate post-operative period. Non-operated, non-epileptic healthy subjects ( $n = 9$ , average age  $33.3 \pm 13.1$  years old; range 23 – 58; all but one right-hand dominant) were scanned on two separate occasions (average inter-scan interval  $6.9 \pm 2.1$  years; range 3.6 – 9.1). In addition, 3 healthy subjects (20, 22, and 33-years of age, all right-hand dominant) were imaged longitudinally (i.e., at baseline and then in a delayed fashion on days 1, 2, 3, 6 and 60) as controls for the longitudinally imaged surgical subgroup.

All MRI data were acquired on a 1.5T Siemens Sonata (Siemens Healthcare, Erlangen, Germany) using an eight-element head coil at the Peter S. Allen MR Research Centre at the University of Alberta. Whole brain, axial, T1-weighted, 3D-MPRAGE) images were obtained aligned to anterior-posterior commissural line with voxel size 1 mm x 1 mm x 1 mm, TR 1890 ms, TE 4.38 ms, and scan time 6:03 min. DTI was acquired using a dual spin-echo, single shot echo-planar imaging sequence with 52 axial-oblique slices with no inter-slice gap; TR = 6400 ms; TE = 88 ms;  $2 \times 2 \times 2 \text{ mm}^3$  voxel resolution (interpolated to 1

x 1 x 2 mm<sup>3</sup>) along six non-collinear diffusion sensitizing gradient directions with  $b = 1,000$  s/mm<sup>2</sup>; 1  $b = 0$  s/mm<sup>2</sup>; 8 averages for a scan time of 7:26 min.

### **5.2.3 DTI analysis of hippocampus**

Raw data were imported and processed to correct for subject motion, DWI signal drift, eddy current and EPI deformations in ExploreDTI (version 1, Utrecht, The Netherlands)(Leemans et al., 2009). Diffusion metrics of interest included FA, MD, AD, and RD, which were calculated using previously determined hippocampal volumes from high resolution T1-weighted images (C. A. Elliott et al., 2016). Each tracing was used as a ROI following affine co-registration of the DTI to T1-weighted image in the motion correction step above. This is distinct from previously published approaches (Pfeuty et al., 2011; Thivard et al., 2007, 2005), which rely on creating hippocampal regions of interest using non-anatomical (diffusion-weighted) images on which boundaries of the hippocampus are less apparent. Each ROI was verified visually for accurate co-registration to both the DTI raw MD map and the T1-weighted image based on anatomical landmarks, by the same tracer (CAE) who traced the hippocampi originally. DTI analysis was carried out both on the entire hippocampus and on hippocampal anatomical subdivisions (head, body, tail) separately based on previously created ROIs.

## 5.2.4 Volumetric analysis of fornix and mammillary bodies

Volumetric analysis of the fornix and mammillary bodies was performed with manual tracing by a single observer (CAE) using ITK-SNAP software ([www.itksnap.org](http://www.itksnap.org); (Yushkevich et al., 2006). Volumetric analysis of the non-operated (contralateral) hippocampus has already been reported as part of a previously published paper (C. A. Elliott et al., 2016). Anatomical boundaries of the structures of interest were viewed simultaneously in three orthogonal planes on 3D-MPRAGE images (Bonilha et al., 2004a). The observer was blinded to surgical status (i.e., pre-resection, post-resection or control) and time point (i.e., post-operative day) by ensuring that anonymized images of patients were interspersed with controls in random order. Images were zoomed to the structure of interest such that the resection cavity (or lack thereof) was not visible. The fornix and mammillary bodies were traced using a protocol described by Copenhaver and colleagues with previously demonstrated robust inter- and intra-rater reliability (Copenhaver et al., 2006). According to this protocol, the fornix and mammillary bodies are considered to be single rather than paired structures; the protocol instructs the observer to segment both sides of these structures together as one, incorporating midline regions that are fused (including part of the body of the fornix, the hippocampal commissure, and midline mammillary body). As a subanalysis, in order to assess potential laterality of the postoperative changes in these structures, the ipsilateral and contralateral portions were separated by an arbitrary approximation of midline (fornix: line between the longitudinal fissure and the cerebral aqueduct on

coronal slices; mammillary bodies: line between the posterior-most aspect of the interpeduncular fossa and the cerebral aqueduct on axial slices).

### **5.2.5 Seizure and neuropsychological outcome**

Seizure outcome was categorized based on the modified Engel classification (Engel et al., 1993a). Accordingly, seizure outcome was dichotomized as either free from disabling seizures (Engel I; including non-disabling simple partial seizures or auras) or not (Engel >I). Each patient underwent pre- and post-operative tests of verbal and figural memory as well as the Wechsler Adult Intelligence Scale (WAIS; standard scores) with full-scale IQ (IQ), verbal comprehension index (VCI), perceptual reasoning index (PRI) and working memory index (WMI). Verbal memory was summarized using an average (VM) of t-scores (population mean = 50, SD = 10) for recognition memory test for words (immediate recall), verbal paired associates II (delayed), logical memory II (delayed) and Rey auditory verbal learning test (RAVLT; delayed). Figural memory (FM) was summarized as an average of t-scores (population mean = 50, SD = 10) for recognition memory for faces, continuous visual memory test (CVMT; delayed) and Rey-Osterreith complex figure task (CFT; delayed). Pre- and post-operative group means were compared for each of these six scores (IQ, VCI, PRI, WMI, VM and FM) separately for dominant and non-dominant hemisphere surgery. Hemispheric dominance was established based on handedness alone 9/17 (53%), fused dichotic listening test 6/17

(35%), fMRI for language lateralization 1/17 (6%) and/or intracarotid etomidate procedure 3/17 (18%).

## **5.2.6 Statistical analysis**

Statistical analyses were performed with Prism software version 7 (Graphpad) and SPSS 24 (IBM). Fisher's exact test was used for categorical variables. The distribution of all continuous data was first evaluated with the Shapiro-Wilk test of normality. A paired t-test or Wilcoxon matched-pairs signed rank test was used for comparison of two paired groups. An unpaired t-test or Mann-Whitney U-test was used to compare two unpaired groups, the latter when data was not normally distributed. The longitudinally imaged group was analyzed with the non-parametric Friedman test with Dunn's post test to correct for multiple comparisons. Pearson correlation analysis was performed to examine the degree to which preoperative contralateral hippocampal DTI metrics (FA, MD, AD, RD) were related to postoperative contralateral hippocampal volume (expressed as a percentage of each patient's preoperative baseline). Performance on verbal and non-verbal memory tests (as well as an aggregate score for each) was analyzed in a two-way mixed ANOVA, with time relative to surgery (preoperative, postoperative) as a within-subject variable and side of resection relative to dominant (language) hemisphere (dominant, non-dominant) as the independent variables. Correlations between postoperative changes of FA and MD and postoperative neuropsychological

scores were tested with Pearson correlation, except when data were not normally distributed in which case Spearman's nonparametric correlation was used. Partial Pearson correlation was also performed to adjust for the preoperative baseline score on each memory test as well as the length of the delay between pre- and post-operative neuropsychological testing (Baxendale et al., 2008; Pfeuty et al., 2011). Holm-Bonferroni correction was used to correct for multiple comparisons. All tests were conducted as two-tailed, with a type 1 error set at  $\alpha = 0.05$ .

## **5.3 Results**

### **5.3.1 Patient characteristics**

Detailed patient demographic data is displayed in Table 5.1. In summary, the mean age was  $39.3 \pm 10.8$  years (range 19 – 59 years) with 44% (11/25) of patients being male. The control group consisted of 12 subjects of similar age ( $t(25)=1.072$ ,  $p = 0.29$ ; average age  $35 \pm 13$  years old; range 20 – 58); 7/12 being male) with no history of epilepsy or any other neurologic or psychiatric disease.

**Table 5.1: Characteristics of TLE surgery patients**

Characteristics of TLE surgery patients with 1-16 from two scan group and 17-25 from the subset of patients with multiple postoperative scans.

Patient	Age(yrs)/Sex/Handedness	MRI Lesion	Pathology	IPIs	SEEG	Surgery	Duration (yrs)	Outcome (EC)
1	38F/R	MTS	MTS	FS	No	Left SAH	37	IIa
2	33M/R	MTS	MTS	None	No	Left SAH	15	Ia
3	21F/R	MTS	MTS	FS	No	Left SAH	10	IIb
4	31M/R	MTS	MTS	None	No	Left SAH	23	Ia
5	55M/R	NL†	MTS	None	No	Left SAH	15	Ia
6	52F/R	MTS	MTS	FS, TBI	No	Left SAH	13	Ia
7	41F/R	MTS	MTS	TBI	No	Right SAH	27	Ia
8	37F/R	MTS	MTS	None	No	Right SAH	36	IIc
9	37F/R	MTS	MTS	FS	No	Right SAH	29	Ia
10	46F/R	MTS	MTS	FS, TBI	No	Right SAH	32	IIa
11	19M/R	MTS	MTS	FS	No	Left ATL	16	Ia
12	44F/R	NL†	MTS	None	No	Left ATL	6	Ia
13	41F/R	MTS	MTS	None	Yes	Left ATL	18	Ia
14	44M/R	MTS	MTS	M	Yes	Left ATL	43	Ic
15	58F/R	MTS	MTS	None	No	Left ATL	47	IIa
16	36F/L	MTS	MTS	FS, TBI	No	Right ATL	16	Ia
17	34M/R	MTS	MTS	None	No	Left SAH	6	Ia
18	45M/R	MTS	MTS	FS	No	Right SAH	28	Ia
19	54F/R	MTS	MTS	None	Yes	Left ATL	26	Ia
20	24M/L	MTS	MTS	FS, M	No	Left ATL	12	Ia
21	39F/R	MTS	Normal	None	No	Right ATL	20	Ia
22	29M/R	MTS	MTS	None	No	Right ATL	11	Ia
23	59M/R	MTS*	MTS	TBI	Yes	Right ATL	29	Ia
24	31M/R	MTS	FCD**	TBI	Yes	Right ATL	7	IIa
25	36F/R	MTS	MTS	TBI	Yes	Right ATL	24	Ia

ATL: Anterior Temporal Lobectomy; EC: Engel Class; FCD: Focal Cortical Dysplasia; FS: febrile seizure; IPI: Initial Precipitating Incident; L: Left-Hand Dominant; M: Meningitis; NL: non-lesional; R: Right-Hand Dominant; SAH: Selective Amygdalohippocampectomy; TBI: traumatic

brain injury. †Two patients reported as non-lesional (NL) on MRI were found to have evidence of MTS on final pathology. \*Bilateral evidence of MTS on MRI, although right significantly more pronounced than left. \*\*Neocortical (temporal) focal cortical dysplasia type 1C, without MTS

Thirteen patients (52%) underwent an ATL and 12 patients (48%) underwent a SAH. Left-sided surgery occurred in 12/25 (48%). Surgical pathology was consistent with MTS in all but two cases (patient #21, MRI consistent with MTS but pathology reported as normal; patient #24, MRI consistent with MTS but pathology reported as a temporal neocortical FCD; Table 5.1). Two patients (#5 and #12) reported to be non-lesional based on MRI had surgical pathology consistent with MTS.

### **5.3.2 Surgical outcome**

Seizure control across all patients, determined at an average of  $5.2 \pm 3.6$  years following surgery, was as follows: Engel I—76% (IA – 72%, IC – 4%), IIA – 16%, IIB – 4%, IIC – 4%. There was no significant difference between seizure freedom rates by surgical approach (SAH – 67%,  $n = 8/12$ ; ATL – 85%,  $n = 11/13$ ;  $p = 0.38$ ; Fisher’s exact test).

### **5.3.3 Baseline hippocampal diffusion metrics**

There was no significant difference in hippocampal FA, MD, AD, and RD values in healthy subjects between sides (FA left:  $0.18 \pm 0.01$ , right:  $0.19 \pm 0.01$ ; MD left:  $0.97 \pm 0.02 \times 10^{-3} \text{ mm}^2/\text{s}$ , right:  $0.97 \pm 0.03 \times 10^{-3} \text{ mm}^2/\text{s}$ ; AD left:  $1.14 \pm 0.03 \times 10^{-3} \text{ mm}^2/\text{s}$ , right:  $1.16 \pm 0.03 \times 10^{-3} \text{ mm}^2/\text{s}$ ; RD left:  $0.88 \pm 0.03 \times 10^{-3} \text{ mm}^2/\text{s}$ , right:  $0.86 \pm 0.03 \times 10^{-3} \text{ mm}^2/\text{s}$ ). Consequently, in subsequent analyses

left and right control hippocampal diffusion metrics were pooled. At baseline, TLE patients showed significant differences in hippocampal FA, MD, AD and RD between operated (ipsilateral, iHC) and non-operated (contralateral, cHC) sides (FA, iHC:  $0.23 \pm 0.05$ , cHC:  $0.18 \pm 0.02$ ,  $p < 0.001$ ; MD, iHC:  $1.08 \pm 0.18 \times 10^{-3}$  mm<sup>2</sup>/s, cHC:  $0.96 \pm 0.07 \times 10^{-3}$  mm<sup>2</sup>/s,  $p = 0.005$ ; AD, iHC:  $1.32 \pm 0.23 \times 10^{-3}$  mm<sup>2</sup>/s, cHC:  $1.14 \pm 0.06 \times 10^{-3}$  mm<sup>2</sup>/s,  $p < 0.001$ ; RD, iHC:  $0.95 \pm 0.17 \times 10^{-3}$  mm<sup>2</sup>/s, cHC:  $0.87 \pm 0.05 \times 10^{-3}$  mm<sup>2</sup>/s,  $p = 0.03$ ; Figure 5.1). At baseline, hippocampal diffusion metrics were significantly different between TLE patients and controls in the iHC, but not the cHC (FA, iHC:  $0.23 \pm 0.05$ , healthy control  $0.18 \pm 0.01$ ,  $p < 0.001$ ; MD, iHC:  $1.08 \pm 0.18 \times 10^{-3}$  mm<sup>2</sup>/s, healthy control  $0.97 \pm 0.03 \times 10^{-3}$  mm<sup>2</sup>/s,  $p = 0.009$ ; AD, iHC:  $1.32 \pm 0.23 \times 10^{-3}$  mm<sup>2</sup>/s, healthy control  $1.15 \pm 0.03 \times 10^{-3}$  mm<sup>2</sup>/s,  $p = 0.001$ ; RD, iHC:  $0.95 \pm 0.17 \times 10^{-3}$  mm<sup>2</sup>/s, healthy control  $0.88 \pm 0.02 \times 10^{-3}$  mm<sup>2</sup>/s,  $p = 0.04$ ; Figure 5.1). Finally, TLE patients demonstrated no differences in baseline ipsilateral or contralateral hippocampal diffusion metrics when analyzed by seizure outcome.

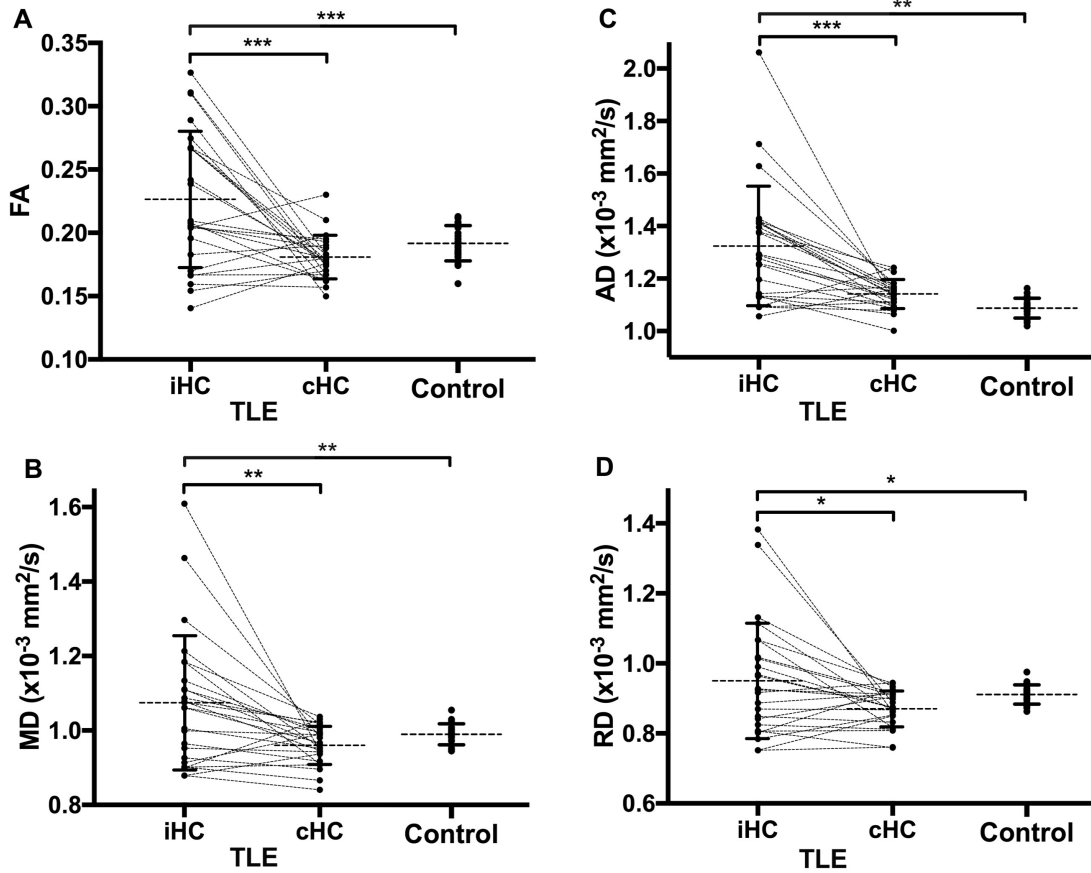


**Figure 5.1: Preoperative diffusion parameters in TLE patients and controls**

Mean preoperative hippocampal diffusion parameters in twenty-five TLE surgery patients (ATL - 13; SAH - 12) for the ipsilateral hippocampus (iHC) versus contralateral hippocampus (cHC) as well as pooled (left and right) hippocampal parameters in twelve healthy controls. The ipsilateral (resected) hippocampus (iHC) showed significant differences in (A) fractional anisotropy (FA), (B) mean diffusivity (MD), (C) axial diffusivity (AD) and (D) radial diffusivity (RD) compared to the contralateral (non-resected) hippocampus (cHC). \* denotes  $p < 0.05$ , \*\*denotes  $p < 0.01$ , \*\*\*denotes  $p < 0.001$ . Error bars denote SD. ATL, anterior temporal lobectomy; SAH, selective amygdalohippocampectomy.

### **5.3.4 Postoperative contralateral hippocampal diffusion metrics**

Postoperatively across all patients ( $n = 25$ ) at an average of  $4.3 \pm 3.0$  years, contralateral hippocampal FA decreased significantly compared to preoperative baseline (preoperative:  $0.18 \pm 0.02$ , postoperative:  $0.17 \pm 0.02$ ;  $Z = -250$ ,  $p = 0.0001$ ; Figure 5.2); by this time contralateral hippocampal FA had also become significantly lower than in healthy controls (postoperative:  $0.17 \pm 0.02$ , control:  $0.18 \pm 0.01$ ;  $t(47) = 3.87$ ,  $p = 0.0003$ ; Figure 5.2). By contrast, postoperative contralateral hippocampal MD increased significantly compared to preoperative baseline (preoperative:  $0.96 \pm 0.05 \times 10^{-3} \text{ mm}^2/\text{s}$ , postoperative:  $0.99 \pm 0.07 \times 10^{-3} \text{ mm}^2/\text{s}$ ;  $p = 0.01$ ; Figure 5.2), though, there was no significant difference between contralateral hippocampal MD in patients after surgery compared to healthy controls (Figure 5.2). No significant change was observed in AD after surgery. Contralateral hippocampal RD did increase significantly following surgery (preoperative:  $0.87 \pm 0.05 \times 10^{-3} \text{ mm}^2/\text{s}$ , postoperative:  $0.91 \pm 0.07 \times 10^{-3} \text{ mm}^2/\text{s}$ ;  $p < 0.0001$ ), though was not significantly different compared to healthy controls. Postoperative DTI metrics were not significantly different between patients free of disabling seizures versus those with ongoing disabling seizures.

In healthy controls, unlike in patients, hippocampal FA and AD did not change over time (inter-scan interval:  $6.9 \pm 2.1$  years). Unexpectedly, in healthy controls, hippocampal MD and RD decreased over time (MD: scan 1,  $0.97 \pm 0.03$

$\times 10^{-3} \text{ mm}^2/\text{s}$ , scan 2,  $0.96 \pm 0.03 \times 10^{-3} \text{ mm}^2/\text{s}$ ,  $t(23) = 4.68$ ,  $p = 0.0001$ ; RD: scan 1,  $0.88 \pm 0.03$ , scan 2  $0.86 \pm 0.03 \times 10^{-3} \text{ mm}^2/\text{s}$ ,  $t(23) = 4.93$ ,  $p < 0.001$ ). Note that this direction of change is opposite to that observed in patients (Figure 5.2).

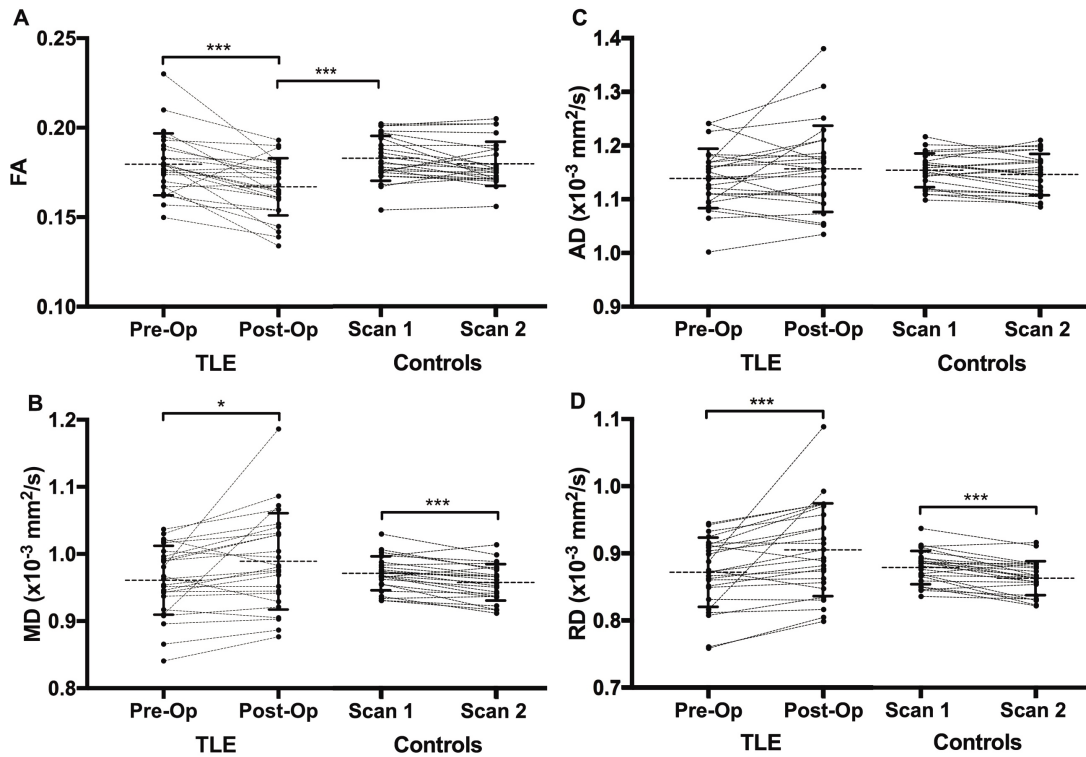


**Figure 5.2: Postoperative changes in hippocampal diffusion compared to healthy controls**

Mean contralateral hippocampal diffusion parameters before and after TLE surgery in twenty-five patients (ATL – 13; SAH – 12) and twelve healthy controls. Mean interval between baseline and follow-up scans was 4.3 years for TLE patients and 6.9 years for healthy controls. In the surgical group, the non-resected hippocampus showed significant (A) postoperative decline in fractional anisotropy (FA), and increase of (B) mean diffusivity (MD) and (D) radial diffusivity (RD) but not (C) axial diffusivity (AD). In the control group, there was no significant change over a similar inter-scan interval in FA or AD (A, C), however, MD and RD decreased significantly over time in the opposite direction compared to TLE surgery patients (B, D). \* denotes  $p < 0.05$ , \*\*\*denotes  $p < 0.001$ . Error bars denote SD. ATL, anterior temporal lobectomy; SAH, selective amygdalohippocampectomy.

Multiple-scan longitudinal analysis (n=9) of postoperative contralateral hippocampal diffusion metrics in TLE patients revealed that progressive changes in FA (decrease), MD (increase), and RD (increase) did not occur until delayed time points (1-3-years; Figure 5.3).

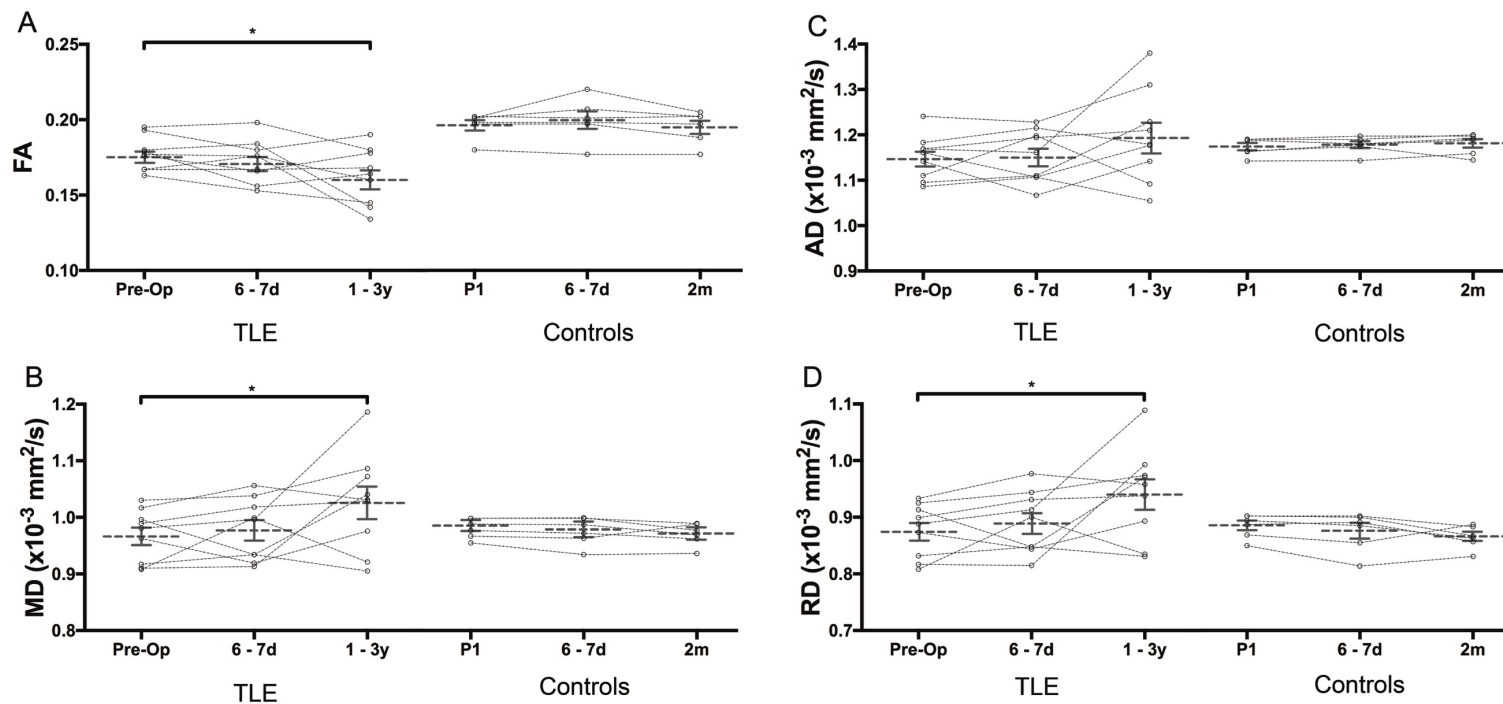


**Figure 5.3: Mean early versus late postoperative contralateral hippocampal diffusion parameters compared with controls**

Mean longitudinal early (6 – 7 days) and delayed (1 – 3 years) individual postoperative contralateral hippocampal diffusion parameters in nine patients compared to before surgery for medically refractory temporal lobe epilepsy (ATL – 7; SAH – 2) and three healthy controls scanned at 6 – 7 days and 2 months after initial scan (P1). Hippocampal diffusion parameters including (A) fractional anisotropy (FA), (B) mean diffusivity (MD), (C) axial diffusivity (AD) and (D) radial diffusivity were not significantly different at 1 week after surgery. Delayed FA, MD and RD (A, B, D) was significantly different compared to preoperatively, as shown, after correction for multiple comparisons (Holm-Bonferroni). \*denotes  $p < 0.05$ , \*\*denotes  $p < 0.01$ . Error bars denote SEM. ATL, anterior temporal lobectomy; SAH, selective amygdalohippocampectomy.

When looking at hippocampal subdivisions, postoperative FA was significantly lower than preoperative for the hippocampal head ( $p = 0.0009$ ) and body ( $p = 0.002$ ) but not tail ( $p = 0.13$ ; Figure 5.4). Also, postoperative hippocampal FA was significantly lower than in healthy subjects across all subdivisions (head,  $p = 0.02$ ; body,  $p = 0.048$ ; tail,  $p = 0.005$ ). Postoperative hippocampal MD, AD and RD were not significantly different for any subdivision compared to before surgery or healthy subjects.

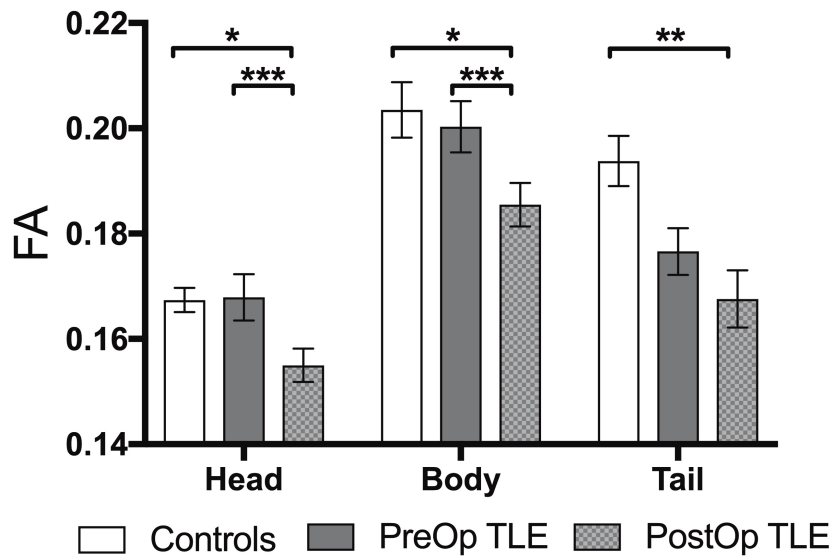


**Figure 5.4: Sub-regional hippocampal fractional anisotropy for before and after TLE surgery as well as in healthy controls**

Mean fractional anisotropy (FA) values across contralateral hippocampal subdivisions (head, body, tail) pre- and post-operatively in 25 patients treated surgically (ATL - 13; SAH - 12) scanned on average 4.3 years after surgery as well as in healthy controls (12). Mean postoperative FA values are significantly lower across all subdivisions relative to healthy controls (head,  $p = 0.02$ ; body,  $p = 0.048$ ; tail,  $p = 0.005$ ) and are significantly lower compared to preoperative values in the hippocampal head ( $p = 0.0009$ ) and body ( $p = 0.002$ ) but not tail ( $p = 0.13$ ). P-values Holm-Bonferroni adjusted for multiple comparisons. Error bars

denote SEM. ATL, anterior temporal lobectomy; SAH, selective amygdalohippocampectomy.

### **5.3.5 Relationship between hippocampal diffusion metrics and hippocampal volume**

There was a negative correlation between mean preoperative contralateral hippocampal MD and delayed postoperative contralateral hippocampal volume expressed as a percentage of each subjects' preoperative baseline ( $r(23) = -0.43$ ,  $p = 0.03$ ; Figure 5.5). This negative correlation was also seen between mean preoperative contralateral hippocampal RD and delayed postoperative contralateral hippocampal volume ( $r(23) = -0.42$ ,  $p = 0.03$ ; Figure 5.5). There was no correlation between either mean preoperative contralateral hippocampal FA or AD and delayed contralateral hippocampal volume. There was no correlation between preoperative hippocampal diffusion metrics on the resected (ipsilateral) side and postoperative contralateral hippocampal volume.

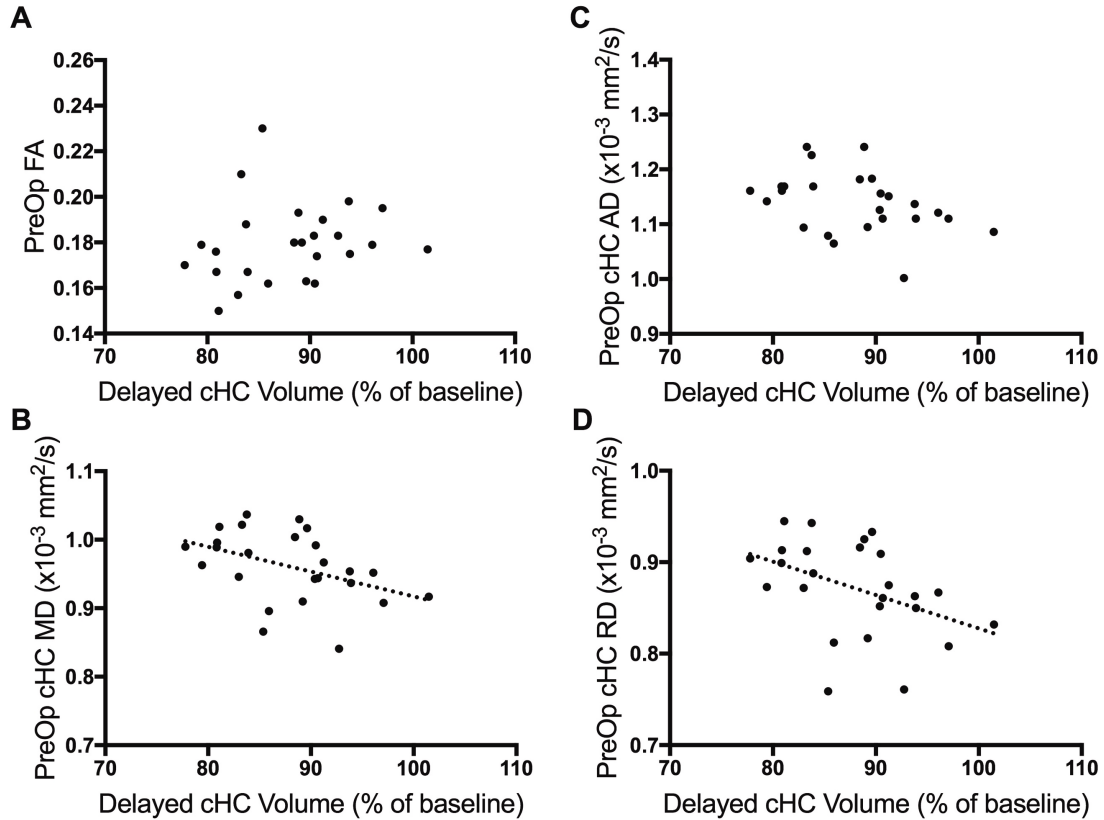


**Figure 5.5: Correlation between preoperative contralateral hippocampal diffusion metrics and delayed postoperative hippocampal volume**

Correlation between preoperative contralateral hippocampal (cHC) diffusion metrics and delayed postoperative hippocampal volume ( $4.3 \pm 3.0$  years post-surgery), expressed as a percentage of baseline for each subject. (A) Fractional anisotropy (FA) is not correlated with delayed postoperative cHC volume ( $r(23) = 0.19$ ,  $p = 0.36$ ). (B) Mean diffusivity (MD) is negative correlated with delayed postoperative cHC volume ( $r(23) = -0.43$ ,  $p = 0.03$ ). (C) Axial diffusivity (AD) is not correlated with delayed postoperative cHC volume ( $r(23) = -0.39$ ,  $p = 0.06$ ). (D) Radial diffusivity (RD) is negatively correlated with delayed postoperative cHC volume ( $r(23) = -0.42$ ,  $p = 0.03$ ).

### 5.3.6 Mammillary body volume loss

After surgery, there was statistically significant volume loss in the mammillary bodies (preoperative:  $117 \pm 22 \text{ mm}^3$ ; postoperative:  $76 \pm 15 \text{ mm}^3$ ;

$t(24) = 10.0, p < 0.0001$ ; Figure 5.6) with 35% mean volume loss relative to baseline.

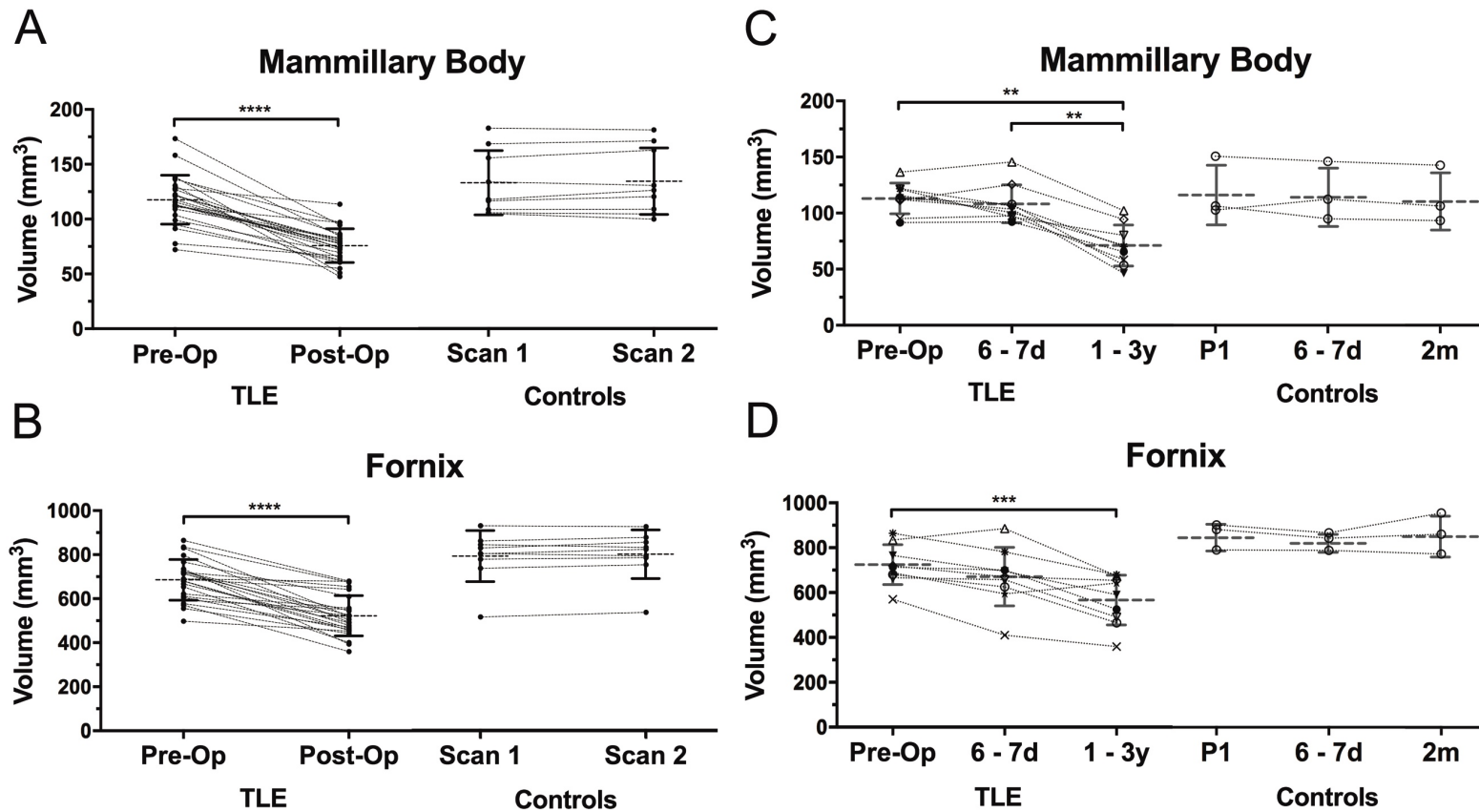


**Figure 5.6: Mammillary body and fornix volume before and after TLE surgery as well as in healthy controls**

Mean mammillary body and fornix volume (mm<sup>3</sup>) pre- and post-operatively in twenty-five patients with medically refractory TLE treated surgically (ATL - 13; SAH - 12; mean post-operative interval  $4.3 \pm 3.0$  years) and twelve healthy controls (mean inter-scan interval  $6.9 \pm 2.1$  years). There was statistically significant post-operative volume loss observed for the mammillary bodies (A) by 36% and the fornix (B) by 24% compared to baseline, in contrast to healthy controls (A, B) with no significant

volume loss over time. A subset of these TLE patients (n = 9; ATL = 7; SAH) were also scanned both early (6 – 7 days) and delayed (1-3 years) as well as three healthy controls scanned at 6 -7 days and 2 months after initial scan (P1). In the multi-scan TLE group there was volume loss in both the mammillary bodies (C) by 37% and the fornix (D) by 22% which was statistically significant only at delayed scan time (1 – 3 years) and not at early (6 – 7 day) scan. Error bars denote SD. \*\*denotes  $p < 0.01$ , \*\*\*denotes  $p < 0.001$ , \*\*\*\*denotes  $p < 0.0001$ . ATL, anterior temporal lobectomy; SAH, selective amygdalohippocampectomy.

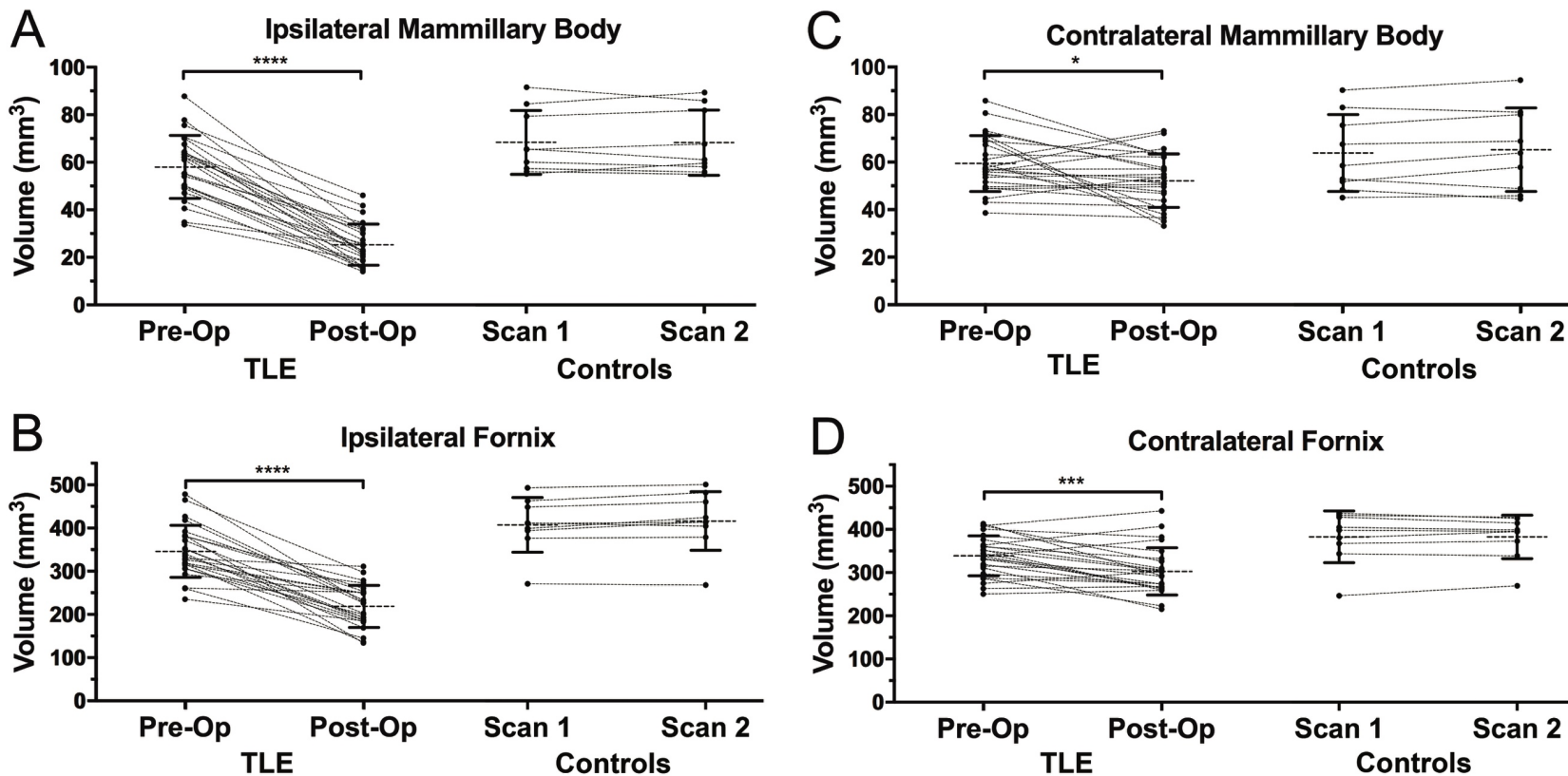


**Figure 5.7: Ipsilateral versus contralateral mammillary body and fornix volume before and after TLE surgery as well as in healthy controls**

Mean ipsilateral and contralateral mammillary body and fornix volume relative to side of resection (mm<sup>3</sup>) pre- and post-operatively in twenty-five patients with medically refractory TLE treated surgically (ATL – 13; SAH – 12; mean post-operative interval  $4.3 \pm 3.0$  years) and twelve healthy controls (mean inter-scan interval  $6.9 \pm 2.1$  years). There was statistically significant post-operative volume loss for both the ipsilateral mammillary body (A) by 56% and the contralateral mammillary

body (C) by 12%. There was statistically significant post-operative volume loss for both the ipsilateral fornix (B) by 37% and the contralateral fornix (D) by 11%. In contrast, there was no significant volume loss in healthy control subjects scanned over a similar inter-scan interval. Error bars denote SD. \*denotes  $p < 0.05$ , \*\*\*denotes  $p < 0.001$ , \*\*\*\*denotes  $p < 0.0001$ . ATL, anterior temporal lobectomy; SAH, selective amygdalohippocampectomy.

Postoperative mammillary body volume loss was more pronounced ipsilateral to the resection cavity, though it did occur bilaterally (ipsilateral volume loss 56%,  $t(24) = 13.5$ ,  $p < 0.0001$ ; contralateral 12%,  $t(24) = 2.6$ ,  $p = 0.02$ , Figure 5.7). In contrast, mammillary body volumes were not significantly different over time in the healthy control group ( $n = 9$ ) with similar inter-scan interval (scan 1:  $132 \pm 29 \text{ mm}^3$ , scan 2:  $134 \pm 30 \text{ mm}^3$ ,  $p = 0.43$ , Figure 5.6). A non-parametric Friedman test of differences among repeated measures in the longitudinally scanned subgroup ( $n = 9$ ; ATL = 7; SAH = 2) revealed a statistically significant effect of time after surgery on mammillary body volume ( $X^2(2) = 15.9$ ,  $p < 0.0001$ ; Figure 5.6). The effect of time was not significant until the most delayed scan when significant mammillary body volume loss between baseline and most delayed scan became apparent (1 – 3 years;  $p = 0.0003$ ; Figure 5.6). In this subgroup, time after surgery had a statistically significant effect on mammillary body volume only for the ipsilateral, but not the contralateral mammillary body (ipsilateral:  $X^2(2) = 14.9$ ,  $p < 0.0001$ ; contralateral:  $X^2(2) = 4.2$ ,  $p = 0.15$ ; data not shown in figure). There was no statistically significant difference in degree of mammillary body volume loss when analyzed by surgical approach (SAH:  $34 \pm 10\%$  versus ATL:  $38 \pm 15\%$ ,  $p = 0.46$ ). Finally, there was no statistically significant difference in the degree of mammillary body volume loss when analyzed by seizure outcome (Engel 1:  $36 \pm 14\%$  versus Engel > 1:  $33 \pm 15\%$ ,  $p = 0.56$ , Mann-Whitney test). There was no significant correlation between postoperative change in mammillary body volume (ipsilateral, contralateral or combined) and pre- or post-operative hippocampal DTI metrics.

### 5.3.7 Fornix volume loss

After surgery, there was statistically significant volume loss in the fornix (preoperative:  $685 \pm 92 \text{ mm}^3$ ; postoperative:  $522 \pm 92 \text{ mm}^3$ ;  $t(24) = 9.0$ ,  $p < 0.0001$ ; Figure 5.6) with 24% mean volume loss relative to baseline. Postoperative fornix volume loss was more pronounced ipsilateral to the resection cavity, though it did occur bilaterally (ipsilateral volume loss 37%,  $t(24) = 9.8$ ,  $p < 0.0001$ ; contralateral 12%,  $t(24) = 4.0$ ,  $p < 0.001$ ). In contrast, fornix volumes were not significantly different over time in the healthy control group ( $n = 9$ ) with similar inter-scan interval (scan 1:  $790 \pm 116 \text{ mm}^3$ , scan 1:  $799 \pm 111 \text{ mm}^3$ ,  $p = 0.11$ , Figure 5.6). A non-parametric Friedman test of differences among repeated measures in the longitudinally scanned subgroup ( $n = 9$ ; ATL = 7; SAH = 2) demonstrated a statistically significant effect of time after surgery on fornix volume ( $X^2(2) = 14.2$ ,  $p < 0.0001$ ; Figure 5.6). The effect of time was not significant until the most delayed scan where significant fornix volume loss between baseline and most delayed scan became apparent (1 – 3 years;  $p = 0.0005$ ; Figure 5.6). In this subgroup, time after surgery had a statistically significant effect on fornix volume only for the ipsilateral, but not the contralateral fornix (ipsilateral:  $X^2(2) = 14.9$ ,  $p < 0.0001$ ; contralateral:  $X^2(2) = 1.6$ ,  $p = 0.57$ ; data not shown in figure). There was no statistically significant difference in degree of fornix volume loss when analyzed by surgical approach (SAH:  $27 \pm 13\%$  versus ATL:  $21 \pm 11\%$ ,  $p = 0.20$ ). Finally, there was no statistically significant difference in the degree of fornix volume loss when analyzed by seizure outcome (Engel 1:  $23 \pm 12\%$  versus Engel > 1:  $28 \pm 10\%$ ,  $p =$

0.33, Mann-Whitney test). There was no significant correlation between postoperative change in fornix volume (ipsilateral, contralateral or combined) and pre- or post-operative hippocampal DTI metrics.

### **5.3.8 Relationship to neuropsychological outcome**

Neuropsychological testing was performed at an average of  $1.7 \pm 2.0$  years post-operatively in 17 of 25 patients ( $n = 8$  dominant temporal lobe surgery). A two-way ANOVA was run on this sample to examine the effect of surgery and side of resection (defined with respect to language laterality, i.e. dominant versus non-dominant) on each measure of verbal and non-verbal memory. Surgery did not result in a significant postoperative difference for any memory score. Side of resection also did not significantly affect memory scores except for the Rey auditory verbal learning test (RAVLT;  $F(1, 15) = 10.1$ ,  $p = 0.006$ ) and the continuous visual memory test (CVMT;  $F(1, 15) = 6.2$ ,  $p = 0.03$ ). RAVLT scores were higher for non-dominant resections both pre- ( $38 \pm 9$ ; mean  $\pm$  SD) and post-operatively ( $42 \pm 12$ ) than dominant resections (preop:  $26 \pm 10$ ; postop:  $29 \pm 6$ ), while CVMT scores were higher for dominant resections both pre- ( $37 \pm 11$ ) and post-operatively ( $50 \pm 11$ ) than non-dominant resections (preop:  $30 \pm 17$ ; postop:  $29 \pm 14$ ). When the four verbal (RMW, LM, VPA and RAVLT) or the three non-verbal (RMF, CVMT, CFT) memory scores were averaged there was no significant difference in the number of patients whose

performance improved after surgery on either verbal or non-verbal average score following dominant or non-dominant surgery.

Given the above differences between patients who underwent dominant versus non-dominant resections, separate scatter plots of postoperative change in the various memory tests (t-scores) versus postoperative change in FA or MD were analyzed using Pearson correlation (or Spearman correlation, where appropriate; Figures 5.8 and 5.9). After accounting for multiple comparisons (9), there was no significant correlation between postoperative change of FA or MD in the contralateral hippocampus and performance on any verbal and non-verbal memory tests. Partial correlation between the postoperative change in performance on each memory test and postoperative change in FA or MD while adjusting for the delay between preoperative and postoperative neuropsychological testing and preoperative baseline performance on each test similarly did not reveal any significant correlation. There was no significant correlation between postoperative change in mammillary body or fornix volume (ipsilateral, contralateral or combined) and any of the neuropsychological tests or aggregate verbal or non-verbal scores.

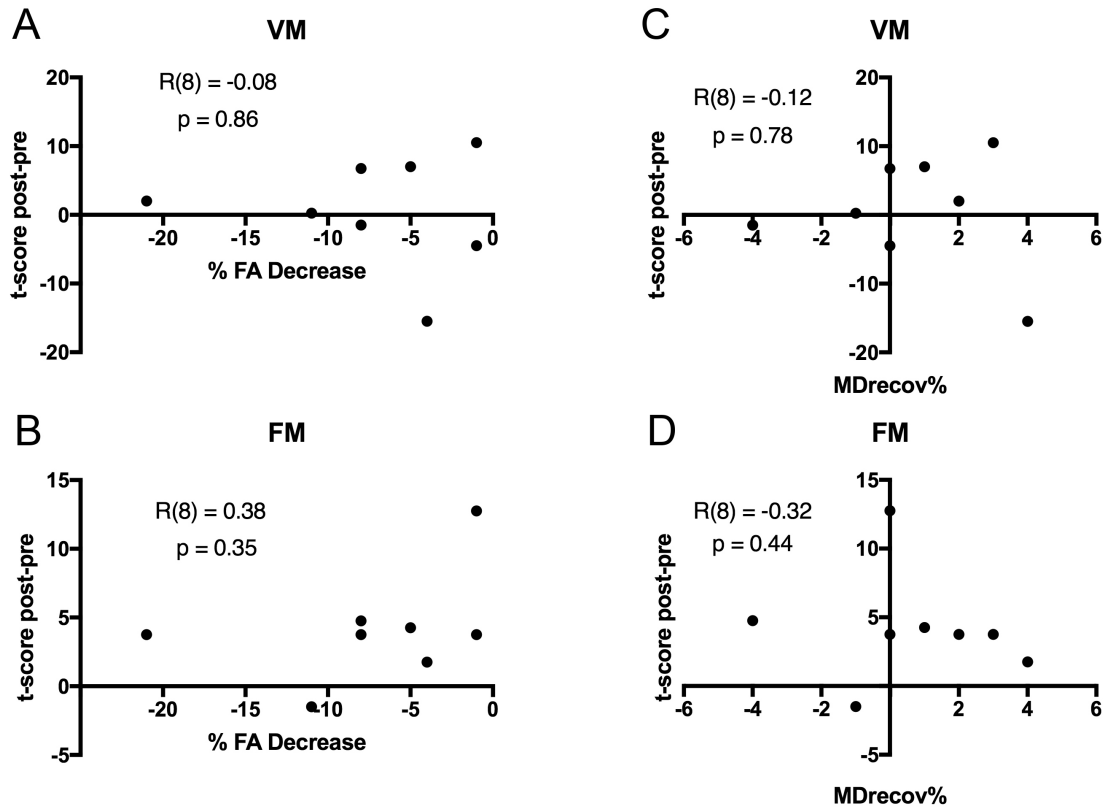


**Figure 5.8: Neuropsychological performance change plotted against diffusion parameter change for dominant resections**

Scatter plots of  $t\text{-scores}_{\text{pre-post}}$  against the postoperative decline in fractional anisotropy (FA) relative to baseline (% FA Decrease; A-B) and against the postoperative increase in mean diffusivity (MD) relative to baseline (MDrecov%; C-D) in the contralateral (non-resected) hippocampus for the dominant resections ( $n = 8$ , ATL – 2, SAH – 6). Correlation coefficients  $R(df)$  and  $p$ -values are presented on each plot (after correction for multiple comparisons). Verbal memory was summarized using an average (VM) of  $t$ -scores (population mean = 50, SD = 10) for recognition memory test for words (immediate recall; RMW), logical memory II (delayed; LM), verbal paired associates II (delayed, VPA), and Rey auditory verbal learning test (delayed, RAVLT). Figural memory was summarized as an average (FM) of  $t$ -scores for recognition memory for faces (RMF), continuous visual memory test (delayed, CVMT) and Rey-Osterreith complex figure (delayed, CFT). ATL, anterior temporal lobectomy; SAH, selective amygdalohippampectomy.

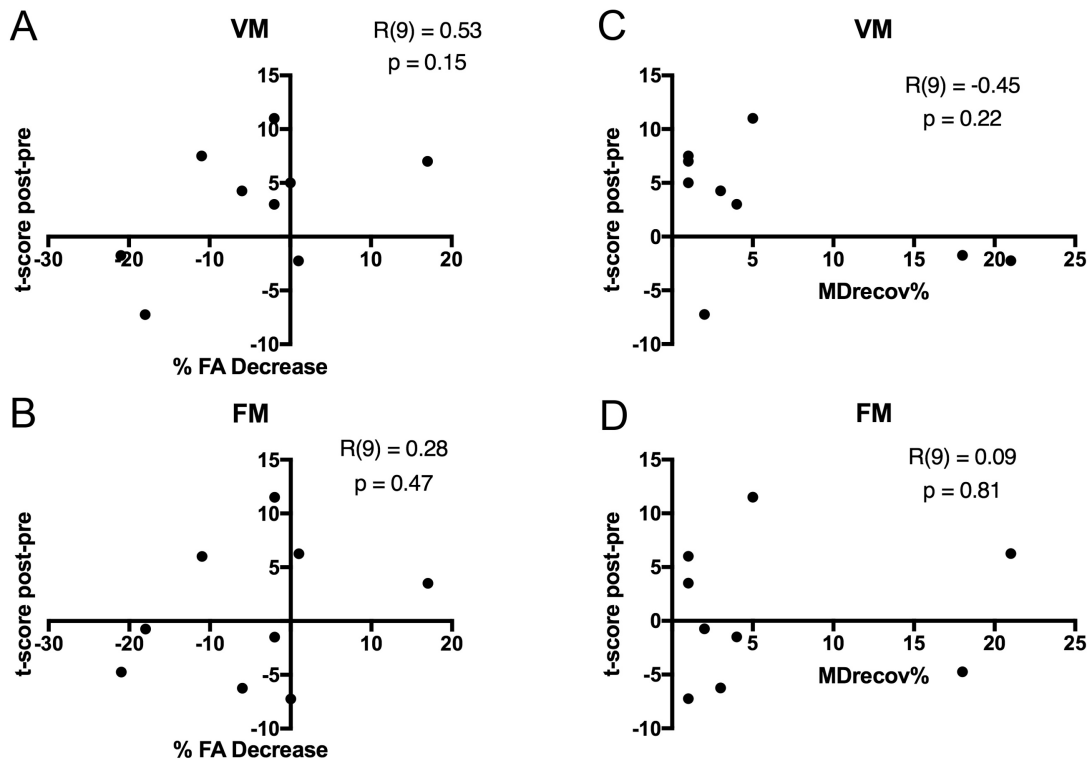


**Figure 5.9: Neuropsychological performance change plotted against diffusion parameter change for non-dominant resections**

Scatter plots of  $t\text{-scores}_{\text{pre-post}}$  against the postoperative decline in fractional anisotropy (FA) relative to baseline (% FA Decrease; A-B) and against the postoperative increase in mean diffusivity (MD) relative to baseline (MDrecov%; C-D) in the contralateral (non-resected) hippocampus for the non-dominant resections (n = 9, ATL = 6, SAH = 3). Correlation coefficients  $R(df)$  and p-values are presented on each plot (after correction for multiple comparisons). Verbal memory was summarized using an average (VM) of t-scores (population mean = 50, SD = 10) for recognition memory test for words (immediate recall; RMW), logical memory II (delayed; LM), verbal paired associates II (delayed, VPA), and Rey auditory verbal learning test (delayed, RAVLT). Figural memory was summarized as an average (FM) of t-scores for recognition memory for faces (RMF), continuous visual memory test (delayed, CVMT) and Rey-Osterreith complex figure (delayed, CFT). ATL, anterior temporal lobectomy; SAH, selective amygdalohippocampectomy.

## 5.4 Discussion

Following TLE surgery, we report significant changes in diffusion metrics within the non-resected, contralateral hippocampus, specifically: 1) reduction of FA; 2) increase of MD; and 3) increase of RD. In contrast to our previously reported changes in hippocampal volume, on longitudinal postoperative imaging these diffusion changes take time to develop, and are not significant at the group level until a delayed time point (1-3 years postoperatively). These diffusion changes are accompanied by delayed limbic circuit structural changes involving bilateral mammillary body and fornix volume loss, though degree of volume loss was not directly correlated with degree of change in diffusion metrics. Neuropsychological analysis revealed that side of resection was the most important predictor of superior preoperative memory performance on tasks attributable to the contralateral hippocampus and there was no correlation between postoperative change in hippocampal diffusion metrics and memory scores. Finally, the degree of postoperative change in hippocampal DTI parameters, mammillary body volume, or fornix volume was not observed to vary significantly based on seizure control.

DTI has been extensively investigated in TLE, revealing global white matter changes which are more severe in the hemisphere and temporal lobe ipsilateral to seizure focus (Otte et al., 2012). Hippocampal DTI is a sensitive measure of tissue microarchitecture as previously demonstrated in a variety of

clinical settings including learning (Sagi et al., 2012), status epilepticus (Förster et al., 2012), cognitive impairment in Alzheimer disease (Fellgiebel et al., 2004; Hong et al., 2010; Müller et al., 2005; Ostojic et al., 2015; Pereira et al., 2014), and schizophrenia (Chiapponi et al., 2014). In TLE, DTI provides information distinct from volumetry without clear correlation between diffusivity changes and the severity of hippocampal atrophy (Düzel et al., 2004; Londono et al., 2003; U. Wiesmann et al., 1999) or disease duration (Thivard et al., 2005).

Diffusion measures taken from non-anatomical ROIs of the hippocampus—as selected on diffusion images—have been reported to predict disease lateralization in some TLE patients, with the hippocampus ipsilateral to the seizure focus reported to have elevated MD and reduced FA (Assaf et al., 2003; Bernhardt et al., 2016; Hugg et al., 1999; Pereira et al., 2006; Salmenpera et al., 2006). However, Ercan et al. found that non-anatomical ROI-based hippocampal DTI measurements are inferior to volumetry for disease lateralization (Ercan et al., 2016). Indeed, these authors found significant ipsilateral hippocampal MD elevation compared to healthy controls in only a minority (28%) of unilateral TLE patients, with significant FA reduction in 57% of unilateral right TLE patients and 28% of unilateral left TLE. Overall, the DTI properties of the hippocampus contralateral to the seizure focus in TLE appear to be more variable, ranging from equivalent to healthy controls (Assaf et al., 2003; Düzel et al., 2004; Ercan et al., 2016; Hugg et al., 1999; Kantarci et al., 2002; U. Wiesmann et al., 1999), to an isolated decrease in FA (Ercan et al.,

2016; Kimiwada et al., 2006; Liacu et al., 2010) to an isolated decrease in MD (Londono et al., 2003; Thivard et al., 2005).

To our knowledge there have been no previous studies examining the trajectory of changes in hippocampal diffusion parameters following TLE surgery. Moreover, our technique—in which DTI metrics are computed within anatomically accurate, three-dimensional, whole-hippocampal volumes of interest based on high-resolution T1-weighted structural MRI scans—is novel. Previous studies have described postoperative hippocampal DTI metrics at a single postoperative time point using regions of interest drawn on non-anatomical, lower resolution diffusion images (Pfeuty et al., 2011; Thivard et al., 2007, 2005). These authors report robust recovery of hippocampal MD, without significant change in FA, in TLE surgery patients with MRI-diagnosed unilateral HS scanned 8 months after surgery (range: 2 – 20 months). In a subsequent study they report a significant positive correlation between recovery in MD and improved performance on auditory verbal span (but not abstract word learning) and aggie figure learning (but not visual-spatial span) in a subsample following right or left temporal lobectomy (Pfeuty et al., 2011). Methodological differences in DTI measurement technique, neuropsychological testing and statistical handling of multiple comparisons may account for the observed differences between our data—which showed no relationship between changes in diffusion metrics and neuropsychological outcomes—and these prior results.

Our results confirm significant preoperative elevation of MD in TLE of the hippocampus ipsilateral to the seizure focus relative to both the contralateral hippocampus and to measures in healthy controls (Assaf et al., 2003; Bernhardt et al., 2016; Hugg et al., 1999; Pereira et al., 2006; Salmenpera et al., 2006). However, we also find significant elevation of FA, AD and RD in the ipsilateral hippocampus in TLE patients prior to surgery relative to both the contralateral hippocampus and healthy controls. This finding of significant elevation of FA prior to surgery in the ipsilateral hippocampus differs from previous reports which relied on measures of hippocampal diffusion using ROIs drawn on non-anatomical (diffusion) images and reflect only part of the entire hippocampus. Our findings do confirm significant postoperative increase in contralateral hippocampal MD following TLE surgery (Pfeuty et al., 2011; Thivard et al., 2007), which does not become statistically significant until the most delayed postoperative scanning time point in our study (1-3 years). In addition, we observe significant postoperative decline of contralateral hippocampal FA by the most delayed scan point. These postoperative hippocampal diffusion changes are contrasted by unexpected decreases in MD and RD and stable FA and AD in healthy subjects scanned over a similar time interval on the same scanner. We are unclear what might account for these changes in MD and RD (which are opposite in direction to the observed postoperative changes in MD/RD in TLE patients) as changes in whole hippocampal diffusion metrics over the life span in healthy subjects have not, to our knowledge, been described.

The contrast in timing of hippocampal volume changes (first week post op) versus DTI changes (observed in a more delayed fashion) may provide some insight into underlying mechanistic processes occurring after temporal lobe surgery. Given the observation that dramatic reductions in volume are observed in the contralateral hippocampus by one week post op (Elliott et al. 2016) without accompanying changes in either MD or FA, it is unlikely that significant fluid shifts (for example, due to dehydration) account for the observed atrophy. Additionally, the observation of late increase in MD, decrease in FA and increase in RD suggests that remodeling of the hippocampus may be occurring after the first week. Previous reports have found evidence of reduced MD and elevated FA are associated with cytotoxic edema (Grossman et al., 2010; Kimura-Ohba et al., 2016; Veeramuthu et al., 2015). Accordingly, the delayed postoperative increases in MD and decrease in FA we observed may suggest that surgery is accompanied by resolution of pre-existing contralateral hippocampal cytotoxic edema, perhaps due to cessation of clinical (or subclinical) electrical bombardment of the contralateral hippocampus by fornical commissural excitatory input from the recently resected, epileptogenic hippocampus. That being said, we also found that the postoperative increase in MD is accompanied by an overshoot in FA normalization, such that postoperative FA actually becomes depressed relative to both baseline and to healthy control values. We propose that this may reflect another mechanism at play. Specifically, we speculate that deafferentation resulting from the surgical removal of hippocampal-hippocampal commissural input results in cellular rearrangement

due to neuronal loss or gliosis and occurs in a more delayed fashion. Interestingly, postoperative fornix and mammillary body volume loss, unlike hippocampal volume loss, do not occur until 1 – 3 years after surgery, suggesting that it may be a combination of both seizure cessation and deafferentation which account for postoperative, circuit-wide changes.

It is important to acknowledge limitations of this study. Firstly, we were not able to include a non-surgical, medically-refractory TLE group for comparison. Secondly, the sample size in our longitudinally scanned group was limited to nine participants as it was quite difficult to recruit subjects willing to participate in early postoperative scanning. Thirdly, the surgical arm included patients who underwent either an ATL (n = 13) or SAH (n = 12); the surgical approach chosen may have different effects on the structural changes measured. Finally, considering the relatively small size of the hippocampus, our DTI results are likely affected by partial volume effects due to the spatial resolution of these scans being 2mm isotropic. Future work at higher MRI field strength with better spatial resolution and more diffusion directions may help to mitigate these technical concerns.

## **5.5 Conclusions**

In conclusion, we show that following TLE surgery, there are significant changes in contralateral hippocampal microstructure, as well as downstream

macrostructural changes in mammillary body and fornix volume. These changes do not become significant until 1-3 years after surgery. The degree of postoperative change in these parameters was not correlated with postoperative seizure outcome nor, as has previously been reported, post-operative memory performance. Further work is necessary to characterize the full extent and clinical significance of structural brain changes occurring after epilepsy surgery.

# **CHAPTER 6: Intraoperative acquisition of diffusion tensor imaging in cranial intraaxial neurosurgery: readout-segmented versus standard single-shot DTI**

**Cameron A. Elliott, Hayden Danyluk, Keith E. Aronyk, Karolyn Au, Donald W. Gross, B. Matt Wheatley, Christian Beaulieu and Tejas Sankar**

This chapter has not yet been submitted for publication.

## **6.1 Introduction**

High-field intraoperative magnetic resonance imaging (iMRI) is increasingly utilized in neurosurgery for intraaxial lesions. The utility of iMRI to improve extent of resection of target tissue has been shown in enhancing (Hatiboglu et al., 2009; Napolitano et al., 2014; Senft et al., 2011) and non-enhancing gliomas (Coburger et al., 2016; Mohammadi et al., 2014; Wu et al., 2014), drug-resistant epilepsy (Kim et al., 2017; Nowell et al., 2017), certain pediatric tumors (Choudhri et al., 2014b; Shah et al., 2012), and pituitary/skull base lesions (Coburger et al., 2014; Sylvester et al., 2015). iMRI contributes to maximal safe resection of target tissue by updating neuronavigational systems with intraoperatively acquired MRI data—collected in surgical position with the cranium and surgical cavity still open—allowing assessment of residual target tissue and its proximity to adjacent non-target tissue, while compensating for

surgically-induced brain deformation (“brain shift”). Brain shift has been shown to be a significant, continuous, unpredictable, diffuse process that can result in anatomical deviation relative to preoperative position of up to 2 cm in either an inward or outward direction (Dorward et al., 1998; Hartkens et al., 2003; Hill et al., 1998; Jacobsohn and Roberts, 1999; Maurer et al., 1998; Nabavi et al., 2001; Nauta and Bonnen, 1998; C Nimsky et al., 2005a). Accurate brain-shift resistant neuronavigational data is particularly important for surgical targets which may be otherwise difficult to identify during surgery, such as diffusely infiltrating gliomas or epileptogenic tissue which may be visually and palpably indistinguishable from healthy brain. Brain-shift resistant neuronavigational information is also important for the accurate delineation of adjacent non-target tissue, which includes white matter tracts that are not readily apparent on standard anatomical MR images (e.g., T1/MPRAGE or T2/FLAIR).

Deterministic, diffusion-tensor imaging (DTI) white matter tractography is commonly used in neurosurgical practice, but is largely limited to the preoperative setting. Spatial distortions and image degradation caused by susceptibility artifact encountered when conventional single-shot echo-planar imaging DTI (SS-DTI) are significant particularly when acquired intraoperatively (SS-iDTI) in surgical position with an open cavity (Irfanoglu et al., 2012; Potgieser et al., 2014). Geometric distortions due to susceptibility artifact can significantly impact DTI-tract reconstructions even in preoperative SS-DTI data such that modelled tracts may terminate in different sulci entirely with spatial inaccuracies ranging from 1.2 – 5.9 mm (median: 2.1 mm) (Albi et al., 2018;

Irfanoglu et al., 2012; Treiber et al., 2016). Although, SS-DTI may mitigate motion-related artifact (generally not an issue for intraoperatively acquired images), it is known to be particularly prone to susceptibility artifact, particularly in areas of the brain where tissue boundaries (e.g. air-tissue interfaces) exist, such as the orbitofrontal cortex and anterior temporal poles which are close to the air-filled frontal and paranasal bony sinuses (Hutton et al., 2002).

Previous investigations of iDTI utilizing SS-DTI are mostly conducted on lower field iMRI (0.3 – 1.5 Tesla) and largely limited to reconstructions of the corticospinal tract (CSpT)(Maesawa et al., 2010; C Nimsky et al., 2005b, 2005a, 2005c; Ostrý et al., 2013; Ozawa et al., 2009; Prabhu et al., 2011; Romano et al., 2011; Shahar et al., 2014). Some reports specifically describe the rationale for limiting analysis to the CSpT, based on its large size, deep location (distant from susceptibility artifact related to the open cranium) and relatively straightforward region of interest-based reconstruction (Romano et al., 2011). These authors show that the intraoperative tract shift of the CSpT relative to its preoperative location ranged from 9.7 mm inward (hereafter indicated by a negative sign, mean inward of  $-5.2 \pm 2.5$  mm) to 11 mm outward (mean outward of  $5.5 \pm 2.4$  mm) in a 1.5-Tesla SS-iDTI study of 20 patients with intraaxial tumor resections (Romano et al., 2011). Another SS-iDTI study at 1.5-Tesla of supratentorial glioma resections in 37 patients identified unpredictable and bidirectional shift of white matter based on measurements directly on colour FA maps, rather than deterministic tractography and was largely limited to the

CSpT (Nimksy et al., 2005). These authors report a maximal shift relative to preoperative location ranging from -8 to 15 mm with mean overall tract shift of  $2.5 \pm 5.8$  mm (Nimksy et al., 2005). Similarly, in a group of 28 patients undergoing pericentral glioma resection in a 1.5-Tesla iMRI, intraoperative CSpT shift using SS-iDTI ranged from -23 to 12 mm with mean absolute tract shift of 6.7 mm (Maesawa et al., 2010). In another investigation at 1.5-Tesla, mean intraoperative CSpT shift was reported as  $3.0 \pm 4.2$  mm (range -8.8 to 19.2 mm), largely driven by more significant intraoperative tract shift in patients with enhancing gliomas compared to minimal shift seen in resection of non-enhancing gliomas (Shahar et al., 2014). A single report of SS-iDTI use at the higher field strength of 3.0-Tesla for CSpT tractography in 25 patients undergoing supratentorial intraaxial resections found the images to be unusable in 9 of 25 (36%) cases due to poor SNR and susceptibility related image distortion (Ostrý et al., 2013). These authors identify a preoperative minimal tumor to CSpT distance of  $2.7 \pm 5.1$  mm (range -6.4 to 18.3 mm) compared to  $5.2 \pm 7.2$  mm (range -12.8 to 22.4mm) for SS-iDTI in surgical position with an open cavity, amongst the 16/25 (64%) where satisfactory iDTI data was obtained. Higher-field iMRI is generally thought to convey superior image quality due to higher SNR with faster acquisitions at higher resolution compared to lower field applications (e.g. 0.3 – 1.5-Tesla) however, this comes at the cost of exacerbated susceptibility artifact which is considerably more pronounced in open cranial surgical field acquisitions (Ginat et al., 2014; Jissendi et al., 2008; Vargas et al., 2009).

One approach to correct EPI distortions observed on presurgical single-shot EPI DTI scans has been the use of image-registration-based post-processing methods (Albi et al., 2018; Merhof et al., 2007) aligned to T1- or T2-weighted structural MRI. Although this approach may successfully correct for 1-2 mm EPI distortions in preoperative data this varies significantly depending on which post-processing pipeline is selected and has not been investigated intraoperatively. It has long been known that multi-shot EPI diffusion techniques can reduce such susceptibility distortions in the acquisition phase (Butts et al., 1996; Robson et al., 1997). Recently, an alternative multi-shot method of DTI acquisition called Readout-Segmented DTI (RS-DTI) has become available which abbreviates sampling time (at the cost of longer overall imaging time) by limiting the portion of k-space filled during each excitation (Frost et al., 2012; Heidemann et al., 2010; Koyasu et al., 2014; Porter and Heidemann, 2009; Robson et al., 1997; Wang et al., 2018). These authors have described a marked reduction in susceptibility and improved T2\* blurring (as assessed by improved sharpness of the grey-white junction) using RS-DTI compared with standard SS-DTI at 3-Tesla or higher. To date, the utility of RS-DTI in minimizing susceptibility artifact in the iMRI setting and specifically for DTI tractography with an open cranium, has not yet been investigated.

The objective of this study was to evaluate the performance of RS-DTI in the iMRI setting for the acquisition of DTI during intraaxial cranial neurosurgery, and to compare it to conventional SS-DTI. Our hypothesis was that RS-DTI would minimize susceptibility artifact-related image degradation commonly

encountered in the 3.0-Tesla iMRI setting and would enable high quality, anatomically-faithful iDTI images. To accomplish this, we acquired both RS-iDTI and SS-iDTI in patients undergoing intraaxial, supratentorial resections in the iMRI suite for suspected low-grade gliomas (14; 64%), high-grade gliomas (7; 32%) and focal cortical dysplasia (1), to evaluate: 1) the severity of regional susceptibility artifact in areas known to be prone to this type of artifact (resection cavity, orbitofrontal, anterior temporal tip); 2) the relative improvement in T2\*-blurring (based on global assessment of sharpness of grey-white matter junction); 3) the feasibility of obtaining surgically relevant white matter tract reconstructions on RS-iDTI with commercially available deterministic DTI tractography software (StealthStation, Medtronic); and 4) the intraoperative change in minimal target-tract distance, maximal intraoperative tract shift and maximal inter-sequence tract difference.

## **6.2 Methods**

### **6.2.1 Participants and ethical approval**

Our study included 22 prospectively enrolled adult patients presenting to the Dan and Bunny Widney Intraoperative MRI surgical suite at the University of Alberta Hospital for cranial, supratentorial, intraaxial resection between October 2016 and December 2017. The study protocol was approved by the University of Alberta Health Research Ethics Board and written informed consent was obtained from all participants.

## **6.2.2 Intraoperative MRI surgical suite**

The iMRI suite (Siemens, Verio, Erlangen, Germany) is a purpose-built 3.0-Tesla IMRIS operating theatre (IMRIS, MN, USA) with radiofrequency shielding. It is equipped with StealthStation i7® (Medtronic, MN, USA) ceiling mounted optical surgical neuronavigation and a Zeiss Pentero navigated surgical microscope (Zeiss, Oberkochen, Germany). The MRI scanner is a superconductive closed-bore 3.0-Tesla magnet that is 173 cm long and has an inner bore diameter of 70 cm. Peak gradient strength is 45 mT/m with a slew rate of 200 T/m/s. The iMRI suite is integrated with a StealthViz™ planning station used for deterministic ROI-based DTI-tractography (StealthStation, v1.0, Medtronic).

## **6.2.3 Image acquisition**

Participants underwent multiple pre- and intra-operative scans at their treating surgeon's discretion. Preoperative iMRI scans were performed following induction of cuffed endotracheal general total intravenous anesthetic on the day of surgery prior to skull clamp pinning (n = 9) or immediately following cranial fixation (n = 1) at the discretion of the treating surgeon. Outpatient preoperative iMRI scans were performed (n = 2), within 2 weeks of surgery, when requested by the treating surgeon (e.g. for functional MRI localization of language or motor cortical areas). Preoperatively only RS-DTI scans were feasible to acquire given clinical time constraints. All participants underwent intraoperative scanning in

surgical position affixed to the operating table with IMRIS head fixation device and the IMRIS two-piece surface head coils, with a total of 8-elements (IMRIS, MN, USA). Intraoperative scanning was performed with dura mater open after target tissue resection to evaluate extent of resection (EOR) and provide updated images for neuronavigation. If residual target tissue was identified on intraoperative imaging, further resection was performed if indicated and safe as judged by the treating surgeon. Additional intraoperative iMRI scans were performed if needed, however, iDTI was only collected on one intraoperative occasion.

Whole brain, axial, T1-weighted, three-dimensional magnetization-prepared rapid-acquired gradient echo (MPRAGE) images were obtained with voxel size  $1 \times 1 \times 1 \text{ mm}^3$ , field of view (FOV) 250 mm, repetition time (TR) 1800 ms, echo time (TE) 2.65 ms and scan time 5 minutes 29 seconds. Single-shot DTI (SS-DTI) images were obtained with voxel size  $1.5 \times 1.5 \times 3 \text{ mm}^3$ , FOV 220 mm, 30 slices, no gap, bandwidth 1530 Hz/Px, GRAPPA R=2, phase partial Fourier 6/8, TR 4900 ms, TE 80 ms, 30 non-collinear diffusion sensitizing gradient directions with  $b = 1000 \text{ s/mm}^2$  and 5  $b = 0 \text{ s/mm}^2$  for total scan time of 3 minutes and 8 seconds. Readout-segmented (readout segmentation of long variable echo-trains; RESOLVE (Porter and Heidemann, 2009)) DTI (RS-DTI) images were obtained with voxel size  $1.5 \times 1.5 \times 3 \text{ mm}^3$ , FOV 220 mm, 30 slices, no gap, bandwidth 503 Hz/Px, GRAPPA R=2, phase partial Fourier off, TR 4300 ms, TE 60 ms, 6 non-collinear diffusion sensitizing gradient directions with  $b = 1000 \text{ s/mm}^2$  and 2  $b = 0 \text{ s/mm}^2$  across 15 readout segments (chosen after an in-

house optimization comparing minimization of susceptibility artifact using readout segments ranging from 7 to 15 – data not shown) for a total scan time of 10 minutes and 34 seconds. In both cases, the slices were aligned along the AC/PC line and were identical for both SS-DTI and RS-DTI.

#### **6.2.4 Comparison of susceptibility artifact and grey-white delineation between RS-DTI and SS-DTI**

Diffusion data preprocessing and rigid-body registration to T1-weighted image space was carried out in ExploreDTI (version 4.8.6, PROVIDI lab, Utrecht, The Netherlands) (Leemans et al., 2009). Single-observer (CAE) quantitative assessment, blinded to diffusion type, was carried out in ITK-SNAP version 3.6.0 ([www.itksnap.org](http://www.itksnap.org)) (Yushkevich et al., 2006). Preprocessing of DTI data in ExploreDTI included signal drift correction (Vos et al., 2017), Gibbs ringing correction (Perrone et al., 2015), as well as subject motion and eddy current induced distortion correction (Leemans and Jones, 2009). Finally, a rigid-body registration of average diffusion images to T1-space was carried out in ExploreDTI. T1-weighted images were corrected for intensity non-linearity using MNI\_N3 (Sled et al., 1998).

Susceptibility artifact was assessed, blinded to DTI-scan type, in two ways in regions known to be prone to this type of image distortion including the resection cavity, orbitofrontal and anterior temporal cortices (Hutton et al.,

2002). First, susceptibility artifact was rated on a four-point scale as in previous studies of MRI artifact (C. Elliott et al., 2016; Wagner et al., 2015) as outlined in Table 6.1. Next, the magnitude of geometric distortion was compared for SS-DTI versus RS-DTI by measuring the anatomic deviation of average diffusion-weighted b1000 images relative to artifact-resistant T1-weighted images at corresponding anatomical points in the same susceptibility prone regions used above. Specifically, anatomical deviation was measured by comparing identical points on the T1-weighted image to anatomically corresponding points on the diffusion image by varying the opacity of the overlaid diffusion image (co-registered to the T1-weighted image). Nine measurements in each patient were performed both ipsilateral and contralateral to side of the resection in the medial and lateral orbitofrontal and anterior temporal regions as well as at the deep, medial and lateral margin of the resection cavity. Regional measurements were excluded when resection completely removed the area of interest (e.g. ipsilateral anterior temporal lobe in anterior temporal lobectomy).

The utility of RS-DTI in reducing T2\*-blurring was assessed with a global blinded rating of the ability to delineate the grey-white matter junction (Table 6.1).

**Table 6.1: Susceptibility artifact and gray-white matter delineation rating scales**

<b>Rating</b>	<b>Regional Artifact</b>	<b>Gray-White</b>
4	No artifact	Crisp
3	Mild artifact, not limiting visualization of anatomy	Good
2	Strong artifact, limiting visualization of anatomy	Poor
1	Profound artifact, visualization of anatomy impossible	Not possible

Adapted from similar published scales (Elliott et al., 2016; Wagner et al., 2015).

### **6.2.5 DTI tractography**

Deterministic, ROI-based, DTI tractography was performed on a StealthViz™ planning station located in the iMRI suite (StealthStation, v1.0, Medtronic). StealthViz™ employs a Fiber Assignment by Continuous Tractography (FACT) approach. Following background masking of non-brain tissue and a quality assurance step for patient motion the software performs a rigid-body registration of non-diffusion weighted (b0) and diffusion weighted image sets to an anatomical scan (MPRAGE) acquired at the same session. Thereafter, fractional anisotropy (FA), directionally-encoded color (DEC) and apparent diffusion coefficient (ADC) maps were computed and manually verified to be accurately registered to anatomic scan.

Tractography was performed by a single observer (CAE) and required approximately 20 minutes to perform. Tractography was performed on both pre- and intra-operatively acquired DTI images for each patient. Tractography parameters were: FA start value of 0.20, seed density of 1, maximum directional change of 60 degrees, minimum fiber length of 20 mm, and 3D object distance (a peri-tract safety margin applied when generating 3D tracts for export) of 1 mm. DEC-maps and anatomical landmarks were used to define ROIs to reconstruct surgically relevant tracts in the area of the craniotomy and specifically in the area of planned target tissue resection at the discretion of the treating surgeon. The CSpT was reconstructed in all patients, as it is the commonly reported tract in previous iDTI investigations. Reconstructed tracts in this study included the CSpT (n = 22), inferior fronto-occipital fasciculus (n = 10), corpus callosum (n = 7), superior longitudinal fasciculus (n = 7), inferior longitudinal fasciculus (n = 5) and uncinate fasciculus (n = 1). Tract reconstruction was carried out using a two-region of interest (ROI) approach (Catani et al., 2002; D. K. Jones et al., 1999; Mori et al., 1999; Mori and Van Zijl, 2002). For example, to reconstruct the corticospinal tract, two ROIs were used including the posterior arm of the internal capsule and the precentral gyrus (identified anatomically and based on DEC-map). Reconstructed tracts were transformed into 3D objects and were exported to an i7 Cranial StealthStation™ neuronavigational system. Exported tracts, each assigned a unique colour, were rigidly registered to a preoperative anatomical reference scan by applying a shared transformation (3D objects were

pre-merged to DTI anatomical reference based on tractography registration process detailed above).

### **6.2.6 Analysis of tractographic data**

As mentioned above, DTI tractography was attempted preoperatively (RS-DTI) and intraoperatively (for both RS-iDTI and SS-iDTI) for surgically relevant tracts. Tractography was rated as feasible if at least one of the surgically relevant tracts could be successfully reconstructed. Tract reconstruction failure of surgically relevant tracts were noted along with the number and identity of tracts which were successfully reconstructed for each DTI scan. The following four measures were made using tract reconstructions using i7 Cranial StealthStation™: 1) target-tract distance (TTD); 2) intraoperative change in TTD; 3) maximal intraoperative tract shift; and 4) maximal inter-sequence (i.e., SS-DTI vs. RS-DTI) intraoperative tract difference. The TTD was defined as the shortest distance between the target tissue and the reconstructed tract. This was measured both pre- and intra-operatively when available. Target tissue was defined for tumour cases either as the area of T1-hypointensity or gadolinium-enhancement, if applicable, while for the single non-lesional epilepsy case it was defined as the resection margin, which could be seen on both pre- and intra-operative scans as the patient was undergoing a repeat resection for ongoing drug-resistant epilepsy. Next, intraoperative change in TTD ( $\Delta$ TTD), our first measure of intraoperative tract shift, was calculated as the difference between the

preoperative and intraoperative TTD. Inward shift of an iDTI-tract relative to preoperative location was assigned a negative (-) sign. Maximal intraoperative tract shift, our second measure of intraoperative tract shift, was defined as the largest distance between pre- and intra-operative tract reconstructions. Finally, the maximum inter-sequence intraoperative tract difference was defined as the largest distance between intraoperative RS-iDTI and SS-iDTI tract reconstructions. In this case, inward shift of the RS-DTI based tract reconstruction relative to SS-DTI was indicated as a negative distance.

### **6.2.7 Statistical analysis**

Statistical analyses were performed with Prism software version 7 (Graphpad). The distribution of all continuous data was first evaluated with the Shapiro-Wilk test of normality. A Welch's *t*-test (for unequal variances) was used to compared ratio scale data (e.g. anatomic deviation measures). A paired sample T-test was used to compare sets of pre- and intra-operative interval ratio scale data. A Mann-Whitney *U* test was used to compare ordinal scale data (e.g. ratings of susceptibility artifact). All tests were conducted as two-tailed, with a type 1 error set at  $\alpha = 0.05$ .

## 6.3 Results

### 6.3.1 Patient characteristics

Clinical characteristics of the 22 patients (mean age  $39 \pm 14$  yrs; 15 male) included in this study are provided in Table 6.2. Preoperative MRI diagnosis was most consistent with low-grade glioma (LGG, as defined by the absence of clear gadolinium enhancement) in 14 (64%), high-grade glioma (HGG, as defined by clear gadolinium enhancement) in seven (32%) and focal cortical dysplasia (FCD) in one. Six cases were repeat resections either for tumour recurrence/residual for suspected HGG (3) or LGG (2) or for ongoing seizures following initial epilepsy resection (1). Final pathologic diagnosis among the 14 suspected LGG was WHO grade II oligodendroglioma (5), WHO grade II astrocytoma (5), WHO grade II central neurocytoma (1), WHO grade I ganglioglioma (1), WHO grade III anaplastic ependymoma (1) and WHO grade IV glioblastoma multiforme (1). Pathologic diagnosis among the seven suspected HGG was WHO grade IV glioblastoma multiforme (4), WHO grade III glioma (1), WHO grade III oligodendroglioma (1) and radiation necrosis (1). Extent of resection (EOR) was assessed by neuroradiologists on the basis of complete removal of target tissue on intraoperative MRI as defined for LGG by hyperintensity on the fluid-attenuation inversion recovery (FLAIR) image or hypointensity of T1-weighted images, for HGG by residual gadolinium enhancement, and for the epilepsy resection for FCD by preoperative epileptogenic zone determination. Gross total resection (GTR) was achieved in

13/22 cases (59%) of which iMRI was used to guide further resection in seven (54%). Among the nine cases where a subtotal or maximal safe resection was achieved, iMRI was used to guide further resection to a functional limit in four (44%). Intraoperative neurophysiological monitoring was used in 4/22 patients.

**Table 6.2: Characteristics of 22 patients with intraaxial iMRI resections**

Pt	Age (yrs), Sex	MRI Dx	CPx	Rpt Resect.	Operation	Pathologic Dx	EOR	Utility of iMRI
1	21 F	LGG	Sz	No	Rt frontal	WHO II oligodendroglioma	GTR	Residual resected
2	25 M	FCD	Sz	Yes	Rt frontal	FCD I	GTR	
3	33 M	LGG	Incidental	No	Lt anterior temporal	WHO II astrocytoma	MSR	
4	24 F	LGG	Sz	No	Lt frontotemporal	WHO II oligodendroglioma	MSR	Residual resected to fx limit
5	61 M	HGG	Sz	No	Lt parieto-occipital	GBM	GTR	
6	36 M	LGG	Sz	No	Lt frontoparietal	WHO III oligodendroglioma	GTR	Residual resected
7	63 M	HGG	Sz	Yes	Lt frontal	WHO III oligodendroglioma	MSR	Residual resected to fx limit
8	49 M	HGG	Sz	No	Rt parietal	GBM	GTR	
9	18 F	LGG	Sz	No	Rt anterior temporal	WHO I ganglioglioma	GTR	
10	36 M	LGG	Sz	No	Lesionectomy, PHG	WHO II astrocytoma	GTR	
11	34 F	LGG	Incidental	No	Lt frontal	WHO II astrocytoma	GTR	Residual resected
12	37 M	LGG	Sz	No	Rt frontotemporal	GBM	GTR	
13	54 M	HGG	Headache	No	Rt temporo-occipital	GBM	GTR	Residual resected
14	57 F	HGG	Sz	No	Rt frontal	WHO II glioma	MSR	
15	34 F	LGG	Residual	Yes	Lt frontal	WHO II central neurocytoma	MSR	Residual resected to fx limit
16	57 M	LGG	Sz	No	Lt frontal	WHO II oligodendroglioma	GTR	Residual resected
17	24 M	LGG	Sz	No	Lt temporal	WHO II astrocytoma	GTR	Residual resected
18	37 F	HGG	Recurrence	Yes	Lt frontotemporal	Radiation necrosis	MSR	
19	37 M	LGG	Residual	Yes	Rt parietal	WHO II oligodendroglioma	MSR	Residual resected to fx limit
20	37 M	LGG	Sz	No	Rt frontoparietal	WHO III ependymoma	GTR	Residual resected
21	26 M	LGG	Sz	No	Rt frontotemporal	WHO II astrocytoma	MSR	Residual resected to fx limit
22	63 M	HGG	Recurrence	Yes	Rt frontal	GBM	MSR	

CPx: Clinical presentation; Dx: diagnosis; EOR: extent of resection; FCD: focal cortical dysplasia; fx: functional; GBM: glioblastoma multiforme; GTR: gross total resection; HGG: high-grade glioma; iMRI: intraoperative MRI; LGG: low-grade glioma; PHG: parahippocampal gyrus; MSR: maximal safe resection; Sz: seizure; WHO: World Health Organization grade.

### **6.3.2 Impact of readout-segmentation iDTI on susceptibility artifact image degradation in presence of resection**

When assessed by visual inspection, RS-iDTI was found to result in significantly less regional susceptibility artifact than SS-iDTI for the resection cavity (RS-iDTI mean rating =  $2.7 \pm 0.5$ , median 3; SS-iDTI mean rating =  $1.4 \pm 0.6$ , median = 1;  $U = 24.5$ ,  $p < 0.0001$ ; Mann-Whitney test), orbitofrontal (RS-iDTI mean rating =  $2.9 \pm 0.5$ , median 3; SS-iDTI mean rating =  $1.2 \pm 0.4$ , median = 1;  $U = 4.5$ ,  $p < 0.0001$ ; Mann-Whitney test) and anterior temporal cortices (RS-iDTI mean rating =  $3.1 \pm 0.4$ , median 3; SS-iDTI mean rating =  $1.9 \pm 0.7$ , median = 2;  $U = 28.5$ ,  $p < 0.0001$ ; Mann-Whitney test)(Figures 6.1 and 6.2).

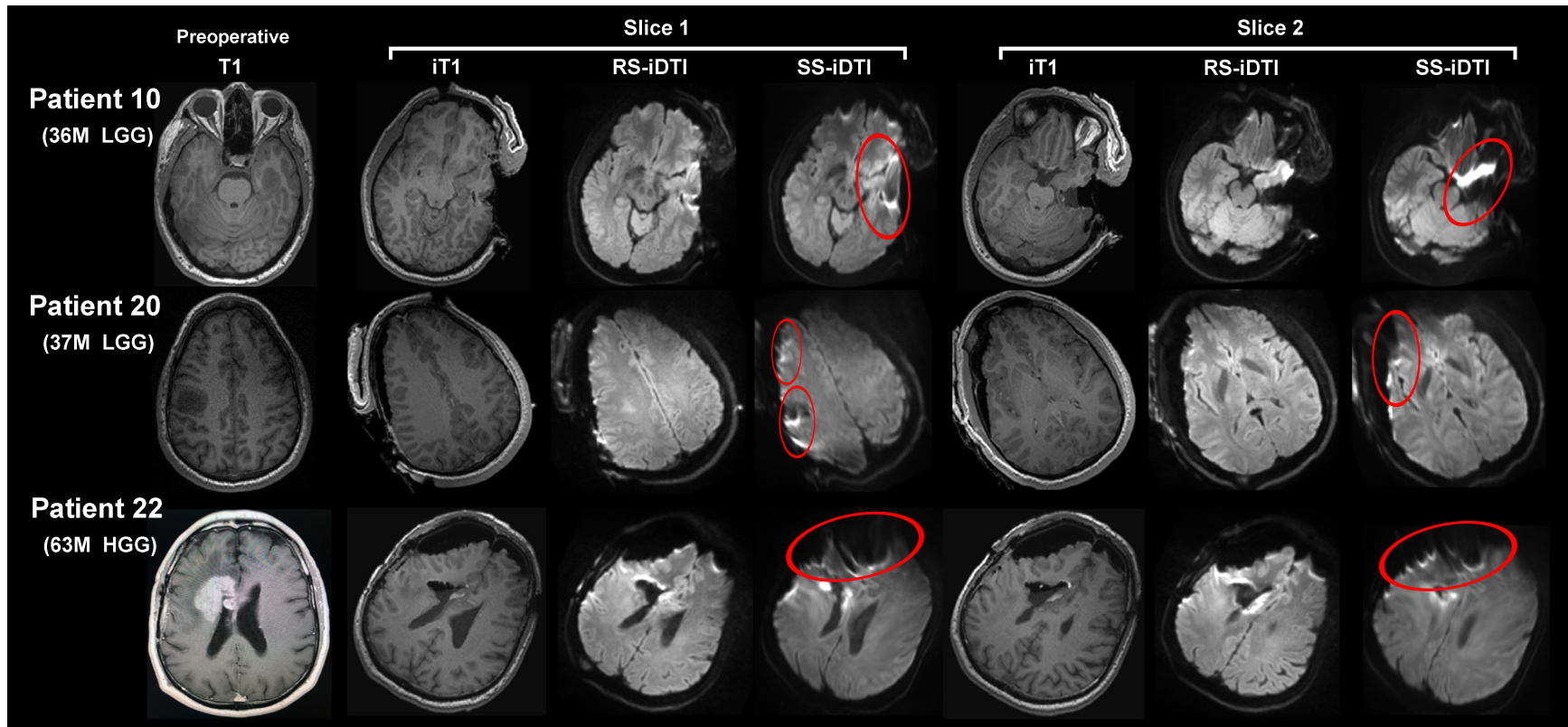


**Figure 6.1: Susceptibility artifact comparison of RS-DTI versus SS-DTI in three iMRI cases**

The pre-operative T1, intraoperative T1-weighted image (iT1), and the intraoperative average b1000 diffusion-weighted images for RS-iDTI and SS-iDTI are shown for two slices in each of three cases. RS-iDTI provides enhanced image quality with reduced susceptibility artifact image degradation and sharper structural delineation compared to SS-iDTI, as highlighted by red ellipses. Please note, in patient 22 the surgeon elected to replace bone flap and fold skin over (without closing dura) to protect the brain from the draping. LGG = low grade glioma; HGG = high-grade glioma.

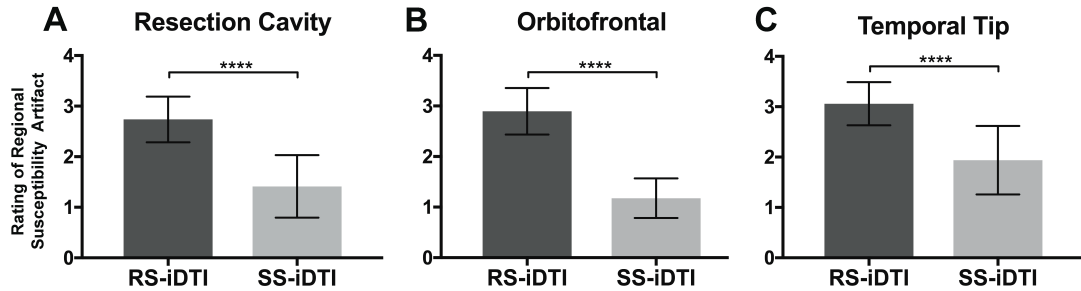


**Figure 6.2: Regional ratings of susceptibility artifact for RS-iDTI versus SS-iDTI**

There was a statistically significant improvement in ratings of regional susceptibility artifact (as defined in Table 1) with readout-segmented (RS-iDTI) compared to conventional single-shot (SS-iDTI) DTI for (A) resection cavity, (B) orbitofrontal cortex and (C) anterior temporal tip. Bars represent mean ratings by sequence type while error bars denote SD. \*\*\*\* denotes  $p < 0.0001$ .

Mean anatomical deviation measured at nine points (ipsilateral and contralateral to side of the resection in the medial and lateral orbitofrontal and anterior temporal regions as well as at the deep, medial and lateral margin of the resection cavity) was also significantly less for RS-iDTI compared to SS-iDTI relative to artifact-resistant intraoperative T1-weighted images (RS-iDTI mean absolute anatomic deviation  $2.7 \pm 0.2$  mm versus SS-iDTI  $7.5 \pm 0.4$  mm; Welch-corrected  $t = 12.0$ ;  $p < 0.0001$ ). Anatomical deviation was also less for RS-iDTI at the resection cavity (RS-iDTI mean absolute anatomic deviation  $2.5 \pm 0.2$  mm versus SS-iDTI  $7.2 \pm 0.6$  mm; Welch-corrected  $t = 8.6$ ;  $p < 0.0001$ ), in the orbitofrontal cortex (RS-iDTI mean absolute anatomic deviation  $2.9 \pm 0.3$  mm versus SS-iDTI  $8.3 \pm 0.6$  mm; Welch-corrected  $t = 8.4$ ;  $p < 0.0001$ ), and at anterior temporal tip (RS-iDTI mean absolute anatomic deviation  $2.6 \pm 0.3$  mm versus SS-iDTI  $6.1 \pm 0.7$  mm; Welch-corrected  $t = 4.4$ ;  $p < 0.001$ )(Figure 6.3).

Anatomical deviation expressed as a signed value (with negative indicating inward shift of DTI relative to T1 reference) is plotted in Figure 6.4.

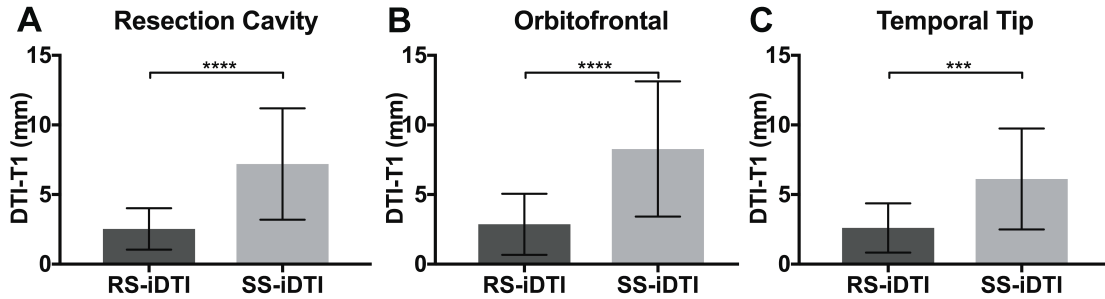


**Figure 6.3: Average absolute anatomical deviation of RS-iDTI compared to SS-iDTI**

Average anatomical deviation was reduced significantly on RS-iDTI relative to SS-iDTI as measured from the absolute value of distance (in mm) between corresponding anatomic points in (A) resection cavity, (B) orbitofrontal cortex, and (C) anterior temporal tip on iDTI versus susceptibility artifact resistant T1-weighted images. \*\*\*\*  $p < 0.0001$ , \*\*\*  $p < 0.001$ . Bars indicate group mean while error bars denote SD.

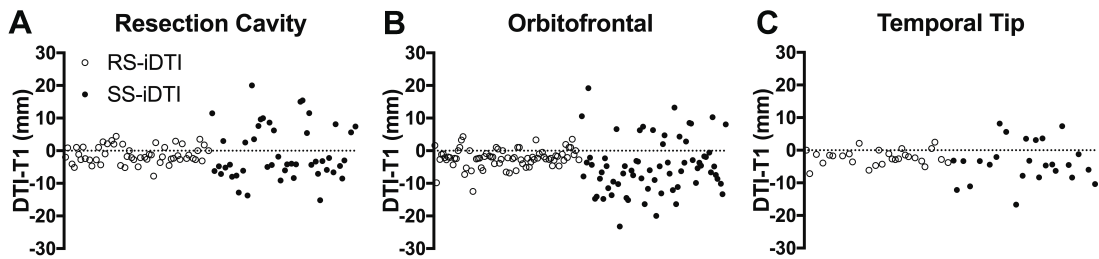


**Figure 6.4: Anatomical deviation of coregistered mean b1000 images for RS- and SS-iDTI relative to T1-reference**

Measured distance (DTI-T1, in mm with negative representing inward shift of DTI) between corresponding anatomic points on susceptibility artifact resistant T1-weighted image showing smaller deviations for readout-segmented (RS-iDTI, open dots) versus conventional single-shot (SS-iDTI, closed dots) DTI for the (A) resection cavity, (B) orbitofrontal cortices and (C) anterior temporal tip. A total of nine measures in regions most prone to susceptibility artifact were made in each subject.

### **6.3.3 Impact of readout-segmentation iDTI on gray-white matter delineation**

The impact of RS-iDTI on the improved ability to delineate the gray-white junction is illustrated qualitatively in Figure 6.1 and quantified in Figure 6.5 (RS-iDTI mean rating =  $3.2 \pm 0.6$ , median 3; SS-iDTI mean rating =  $1.6 \pm 0.5$ , median = 1;  $U = 11$ ,  $p < 0.0001$ ; Mann-Whitney test).

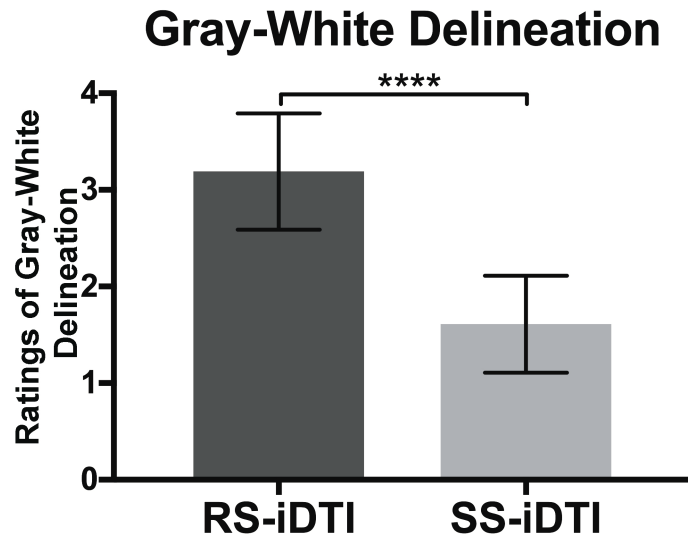


**Figure 6.5: Global ratings of gray-white matter delineation on average b1000 diffusion images**

Global ratings of gray-white matter delineation (as defined in Table 1) were significantly better for readout-segmented (RS-iDTI) versus conventional single-shot (SS-iDTI) DTI. \*\*\*\* denotes  $p < 0.0001$ . Bars represent mean ratings by sequence type while error bars denote SD.

### 6.3.4 Feasibility of intraoperative DTI tractography

The pre- and intra-operative tractography process (acquisition, processing, analysis and export to neuronavigation) could be conducted on-the-fly, immediately after intraoperative acquisition during surgery. Intraoperative DTI-tractography was feasible (successful reconstruction of at least one surgically relevant tract) in all 22 cases for RS-DTI and 20/21 cases for SS-iDTI (Table 6.3). SS-iDTI tract reconstruction failure, of at least one surgically relevant tract, occurred in 8/21 for which RS-iDTI permitted successful reconstruction in 5 of these 8. Thus RS-iDTI could reconstruct all the tracts deemed critical for a given surgery in 18 of 22 patients. Tract reconstruction

failures were thought to be due to susceptibility related image degradation which was more prominent on SS-iDTI images.

**Table 6.3: A comparison of reconstruction of surgically relevant tracts for preoperative RS-DTI and intraoperative RS-iDTI and SS-iDTI in 22 iMRI patients described in Table 6.2**

Pt	Preoperative RS-DTI							Intraoperative RS-iDTI							Intraoperative SS-iDTI							
	Total	CSpT	IFOF	CC	SLF	ILF	UF	Total	CSpT	IFOF	CC	SLF	ILF	UF	Total	CSpT	IFOF	CC	SLF	ILF	UF	
1	3	+	+	+				3	+	+	+				3	+	+	+				
2	3	+	+	+				3	+	+	+				3	+	+	+				
3	3	+	+	+				3	+	+	+				3	+	+	+				
4	3	+		+	∅	+		2	+		+	∅	∅		2	+		+	∅	∅		
5	3	+	+	+				2	+	∅	+				2	+	∅	+				
6	3	+		+	+			2	+		+	+			2	+		+	+			
7*	2	+	+					1	+	+					1	+	∅					
8	3	+	+	+				3	+	+	+				3	+	+	+				
9	3	+	+			+		2	+	+			∅		n/a							
10	5	+	+		+	+	+	4	+	+		+	C	+	4	+	+		+	C	+	
11	3	+	+		+			3	+	+		+			3	+	+		+			
12	2	+			+			2	+			+			2	+			+			
13	n/a							1	+						1	+						
14*	n/a							3	+	+		+			2	+	+		∅			
15*	n/a							1	+						0	∅						
16	n/a							2	+			+			2	+			+			
17	n/a							3	+			+	+		3	+			+	+		
18	n/a							1	+						1	+						
19*	n/a							2	+				+		1	+					∅	
20	n/a							1	+						1	+						
21*	n/a							1	+						0	∅						
22	n/a							1	+						1	+						

CSpT: corticospinal tract; IFOF: inferior fronto-occipital fasciculus; CC: corpus callosum; SLF: superior longitudinal fasciculus; ILF: inferior longitudinal fasciculus; UF: uncinata fasciculus; +: successfully reconstructed; ∅: unsuccessfully reconstructed; C: cut (i.e. resected); n/a: scan not collected; \*: indicates superior performance of RS-iDTI compared to SS-iDTI.

### 6.3.5 Intraoperative tract shift analyses

Mean tract-to-target (TTD), defined as the shortest distance between the target tissue and the reconstructed tract, was not significantly different between pre-operatively acquired RS-DTI ( $6.8 \pm 7.0$  mm, range: 0 – 27.0 mm) and intraoperatively acquired RS-iDTI ( $9.6 \pm 10.7$  mm, range: 0 – 34.6,  $t(29)=1.88$ ,  $p = 0.07$ ) or intraoperatively acquired SS-iDTI ( $10.1 \pm 11.7$  mm, range: 0 – 37.4,  $t(29)=1.57$ ,  $p = 0.13$ ), for the 12 cases in which pre-operative DTI had been acquired (Table 6.4). When looking exclusively at intraoperatively acquired DTI data in the 21 subjects with both RS-iDTI and SS-DTI, there was also no statistically significant difference in mean TTD for RS-iDTI ( $10.7 \pm 12.1$  mm, range 0 – 34.6) versus SS-iDTI ( $11.1 \pm 12.0$  mm, range 0 – 37.8,  $t(40)=0.33$ ,  $p = 0.74$ ). Similarly, mean of the absolute value of intraoperative change in TTD was not significantly different by DTI sequence type ( $\Delta$ TTD RS-iDTI:  $5.4 \pm 4.4$  mm, range: -16.8 – 11.4 versus  $\Delta$ TTD SS-iDTI:  $6.0 \pm 5.0$  mm, range: -19.0 – 12;  $t(29)=0.59$ ,  $p = 0.56$ ; Table 6.4). Despite this, in certain cases, differences between TTD were marked (Figure 6.6). Moreover, in the 14 LGG cases alone, the mean signed intraoperative change in TTD was significantly different by DTI sequence type at the group level with  $\Delta$ TTD RS-iDTI:  $-3.9 \pm 6.7$  mm, range: -16.8 to 4.7 versus  $\Delta$ TTD SS-iDTI:  $-0.6 \pm 6.0$  mm, range: -13.6 to 5.9;  $t(17)=2.18$ ,  $p = 0.04$  (Table 6.4).

The mean of the absolute value of maximal intraoperative tract shift was not statistically different between RS-iDTI tract reconstructions ( $9.7 \pm 3.9$  mm,

range: -21.4 to 11.4 mm) and SS-iDTI ( $9.5 \pm 5.4$  mm, range: -22 to 26 mm;  $t(29)=0.35$ ,  $p = 0.73$  (Table 6.4). Finally, the mean maximum inter-sequence intraoperative tract difference, as measured by deviation of RS-iDTI modelled tracts from SS-iDTI modelled tracts, was  $9.5 \pm 5.7$  mm (range: -27.1 to 18.7 mm; Table 6.4 and Figure 6.7).

**Table 6.4: Summary of intraoperative tract analyses**

Measure (mean $\pm$ SD (range), mm)	RS-DTI	SS-DTI	p-value
<b>Preoperative TTD</b>	$6.8 \pm 7.0$ (0 – 27.0)	n/a	0.07 <sup>†</sup>
<b>Intraoperative TTD</b>	$9.6 \pm 10.7$ (0 – 34.6)	$10.1 \pm 11.7$ (0 – 37.4)	0.13
<b><math>\Delta</math>TTD</b>	$5.4 \pm 4.4$ (-16.8 – 11.4)	$6.0 \pm 5.0$ (-19.0 – 12)	0.56
<b>Maximal tract shift</b>	$9.7 \pm 3.9$ (-21.4 – 11.4)	$9.5 \pm 5.4$ (-22 – 26)	0.73
<b>Maximal inter-sequence tract difference</b>	$9.5 \pm 5.7$ (-27.1 – 18.7)		

TTD: target-tract distance, the shortest distance between the target tissue and the reconstructed tract on T1-weighted images;  $\Delta$ TTD: mean absolute value of intraoperative change in TTD (signed range provided with inward shift of iDTI-tract relative to preoperative location assigned a negative (-) sign), <sup>†</sup>paired t-test compared to RS-iDTI TTD.

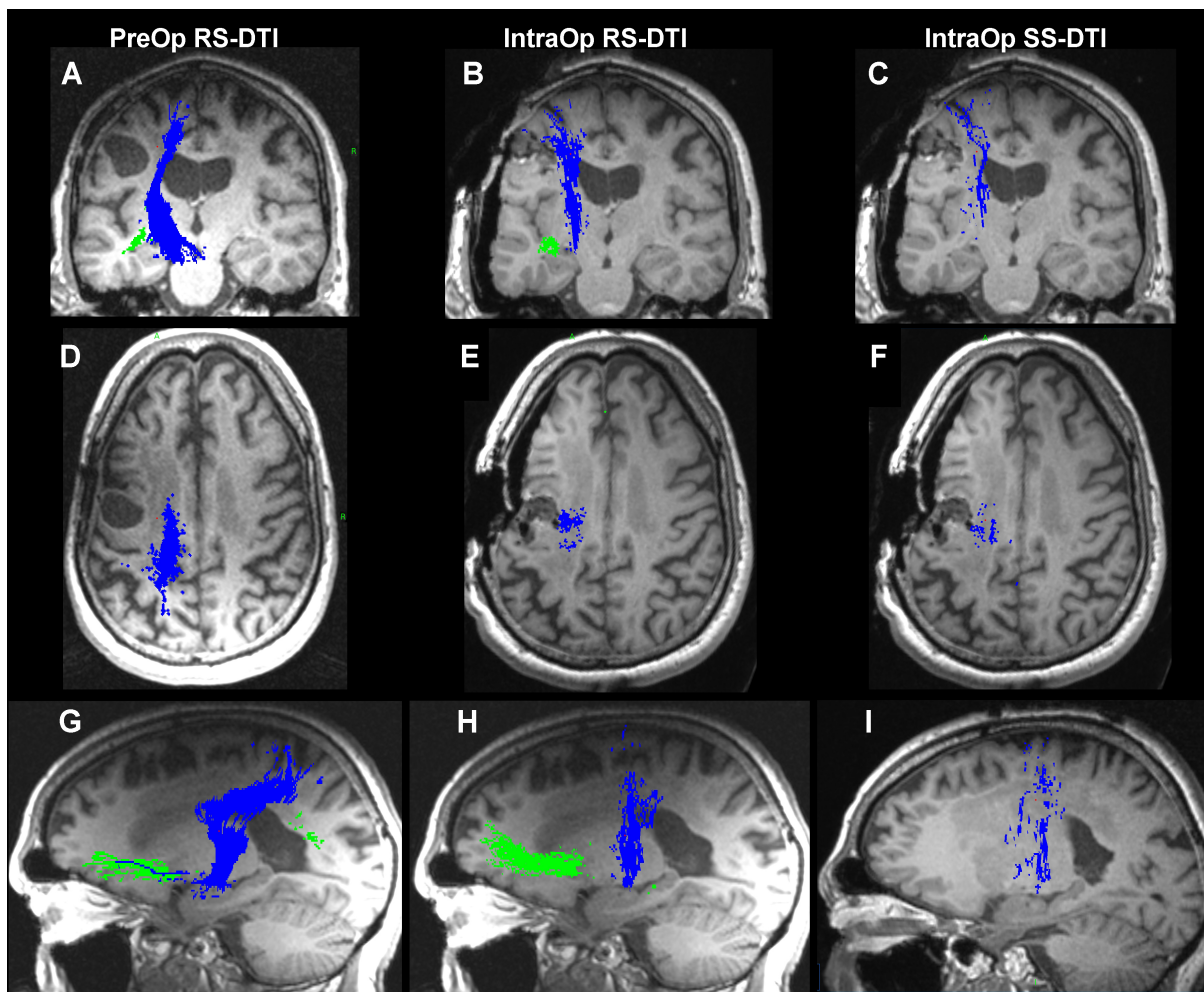


**Figure 6.6: Differences in intraoperative tractographic output and intraoperative shift in target-tract distance**

Representative example comparing multi-planar preoperative (A, D, G) and intraoperative tract reconstructions acquired in surgical position, with dura and cranium open for RS-iDTI data (B, E, H) and SS-iDTI data (C, F, I) in patient #7 (63M, HGG) of the corticospinal tract (blue) and inferior fronto-occipital fasciculus (green). RS-iDTI routinely demonstrated more robust tract reconstructions with fewer tractographic failures (e.g., IFOF failure in panel I) than SS-iDTI.

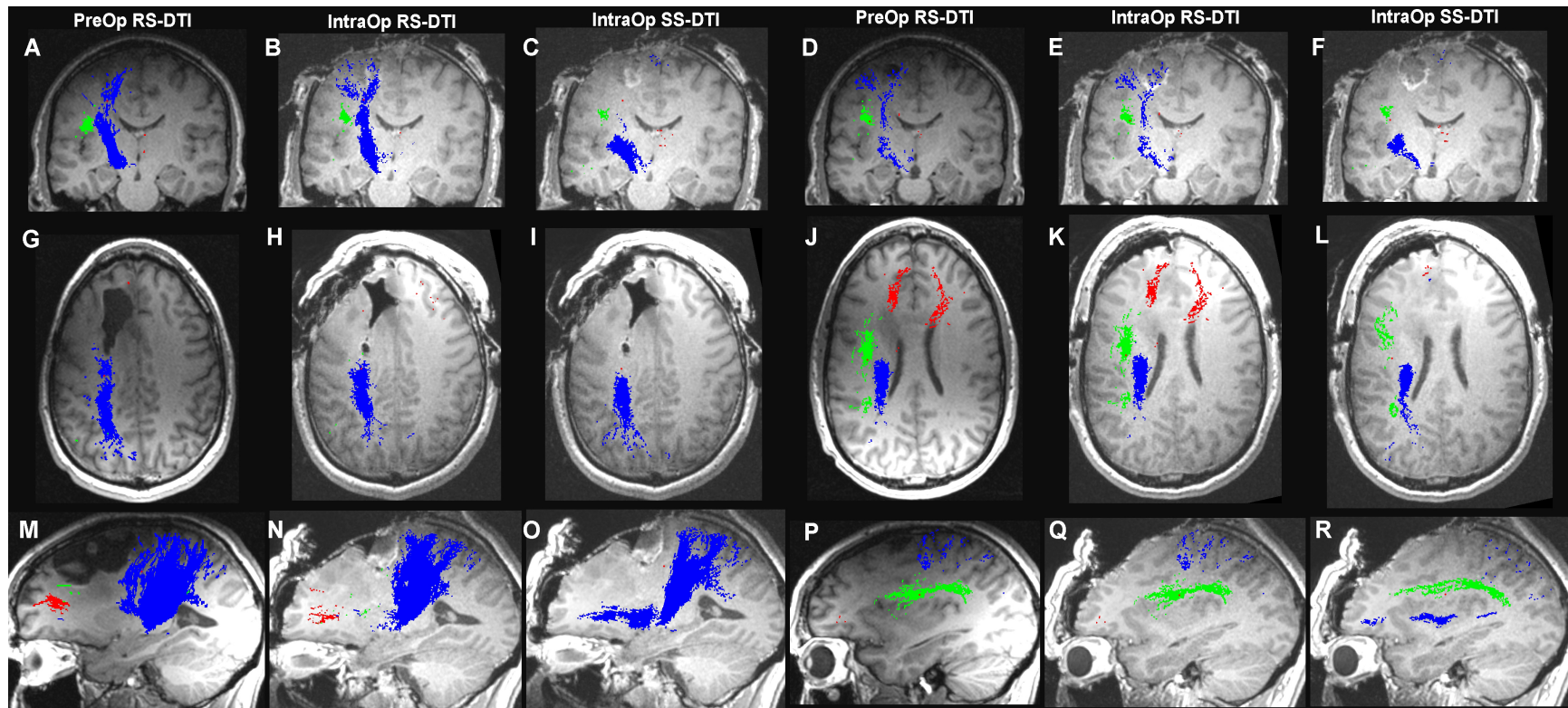


**Figure 6.7: Differences in intraoperative tractographic output and intraoperative tract shift in target-tract distance**

Representative example comparing multi-planar preoperative (A, D, G, J, M, P) and intraoperative tract reconstructions at two identical locations acquired in surgical position, with dura and cranium open for RS-iDTI data (B, E, H, K, N, Q) and SS-iDTI data (C, F, I, L, O, R) in patient #6 (36M, HGG) of the corticospinal tract (blue), superior longitudinal fasciculus (green) and anterior corpus callosum (red). RS-iDTI routinely demonstrated more robust tract reconstructions with fewer tractographic failures than SS-iDTI. Large inter-sequence differences were demonstrated between RS-iDTI and SS-iDTI modelled tracts.

## 6.4 Discussion

In this study, we show for the first time that RS-iDTI performed in a clinical 3-Tesla iMRI surgical setting significantly mitigates susceptibility artifact related image distortion that typically distorts cranial intraoperative DTI acquisition. RS-iDTI significantly reduced regional susceptibility artifact image degradation, enhanced global grey-white matter delineation, and minimized anatomic deviation of DTI images relative to artifact-resistant T1-weighted images. RS-iDTI resulted in improved tractography feasibility, more robust tract reconstructions as well as large, clinically important differences in modeled tracts between sequences. Finally, when limited to pathologically proven low grade glioma cases alone, mean intraoperative change in target-to-tract distance was significantly different in tract reconstructions generated based on RS-iDTI versus SS-iDTI data.

Deterministic DTI-tractography, although commonplace for preoperative planning in cranial neurosurgery, is not widely used in the iMRI setting to update neuronavigational systems with the modelled position of surgically relevant white matter tracts based on intraoperatively acquired DTI data. This is largely a technical limitation based on geometrical distortion and poor image quality related to susceptibility artifact when conventional SS-DTI is used to acquire intraoperative DTI of the open cranial surgical field, particularly at higher fields such as 3-Tesla. Although the gold standard intraoperative technique of direct cortical or subcortical electrical stimulation can provide reliable real-time spatial

information regarding the intraoperative position of many white matter tracts, it is not available for all tracts and requires awake resection (except for monitoring of the CSpT), which may not be tolerated by all patients, leaving white matter at risk.

Several previous iDTI investigations, focused on CSpT reconstructions in iMRI installations of 1.5-Tesla field strength or less, have identified significant, bidirectional intraoperative tract shift ranging from -23 to 19.2 mm (Maesawa et al., 2010; C Nimsky et al., 2005b; Ostrý et al., 2013; Ozawa et al., 2009; Prabhu et al., 2011; Romano et al., 2011; Shahar et al., 2014; Yang et al., 2017). One previous study by Ostry et al., (2013) examined the feasibility of SS-iDTI at 3-Tesla and found images unusable in 9/25 (36%) due to image degradation and spatial distortion secondary to susceptibility artifact. Our results confirm this finding of Ostry et al., with intraoperative tractography failures due to susceptibility artifact also occurring in 8/21 (38%), including 4/22 (18%) in which RS-iDTI was found to allow intraoperative DTI tractography where SS-iDTI had failed (Table 6.3). To our knowledge there have been no previous studies examining the impact of DTI sequence type in the iMRI setting, in particular RS-iDTI, on deterministic tractographic output. In the preoperative setting, previous investigations examining the impact of susceptibility artifact related geometric distortions on DTI output have found it to be a significant problem which may result in clinically significant inaccuracies of tract position (Jones and Cercignani, 2010; Treiber et al., 2016).

Our results confirm significant, bidirectional intraoperative tract shift, which varies from a mean of 2.3 mm inward—when measured at the shortest distance between a surgical target and a tract of interest—to up to 9.7 mm when measured at the point of maximum intraoperative tract shift. However, we also find marked differences in tractographic output by DTI sequence type, which when combined with our observation of RS-iDTI being associated with significantly less regional susceptibility artifact and geometric distortion relative to SS-iDTI, suggests that RS-iDTI is a superior sequence for intraoperative white matter tractography. Finally, our observation of significantly lower mean intraoperative change in target-to-tract distance amongst the subsample of pathologically proven low-grade gliomas for tract reconstructions generated with SS-iDTI than RS-iDTI suggest that previous reports of insignificant intraoperative mean tumor-to-corticospinal distance shifts amongst nonenhancing tumors (as opposed to enhancing tumors) may be at least partially attributable to geometric distortions associated with the intraoperative single-shot DTI employed (Shahar et al., 2014). Unfortunately, due to lower number of high grade gliomas and inability to collect preoperative DTI in all patients, we were unable to analyze the intraoperative change in TTD for enhancing tumors.

There are important limitations of this study. First, this a single-centre study with small sample size, consisting mostly of LGG patients. Second, although it was our intention to collect preoperative DTI data on all patients,

practically this was not always possible in the clinical iMRI setting. Specifically, if at the time of surgery participants already had suitable preoperative MRI data available—obtained from other scanners—it was not always feasible to collect repeat preoperative imaging after induction of anesthesia on the iMRI scanner including candidate DTI sequences. Similarly, in the cases where preoperative DTI was collected it was frequently limited to RS-DTI due to time constraints. In addition, this limitation necessitated using preoperative RS-DTI as a baseline for intraoperative tract shift analysis for both intraoperative RS-iDTI and SS-iDTI. Third, collection of intraoperative neurophysiological data was not part of the inclusion criteria and was only collected in a small fraction of participants (n = 4). When direct electrical stimulation (cortical or subcortical) was collected, it was limited to interrogation of the corticospinal tract. As a result, we were not able to assess the correlation between distance from stimulation point and modelled tract location with stimulation current, as has been done in previous iDTI reports (Kinoshita et al., 2005; Maesawa et al., 2010; Nossek et al., 2011; Ostrý et al., 2013; Prabhu et al., 2011), but not in others (C Nimsy et al., 2005b; Nimsy et al., 2006; Romano et al., 2011; Shahar et al., 2014). Evaluating the correlation between stimulation and tractographic output from RS-iDTI versus SS-iDTI is an important next step. Next, our selected RS-DTI scan parameters of 15 readout segments (to minimize open cranial susceptibility distortions) allowed only 6 diffusion gradient directions (which was sufficient for tensor calculation and standard deterministic tractography) resulted in a scan duration

that is arguably at the upper limit for use in the clinical preoperative (e.g., awake) or intraoperative setting. Finally, the iMRI environment presents some technical challenges which may limit SNR and image quality such as receive coil limitations (e.g. typically limited to 8-element, two-piece, flexible surface coils) and non-supine, non-neutral head positions which may necessitate scanning away from isocentre which may impact static field homogeneity or gradient linearity.

## **6.5 Conclusions**

Readout-segmented DTI significantly reduces susceptibility artifact related image degradation and geometric distortion, enhances signal-to-noise and provides more robust clinical tractographic output than conventional single-shot DTI. Significant differences exist between clinical tractographic output generated from readout-segmented versus single-shot intraoperative DTI which need to be verified using gold standard neurophysiological interrogation of tract reconstructions.

# Chapter 7: General discussion and Conclusions

Cameron A. Elliott

## 7.1 General discussion

This thesis demonstrates that structural changes of the brain during and following neurosurgical intervention—as detected in vivo using MRI—relate to clinically relevant surgical outcome variables. The thesis also shows that intraoperative MRI acquisition can be optimized to provide more clinically useful information to the neurosurgeon (i.e., iDTI), which can further improve patient outcome. Overall, the thesis emphasizes that the perioperative period (including both the intraoperative period as well as the early and delayed postoperative period) represents a unique opportunity to understand the evolution of structural and functional consequences of invasive neurosurgical treatment.

The key novel findings that emerge in the original work included in this thesis are as follows:

- 1) *The ultimate, long-term structural and functional consequence of infantile TBI suspected to be secondary to NAT is predicted by areas of*

*restricted diffusion on clinically-acquired, early (<7 days post-injury) DWI.* This finding was demonstrated in chapter 3 in a small group of 4 patients with relatively small traumatic subdural hematomas accompanied by extensive, but predominantly unilateral, areas of restricted diffusion, the distribution of which corresponded with areas of delayed cerebral atrophy on structural MRI accompanied by expected neurological deficits.

2) *Longitudinal structural MRI and manual volumetry—including ultra-early postoperative and delayed postoperative scans—can effectively characterize the extent and time course of limbic circuit structural consequences following resective surgery for drug resistant TLE.* This finding was demonstrated in both chapters 4 and 5 in a group of 26 TLE patients with DRE treated with resective surgery. The novelty of this work stems largely from the within-subjects, longitudinal nature of the scanning protocol and from the focus on the early postoperative period. Our conclusion that ultra-early postoperative structural changes of the brain (i.e., contralateral, non-resected hippocampal volume loss) relate to clinically meaningful surgical outcome variables (e.g. seizure control) is also a novel concept.

*Key specific findings include the following:*

- Significant postoperative volume loss occurs following resective surgery for TLE within the limbic circuit including within the contralateral hippocampus, mammillary bodies and fornix.
- The time course of postoperative volume loss differs significantly by structure. Volume loss in the contralateral hippocampus begins immediately and progresses rapidly over the first postoperative week, while volume loss in the mammillary bodies and fornix (which occurs bilaterally) occurs only in a delayed fashion (taking 1-3 years to develop). This observed difference in volumetric response to TLE surgery may relate to variable susceptibility of limbic structures to the impact of resective surgery or a variable response to postoperative seizure cessation.
- Although the hippocampus is well-known to be capable of mounting rapid neuroplastic changes in volume in response to a variety of stimuli, the observation of this in the ultra-early postoperative period is a novel finding.
- Postoperative, contralateral hippocampal volume loss (but not mammillary body or fornix volume) is significantly more pronounced in patients with ongoing, disabling seizures following TLE surgery and is a potential biomarker of surgical failure that may be identifiable based on early postoperative MRI

and may help to tailor ongoing treatment based on risk of seizure recurrence.

- Hippocampal subregional (head, body and tail) volumetric analysis revealed that the bulk of postoperative volume loss occurred in the hippocampal body and to a lesser extent the head. Although further investigations are needed, this may relate to more pronounced disconnection of hippocampal-hippocampal connections in the hippocampal body versus the head or tail.
- The observed postoperative limbic circuit volumetric changes were not accompanied by significant postoperative neuropsychological deficits. In fact, we observed a postoperative improvement in figural memory following dominant TLE surgery (Table 4.3). Specifically, there was no significant postoperative decline in tests of verbal and figural memory (which are thought to be hippocampally-mediated) attributable to postoperative volume loss in the shrinking non-resected hippocampus.

*3) Longitudinal postoperative measures of hippocampal diffusion are a sensitive in vivo measure of tissue microarchitecture which should be applied using anatomically accurate, whole hippocampal volumes of interest drawn on high-resolution T1-weighted images. This finding was demonstrated in chapter 5 in a group of 25 TLE surgery patients*

compared to 12 healthy control subjects scanned at similar intervals. This is a novel approach to computing diffusion metrics in the hippocampus; prior attempts in the literature at measuring postoperative hippocampal diffusion have employed vague regions of interest drawn on lower resolution, non-anatomical raw diffusion images.

*Key specific findings include the following:*

- In contrast to observed postoperative hippocampal volume loss, postoperative diffusion metric changes develop in a delayed fashion, not becoming significantly different from baseline until delayed (1-3 year) postoperative scans. Specifically, we identified postoperative reduction in hippocampal FA accompanied by increase in hippocampal MD and RD.
- Hippocampal diffusion analysis by anatomical subdivision (hippocampal head, body and tail) identified significantly lower mean postoperative FA across all subdivisions relative to healthy controls as well as relative to preoperative values limited to the hippocampal head and body (Figure 5.4).
- Postoperative changes in hippocampal diffusion metrics were not significantly different when analyzed by postoperative seizure control.

- These postoperative hippocampal diffusion metrics taken together with the postoperative manual volumetry results for limbic circuit structures provide novel insight into the potential etiology of postoperative structural changes of the brain following TLE surgery. First, the observed early postoperative hippocampal volume loss is unlikely the result of postoperative mechanical deformation due to craniotomy or CSF egress (based on stability of the periventricular caudate nucleus after TLE surgery, Figure 4.9), nor is it due to postoperative fluid shifts (e.g., due to dehydration) given that there are no observed early postoperative changes in diffusion metrics. The observed late postoperative reduction in FA and elevation in MD/RD suggests that a delayed remodeling process in the contralateral hippocampus is occurring, which we speculate may reflect resolution of pre-existing hippocampal cytotoxic edema (characterized by elevated FA and reduced MD (Grossman et al., 2010; Kimura-Ohba et al., 2016; Veeramuthu et al., 2015)). In addition, these findings are also consistent with the postoperative consequences of deafferentation (loss of hippocampal-hippocampal commissural input), which may account for the relative overshoot of the observed postoperative overshoot in hippocampal FA normalization.

4) *Technical limitations of intraoperatively acquired DTI, largely due to the image degradation and geometric distortion of susceptibility artifact associated with DTI acquisition in the surgical position while the cranium and dura are open, can be minimized with readout-segmented DTI (RS-iDTI) permitting real-time, clinical deterministic tractography during cranial resective neurosurgery.* This finding was demonstrated in chapter 6 in a group of 22 iMRI surgery patients. This is a novel finding which has the potential to significantly impact clinical neurosurgical practice by extending our ability to update neuronavigational systems with the intraoperative position of surgically relevant white matter tracts.

Key findings include the following:

- RS-iDTI is associated with significantly less regional susceptibility artifact and enhanced global gray-white matter delineation compared to conventional SS-iDTI.
- RS-iDTI significantly reduces regional geometric distortion of mean DTI images relative to susceptibility artifact resistant intraoperative MPRAGE compared to SS-iDTI.
- RS-iDTI improves feasibility of tractography based on intraoperatively-acquired, open surgical field DTI and permits

more robust reconstructions of a wider variety of surgically-relevant white matter tracts than SS-DTI.

- RS-iDTI, although requiring significantly longer acquisition time than SS-iDTI (~10 minutes versus ~3 minutes, respectively), can be conducted on-the-fly, using widely available clinical DTI software in the iMRI environment.
- Intraoperative tract shift is a significant, unpredictable, and bidirectional process that is ubiquitous in supratentorial, cranial resective neurosurgery.
- Significant differences exist in modeled tract position using deterministic clinical tractography analysis of RS-iDTI versus SS-iDTI data.

## **7.2 Thesis limitations**

A number of general limitations relevant to the studies presented in this thesis need to be considered.

### **7.2.1 Small sample size**

All studies in this thesis are single-centred investigations with fewer than 40 participants, which may limit our statistical power particularly for secondary

analyses. Study #1, in particular, should be considered a proof-of-principle study suggesting—but not proving conclusively—that DWI provides relevant prognostic information on structural and functional outcome at the individual patient level. It is important to highlight that in studies #1 and #2, ensuring adequately long postoperative surveillance of clinically relevant outcome variables (e.g., delayed clinical examination in study #1 and delayed assessment of seizure outcome in study #2) frequently limits sample size due to a variety of clinical factors which hamper long-term clinical and radiographic follow-up. In study #2, delayed postoperative neuropsychological assessment could not be collected in more than 30% of study participants. In the longitudinally imaged postoperative group in study #2, another important factor affecting sample size and recruitment was patient tolerance of rigorous, ultra-early postoperative imaging involving up to 4 scans in the first postoperative week. Although a larger-scale, multi-centred study of the perioperative changes identified in this thesis is an important next step (discussed below in 7.2.2), performing such a study using manual volumetry techniques would—thanks to the laborious nature of this method—likely limit sample size to 50 – 100 patients (see section 1.2.2.3.1). Also, although automated volumetry techniques would be an interesting to explore, their application to the abnormal postoperative brain is fraught with challenges that have yet to be overcome (section 1.2.2.3.2). Finally, multi-centred designs or, similarly, multi-scanner clinical studies within an

institution, when analyzed for volumetry would introduce a new source of error due to interscanner variability (Biberacher et al., 2016).

### **7.2.2 Confounding factors**

It is important to acknowledge several potentially confounding clinical factors of the results presented in this thesis. For example, in study #1, the impact of non-convulsive status epilepticus on the presented results is unclear, given (as explained in chapter 3) the lack of continuous EEG in the pediatric intensive care unit during these patients' admissions. In study #2, surgical treatment (i.e., ATL versus SAH) and postoperative AED regimens were heterogeneous. Moreover, we were not able to include a non-surgical, drug-resistant TLE group to compare to our TLE surgical group, and as such, comparisons were made to longitudinal changes in healthy control subjects of similar age.

## **7.3 Future directions**

The findings presented in this thesis clearly establish the perioperative period as a novel opportunity to explore the evolution of structural and functional consequences of neurosurgical diseases and their relationship to clinically relevant outcome variables. Directions for future work are specifically highlighted, for each study, below.

Specifically, in the area of pediatric TBI, future work will include a prospective longitudinal study examining the relationship between acute diffusion brain changes and delayed structural and functional outcomes in infants. Inclusion of patients suffering from suspected or proven NAT as well as those with accidental TBI may help to develop early post-incident MRI-based markers of NAT related TBI or may further help to develop our ability to use acute DWI scans to prognosticate relevant patient outcomes.

With respect to study #2, future efforts will focus on expanding our understanding of structural changes of the brain after TLE surgery using larger data sets collected from the clinical setting (rather than from dedicated research protocols) across different scanners and surgical centres. If a structural MRI biomarker is to be of clinical use, then the ability to measure it on widely available clinical T1-weighted images, regardless of scanner or centre, would be a significant step forward. In addition, given the laborious nature of manual volumetry, future work should investigate the reliability of applying automated volumetric techniques to the postoperative brain, compared to the gold standard of manual volumetry. In this way, putative biomarkers of seizure outcome, such as contralateral hippocampal volume, may be evaluated in larger sample sizes accompanied by adequate postoperative seizure surveillance. With respect to hippocampal diffusion in TLE, future research will explore replication of these findings using higher spatial resolution DTI images which will allow examination of the relationship between hippocampal subfield DTI metrics and how they

predict ILAE HS subtype, which has been shown to relate with post-surgical seizure control (Blümcke et al., 2013).

Finally, with respect to intraoperative DTI applications (study #3), next steps will focus on routine neurophysiological interrogation of white matter tracts using cortical and subcortical DES to confirm that iDTI with reduced susceptibility-artifact and geometrical distortion translates into more accurate spatial information about white matter tracts. This will no doubt prove to be a challenging goal, requiring awake craniotomies such that white matter tracts apart from the CSpT (such as those involved with productive and receptive speech) can be stimulated, and the distance from stimulation sites to reconstructed tracts can be determined to generate a distance-current relationship.

## **7.4 Conclusions**

In summary, this thesis provides novel evidence linking perioperative changes in brain structure—as detected in vivo using MRI—to clinically relevant surgical outcome variables across a variety of neurosurgical diseases. The thesis also shows that intraoperative MRI acquisition can be optimized to provide more clinically useful information to the neurosurgeon (i.e., iDTI). The presented data establish the perioperative period as a novel opportunity to interrogate brain structure using MRI in a longitudinal fashion using a variety of macrostructural

or microstructural measures which as demonstrated in this thesis may serve as putative biomarkers of patient outcome. For the time being, it remains difficult to extend these techniques to the clinical realm to permit the generalizability and broad utility of such biomarkers while ensuring the adequate long-term postoperative surveillance necessary to ensure the durability of clinically relevant outcomes.

## References

Ahmadi, M., Hagler Jr, D., McDonald, C., Tecoma, E., Iragui, V., Dale, A., Halgren, E.,  
2009. Side matters: diffusion tensor imaging tractography in left and right  
temporal lobe epilepsy. *Am. J. Neuroradiol.* 30, 1740–1747.  
doi:10.3174/ajnr.A1650.Side

Akai, H., Mori, H., Aoki, S., Masutani, Y., Kawahara, N., Shibahara, J., Ohtomo, K.,  
2005. Diffusion Tensor Tractography of Gliomatosis Cerebri. *J. Comput.*  
*Assist. Tomogr.* 29, 127–129. doi:10.1097/01.rct.0000148453.29579.51

Albi, A., Meola, A., Zhang, F., Kahali, P., Rigolo, L., Tax, C.M.W., Ciris, P.A., Essayed,  
W.I., Unadkat, P., Norton, I., Rathi, Y., Olubiyi, O., Golby, A.J., O'Donnell, L.J.,  
2018. Image Registration to Compensate for EPI Distortion in Patients with  
Brain Tumors: An Evaluation of Tract-Specific Effects. *J. Neuroimaging* 1–10.  
doi:10.1111/jon.12485

Alex, Mamourian, e. C., Rodichok, L., Towfighi, J., 1995. The Asymmetric  
Mamillary Body: Association with Medial Temporal Lobe Disease  
Demonstrated with MR 1–11.

Alexander, A.L., Lee, J.E., Lazar, M., Field, A.S., 2007. Diffusion tensor imaging of  
the brain. *Neurotherapeutics* 4, 316–329. doi:10.1016/j.nurt.2007.05.011

Anderson, V., Catroppa, C., Morse, S., Haritou, F., Rosenfeld, J., 2005. Functional  
plasticity or vulnerability after early brain injury? *Pediatrics* 116, 1374–

1382. doi:10.1542/peds.2004-1728

Anderson, V., Catroppa, C., Morse, S., Haritou, F., Rosenfeld, J., 2000. Recovery of intellectual ability following traumatic brain injury in childhood: impact of injury severity and age at injury. *Pediatr. Neurosurg.* 32, 282–290.  
doi:10.1159/000028956

Andersson, D., Wilhelmsson, U., Nilsson, M., Kubista, M., Ståhlberg, A., Pekna, M., Pekny, M., 2013. Plasticity Response in the Contralesional Hemisphere after Subtle Neurotrauma: Gene Expression Profiling after Partial Deafferentation of the Hippocampus. *PLoS One* 8. doi:10.1371/journal.pone.0070699

Andersson, J.L.R., Jenkinson, M., Smith, S., 2007. Non-linear registration, aka spatial normalisation. FMRIB Technical Report TR07JA2., FMRIB Technical Report TR07JA2.

Araújo, D., Santos, A.C., Velasco, T.R., Wichert-Ana, L., Terra-Bustamante, V.C., Alexandre, V., Carlotti, C.G., Assirati, J. a., Machado, H.R., Walz, R., Leite, J.P., Sakamoto, A.C., kec, Araujo, D., Santos, A.C., Velasco, T.R., Wichert-Ana, L., Terra-Bustamante, V.C., Alexandre, V., Carlotti, C.G., Assirati, J. a., Machado, H.R., Walz, R., Leite, J.P., Sakamoto, A.C., 2006. Volumetric evidence of bilateral damage in unilateral mesial temporal lobe epilepsy. *Epilepsia* 47, 1354–1359. doi:10.1111/j.1528-1167.2006.00605.x

Arfanakis, K., Arfanakis, K., Hermann, B.P., Hermann, B.P., Rogers, B.P., Rogers,

- B.P., Carew, J.D., Carew, J.D., Seidenberg, M., Seidenberg, M., Meyerand, M.E., Meyerand, M.E., 2002. Diffusion tensor MRI in temporal lobe epilepsy. *Magn. Reson. Imaging* 20, 511–9. doi:10.1016/S0730-725X(02)00509-X
- Arruda, F., Cendes, F., Andermann, F., Dubeau, F., Villemure, J.G., Jones-Gotman, M., Poulin, N., Arnold, D.L., Olivier, a, 1996. Mesial atrophy and outcome after amygdalohippocampectomy or temporal lobe removal. *Ann. Neurol.* 40, 446–450. doi:10.1002/ana.410400314
- Ashwal, S., Wycliffe, N.D., Holshouser, B.A., 2011. Advanced neuroimaging in children with nonaccidental trauma. *Dev. Neurosci.* 32, 343–360. doi:10.1159/000316801
- Assaf, B.A., Mohamed, F.B., Abou-Khaled, K.J., Williams, J.M., Yazeji, M.S., Haselgrove, J., Faro, S.H., 2003. Diffusion tensor imaging of the hippocampal formation in temporal lobe epilepsy. *AJNR Am. J. Neuroradiol.* 24, 1857–1862.
- Bandstra, N.F., Camfield, C.S., Camfield, P.R., 2008. Stigma of epilepsy. *Can. J. Neurol. Sci.* 35, 436–40. doi:DOI: 10.1017/S0317167100009082
- Barnes, J., Ridgway, G.R., Bartlett, J., Henley, S.M.D., Lehmann, M., Hobbs, N., Clarkson, M.J., MacManus, D.G., Ourselin, S., Fox, N.C., 2010. Head size, age and gender adjustment in MRI studies: A necessary nuisance? *Neuroimage* 53, 1244–1255. doi:10.1016/j.neuroimage.2010.06.025

- Barnes, P.D., 2011. Imaging of Nonaccidental Injury and the Mimics: Issues and Controversies in the Era of Evidence-Based Medicine. *Radiol. Clin. North Am.* 49, 205–229. doi:10.1016/j.rcl.2010.08.001
- Bartolomei, F., Chauvel, P., Wendling, F., 2008. Epileptogenicity of brain structures in human temporal lobe epilepsy: a quantified study from intracerebral EEG. *Brain* 131, 1818–1830.
- Basser, P.J., Jones, D.K., 2002. Diffusion-tensor MRI: theory, experimental design and data analysis - a technical review. *NMR Biomed* 15, 456–467. doi:10.1002/nbm.783
- Basser, P.J., Pajevic, S., Pierpaoli, C., Duda, J., Aldroubi, A., 2000. In Vivo Fiber Tractography. *Magnetic Reson. Med.* 44, 625–632. doi:10.1002/1522-2594(200010)44
- Bastin, M.E., Rana, A.K., Wardlaw, J.M., Armitage, P.A., Keir, S.L., 2000. A study of the apparent diffusion coefficient of grey and white matter in human ischaemic stroke. *Neuroreport* 11, 2867–2874.
- Baxendale, S., Thompson, P., Duncan, J., 2008. Improvements in memory function following anterior temporal lobe resection for epilepsy 1319–1325.
- Behrens, T.E.J., Berg, H.J., Jbabdi, S., Rushworth, M.F.S., Woolrich, M.W., 2007. Probabilistic diffusion tractography with multiple fibre orientations: What can we gain? *Neuroimage* 34, 144–155.

doi:10.1016/j.neuroimage.2006.09.018

Bello, L., Gambini, A., Castellano, A., Carrabba, G., Acerbi, F., Fava, E., Giussani, C., Cadioli, M., Blasi, V., Casarotti, A., Papagno, C., Gupta, A.K., Gaini, S., Scotti, G., Falini, A., 2008. Motor and language DTI Fiber Tracking combined with intraoperative subcortical mapping for surgical removal of gliomas.

Neuroimage 39, 369–82. doi:10.1016/j.neuroimage.2007.08.031

Bengtson, M., Martin, R., Sawrie, S., Gilliam, F., Faught, E., Morawetz, R., Kuzniecky, R., Trenerry, M.R., 2000. Gender, memory, and hippocampal volumes: relationships in temporal lobe epilepsy to the editor. *Epilepsy Behav.* 1, 195–196. doi:10.1006/ebeh.2000.0051

Berg, A.T., 2004. Understanding the delay before epilepsy surgery: who develops intractable focal epilepsy and when? *CNS Spectr.* 9, 136–144.

Berkovic, S.F., Andermann, F., Olivier, A., Ethier, R., Melanson, D., Robitaille, Y., Kuzniecky, R., Peters, T., Feindel, W., 1991. Hippocampal sclerosis in temporal lobe epilepsy demonstrated by magnetic resonance imaging. *Ann. Neurol.* 29, 175–82. doi:10.1002/ana.410290210

Berkovic, S.F., McIntosh, a M., Kalnins, R.M., Jackson, G.D., Fabinyi, G.C., Brazenor, G. a, Bladin, P.F., Hopper, J.L., 1995. Preoperative MRI predicts outcome of temporal lobectomy: an actuarial analysis. *Neurology* 45, 1358–1363. doi:10.1212/WNL.45.7.1358

- Bernasconi, A., Bernasconi, N., Caramanos, Z., Reutens, D.C., Andermann, F., Tampieri, D., Pike, B.G., Arnold, D.L., 2000. T2 relaxometry can lateralize mesial temporal lobe epilepsy in patients with normal MRI. *Neuroimage* 12, 739–746. doi:10.1006/nimg.2000.0622
- Bernasconi, N., 2003. Mesial temporal damage in temporal lobe epilepsy: a volumetric MRI study of the hippocampus, amygdala and parahippocampal region. *Brain* 126, 462–469. doi:10.1093/brain/awg034
- Bernasconi, N., Andermann, F., Arnold, D.L., Bernasconi, A., 2003. Entorhinal cortex MRI assessment in temporal, extratemporal, and idiopathic generalized epilepsy. *Epilepsia* 44, 1070–1074. doi:10.1046/j.1528-1157.2003.64802.x
- Bernasconi, N., Bernasconi, A., Caramanos, Z., Dubeau, F., Richardson, J., Andermann, F., Arnold, D., 2001. Entorhinal cortex atrophy in epilepsy patients exhibiting normal hippocampal volumes. *Neurology* 56, 1335–1339.
- Bernasconi, N., Duchesne, S., Janke, A., Lerch, J., Collins, D.L., Bernasconi, A., 2004. Whole-brain voxel-based statistical analysis of gray matter and white matter in temporal lobe epilepsy. *Neuroimage* 23, 717–723. doi:10.1016/j.neuroimage.2004.06.015
- Bernasconi, N., Natsume, J., Bernasconi, A., 2005. Progression in temporal lobe

epilepsy: differential atrophy in mesial temporal structures. *Neurology* 65, 223–228. doi:10.1212/01.wnl.0000169066.46912.fa

Bernhardt, B.C., Bernasconi, A., Liu, M., Hong, S.-J., Caldairou, B., Goubran, M., Guiot, M.C., Hall, J., Bernasconi, N., 2016. The spectrum of structural and functional imaging abnormalities in temporal lobe epilepsy. *Ann. Neurol.* 1–12. doi:10.1002/ana.24691

Bernhardt, B.C., Bernasconi, N., Concha, L., Bernasconi, A., 2010. Cortical thickness analysis in temporal lobe epilepsy: Reproducibility and relation to outcome. *Neurology* 74, 1776–84. doi:10.1212/WNL.0b013e3181e0f80a

Bernhardt, B.C., Kim, H., Bernasconi, N., 2013. Patterns of subregional mesiotemporal disease progression in temporal lobe epilepsy. *Neurology* 81, 1840–1847. doi:10.1212/01.wnl.0000436069.20513.92

Bernhardt, B.C., Worsley, K.J., Besson, P., Concha, L., Lerch, J.P., Evans, A.C., Bernasconi, N., 2008. Mapping limbic network organization in temporal lobe epilepsy using morphometric correlations: Insights on the relation between mesiotemporal connectivity and cortical atrophy. *Neuroimage* 42, 515–524. doi:10.1016/j.neuroimage.2008.04.261

Biberacher, V., Schmidt, P., Keshavan, A., Boucard, C.C., Righart, R., Sämann, P., Preibisch, C., Fröbel, D., Aly, L., Hemmer, B., Zimmer, C., Henry, R.G., Mühlau, M., 2016. Intra- and interscanner variability of magnetic resonance imaging

based volumetry in multiple sclerosis. *Neuroimage* 142, 188–197.

doi:10.1016/j.neuroimage.2016.07.035

Bilir, E., Craven, W., Hugg, J., Gilliam, F., Martin, R., Faught, E., Kuzniecky, R., 1998.

Volumetric MRI of the limbic system: anatomic determinants.

*Neuroradiology* 40, 138–44.

Biousse, V., Suh, D.Y., Newman, N.J., Davis, P.C., Mapstone, T., Lambert, S.R., 2002.

Diffusion-weighted magnetic resonance imaging in Shaken Baby Syndrome.

*Am. J. Ophthalmol.* 133, 249–55.

Black, P., Moriarty, T., Alexander, E., Stieg, P., Woodard, E., Gleason, P., Martin, C.,

Kikinis, R., Schwartz, R., Jolesz, F., 1997. Development and implementation

of intraoperative magnetic resonance imaging and its neurosurgical

applications. *Neurosurgery* 41, 831–845.

Blaus, B., 2014. Medical gallery of Blausen Medical 2014. *WikiJournal Med.* 1.

doi:10.15347/wjm/2014.010

Bloch, F., 1946. Nuclear induction. *Phys Rev* 70, 460–474.

Blümcke, I., 2009. Neuropathology of focal epilepsies: A critical review. *Epilepsy*

*Behav.* 15, 34–39. doi:10.1016/j.yebeh.2009.02.033

Blümcke, I., 2009. Neuropathology of focal epilepsies: A critical review. *Epilepsy*

*Behav.* 15, 34–39. doi:10.1016/j.yebeh.2009.02.033

- Blümcke, I., Pauli, E., Clusmann, H., Schramm, J., Becker, A., Elger, C., Merschhemke, M., Meencke, H.J., Lehmann, T., Deimling, A., Scheiwe, C., Zentner, J., Volk, B., Romstöck, J., Stefan, H., Hildebrandt, M., Von Deimling, A., Scheiwe, C., Zentner, J., Volk, B., Romstöck, J., Stefan, H., Hildebrandt, M., 2007. A new clinico-pathological classification system for mesial temporal sclerosis. *Acta Neuropathol.* 113, 235–244. doi:10.1007/s00401-006-0187-0
- Blumcke, I., Spreafico, R., 2012. Cause matters: a neuropathological challenge to human epilepsies. *Brain Pathol.* 22, 347–349.
- Blümcke, I., Thom, M., Aronica, E., Armstrong, D.D., Bartolomei, F., Bernasconi, A., Bernasconi, N., Bien, C.G., Cendes, F., Coras, R., Cross, J.H., Jacques, T.S., Kahane, P., Mathern, G.W., Miyata, H., Moshé, S.L., Oz, B., Özkara, Ç., Perucca, E., Sisodiya, S., Wiebe, S., Spreafico, R., 2013. International consensus classification of hippocampal sclerosis in temporal lobe epilepsy: A Task Force report from the ILAE Commission on Diagnostic Methods. *Epilepsia* 54, 1315–1329. doi:10.1111/epi.12220
- Boccardi, M., Bocchetta, M., Apostolova, L.G., Barnes, J., Bartzokis, G., Corbetta, G., Decarli, C., Ganzola, R., Gerritsen, L., Henneman, W., Killiany, R.J., Malykhin, N., Pasqualetti, P., Pruessner, J.C., Redolfi, A., Soininen, H., Tolomeo, D., Wang, L., Watson, C., Wolf, H., Duvernoy, H., Duchesne, S., Frisoni, G.B., 2015. Delphi definition of the EADC-ADNI Harmonized Protocol for hippocampal

segmentation on magnetic resonance. *Alzheimer's Dement.* 11, 126–138.  
doi:10.1016/j.jalz.2014.02.009.Delphi

Boccardi, M., Bocchetta, M., Apostolova, L.G., Preboske, G., Robitaille, N.,  
Pasqualetti, P., Collins, L.D., Duchesne, S., Jack, C.R., Frisoni, G.B., 2014.  
Establishing Magnetic Resonance Images Orientation for the EADC-ADNI  
Manual Hippocampal Segmentation Protocol. *J. Neuroimaging* 24, 509–514.  
doi:10.1111/jon.12065

Boccardi, M., Ganzola, R., Bocchetta, M., Pievani, M., Redolfi, A., Bartzokis, G.,  
Camicioli, R., Czernansky, J., de Leon, M., DeToledo-Morrell, L., Killiany, R.,  
Lehericy, S., Pantel, J., Pruessner, J., Soininen, H., Watson, C., Duchesne, S.,  
Jack, C.J., Frisoni, G., 2011. Survey of protocols for the manual segmentation  
of the hippocampus: preparatory steps towards a joint EADC-ADNI  
harmonized protocol. *J. Alzheimer's Dis.* 26, 1–24. doi:10.3233/JAD-2011-  
0004.Survey

Bonilha, L., Edwards, J.C., Kinsman, S.L., Morgan, P.S., Fridriksson, J., Rorden, C.,  
Rumboldt, Z., Roberts, D.R., Eckert, M.A., Halford, J.J., 2010.  
Extrahippocampal gray matter loss and hippocampal deafferentation in  
patients with temporal lobe epilepsy. *Epilepsia* 51, 519–528.  
doi:10.1111/j.1528-1167.2009.02506.x

Bonilha, L., Keller, S.S., 2015. Quantitative MRI in refractory temporal lobe  
epilepsy: relationship with surgical outcomes. *Quant. Imaging Med. Surg.* 5,

204–24. doi:10.3978/j.issn.2223-4292.2015.01.01

Bonilha, L., Kobayashi, E., Cendes, F., Li, L.M., 2004a. Protocol for volumetric segmentation of medial temporal structures using high-resolution 3-D magnetic resonance imaging. *Hum. Brain Mapp.* 22, 145–154.  
doi:10.1002/hbm.20023

Bonilha, L., Rorden, C., Castellano, G., Pereira, F., Rio, P.A., Cendes, F., Li, L.M., 2004b. Voxel-based morphometry reveals gray matter network atrophy in refractory medial temporal lobe epilepsy. *Arch. Neurol.* 61, 1379–1384.  
doi:10.1001/archneur.61.9.1379

Bonilha, L., Rorden, C., Halford, J.J., Eckert, M., Appenzeller, S., Cendes, F., Li, L.M., 2007. Asymmetrical extra-hippocampal grey matter loss related to hippocampal atrophy in patients with medial temporal lobe epilepsy. *J. Neurol. Neurosurg. Psychiatry* 78, 286–294. doi:10.1136/jnnp.2006.103994

Bonnier, C., Mesples, B., Gressens, P., 2004. Animal models of shaken baby syndrome: Revisiting the pathophysiology of this devastating injury. *Pediatr. Rehabil.* 7, 165–171. doi:10.1080/13638490410001703325

Bonnier, C., Nassogne, M.-C., Saint-Martin, C., Mesples, B., Kadhim, H., Sébire, G., 2003. Neuroimaging of intraparenchymal lesions predicts outcome in shaken baby syndrome. *Pediatrics* 112, 808–814.  
doi:10.1542/peds.112.4.808

- Bouchet, C., Cazauvieilh, C., 1825. De l'épilepsie considérée dans ses rapports avec l'aliénation mentale. Recherche sur la nature et le siège de ces deux maladies. *Arch Gen Med* 510–542.
- Brant-Zawadzki, M., Gillan, G., Nitz, W., 1992. MP RAGE: a three-dimensional, T1-weighted, gradient-echo sequence--initial experience in the brain. *Radiology* 182, 769–775. doi:10.1148/radiology.182.3.1535892
- Briellmann, R.S., Syngeniotis, A., Jackson, G.D., 2001. Comparison of hippocampal volumetry at 1.5 tesla and at 3 tesla. *Epilepsia* 42, 1021–1024. doi:10.1046/j.1528-1157.2001.0420081021.x
- Brierley, J.B., Excell, B.J., 1966. The Effects of Profound Systemic Hypotension upon the Brain of M. Rhesus: Physiological and Pathological Observations. *Brain* 89, 269–298.
- Brinkmann, B.H., Manduca, A., Robb, R.A., 1998. Optimized homomorphic unsharp masking for MR grayscale inhomogeneity correction. *IEEE Trans. Med. Imaging* 17, 161–171. doi:10.1109/42.700729
- Broca, P., 1878. Anatomie comparée des circonvolutions cérébrales: le grande lobe limbique et la scissure limbique dans la série des mammifères. *Rev D'Anthropol* 1, 385–498.
- Brody, A.S., Frush, D.P., Huda, W., Brent, R.L., 2007. Radiation Risk to Children From Computed Tomography. *Pediatrics* 120, 677–682.

doi:10.1542/peds.2007-1910

Bronen, R., Cheung, G., Charles, J., 1989. Mesial temporal sclerosis: comparison of MR, CT, angiography, EEG, and pathology. *Am. J. Neuroradiol.* 10, 897.

Bronen, R.A., Cheung, G., Charles, J.T., Kim, J.H., Spencer, D.D., Spencer, S.S., Sze, G., McCarthy, G., 1991. Imaging findings in hippocampal sclerosis: Correlation with pathology. *Am. J. Neuroradiol.* 12, 933–940. doi:epilepsy-Converted #99; Used to be #1969

Bronen, R.A., Fulbright, R.K., Kim, J.H., Spencer, S.S., Spencer, D.D., Al-Rodhan, N.R., 1995. Regional distribution of MR findings in hippocampal sclerosis. *AJNR. Am. J. Neuroradiol.* 16, 1193–1200.

Bucholz, R., McDurmont, L., 2009. The history, current status, and future of the stealthstation treatment guidance system. Springer Nature.

Buga, a. M., Sascau, M., Pisoschi, C., Herndon, J.G., Kessler, C., Popa-Wagner, a., 2008. The genomic response of the ipsilateral and contralateral cortex to stroke in aged rats. *J. Cell. Mol. Med.* 12, 2731–2753. doi:10.1111/j.1582-4934.2008.00252.x

Butts, K., De Crespigny, A., Pauly, J.M., Moseley, M., 1996. Diffusion-weighted interleaved echo-planar imaging with a pair of orthogonal navigator echoes. *Magn. Reson. Med.* 35, 763–770. doi:10.1002/mrm.1910350518

Caciagli, L., Bernasconi, A., Wiebe, S., Koepp, M.J., Bernasconi, N., Bernhardt, B.C.,

2017. A meta-Analysis on progressive atrophy in intractable temporal lobe epilepsy: Time is brain? *Neurology* 89, 506–516.

doi:10.1212/WNL.0000000000004176

Cajal S, R. y, 1894. The Croonian Lecture: La Fine Structure des Centres Nerveux. *Proc R Soc L.* 55, 444–468.

Caramanos, Z., Fonov, V.S., Francis, S.J., Narayanan, S., Pike, G.B., Collins, D.L., Arnold, D.L., 2010. Gradient distortions in MRI: Characterizing and correcting for their effects on SIENA-generated measures of brain volume change. *Neuroimage* 49, 1601–1611.

doi:10.1016/j.neuroimage.2009.08.008

Catani, M., Howard, R.J., Pajevic, S., Jones, D.K., 2002. Virtual in Vivo interactive dissection of white matter fasciculi in the human brain. *Neuroimage* 17, 77–94. doi:10.1006/nimg.2002.1136

Catani, M., Thiebaut de Schotten, M., 2008. A diffusion tensor imaging tractography atlas for virtual in vivo dissections. *Cortex* 44, 1105–1132.

doi:10.1016/j.cortex.2008.05.004

CDC, 1990. Childhood injuries in the United States, *Am J Dis Child.*

Cendes, F., Andermann, F., Dubeau, F., Matthews, P.M., Arnold, D., 1997.

Normalization of neuronal metabolic dysfunction after surgery for temporal lobe epilepsy: Evidence from proton MR spectroscopic imaging. *Neurology*

49, 1525–1533.

Cendes, F., Andermann, F., Gloor, P., Evans, A., Jones-Gotman, M., Watson, C., Melanson, D., Oliver, A., Peters, T., Lopes-Cendes, I., 1993a. MRI volumetric measurement of amygdala and hippocampus in temporal lobe epilepsy. *Neurology* 43, 719–725.

Cendes, F., Andermann, F., Preul, M.C., Arnold, D.L., 1994. Lateralization of temporal lobe epilepsy based on regional metabolic abnormalities in proton magnetic resonance spectroscopic images. *Ann. Neurol.* 35, 211–216.  
doi:10.1002/ana.410350213

Cendes, F., Knowlton, R.C., Novotny, E., Min, L.L., Antel, S., Sawrie, S., Laxer, K.D., Arnold, D., 2002. Magnetic resonance spectroscopy in epilepsy: Clinical issues. *Epilepsia* 43, 32–39. doi:10.1046/j.1528-1157.2002.043s1032.x

Cendes, F., Leproux, F., Melanson, D., Ethier, R., Evans, A., Peters, T., Andermann, F., 1993b. MRI of amygdala and hippocampus in temporal lobe epilepsy. *J Comput Assist Tomogr* 17, 206–210.

Chalela, J., Wolf, R., Maldjian, J., Kasner, S., 2001. MRI identification of early white matter injury in anoxic-ischemic encephalopathy. *Neurology* 56, 481–485.

Chan, S., Erickson, J., Yoon, S., 1997. Limbic System malities Associated with Mesial Temporal Sclerosis : A Model of Chronic Cerebral Changes Due to. *Radio* 17, 1095–1110.

- Chatzikonstantinou, A., Gass, A., Förster, A., Hennerici, M.G., Szabo, K., 2011.  
Features of acute DWI abnormalities related to status epilepticus. *Epilepsy Res.* 97, 45–51. doi:10.1016/j.eplepsyres.2011.07.002
- Chau, W., McIntosh, A.R., 2005. The Talairach coordinate of a point in the MNI space: How to interpret it. *Neuroimage* 25, 408–416.  
doi:10.1016/j.neuroimage.2004.12.007
- Chiapponi, C., Piras, F., Fagioli, S., Girardi, P., Caltagirone, C., Spalletta, G., 2014.  
Hippocampus age-related microstructural changes in schizophrenia: A case-control mean diffusivity study. *Schizophr. Res.* 157, 214–217.  
doi:10.1016/j.schres.2014.05.028
- Cho, K., 2001. Chronic “jet lag” produces temporal lobe atrophy and spatial cognitive deficits. *Nat. Neurosci.* 4, 567–568. doi:10.1038/88384
- Choudhri, A., Chin, E., Klimo, P., Boop, F., 2014a. Spatial distortion due to field inhomogeneity in 3.0 tesla intraoperative MRI. *Neuroradiol. J.* 27, 387–392.  
doi:10.15274/NRJ-2014-10081
- Choudhri, A., Klimo, P., Auschwitz, T., Whitehead, M., Boop, F., 2014b. 3T Intraoperative MRI for Management of Pediatric CNS Neoplasms. *Pediatrics* 35, 2382–2387.
- Clusmann, H., Schramm, J., Kral, T., Helmstaedter, C., Ostertun, B., Fimmers, R., Haun, D., Elger, C.E., 2002. Prognostic factors and outcome after different

types of resection for temporal lobe epilepsy. *J. Neurosurg.* 97, 1131–1141.  
doi:10.3171/jns.2002.97.5.1131

Coan, A.C., Kobayashi, E., 2004. Abnormalities of hippocampal signal intensity in patients with familial mesial temporal lobe epilepsy. *Braz J Med Biol Res* 37, 827–832. doi:10.1177/1043454203254645

Coan, A.C., Kubota, B., Bergo, F.P.G., Campos, B.M., Cendes, F., 2014. 3T MRI quantification of hippocampal volume and signal in mesial temporal lobe epilepsy improves detection of hippocampal sclerosis. *Am. J. Neuroradiol.* 35, 77–83. doi:10.3174/ajnr.A3640

Coburger, J., König, R., Seitz, K., Bätzner, U., Wirtz, C.R., Hlavac, M., 2014. Determining the utility of intraoperative magnetic resonance imaging for transsphenoidal surgery: a retrospective study. *J. Neurosurg.* 120, 346–356. doi:10.3171/2013.9.JNS122207

Coburger, J., Merkel, A., Scherer, M., Schwartz, F., Gessler, F., Roder, C., Pala, A., König, R., Bullinger, L., Nagel, G., Jungk, C., Bisdas, S., Nabavi, A., Ganslandt, O., Seifert, V., Tatagiba, M., Senft, C., Mehdorn, M., Unterberg, A.W., Rössler, K., Wirtz, C.R., 2016. Low-grade glioma surgery in intraoperative magnetic resonance imaging: Results of a multicenter retrospective assessment of the german study group for intraoperative magnetic resonance imaging. *Neurosurgery* 78, 775–785. doi:10.1227/NEU.0000000000001081

- Coburger, J., Wirtz, C., Konig, R., 2017. Impact of extent of resection and recurrent surgery on clinical outcome and overall survival in a consecutive series of 170 patients for glioblastoma in intraoperative high field magnetic resonance imaging. *J Neurosurg Sci* 61, 233–244.
- Coenen, V., Krings, T., Mayfrank, L., Polin, R., Reinges, M., Thron, A., Gilsbach, J., 2001. Three-dimensional visualization of the pyramidal tract in a neuronavigation system during brain tumor surgery: first experiences and technical note. *Neurosurgery* 49, 86–93.
- Cohen-Adad, J., 2012. High-Resolution DWI in Brain and Spinal Cord with syngo RESOLVE 1. Siemens Magnetom - *Clin. Neurol.* 510, 16–23.
- Cohen-Gadol, A. a, Wilhelmi, B.G., Collignon, F., White, J.B., Britton, J.W., Cambier, D.M., Christianson, T.J.H., Marsh, W.R., Meyer, F.B., Cascino, G.D., 2006. Long-term outcome of epilepsy surgery among 399 patients with nonlesional seizure foci including mesial temporal lobe sclerosis. *J. Neurosurg.* 104, 513–524. doi:10.3171/jns.2006.104.4.513
- Cole, A., 2004. Status epilepticus and peri-ictal imaging. *Epilepsia* 45, 72–77.
- Colon-Perez, L.M., Triplett, W., Bohsali, A., Corti, M., Nguyen, P.T., Patten, C., Mareci, T.H., Price, C.C., 2016. A majority rule approach for region-of-interest-guided streamline fiber tractography. *Brain Imaging Behav.* 10, 1137–1147. doi:10.1007/s11682-015-9474-5

- Concha, L., Beaulieu, C., Collins, D.L., Gross, D.W., 2009. White-matter diffusion abnormalities in temporal-lobe epilepsy with and without mesial temporal sclerosis. *J. Neurol. Neurosurg. Psychiatry* 80, 312–319.  
doi:10.1136/jnnp.2007.139287
- Concha, L., Beaulieu, C., Gross, D.W., 2005a. Bilateral limbic diffusion abnormalities in unilateral temporal lobe epilepsy. *Ann. Neurol.* 57, 188–196. doi:10.1002/ana.20334
- Concha, L., Beaulieu, C., Wheatley, B.M., Gross, D.W., 2007. Bilateral White Matter Diffusion Changes Persist after Epilepsy Surgery. *Epilepsia* 48, 931–940.  
doi:10.1111/j.1528-1167.2007.01006.x
- Concha, L., Gross, D.W., Beaulieu, C., L, C., Concha, L., Gross, D.W., Beaulieu, C., L, C., 2005b. Diffusion Tensor Tractography of the Limbic System. *AJNR. Am. J. Neuroradiol.* 26, 1–8.
- Concha, L., Livy, D.J., Beaulieu, C., Wheatley, B.M., Gross, D.W., 2010. In Vivo Diffusion Tensor Imaging and Histopathology of the Fimbria-Fornix in Temporal Lobe Epilepsy. *J. Neurosci.* 30, 996–1002.  
doi:10.1523/JNEUROSCI.1619-09.2010
- Cook, M.J., Fish, D.R., Shorvon, S.D., Straughan, K., Stevens, J.M., 1992. Hippocampal volumetric and morphometric studies in frontal and temporal lobe epilepsy. *Brain* 115 ( Pt 4, 1001–1015. doi:10.1093/brain/115.4.1001

- Copenhaver, B.R., Rabin, L. a., Saykin, A.J., Roth, R.M., Wishart, H. a., Flashman, L. a., Santulli, R.B., McHugh, T.L., Mamourian, A.C., 2006. The fornix and mammillary bodies in older adults with Alzheimer's disease, mild cognitive impairment, and cognitive complaints: A volumetric MRI study. *Psychiatry Res. - Neuroimaging* 147, 93–103. doi:10.1016/j.psychresns.2006.01.015
- Corkin, S., 1965. Tactually guided maze learning in man: Effects of unilateral cortical excisions and bilateral hippocampal lesions. *Neuropsychologia* 3, 339–352.
- D'Agostino, E., Maes, F., Vandermeulen, D., Suetens, P., 2003. A viscous fluid model for multimodal non-rigid image registration using mutual information. *IEEE Trans. Med. Image Anal.* 7, 565–575. doi:Doi 10.1016/S1361-8415(03)00039-2
- Dale, A., Fischl, B., Sereno, M., 1999. Cortical Surface-Based Analysis. *Neuroimage* 9, 179–194. doi:10.1006/nimg.1998.0395
- Damadian, R., 1971. Tumor detection by nuclear magntic resonance. *Science* (80-. ). 171, 1151.
- Damadian, R., Goldsmith, M., Minkoff, L., 1977. NMR in cancer: XVI. FONAR image of the live human body. *Physiol Chem Phys* 9, 97.
- Davis, P., Wright, E., 1977. A new method for measuring cranial cavity volume and its application to the assessment of cerebral atrophy at autopsy.

Neuropathol. Appl. Neurobiol. 3, 341–358. doi:10.1111/j.1365-2990.1977.tb00595.x

de Tisi, J., Bell, G.S., Peacock, J.L., McEvoy, A.W., Harkness, W.F.J., Sander, J.W., Duncan, J.S., Tisi BA, J., Tisi, J., MD, G.S.B., Peacock, P.J.L., FRCS, A.W.M., FRCS, W.F.H., S, P.J.W., FRCP, e., FRCP, P.J.S.D., 2011. The long-term outcome of adult epilepsy surgery, patterns of seizure remission, and relapse: a cohort study. *Lancet* 378, 1388–1395. doi:10.1016/S0140-6736(11)60890-8

DeCarli, C., Hatta, J., Fazilat, S., Fazilat, S., Gaillard, W.D., Theodore, W.H., 1998. Extratemporal atrophy in patients with complex partial seizures of left temporal origin. *Ann. Neurol.* 43, 41–45. doi:10.1002/ana.410430110

Deitch, J.S., Rubel, E.W., 1989. Changes in neuronal cell bodies in N. laminaris during deafferentation-induced dendritic atrophy. *J. Comp. Neurol.* 281, 259–268. doi:10.1002/cne.902810208

Despotović, I., Goossens, B., Philips, W., 2015. MRI segmentation of the human brain: Challenges, methods, and applications. *Comput. Math. Methods Med.* 2015. doi:10.1155/2015/450341

Devinsky, O., Spruill, T., Thurman, D., Friedman, D., 2016. Recognizing and preventing epilepsy-related mortality A call for action. *Neurology* 86, 779–786. doi:10.1212/WNL.0000000000002253

Donaire, A., Carreno, M., Gómez, B., Fossas, P., Bargalló, N., Agudo, R., Falip, M.,

- Setoain, X., Boget, T., Raspall, T., Obach, V., Rumiá, J., 2006. Cortical laminar necrosis related to prolonged focal status epilepticus. *J. Neurol. Neurosurg. Psychiatry* 77, 104–6. doi:10.1136/jnnp.2004.058701
- Dorward, N.L., Alberti, O., Velani, B., Gerritsen, F.A., Harkness, W.F.J., Kitchen, N.D., Thomas, D.G.T., 1998. Postimaging brain distortion: magnitude, correlates, and impact on neuronavigation. *J. Neurosurg.* 88, 656–662. doi:10.3171/jns.1998.88.4.0656
- Droby, A., Lukas, C., Schänzer, A., Spiwoкс-Becker, I., Giorgio, A., Gold, R., De Stefano, N., Kugel, H., Deppe, M., Wiendl, H., Meuth, S.G., Acker, T., Zipp, F., Deichmann, R., 2015. A human post-mortem brain model for the standardization of multi-centre MRI studies. *Neuroimage* 110, 11–21. doi:10.1016/j.neuroimage.2015.01.028
- Duffau, H., 2014. Diffusion Tensor Imaging Is a Research and Educational Tool, but Not Yet a Clinical Tool. *World Neurosurg.* 82, 10–12. doi:10.1016/j.wneu.2013.08.054
- Duhaime, A., Alario, A.J., Lewander, J., Schult, L., Sutton, L.N., Seidl, T.S., Nudelman, S., Budenz, D., Hertle, R., Tsiaras, W., Loporchio, S., Lewander, W.J., Schut, L., Sutton, L.N., Seidl, T.S., Nudelman, S., Budenz, D., Hertle, R., Tsiaras, W., 1992. Head injury in very young children: mechanisms, injury types, and ophthalmologic findings in 100 hospitalized patients younger than 2 years of age. *Pediatrics* 90, 170–185. doi:10.1016/S0196-

0644(05)80277-X

Duhaime, A., Christian, C., Rorke, L., Zimmerman, R., 1998. Nonaccidental head injury in infants—the “shaken-baby syndrome.” *N. Engl. J. Med.* 338, 1822–1829. doi:10.1056/NEJM199806183382507

Duncan, J.S., 1996. Magnetic resonance spectroscopy. *Epilepsia* 37, 598–605. doi:10.1111/j.1528-1157.1996.tb00622.x

Duning, Heindel, W., Knecht, S., 2005. Deyhydration Confounds the Assessment of Brain Atrophy. *Neurology* 18–21.

Durkin, M.S., Olsen, S., Barlow, B., Virella, A., Connolly, E.S., 1998. The epidemiology of urban pediatric neurological trauma: Evaluation of, and implications for, injury prevention programs. *Neurosurgery* 42, 300–310. doi:10.1097/00006123-199802000-00052

Durnford, A.J., Rodgers, W., Kirkham, F.J., Mullee, M. a., Whitney, A., Prevett, M., Kinton, L., Harris, M., Gray, W.P., 2011. Very good inter-rater reliability of Engel and ILAE epilepsy surgery outcome classifications in a series of 76 patients. *Seizure* 20, 809–812. doi:10.1016/j.seizure.2011.08.004

Duvernoy, H., 1998. *The Human Hippocampus: Functional Anatomy, Vascularization and Serial Sections with MRI.* Springer-Verlag, Berlin.

Duvernoy, H., Cattin, F., Naidich, T., Fatterpekar, G., Raybaud, C., Risold, P., Salvolini, U., Scarabino, T., 2005. *Sectional Anatomy and Magnetic*

Resonance Imaging. *Hum. Hippocampus* 129–217.

Düzel, E., Kaufmann, J., Guderian, S., Szentkuti, A., Schott, B., Bodammer, N., Hopf, M., Kanowski, M., Tempelmann, C., Heinze, H.J., 2004. Measures of hippocampal volumes, diffusion and <sup>1</sup>H MRS metabolic abnormalities in temporal lobe epilepsy provide partially complementary information. *Eur. J. Neurol.* 11, 195–205. doi:10.1046/j.1351-5101.2003.00737.x

Dwivedi, R., Ramanujam, B., Chandra, P.S., Sapra, S., Gulati, S., Kalaivani, M., Garg, A., Bal, C.S., Tripathi, M., Dwivedi, S.N., Sagar, R., Sarkar, C., Tripathi, M., 2017. Surgery for Drug-Resistant Epilepsy in Children. *N. Engl. J. Med.* 377, 1639–1647. doi:10.1056/NEJMoa1615335

Ebisu, T., Naruse, S., Horikawa, Y., Ueda, S., Tanaka, C., Uto, M., Umeda, M., Higuchi, T., 1993. Discrimination between different types of white matter edema with diffusion-weighted MR imaging. *J. Magn. Reson. Imaging* 3, 863–868. doi:10.1002/jmri.1880030612

Einstein, A., 1905. Über die von der molekularkinetischen Theorie der wärme geforderte Bewegung von in ruhenden Flüssigkeiten suspendierten Teilchen. *Ann Phys.* 4, 549–560.

Elliott, C., Fox, R., Ashforth, R., Gourishankar, S., Nataraj, A., 2016. Magnetic resonance imaging artifact following anterior cervical discectomy and fusion with a trabecular metal cage. *J. Neurosurg. Spine* 24, 496–501.

doi:10.3171/2015.5.SPINE14219

Elliott, C.A., Gross, D., Wheatley, B.M., Beaulieu, C., Sankar, T., 2016. Progressive contralateral hippocampal atrophy following surgery for medically refractory temporal lobe epilepsy. *Epilepsy Res.* 125, 62–71.  
doi:10.1016/j.epilepsyres.2016.06.007

Elliott, C.A., Gross, D.W., Wheatley, B.M., Beaulieu, C., Sankar, T., 2018. Longitudinal hippocampal and extra-hippocampal microstructural and macrostructural changes following temporal lobe epilepsy surgery. *Epilepsy Res.* 140, 128–137. doi:10.1016/j.epilepsyres.2018.01.008

Elliott, C.A., Ramaswamy, V., Jacob, F.D., Sankar, T., Mehta, V., 2017. Early diffusion restriction of white matter in infants with small subdural hematomas is associated with delayed atrophy. *Child's Nerv. Syst.* 33, 289–295. doi:10.1007/s00381-016-3271-3

Elster, A., 2015. Questions and answers in MRI [WWW Document]. MRIquestions.com. URL <http://mriquestions.com/index.html> (accessed 3.23.17).

Engel, J., 2016. What can we do for people with drug-resistant epilepsy? *Neurology* 87, 2483–2489. doi:10.1212/WNL.0000000000003407

Engel, J., 2001. ILAE Commission Report A Proposed Diagnostic Scheme for People with Epileptic Seizures and with Epilepsy : Report of the ILAE Task

Force on Classification and Terminology De mo ( V isi t htt p :/ / w lit me rg  
er . co m ) ( V isi t htt p :/ / w ww De fsp. Epilepsia 42, 796–803.

doi:10.1046/j.1528-1157.2001.10401.x

Engel, J., Cascino, G., Ness, P., Rasmussen, T., LM, O., 1993a. Surgical treatment of  
the epilepsies. Raven Press, NY.

Engel, J., Cascino, G., Ness, P., Rasmussen, T., Ojemann, L., 1993b. Outcome with  
respect to epileptic seizures., in: Engel, J. (Ed.), Surgical Treatment of the  
Epilepsies. Raven Press, NY.

Engel, J., Mcdermott, M.P., Wiebe, S., Langfitt, J.T., Stern, J.M., Dewar, S., Sperling,  
M.R., Gardiner, I., Erba, G., Jacobs, M., Vinters, H. V, Mintzer, S., Kieburtz, K.,  
2012. Early Surgical Therapy for Drug-Resistant Temporal Lobe Epilepsy  
307.

England, M.J., Liverman, C.T., Schultz, A.M., Strawbridge, L.M., 2012. A Summary  
of the Institute of Medicine Report: Epilepsy Across the Spectrum:  
Promoting Health and Understanding. Epilepsy Behav 25, 266–276.  
doi:10.1016/j.jacc.2007.01.076.White

Ercan, K., Gunbey, H.P., Bilir, E., Zan, E., Arslan, H., 2016. Comparative  
Lateralizing Ability of Multimodality MRI in Temporal Lobe Epilepsy. Dis.  
Markers 2016. doi:10.1155/2016/5923243

Eritaia, J., Wood, S.J., Stuart, G.W., Bridle, N., Dudgeon, P., Maruff, P., Velakoulis, D.,

- Pantelis, C., 2000. An optimized method for estimating intracranial volume from magnetic resonance images. *Magn. Reson. Med.* 44, 973–7.  
doi:10.1002/1522-2594(200012)44:6<973::AID-MRM21>3.0.CO;2-H [pii]
- Essayed, W.I., Zhang, F., Unadkat, P., Cosgrove, G.R., Golby, A.J., O'Donnell, L.J., 2017. White matter tractography for neurosurgical planning: A topography-based review of the current state of the art. *NeuroImage Clin.* 15, 659–672.  
doi:10.1016/j.nicl.2017.06.011
- Falconer, M., 1953. Discussion on the surgery of temporal lobe epilepsy: surgical and pathological aspects. *Proc R Soc Med* 46, 971–974.
- Falconer, M.A., Taylor, D.C., 1968. Surgical treatment of drug-resistant epilepsy due to mesial temporal sclerosis. *Arch. Neurol.* 19, 353–361.
- Feindel, W., 1991. Development of Surgical Therapy of Epilepsy at the Montreal Neurological Institute. *Can. J. Neurol. Sci. / J. Can. des Sci. Neurol.* 18, 549–553. doi:10.1017/S0317167100032674
- Feindel, W., Leblanc, R., Almeida, A.N., De Almeida, A.N., Almeida, A.N., 2009. Epilepsy Surgery: Historical Highlights 1909-2009. *Epilepsia* 50, 131–151.  
doi:10.1111/j.1528-1167.2009.02043.x
- Fellgiebel, A., Wille, P., Müller, M.J., Winterer, G., Scheurich, A., Vucurevic, G., Schmidt, L.G., Stoeter, P., 2004. Ultrastructural hippocampal and white matter alterations in mild cognitive impairment: a diffusion tensor imaging

- study. *Dement Geriatr Cogn Disord* 18, 101–8. doi:10.1159/000077817
- Fellgiebel, A., Yakushev, I., 2011. Diffusion tensor imaging of the hippocampus in MCI and early Alzheimers Disease. *J. Alzheimer's Dis.* 26, 257–262. doi:10.3233/JAD-2011-0001
- Fernandes, D.A., Yasuda, C.L., Lopes, T.M.T.M.T.M.T.M., Enrico, G., Alessio, A.A.A., Tedeschi, H., de Oliveira, E., Cendes, F., 2014. Long-term postoperative atrophy of contralateral hippocampus and cognitive function in unilateral refractory MTLE with unilateral hippocampal sclerosis. *Epilepsy Behav.* 36, 108–114. doi:10.1016/j.yebeh.2014.04.028
- Fick, A., 1855. Uber diffusion. *Ann Phys* 94, 59.
- Figaji, A.A., 2017. Anatomical and Physiological Differences between Children and Adults Relevant to Traumatic Brain Injury and the Implications for Clinical Assessment and Care. *Front. Neurol.* 8, 1–15. doi:10.3389/fneur.2017.00685
- Fink, G., 2011. Stress Controversies: Post-Traumatic Stress Disorder, Hippocampal Volume, Gastroduodenal Ulceration. *J. Neuroendocrinol.* 23, 107–117. doi:10.1111/j.1365-2826.2010.02089.x
- Firbank, M.J., Harrison, R.M., Williams, E.D., Coulthard, a, 2000. Quality assurance for MRI: practical experience 1,2. *Radiology* 73, 376–383. doi:10.1259/bjr.73.868.10844863

- Fisher, R.S., Acevedo, C., Arzimanoglou, A., Bogacz, A., Cross, J.H., Elger, C.E., Engel, J., Forsgren, L., French, J.A., Glynn, M., Hesdorffer, D.C., Lee, B.I., Mathern, G.W., Moshé, S.L., Perucca, E., Scheffer, I.E., Tomson, T., Watanabe, M., Wiebe, S., 2014. ILAE Official Report: A practical clinical definition of epilepsy. *Epilepsia* 55, 475–482. doi:10.1111/epi.12550
- Fisher, R.S., Boas, W.E., Blume, W., Elger, C., Genton, P., Lee, P., Engel, J., 2005. Epileptic Seizures and Epilepsy: Definitions Proposed by the International League Against Epilepsy(ILAE) and the International Bureau for Epilepsy(IBE). *Epilepsia* 46, 470–472. doi:10.1111/j.1528-1167.2005.00273\_1.x
- Fisher, R.S., Cross, J.H., D'Souza, C., French, J.A., Haut, S.R., Higurashi, N., Hirsch, E., Jansen, F.E., Lagae, L., Moshé, S.L., Peltola, J., Roulet Perez, E., Scheffer, I.E., Schulze-Bonhage, A., Somerville, E., Sperling, M., Yacubian, E.M., Zuberi, S.M., 2017. Instruction manual for the ILAE 2017 operational classification of seizure types. *Epilepsia* 1–12. doi:10.1111/epi.13671
- Fitzpatrick, J., 2010. The role of registration in accurate surgical guidance. *Proc Inst Mech Eng H* 224, 607–622.
- Focke, N.K., Yogarajah, M., Bonelli, S.B., Bartlett, P.A., Symms, M.R., Duncan, J.S., 2008. Voxel-based diffusion tensor imaging in patients with mesial temporal lobe epilepsy and hippocampal sclerosis. *Neuroimage* 40, 728–737. doi:10.1016/j.neuroimage.2007.12.031

Förster, A., Griebbe, M., Gass, A., Kern, R., Hennerici, M.G., Szabo, K., 2012.

Diffusion-weighted imaging for the differential diagnosis of disorders affecting the hippocampus. *Cerebrovasc. Dis.* 33, 104–115.

doi:10.1159/000332036

Frisoni, G., Fox, N., Jack, C.J., Scheltens, P., Thompson, P., 2010. The clinical use of structural MRI in Alzheimer disease. *Nat Rev Neurol* 6, 67–77.

Frisoni, G.B., Jack, C.R., 2011. Harmonization of magnetic resonance-based manual hippocampal segmentation: A mandatory step for wide clinical use. *Alzheimer's Dement.* 7, 171–174. doi:10.1016/j.jalz.2010.06.007

Frisoni, G.B., Jack, C.R., Bocchetta, M., Bauer, C., Frederiksen, K.S., Liu, Y., Preboske, G., Swihart, T., Blair, M., Cavado, E., Grothe, M.J., Lanfredi, M., Martinez, O., Nishikawa, M., Portegies, M., Stoub, T., Ward, C., Apostolova, L.G., Ganzola, R., Wolf, D., Barkhof, F., Bartzokis, G., DeCarli, C., Csernansky, J.G., deToledo-Morrell, L., Geerlings, M.I., Kaye, J., Killiany, R.J., Lehericy, S., Matsuda, H., O'Brien, J., Silbert, L.C., Scheltens, P., Soininen, H., Teipel, S., Waldemar, G., Fellgiebel, A., Barnes, J., Firbank, M., Gerritsen, L., Henneman, W., Malykhin, N., Pruessner, J.C., Wang, L., Watson, C., Wolf, H., deLeon, M., Pantel, J., Ferrari, C., Bosco, P., Pasqualetti, P., Duchesne, S., Duvernoy, H., Boccardi, M., 2014. The EADC-ADNI Harmonized Protocol for manual hippocampal segmentation on magnetic resonance: Evidence of validity. *Alzheimer's Dement.* 1–15. doi:10.1016/j.jalz.2014.05.1756

- Frost, R., Porter, D. a., Miller, K.L., Jezzard, P., 2012. Implementation and assessment of diffusion-weighted partial Fourier readout-segmented echo-planar imaging. *Magn. Reson. Med.* 68, 441–451. doi:10.1002/mrm.23242
- Fuerst, D., Shah, J., Shah, A., Watson, C., 2003. Hippocampal sclerosis is a progressive disorder: a longitudinal volumetric MRI study. *Ann. Neurol.* 53, 413–6. doi:10.1002/ana.10509
- Ganzetti, M., Wenderoth, N., Mantini, D., 2016. Intensity Inhomogeneity Correction of Structural MR Images: A Data-Driven Approach to Define Input Algorithm Parameters. *Front. Neuroinform.* 10, 1–14. doi:10.3389/fninf.2016.00010
- Garcia-Finana, M., Cruz-Orive, L., Mackay, C., Pakkenberg, B., Roberts, N., 2003. Comparison of MR imaging against physical sectioning to estimate the volume of human cerebral compartments. *Neuroimage* 18, 505–516.
- Garcia-Finana, M., Keller, S., Roberts, N., 2009. Confidence intervals for the volume of brain structures in Cavalieri sampling with local errors. *J Neurosci Methods* 179, 71–77.
- Gates, J.R., Cruz-rodriguez, R., 1990. *Mesial Temporal Sclerosis : Pathogenesis , Diagnosis , and Management.*
- Geddes, J.F., Hackshaw, a K., Vowles, G.H., Nickols, C.D., Whitwell, H.L., 2001a. Neuropathology of inflicted head injury in children. I. Patterns of brain

damage. *Brain* 124, 1290–1298. doi:10.1093/brain/124.7.1290

Geddes, J.F., Vowles, G.H., Hackshaw, a K., Nickols, C.D., Scott, I.S., Whitwell, H.L.,  
2001b. Neuropathology of inflicted head injury in children. II. Microscopic  
brain injury in infants. *Brain* 124, 1299–1306.  
doi:10.1093/brain/124.7.1299

Gerard, I.J., Kersten-Oertel, M., Petrecca, K., Sirhan, D., Hall, J.A., Collins, D.L.,  
2017. Brain shift in neuronavigation of brain tumors: A review. *Med. Image  
Anal.* 35, 403–420. doi:10.1016/j.media.2016.08.007

Gering, D.T., Nabavi, a, Kikinis, R., Hata, N., O'Donnell, L.J., Grimson, W.E., Jolesz,  
F. a, Black, P.M., Wells, W.M., 2001. An integrated visualization system for  
surgical planning and guidance using image fusion and an open MR. *J. Magn.  
Reson. Imaging* 13, 967–975.

Geuze, E., Vermetten, E., Bremner, J.D., 2005. MR-based in vivo hippocampal  
volumetrics: 1. Review of methodologies currently employed. *Mol.  
Psychiatry* 10, 147–159. doi:10.1038/sj.mp.4001580

Ghahreman, A., Bhasin, V., Chaseling, R., Andrews, B., Lang, E.W., 2005.  
Nonaccidental head injuries in children: a Sydney experience. *J. Neurosurg.  
Pediatr.* 103, 213–218. doi:10.3171/ped.2005.103.3.0213

Gildenberg, P., 1997. Where have we been? Where are we going? *Stereotact.  
Funct. Neurosurg.* 68, 1–9.

- Gill, A., Shellock, F.G., 2012. Assessment of MRI issues at 3-Tesla for metallic surgical implants: Findings applied to 61 additional skin closure staples and vessel ligation clips. *J. Cardiovasc. Magn. Reson.* 14, 3. doi:10.1186/1532-429X-14-3
- Ginat, D.T., Swearingen, B., Curry, W., Cahill, D., Madsen, J., Schaefer, P.W., 2014. 3 Tesla intraoperative MRI for brain tumor surgery. *J. Magn. Reson. Imaging* 39, 1357–1365. doi:10.1002/jmri.24380
- Golby, A.J., Kindlmann, G., Nortion, I., Yarmarkovich, A., Pieper, S., Kikinis, R., 2011. Interactive diffusion tensor tractography visualization for neurosurgical planning. *Neurosurgery* 68, 496–505. doi:10.1227/NEU.0b013e3182061ebb.Interactive
- Goldstein, J.L., Leonhardt, D., Kmytyuk, N., Kim, F., Wang, D., Wainwright, M.S., 2011. Abnormal neuroimaging is associated with early in-hospital seizures in pediatric abusive head trauma. *Neurocrit. Care* 15, 63–69. doi:10.1007/s12028-010-9468-5
- Gong, G., Concha, L., Beaulieu, C., Gross, D.W., 2008. Thalamic diffusion and volumetry in temporal lobe epilepsy with and without mesial temporal sclerosis. *Epilepsy Res.* 80, 184–193. doi:10.1016/j.epilepsyres.2008.04.002
- Gong, G., Concha, L., Beaulieu, C., Gross, D.W., 2008. Thalamic diffusion and volumetry in temporal lobe epilepsy with and without mesial temporal

- sclerosis. *Epilepsy Res.* 80, 184–193. doi:10.1016/j.epilepsyres.2008.04.002
- Gronenschild, E.H.B.M., Habets, P., Jacobs, H.I.L., Mengelers, R., Rozendaal, N., van Os, J., Marcelis, M., 2012. The effects of FreeSurfer version, workstation type, and Macintosh operating system version on anatomical volume and cortical thickness measurements. *PLoS One* 7. doi:10.1371/journal.pone.0038234
- Gross, D.W., Concha, L., Beaulieu, C., 2006. Extratemporal White Matter Abnormalities in Mesial Temporal Lobe Epilepsy Demonstrated with Diffusion Tensor Imaging. *Epilepsia* 47, 1360–1363. doi:10.1111/j.1528-1167.2006.00603.x
- Grossman, E.J., Inglese, M., Bammer, R., 2010. Mild traumatic brain injury: is diffusion imaging ready for primetime in forensic medicine? *Top Magn Reson Imaging* 21, 379–386. doi:10.1097/RMR.0b013e31823e65b8.Mild
- Guo, K., Meints, K., Hall, C., Hall, S., Mills, D., 2009. Left gaze bias in humans, rhesus monkeys and domestic dogs. *Anim. Cogn.* 12, 409–418. doi:10.1007/s10071-008-0199-3
- Hagemann, G., Ugur, T., Schleussner, E., Mentzel, H.-J., Fitzek, C., Witte, O.W., Gaser, C., 2011. Changes in Brain Size during the Menstrual Cycle. *PLoS One* 6, e14655. doi:10.1371/journal.pone.0014655
- Hartkens, T., Hill, D., Castellno-Smith, A., Hawkes, D., Maurer, C., Martin, A., Hall, W., Liu, H., Truwit, C., 2003. Measurement and analysis of brain deformation

- during neurosurgery - Research Portal, King's College, London. *IEEE Trans. Med. Imaging* 22, 82–92.
- Hatiboglu, M., Weinberg, J., Suki, D., Tummala, S., Rao, G., Sawaya, R., Prabhu, S., 2010. Utilization of intraoperative motor mapping in glioma surgery with high-field intraoperative magnetic resonance imaging. *Stereotact. Funct. Neurosurg.* 88, 345–352.
- Hatiboglu, M.A., Weinberg, J.S., Suki, D., Rao, G., Prabhu, S.S., Shah, K., Jackson, E., Sawaya, R., 2009. Impact of intraoperative high-field magnetic resonance imaging guidance on glioma surgery: A prospective volumetric analysis. *Neurosurgery* 64, 1073–1081. doi:10.1227/01.NEU.0000345647.58219.07
- Heckers, S., 2001. Neuroimaging studies of the hippocampus in schizophrenia. *Hippocampus* 11, 520–528. doi:10.1002/hipo.1068
- Heidemann, R.M., Porter, D.A., Anwander, A., Feiweier, T., Heberlein, K., Knösche, T.R., Turner, R., 2010. Diffusion imaging in humans at 7T using readout-segmented EPI and GRAPPA. *Magn. Reson. Med.* 64, 9–14. doi:10.1002/mrm.22480
- Heiniger, P., El-Koussy, M., Schindler, K., Lövblad, K.O., Kiefer, C., Oswald, H., Wissmeyer, M., Mariani, L., Donati, F., Schroth, G., Weder, B., 2002. Diffusion and perfusion MRI for the localisation of epileptogenic foci in drug-resistant epilepsy. *Neuroradiology* 44, 475–480. doi:10.1007/s00234-002-0785-z

- Helmstaedter, C., Richter, S., Röske, S., Oltmanns, F., Schramm, J., Lehmann, T.N.,  
2008. Differential effects of temporal pole resection with  
amygdalohippocampectomy versus selective amygdalohippocampectomy  
on material-specific memory in patients with mesial temporal lobe epilepsy.  
*Epilepsia* 49, 88–97. doi:10.1111/j.1528-1167.2007.01386.x
- Hendler, T., Pianka, P., Sigal, M., Kafri, M., Ben-Bashat, D., Constantini, S., Graif, M.,  
Fried, I., Assaf, Y., 2003. Delineating gray and white matter involvement in  
brain lesions: three-dimensional alignment of functional magnetic  
resonance imaging and diffusion-tensor imaging. *J. Neurosurg.* 99, 1018–  
1027. doi:10.3171/jns.2003.99.6.1018
- Hergan, K., Schaefer, P.W., Sorensen, a G., Gonzalez, R.G., Huisman, T. a G.M.,  
2002. Diffusion-weighted MRI in diffuse axonal injury of the brain. *Eur.*  
*Radiol.* 12, 2536–41. doi:10.1007/s00330-002-1333-2
- Hill, D.L.G., Maurer, C.R., Maciunas, R.J., Barwise, J.A., Fitzpatrick, J.M., Wang, M.Y.,  
1998. Measurement of intraoperative brain surface deformation under a  
craniotomy. *Neurosurgery* 43, 514–526. doi:10.1097/00006123-  
199809000-00066
- Hirano, A., Zimmerman, H., 1971. Some New Pathological Findings in The Central  
Myelinated Axon. *J Neuropathol Exp Neurol* 30, 325–336.
- Holloway, M., Bye, A., Moran, K., 1994. Non-accidental head injury in children.

Med. J. Aust. 160, 786–789.

Holodny, A.I., Ollenschleger, M.D., Liu, W., Schulder, M., Kalnin, A.J., 2001.

Identification of the Corticospinal Tracts Achieved Using Blood-oxygen-level – dependent and Diffusion Functional MR Imaging in Patients with Brain Tumors. *Ajnr* 83–88.

Hong, Y.J., Yoon, B., Shim, Y.S., Cho, A.H., Lim, S.C., Ahn, K.J., Yang, D.W., 2010.

Differences in microstructural alterations of the hippocampus in Alzheimer disease and idiopathic normal pressure hydrocephalus: A diffusion tensor imaging study. *Am. J. Neuroradiol.* 31, 1867–1872. doi:10.3174/ajnr.A2207

Hou, Z., 2006. A review on MR image intensity inhomogeneity correction. *Int. J. Biomed. Imaging* 2006, 1–11. doi:10.1155/IJBI/2006/49515

Huang, H., Ceritoglu, C., Li, X., Qiu, A., Miller, M.I., van Zijl, P.C.M., Mori, S., 2008.

Correction of B0-Susceptibility Induced Distortion in Diffusion-weighted Images Using Large-Deformation Diffeomorphic Metric Mapping. *Magn. Reson. Imaging* 26, 1294–1302. doi:10.1016/j.mri.2008.03.005. Correction

Hugg, J.W., Butterworth, E.J., Kuzniecky, R.I., 1999. Diffusion mapping applied to

mesial temporal lobe epilepsy: preliminary observations. *Neurology* 53, 173–176. doi:10.1212/WNL.53.1.173

Hugg, J.W., Kuzniecky, R.I., Gilliam, F.G., Morawetz, R.B., Faught, R.E.,

Hetherington, H.P., 1996. Normalization of Contralateral Metabolic Function

Following Temporal Lobectomy Demonstrated by <sup>1</sup>H Magnetic Resonance Spectroscopic Imaging 236–239.

Hugg, J.W., Laxer, K.D., Matson, G.B., Maudsley, a a, Weiner, M.W., 1993. Neuron loss localizes human temporal lobe epilepsy by in vivo proton magnetic resonance spectroscopic imaging. *Ann. Neurol.* 34, 788–94.

doi:10.1002/ana.410340606

Huppertz, H.J., Kröll-Seger, J., Klöppel, S., Ganz, R.E., Kassubek, J., 2010. Intra- and interscanner variability of automated voxel-based volumetry based on a 3D probabilistic atlas of human cerebral structures. *Neuroimage* 49, 2216–2224. doi:10.1016/j.neuroimage.2009.10.066

Hutton, C., Bork, A., Josephs, O., Deichmann, R., Ashburner, J., Turner, R., 2002. Image distortion correction in fMRI: A quantitative evaluation. *Neuroimage* 16, 217–240. doi:10.1006/nimg.2001.1054

Ichord, R.N., Naim, M., Pollock, A.N., Nance, M.L., Margulies, S.S., Christian, C.W., 2007. Hypoxic-ischemic injury complicates inflicted and accidental traumatic brain injury in young children: the role of diffusion-weighted imaging. *J. Neurotrauma* 24, 106–118. doi:10.1089/neu.2006.0087

Imagawa, K.K., Hamilton, A., Ceschin, R., Tokar, E., Pham, P., Bluml, S., Wisnowski, J., Panigrahy, A., 2014. Characterization of Microstructural Injury: A Novel Approach in Infant Abusive Head Trauma-Initial Experience. *J. Neurotrauma*

31, 1632–8. doi:10.1089/neu.2013.3228

Insausti, R., Juottonen, K., Soininen, H., Insausti, A., Partanen, K., Vainio, P., Laakso, M., Pitkanen, A., 1998. MR volumetric analysis of the human entorhinal, perirhinal and temporopolar cortices. *Am. J. Neuroradiol.* 19, 659–671.

Irfanoglu, M., Walker, L., Sarlls, J., Marengo, S., Pierpaoli, C., 2012. Effects of image distortions originating from susceptibility and concomitant fields on diffusion MRI tractography results. *Neuroimage* 61, 275–288.  
doi:10.1109/TMI.2012.2196707.Separate

Ius, T., Isola, M., Budai, R., Pauletto, G., Tomasino, B., Fadiga, L., Skrap, M., 2012. Low-grade glioma surgery in eloquent areas: volumetric analysis of extent of resection and its impact on overall survival. A single-institution experience in 190 patients. *J. Neurosurg.* 117, 1039–1052.  
doi:10.3171/2012.8.JNS12393

Jack, C.R., Sharbrough, F.W., Cascino, G.D., Hirschorn, K.A., Brien, P.C.O., Marsh, W.R., 1992. Magnetic Resonance Image-Based hippocampal volumetry: correlation with outcome after temporal lobectomy 138–146.

Jack, C.R.J., Bentley, M.D., Twomey, C.K., Zinsmeister, A.R., 1990a. MR imaging-based volume measurements of the hippocampal formation and anterior temporal lobe: validation studies. *Radiology* 175, 423–429.

- Jack, C.R.J., Sharbrough, F.W., Twomey, C.K., Cascino, G.D., Hirschorn, K.A., Marsh, W.R., Zinsmeister, A.R., Scheithauer, B., 1990b. Temporal lobe seizures: lateralization with MR volume measurements of the hippocampal formation. *Radiology* 175, 423–239.
- Jackson, G., Berkovic, S., Duncan, J., Connelly, A., 1993. Optimizing the diagnosis of hippocampal sclerosis using MR imaging. *Am. J. Neuroradiol.* 14, 753–762.
- Jackson, G., Berkovic, S., Tress, B., Kalnins, R., Fabinyi, G., Bladin, P., 1990. Hippocampal sclerosis can reliably be detected by magnetic resonance imaging. *Neurology* 40, 1869–1875.
- Jackson, G., Kuzniecky, R., Cascino, G., 1994. Hippocampal sclerosis without detectable hippocampal atrophy. *Neurology* 44, 42–46.
- Jacobsohn, E., Roberts, D., 1999. Gregg M. Eschun MD, Eric Jacobsohn MD, Daniel Roberts MD, Barney Sneiderman LLM\* 497–504.
- Jagannathan, P., Jagannathan, J., 2008. Molecular mechanisms of traumatic brain injury in children. A review. *Neurosurg. Focus* 25, E12.  
doi:10.3171/FOC.2008.25.10.E6
- Jayawant, S., Rawlinson, A., Gibbon, F., Price, J., Schulte, J., Sharples, P., Sibert, J.R., Kemp, A.M., 1998. Subdural haemorrhages in infants: population based study. *Bmj* 317, 1558–1561. doi:10.1136/bmj.317.7172.1558

- Jewell, G., McCourt, M.E., 2000. Pseudoneglect: a review and meta- analysis of performance factors in line bisection tasks. *Neuropsychologia* 38, 93–110.
- Jissendi, P., Baudry, S., Baleriaux, D., 2008. Diffusion tensor imaging (DTI) and tractography of the cerebellar projections to prefrontal and posterior parietal cortices. *J Neuroradiol.* 35, 42–50.
- Jones, D.K., Cercignani, M., 2010. Twenty-five pitfalls in the analysis of diffusion MRI data. *NMR Biomed.* 23, 803–820. doi:10.1002/nbm.1543
- Jones, D.K., Horsfield, M.A., Simmons, A., 1999. Optimal strategies for measuring diffusion in anisotropic systems by magnetic resonance imaging. *Magn. Reson. Med.* 42, 515–525. doi:10.1002/(SICI)1522-2594(199909)42:3<515::AID-MRM14>3.0.CO;2-Q
- Jones, D.K., Simmons, A., Williams, S.C., Horsfield, M.A., 1999. Non-invasive assessment of axonal fiber connectivity in the human brain via diffusion tensor MRI. *Magn. Reson. Med.* 42, 37–41. doi:10.1002/(SICI)1522-2594(199907)42:1<37::AID-MRM7>3.0.CO;2-O [pii]
- Josephson, C., Dykeman, J., Fiest, K., Liu, X., 2013. Systematic review and meta-analysis of standard vs selective temporal lobe epilepsy surgery. *Neurology.*
- Jovicich, J., Czanner, S., Han, X., Salat, D., van der Kouwe, A., Quinn, B., Pacheco, J., Albert, M., Killiany, R., Blacker, D., Maguire, P., Rosas, D., Makris, N., Gollub, R., Dale, A., Dickerson, B.C., Fischl, B., 2009. MRI-derived measurements of

human subcortical, ventricular and intracranial brain volumes: Reliability effects of scan sessions, acquisition sequences, data analyses, scanner upgrade, scanner vendors and field strengths. *Neuroimage* 46, 177–192.  
doi:10.1016/j.neuroimage.2009.02.010

Kahane, P., Bartolomei, F., 2010. Temporal lobe epilepsy and hippocampal sclerosis: Lessons from depth EEG recordings. *Epilepsia* 51, 59–62.  
doi:10.1111/j.1528-1167.2009.02448.x

Kalviainen, R., Salmenpera, T., Partanen, K., Vainio, P., Riekkinen, P., Pitkänen A, S., 1997. MRI volumetry and T2 relaxometry of the amygdala in newly diagnosed and chronic temporal lobe epilepsy. *Epilepsia* 38, 39–50.

Kamada, K., Todo, T., Masutani, Y., Aoki, S., Ino, K., R.T., Morita, A., Saito, N., 2007. Visualization of the frontotemporal language fibers by tractography combined with functional magnetic resonance imaging and magnetoencephalography. *J. Neurosurg.* 106, 90–98.  
doi:10.3171/jns.2007.106.1.90

Kamada, K., Todo, T., Masutani, Y., Aoki, S., Ino, K., Takano, T., Kirino, T., Kawahara, N., Morita, A., 2005. Combined use of tractography-integrated functional neuronavigation and direct fiber stimulation. *J. Neurosurg.* 102, 664–672. doi:10.3171/jns.2005.102.4.0664

Kanner, A.M., 2011. Hippocampal atrophy: Another common pathogenic

mechanism of depressive disorders and epilepsy? *Epilepsy Curr.* 11, 149–150. doi:10.5698/1535-7511-11.5.149

Kantarci, K., 2014. Fractional Anisotropy of the Fornix and Hippocampal Atrophy in Alzheimers Disease. *Front. Aging Neurosci.* 6, 1–4.  
doi:10.3389/fnagi.2014.00316

Kantarci, K., Shin, C., Britton, J., So, E., Cascino, G., Jack Jr, C., 2002. Comparative diagnostic utility of 1H MRS and DWI in evaluation of temporal lobe epilepsy. *Neurology* 58, 1745–1753.

Keller, S., Schoene-Bake, J., Gerdes, J.S., Weber, B., Deppe, M., 2012. Concomitant Fractional Anisotropy and Volumetric Abnormalities in Temporal Lobe Epilepsy: Cross-Sectional Evidence for Progressive Neurologic Injury. *PLoS One* 7, e46791. doi:10.1371/journal.pone.0046791

Keller, S.S., Baker, G., Downes, J.J., Roberts, N., 2009. Quantitative MRI of the prefrontal cortex and executive function in patients with temporal lobe epilepsy. *Epilepsy Behav.* 15, 186–95. doi:10.1016/j.yebeh.2009.03.005

Keller, S.S., Cresswell, P., Denby, C., Wieshmann, U., Eldridge, P., Baker, G., Roberts, N., 2007. Persistent seizures following left temporal lobe surgery are associated with posterior and bilateral structural and functional brain abnormalities. *Epilepsy Res.* 74, 131–139.  
doi:10.1016/j.eplepsyres.2007.02.005

- Keller, S.S., Mackay, C.E., Barrick, T.R., Wieshmann, U.C., Howard, M.A., Roberts, N., 2002. Voxel-based morphometric comparison of hippocampal and extrahippocampal abnormalities in patients with left and right hippocampal atrophy. *Neuroimage* 16, 23–31. doi:10.1006/nimg.2001.1072
- Keller, S.S., Roberts, N., 2009. Measurement of brain volume using MRI: Software, techniques, choices and prerequisites. *J. Anthropol. Sci.* 87, 127–151.
- Keller, S.S., Roberts, N., 2008. Voxel-based morphometry of temporal lobe epilepsy: An introduction and review of the literature. *Epilepsia* 49, 741–757. doi:10.1111/j.1528-1167.2007.01485.x
- Keller, S.S., Schoene-Bake, J.C., Gerdes, J.S., Weber, B., Deppe, M., 2012. Concomitant Fractional Anisotropy and Volumetric Abnormalities in Temporal Lobe Epilepsy: Cross-Sectional Evidence for Progressive Neurologic Injury. *PLoS One* 7, e46791. doi:10.1371/journal.pone.0046791
- Keller, S.S., Wieshmann, U.C., Mackay, C.E., Denby, C.E., Webb, J., Roberts, N., 2002. Voxel based morphometry of grey matter abnormalities in patients with medically intractable temporal lobe epilepsy: effects of side of seizure onset and epilepsy duration. *J. Neurol. Neurosurg. Psychiatry* 73, 648–655. doi:10.1136/jnnp.73.6.648
- Kemmotsu, N., Girard, H.M., Bernhardt, B.C., Bonilha, L., Lin, J.J., Tecoma, E.S., Iragui, V.J., Hagler, D.J., Halgren, E., McDonald, C.R., 2011. MRI analysis in

temporal lobe epilepsy: Cortical thinning and white matter disruptions are related to side of seizure onset. *Epilepsia* 52, 2257–2266.

doi:10.1111/j.1528-1167.2011.03278.x

Kemp, a. M., Rajaram, S., Mann, M., Tempest, V., Farewell, D., Gawne-Cain, M.L., Jaspán, T., Maguire, S., 2009. What neuroimaging should be performed in children in whom inflicted brain injury (iBI) is suspected? A systematic review. *Clin. Radiol.* 64, 473–483. doi:10.1016/j.crad.2008.11.011

Kemp, a M., Stoodley, N., Cobley, C., Coles, L., Kemp, K.W., 2003. Apnoea and brain swelling in non-accidental head injury. *Arch. Dis. Child.* 88, 472-476; discussion 472-476. doi:10.1136/adc.88.6.472

Kempton, M.J., Ettinger, U., Foster, R., Williams, S.C.R., Calvert, G.A., Hampshire, A., Zelaya, F.O., O’Gorman, R.L., McMorris, T., Owen, A.M., Smith, M.S., 2011. Dehydration affects brain structure and function in healthy adolescents. *Hum. Brain Mapp.* 32, 71–79. doi:10.1002/hbm.20999

Kim, G.-H., Seo, J.H., Schroff, S., Chen, P.-C., Lee, K.H., Baumgartner, J., 2017. Impact of intraoperative 3-T MRI with diffusion tensor imaging on hemispherectomy. *J. Neurosurg. Pediatr.* 19, 63–69. doi:10.3171/2016.4.PEDS15568

Kim, H., Piao, Z., Liu, P., Bingaman, W., Diehl, B., 2008. Secondary white matter degeneration of the corpus callosum in patients with intractable temporal

- lobe epilepsy: A diffusion tensor imaging study. *Epilepsy Res.* 81, 136–142.  
doi:10.1016/j.eplepsyres.2008.05.005
- Kim, J.H., Tien, R.D., Felsberg, G.J., Osumi, A.K., Lee, N., 1995. Clinical Significance of Asymmetry of the Fornix and Mamillary Body on MR in Hippocampal Sclerosis 1–13.
- Kim, M.W., Bang, M.S., Han, T.R., Ko, Y.J., Yoon, B.W., Kim, J.H., Kang, L.M., Lee, K.M., Kim, M.H., 2005. Exercise increased BDNF and trkB in the contralateral hemisphere of the ischemic rat brain. *Brain Res.* 1052, 16–21.  
doi:10.1016/j.brainres.2005.05.070
- Kimiwada, T., Juhász, C., Makki, M., Muzik, O., Chugani, D.C., Asano, E., Chugani, H.T., 2006. Hippocampal and thalamic diffusion abnormalities in children with temporal lobe epilepsy. *Epilepsia* 47, 167–75.
- Kimura-Ohba, S., Yang, Y., Thompson, J., Kimura, T., Salayandia, V.M., Cosse, M., Yang, Y., Sillerud, L.O., Rosenberg, G.A., 2016. Transient increase of fractional anisotropy in reversible vasogenic edema. *J. Cereb. Blood Flow Metab.* 36, 1731–1743. doi:10.1177/0271678X16630556
- Kimura, D., 1963. Right temporal-lobe damage. *Arch. Neurol.* 8, 264–271.
- King, W.J., MacKay, M., Sirnick, A., Canadian Shaken Baby Study Group, 2003. Shaken baby syndrome in Canada: clinical characteristics and outcomes of hospital cases. *CMAJ* 168, 155–9.

- Kinoshita, M., Yamada, K., Hashimoto, N., Kato, A., Izumoto, S., Baba, T., Maruno, M., Nishimura, T., Yoshimine, T., 2005. Fiber-tracking does not accurately estimate size of fiber bundle in pathological condition: initial neurosurgical experience using neuronavigation and subcortical white matter stimulation. *Neuroimage* 25, 424–9. doi:10.1016/j.neuroimage.2004.07.076
- Koo, T.K., Li, M.Y., 2016. A Guideline of Selecting and Reporting Intraclass Correlation Coefficients for Reliability Research. *J. Chiropr. Med.* 15, 155–163. doi:10.1016/j.jcm.2016.02.012
- Koyasu, S., Iima, M., Umeoka, S., Morisawa, N., Porter, D.A., Ito, J., Le Bihan, D., Togashi, K., 2014. The clinical utility of reduced-distortion readout-segmented echo-planar imaging in the head and neck region: initial experience. *Eur. Radiol.* 24, 3088–3096. doi:10.1007/s00330-014-3369-5
- Kuzniecky, R., De Le Sayette, V., Ethier, R., Melanson, D., Andermann, F., Berkovic, S., Robitaille, Y., Olivier, A., Peters, T., Feindel, W., 1987. Magnetic resonance imaging in temporal lobe epilepsy: pathological correlations. *Ann. Neurol.* 22, 341–347.
- Kuzniecky, R.I., Burgard, S., Bilir, E., Morawetz, R., Gilliam, F., Faught, E., Black, L., Palmer, C., 1996. Qualitative MRI segmentation in mesial temporal sclerosis: clinical correlations. *Epilepsia* 37, 433–439. doi:10.1111/j.1528-1157.1996.tb00588.x

- Kwan, P., Arzimanoglou, A., Berg, A.T., Brodie, M.J., Hauser, W.A., Mathern, G., Moshé, S.L., Perucca, E., Wiebe, S., French, J., 2010. Definition of drug resistant epilepsy: Consensus proposal by the ad hoc Task Force of the ILAE Commission on Therapeutic Strategies. *Epilepsia* 51, 1069–1077. doi:10.1111/j.1528-1167.2009.02397.x
- Kwan, P., Brodie, M., 2000. Early Identification of Refractory Epilepsy 342, 314–319.
- Kwan, P., Schachter, S.C., Brodie, M.J., 2011. Drug-Resistant Epilepsy. *N. Engl. J. Med.* 919–926.
- Lansberg, M., O'Brien, M., Norbash, A., Moseley, M., Morrell, M., Albers, G., 1999. MRI abnormalities associated with partial status epilepticus. *Neurology* 52, 1021–1027.
- LaRiviere, M.J., Gross, R.E., 2016. Stereotactic Laser Ablation for Medically Intractable Epilepsy: The Next Generation of Minimally Invasive Epilepsy Surgery. *Front. Surg.* 3. doi:10.3389/fsurg.2016.00064
- Lauterbur, P., 1973. Image formation by induced local interactions: Examples employing nuclear magnetic resonance. *Nature* 242, 190–191.
- Lawes, I.N.C., Barrick, T.R., Murugam, V., Spierings, N., Evans, D.R., Song, M., Clark, C.A., 2008. Atlas-based segmentation of white matter tracts of the human brain using diffusion tensor tractography and comparison with classical

dissection. *Neuroimage* 39, 62–79. doi:10.1016/j.neuroimage.2007.06.041

Lawson, J. a, Vogrin, S., Bleasel, a F., Cook, M.J., Bye, a M., 2000. Cerebral and cerebellar volume reduction in children with intractable epilepsy. *Epilepsia* 41, 1456–1462.

Lee, W., Andermann, F., Dubeau, F., Bernasconi, A., Macdonald, D., Evans, A., Reutens, D.C., 1998. Morphometric Analysis of the Temporal Lobe in Temporal Lobe Epilepsy 39.

Leemans, A., Jeurissen, B., Sijbers, J., Jones, D., 2009. ExploreDTI: a graphical toolbox for processing, analyzing, and visualizing diffusion MR data. *Proc. 17th Sci. Meet. Int. Soc. Magn. Reson. Med.* 17, 3537.

Leemans, A., Jones, D.K., 2009. The B-matrix must be rotated when correcting for subject motion in DTI data. *Magn. Reson. Med.* 61, 1336–1349.  
doi:10.1002/mrm.21890

Lencz, T., McCarthy, G., Bronen, R.A., Scott, T.M., Inserni, J.A., Sass, K.J., Novelly, R.A., Kim, J.H., Spencer, D.D., 1992. Quantitative magnetic resonance imaging in temporal lobe epilepsy: relationship to neuropathology and neuropsychological function. *Ann Neurol* 31, 629–637.  
doi:10.1002/ana.410310610

Levira, F., Thurman, D.J., Sander, J.W., Hauser, W.A., Hesdorffer, D.C., Masanja, H., Odermatt, P., Logroscino, G., Newton, C.R., 2017. Premature mortality of

epilepsy in low- and middle-income countries: A systematic review from the Mortality Task Force of the International League Against Epilepsy. *Epilepsia* 58, 6–16. doi:10.1111/epi.13603

Levy-Reis, I., Gonzalez-Atavales, J., King, D., French, J., Alsop, D., Detre, J., 2000. Hippocampal imaging and volumetry in temporal lobe epilepsy at 1.5 and 4 Tesla, in: *Proceedings of the International Society for Magnetic Resonance in Medicine*.

Liacu, D., de Marco, G., Ducreux, D., Bouilleret, V., Masnou, P., Idy-Peretti, I., 2010. Diffusion tensor changes in epileptogenic hippocampus of TLE patients. *Neurophysiol. Clin.* 40, 151–7. doi:10.1016/j.neucli.2010.01.003

Lin, J.J., Riley, J.D., Juranek, J., Cramer, S.C., 2008. Vulnerability of the frontal-temporal connections in temporal lobe epilepsy. *Epilepsy Res.* 82, 162–170. doi:10.1016/j.eplepsyres.2008.07.020

Liu, M., Gross, D.W., Wheatley, B.M., Concha, L., Beaulieu, C., 2013. The acute phase of Wallerian degeneration: Longitudinal diffusion tensor imaging of the fornix following temporal lobe surgery. *Neuroimage* 74, 128–139. doi:10.1016/j.neuroimage.2013.01.069

Londono, A., Castillo, M., Lee, Y.Z., Smith, J.K., 2003. Apparent diffusion coefficient measurements in the hippocampi in patients with temporal lobe seizures. *AJNR Am J Neuroradiol* 24, 1582–1586.

- Looi, J.C.L., Lindberg, O., Liberg, B., Tatham, V., Kumar, R., Maller, J., Millard, E., Sachdev, P., Högberg, G., Pagani, M., Botes, L., Engman, E.-L.L., Zhang, Y., Svensson, L., Wahlund, L.-O.O., 2008. Volumetrics of the caudate nucleus: reliability and validity of a new manual tracing protocol. *Psychiatry Res.* 163, 279–88. doi:10.1016/j.psychresns.2007.07.005
- Lorente de No R, 1928. Ein Beitrag zur Kenntnis der Gefassverteilung in der Hirnrinde (International brain research organisation, monograph series, vol II). *J psychol neurol* 35, 19–31.
- Macchia, R.J., Termine, J.E., Buchen, C.D., 2007. Raymond V. Damadian, M.D.: Magnetic Resonance Imaging and the Controversy of the 2003 Nobel Prize in Physiology or Medicine. *J. Urol.* 178, 783–785. doi:10.1016/j.juro.2007.05.019
- MacDonald, D., Kabani, N., Avis, D., Evans, A.C., 2000. Automated 3-D extraction of inner and outer surfaces of cerebral cortex from MRI. *Neuroimage* 12, 340–356. doi:10.1006/nimg.1999.0534
- MacRae, D., Blümcke, I., Thom, M., Wiestler, O.D., 2002. Ammon's Horn Sclerosis: A Maldevelopmental Disorder Associated with Temporal Lobe Epilepsy. *Brain Pathol.* 12, 1–13. doi:10.1111/j.1750-3639.2002.tb00436.x
- Maesawa, S., Fujii, M., Nakahara, N., Watanabe, T., Wakabayashi, T., Yoshida, J., 2010. Intraoperative tractography and motor evoked potential (MEP)

- monitoring in surgery for gliomas around the corticospinal tract. *World Neurosurg.* 74, 153–61. doi:10.1016/j.wneu.2010.03.022
- Malmgren, K., Thom, M., 2012. Hippocampal sclerosis-Origins and imaging. *Epilepsia* 53, 19–33. doi:10.1111/j.1528-1167.2012.03610.x
- Maltbie, E., Bhatt, K., Paniagua, B., Smith, R., Graves, M., Mosconi, M., Peterson, S., White, S., Blocher, J., El-Sayed, M., Hazlett, H., Styner, M., 2012. Asymmetric bias in user guided segmentations of brain structures. *Neuroimage* 59, 1315–1323.
- Malykhin, N. V., Bouchard, T.P., Ogilvie, C.J., Coupland, N.J., Seres, P., Camicioli, R., 2007. Three-dimensional volumetric analysis and reconstruction of amygdala and hippocampal head, body and tail. *Psychiatry Res. Neuroimaging* 155, 155–165. doi:10.1016/j.psychresns.2006.11.011
- Marcoux, F.W., Morawetz, R.B., Crowell, R.M., DeGirolami, U., Halsey, J.H., 1982. Differential regional vulnerability in transient focal cerebral ischemia. *Stroke.* 13, 339–346. doi:10.1161/01.STR.13.3.339
- Margerison, J.H., Corsellis, J. a N., 1966. Epilepsy and the temporal lobes. *Brain* 89, 499–530.
- Mark, L., Daniels, D., Naidich, T., Hendrix, L., 1995. Limbic connections. *AJNR Am. J. Neuroradiol.* 16, 1303–1306.
- Mascott, C., 2005. Comparison of magnetic tracking and optical tracking by

simultaneous use of two independent frameless stereotactic systems.  
Neurosurgery 57, 295–301.

Maurer, C.R., Hill, D.L.G., Martin, J., Liu, H., McCue, M., Rueckert, D., Lloret, D., Hall, W.A., Maxwell, R.E., Hawkes, D.J., Truwit, C.L., 1998. Investigation of Intraoperative Brain Deformation Preliminary Results. IEEE Trans. Med. Imaging 17, 817–825.

McDonald, C.R., Hagler, D.J., Girard, H.M., Pung, C., Ahmadi, M.E., Holland, D., Patel, R.H., Barba, D., Tecoma, E.S., Iragui, V.J., Halgren, E., Dale, a. M., 2010. Changes in fiber tract integrity and visual fields after anterior temporal lobectomy. Neurology 75, 1631–1638.  
doi:10.1212/WNL.0b013e3181fb44db

McIntosh, A., Wilson, S., Berkovic, S., 2001. Seizure outcome after temporal lobectomy: Current research practice and findings. Epilepsia 42, 1288–1307.

McIntosh, A.M., Kalnins, R.M., Mitchell, L.A., Fabinyi, G.C. a, Briellmann, R.S., Berkovic, S.F., 2004. Temporal lobectomy: Long-term seizure outcome, late recurrence and risks for seizure recurrence. Brain 127, 2018–2030.  
doi:10.1093/brain/awh221

McKinney, A.M., Thompson, L.R., Truwit, C.L., Velders, S., Karagulle, A., Kiragu, A., 2008. Unilateral hypoxic-ischemic injury in young children from abusive

head trauma, lacking craniocervical vascular dissection or cord injury.

*Pediatr. Radiol.* 38, 164–174. doi:10.1007/s00247-007-0673-0

Merhof, D., Soza, G., Stadlbauer, A., Greiner, G., Nimsky, C., 2007. Correction of susceptibility artifacts in diffusion tensor data using non-linear registration.

*Med. Image Anal.* 11, 588–603. doi:10.1016/j.media.2007.05.004

Mert, A., Gan, L.S., Knosp, E., Sutherland, G.R., Wolfsberger, S., 2013. Advanced cranial navigation. *Neurosurgery* 72, 43–53.

doi:10.1227/NEU.0b013e3182750c03

Milner, B., 1971. Interhemispheric differences in the localization of psychological processes in man. *Br. Med. Bull.* 27, 272–277.

Milner, B., 1968. Visual recognition and recall after right temporal-lobe excision in man. *Neuropsychologia* 6, 191–209.

Mislow, J.M.K., Golby, A.J., Black, P.M., 2009. Origins of Intraoperative MRI.

*Neurosurg. Clin. N. Am.* 20, 137–146. doi:10.1016/j.nec.2009.04.002

Mitchell, L., Jackson, G., Kalnins, R., Saling, M., Fitt, G., Ashpole, R., Berkovic, S., 1999. Anterior temporal abnormality in temporal lobe epilepsy: A quantitative MRI and histopathologic study. *Neurology* 52, 327–336.

Mohammadi, A.M., Sullivan, T.B., Barnett, G.H., Recinos, V., Angelov, L., Kamian, K., Vogelbaum, M.A., 2014. Use of high-field intraoperative magnetic resonance imaging to enhance the extent of resection of enhancing and

nonenhancing gliomas. *Neurosurgery* 74, 339–348.

doi:10.1227/NEU.0000000000000278

Moorhead, T.W.J., Gountouna, V.E., Job, D.E., McIntosh, A.M., Romaniuk, L., Lymer, G.K.S., Whalley, H.C., Waiter, G.D., Brennan, D., Ahearn, T.S., Cavanagh, J., Condon, B., Steele, J.D., Wardlaw, J.M., Lawrie, S.M., 2009. Prospective multi-centre Voxel Based Morphometry study employing scanner specific segmentations: procedure development using CaliBrain structural MRI data. *BMC Med. Imaging* 9, 8. doi:10.1186/1471-2342-9-8

Morey, R. a., Selgrade, E.S., Wagner, H.R., Huettel, S. a., Wang, L., McCarthy, G., 2010. Scan-rescan reliability of subcortical brain volumes derived from automated segmentation. *Hum. Brain Mapp.* 31, 1751–1762. doi:10.1002/hbm.20973

Morey, R., Petty, C., Xu, Y., Hayes, J., Wagner, H., Lewis, D., LaBar, K., Styner, M., McCarthy, G., 2008. A comparison of automated segmentation and manual tracing for quantifying hippocampal and amygdala volumes. *Neuroimage* 45, 855–866.

Mori, S., Crain, B., Chacko, V., Van Zijl, P., 1999. Three-dimensional tracking of axonal projections in the brain by magnetic resonance imaging. *Ann Neurol* 45, 265–269.

Mori, S., Frederiksen, K., van Zijl, P., Stieltjes, B., Kraut, M., Solyaiyappan, M.,

- Pomper, M., 2002. Brain white matter anatomy of tumor patients evaluated with diffusion tensor imaging. *Ann Neurol* 51, 377–380.
- Mori, S., Van Zijl, P.C.M., 2002. Fiber tracking: Principles and strategies - A technical review. *NMR Biomed.* 15, 468–480. doi:10.1002/nbm.781
- Moritani, T., Smoker, W.R.K., Sato, Y., Numaguchi, Y., Westesson, P.A., 2005. Diffusion-Weighted Imaging of Acute Excitotoxic Brain Injury 216–228.
- Morris, A., 1956. Temporal lobectomy with removal of uncus, hippocampus, and amygdala. *Arch Neurol Psychiatry* 79.
- Mueller, S., Schuff, N., Yaffe, K., Madison, C., Miller, B., Weiner, M., 2010. Hippocampal atrophy patterns in mild cognitive impairment and Alzheimer's disease. *Hum. Brain Mapp.* 31, 1339–1347.
- Müller, M.J., Greverus, D., Dellani, P.R., Weibrich, C., Wille, P.R., Scheurich, A., Stoeter, P., Fellgiebel, A., 2005. Functional implications of hippocampal volume and diffusivity in mild cognitive impairment. *Neuroimage* 28, 1033–1042. doi:10.1016/j.neuroimage.2005.06.029
- Munnich, T., Klein, J., Hattingen, E., Noack, A., Herrmann, E., Seifert, V., Senft, C., MT, F., 2018. Tractography Verified by Intraoperative Magnetic Resonance Imaging and Subcortical Stimulation. *Oper. Neurosurg.* 0, 1–14. doi:10.1093/ons/opy062
- Nabavi, A., McL. Black, P., Gering, D.T., Westin, C.F., Mehta, V., Pergolizzi, R.S.,

- Ferrant, M., Warfield, S.K., Hata, N., Schwartz, R.B., Wells, W.M., Kikinis, R., Jolesz, F. a., 2001. Serial intraoperative magnetic resonance imaging of brain shift. *Neurosurgery* 48, 787–798. doi:10.1227/00006123-200104000-00019
- Nagasaka, T., Shindo, K., Hiraide, M., Sugimoto, T., Shiozawa, Z., 2002. Ipsilateral thalamic MRI abnormality in an epilepsy patient. *Neurology* 58, 641–644.
- Nakamura, K., Brown, R.A., Narayanan, S., Collins, D.L., Arnold, D.L., 2015. Diurnal fluctuations in brain volume: Statistical analyses of MRI from large populations. *Neuroimage* 118, 126–132. doi:10.1016/j.neuroimage.2015.05.077
- Nakano, I., 1998. The limbic system: an outline and brief history of the concept. *Neuropathology* 18, 211–214.
- Namer, I.J., Waydelich, R., Armspach, J.P., Hirsch, E., Marescaux, C., Grucker, D., 1998. Contribution of T2relaxation time mapping in the evaluation of cryptogenic temporal lobe epilepsy. *Neuroimage* 7, 304–313. doi:10.1006/nimg.1998.0331
- Napolitano, M., Vaz, G., Lawson, T.M., Docquier, M.A., van Maanen, A., Duprez, T., Raftopoulos, C., 2014. Glioblastoma surgery with and without intraoperative MRI at 3.0T. *Neurochirurgie* 60, 143–150. doi:10.1016/j.neuchi.2014.03.010

Natsume, J., Bernasconi, N., Andermann, F., Bernasconi, A., 2003. MRI volumetry of the thalamus in temporal, extratemporal, and idiopathic generalized epilepsy. *Neurology* 60, 1296–1300.

doi:10.1212/01.WNL.0000058764.34968.C2

Nauta, H.J.W., Bonnen, J.G., 1998. Problem of intraoperative anatomical shift in image-guided surgery. *Surg. Syst. Proc.* 3262, 229–233.

doi:10.1117/12.309473

Nazem-Zadeh, M.R., Schwalb, J.M., Elisevich, K. V., Bagher-Ebadian, H., Hamidian, H., Akhondi-Asl, A.R., Jafari-Khouzani, K., Soltanian-Zadeh, H., 2014.

Lateralization of temporal lobe epilepsy using a novel uncertainty analysis of MR diffusion in hippocampus, cingulum, and fornix, and hippocampal volume and FLAIR intensity. *J. Neurol. Sci.* 342, 152–161.

doi:10.1016/j.jns.2014.05.019

Ngugi, A., Bottomley, C., Kleinschmidt, I., Sander, J., Newton, C., 2010. Estimation of the burden of active and life-time epilepsy: a meta-analytic approach.

*Epilepsia* 51, 883–890.

Niemeyer, P., 1958. The transventricular amygdala-hippocampectomy in the temporal lobe epilepsy. Charles C Thomas, Springfield, Il.

Nilsson, D., Go, C., Rutka, J.T., Rydenhag, B., Mabbott, D.J., Snead, O.C., Raybaud, C.R., Widjaja, E., 2008. Bilateral diffusion tensor abnormalities of temporal

lobe and cingulate gyrus white matter in children with temporal lobe epilepsy. *Epilepsy Res.* 81, 128–135. doi:10.1016/j.eplepsyres.2008.05.002

Nimsky, C., Ganslandt, O., Hastreiter, P., Wang, R., Benner, T., Sorensen, A., Fahlbusch, R., 2005. Preoperative and intraoperative diffusion tensor imaging-based fiber tracking in glioma surgery. *Neurosurgery* 56, 130–138. doi:10.1227/01.NEU.0000144842.18771.30

Nimsky, C., Ganslandt, O., Cerny, S., Hastreiter, P., Greiner, G., Fahlbusch, R., 2000. Quantification of, visualization of, and compensation for brain shift using intraoperative magnetic resonance imaging. *Neurosurgery* 47, 1070–1080. doi:10.1097/00006123-200011000-00008

Nimsky, C., Ganslandt, O., Fahlbusch, R., 2005a. 1.5 T: intraoperative imaging beyond standard anatomic imaging. *Neurosurg. Clin. N. Am.* 16, 185–200. doi:10.1016/j.nec.2004.07.001

Nimsky, C., Ganslandt, O., Hastreiter, P., Wang, R., Benner, T., Sorensen, A., Fahlbusch, R., 2005b. Intraoperative Diffusion-Tensor MR Imaging: Shifting of White Matter Tracts during Neurosurgical Procedures—Initial Experience<sup>1</sup>. *Radiology* 234, 218–225. doi:10.1148/radiol.2341031984

Nimsky, C., Ganslandt, O., Hastreiter, P., Wang, R., Benner, T., Sorensen, A.G., Fahlbusch, R., 2005. Preoperative and intraoperative diffusion tensor imaging-based fiber tracking in glioma surgery. *Neurosurgery* 56, 130–137.

doi:10.1227/01.NEU.0000144842.18771.30

Nimsky, C., Ganslandt, O., Merhof, D., Sorensen, a G., Fahlbusch, R., 2006.

Intraoperative visualization of the pyramidal tract by diffusion-tensor-imaging-based fiber tracking. *Neuroimage* 30, 1219–29.

doi:10.1016/j.neuroimage.2005.11.001

Nimsky, C., Grummich, P., Ag, S., Fahlbusch, R., Ganslandt, O., 2005c. Visualization of the pyramidal tract in glioma surgery by integrating diffusion tensor imaging in functional neuronavigation . *PubMed Commons* 7–8.

Niu, C., Liu, X., Yang, Y., Zhang, K., Min, Z., Wang, M., Li, W., Guo, L., Lin, P., Zhang, M., 2016. Assessing Region of Interest Schemes for the Corticospinal Tract in Patients With Brain Tumors. *Medicine (Baltimore)*. 95, e3189.

doi:10.1097/MD.0000000000003189

Nordenskjold, R., Malmberg, F., Larsson, E.M., Simmons, A., Brooks, S.J., Lind, L., Ahlstrom, H., Johansson, L., Kullberg, J., 2013. Intracranial volume estimated with commonly used methods could introduce bias in studies including brain volume measurements. *Neuroimage* 83, 355–360.

doi:10.1016/j.neuroimage.2013.06.068

Nossek, E., Korn, A., Shahar, T., Kanner, A.A., Yaffe, H., Marcovici, D., Ben-Harosh, C., Ben Ami, H., Weinstein, M., Shapira-Lichter, I., Constantini, S., Hendler, T., Ram, Z., 2011. Intraoperative mapping and monitoring of the corticospinal

tracts with neurophysiological assessment and 3-dimensional ultrasonography-based navigation. *J. Neurosurg.* 114, 738–746.

doi:10.3171/2010.8.JNS10639

Noulhiane, M., Samson, S., Clémenceau, S., Dormont, D., Baulac, M., Hasboun, D., Cl, S., 2006. A volumetric MRI study of the hippocampus and the parahippocampal region after unilateral medial temporal lobe resection. *J. Neurosci. Methods* 156, 293–304. doi:10.1016/j.jneumeth.2006.02.021

Novy, J., Belluzo, M., Caboclo, L., Catarino, C., Yogarajah, M., Martinian, L., Peacock, J., Bell, G., Koepp, M., Thom, M., Sander, J., Sisodiya, S., 2013. The lifelong course of chronic epilepsy: the Chalfont experience. *Brain* 136, 3187–3199.

Nowell, M., Sparks, R., Zombori, G., Miserocchi, A., Rodionov, R., Diehl, B., Wehner, T., White, M., Ourselin, S., McEvoy, A., Duncan, J., 2017. Resection planning in extratemporal epilepsy surgery using 3D multimodality imaging and intraoperative MRI. *Br. J. Neurosurg.* 31, 468–470.

doi:10.1080/02688697.2016.1265086

Nugent, A.A.C., Luckenbaugh, D. a., Wood, S.E.S., Bogers, W., Zarate, C.J. a., Drevets, W.C.W., 2013. Automated subcortical segmentation using FIRST: Test-retest reliability, interscanner reliability, and comparison to manual segmentation. *Hum. Brain Mapp.* 34, 2313–2329. doi:10.1002/hbm.22068

- Oikawa, H., Sasaki, M., Tamakawa, Y., Kamei, a, 2001. The circuit of Papez in mesial temporal sclerosis: MRI. *Neuroradiology* 43, 205–10.
- Olivier, A., 2000. Amygdalohippocampectomy in Temporal Lobe Epilepsy. *Can. J. Neurol. Sci.* 27, S68–S76.
- Ostojic, J., Kozic, D., Pavlovic, A., Semnic, M., Todorovic, A., Petrovic, K., Covickovic-Sternic, N., 2015. Hippocampal diffusion tensor imaging microstructural changes in vascular dementia. *Acta Neurol. Belg.* 115, 557–562. doi:10.1007/s13760-014-0419-3
- Ostrý, S., Belšan, T., Otáhal, J., Beneš, V., Netuka, D., 2013. Is intraoperative diffusion tensor imaging at 3.0T comparable to subcortical corticospinal tract mapping? *Neurosurgery* 73, 797–807. doi:10.1227/NEU.0000000000000087
- Otte, W.M., Van Eijsden, P., Sander, J.W., Duncan, J.S., Dijkhuizen, R.M., Braun, K.P.J., 2012. A meta-analysis of white matter changes in temporal lobe epilepsy as studied with diffusion tensor imaging. *Epilepsia* 53, 659–667. doi:10.1111/j.1528-1167.2012.03426.x
- Ozawa, N., Muragaki, Y., Nakamura, R., Hori, T., Iseki, H., 2009. Shift of the pyramidal tract during resection of the intraaxial brain tumors estimated by intraoperative diffusion-weighted imaging. *Neurol. Med. Chir. (Tokyo)*. 49, 51–6.

- Ozkara, C., Aronica, E., 2012. Hippocampal sclerosis, in: Stefan, H., Theodore, W. (Eds.), *Handbook of Clinical Neurology*. Elsevier B.V., Amsterdam, The Netherlands, pp. 621–639.
- Paglioli, E., Palmi, A., Paglioli, E., Da Costa, J., Portuguese, M., Martinez, J. V., Calcagnotto, M.E., Hoefel, J.R., Raupp, S., Barbosa-Coutinho, L., 2004. Survival analysis of the surgical outcome of temporal lobe epilepsy due to hippocampal sclerosis 10, 233–236.
- Pantoni, L., Garcia, J., Gutierrez, J., 1999. Cerebral white matter is highly vulnerable to ischemia. *Stroke* 27, 1641–1647.
- Papez, J., 1937. A proposed mechanism of emotion. *Arch Neurol Psychiatry* 38, 725–743.
- Pardoe, H.R., Pell, G.S., Abbott, D.F., Jackson, G.D., 2011. Hippocampal volume assessment in temporal lobe epilepsy: How good is automated segmentation? *Epilepsia* 50, 2586–2592. doi:10.1111/j.1528-1167.2009.02243.x.Hippocampal
- Parizel, P.M., Van Goethem, J.W., Özsarlak, Ö., Maes, M., Phillips, C.D., 2005. New developments in the neuroradiological diagnosis of craniocerebral trauma. *Eur. Radiol.* 15, 569–581. doi:10.1007/s00330-004-2558-z
- Patenaude, B., Smith, S.M., Kennedy, D., Jenkinson, M., 2011. A Bayesian Model of Shape and Appearance for Subcortical Brain. *Neuroimage* 56, 907–922.

doi:10.1016/j.neuroimage.2011.02.046.A

Pekna, M., Pekny, M., Nilsson, M., 2012. Modulation of neural plasticity as a basis for stroke rehabilitation. *Stroke* 43, 2819–2828.

doi:10.1161/STROKEAHA.112.654228

Penfield, W., Baldwin, M., 1952. Temporal lobe seizures and the technique of subtotal temporal lobectomy. *Ann. Surg.* 136, 625–634.

Pereira, J.B., Valls-Pedret, C., Ros, E., Palacios, E., Falcon, C., Bargallo, N., Bartres-Faz, D., Wahlund, L.O., Westman, E., Junque, C., 2014. Regional vulnerability of hippocampal subfields to aging measured by structural and diffusion MRI. *Hippocampus* 24, 403–414. doi:10.1002/hipo.22234

Pereira, P.M.G., Oliveira, E., Rosado, P., 2006. Apparent diffusion coefficient mapping of the hippocampus and the amygdala in pharmaco-resistant temporal lobe epilepsy. *Am. J. Neuroradiol.* 27, 671–683.

Perrone, D., Aelterman, J., Pižurica, A., Jeurissen, B., Philips, W., Leemans, A., 2015. The effect of Gibbs ringing artifacts on measures derived from diffusion MRI. *Neuroimage* 120, 441–455.

doi:10.1016/j.neuroimage.2015.06.068

Pfeuty, M., Thivard, L., Dupont, S., Adam, C., Baulac, M., Samson, S., 2011. Postoperative recovery of hippocampal contralateral diffusivity in medial temporal lobe epilepsy correlates with memory functions. *J. Neurol.*

Neurosurg. Psychiatry 82, 340–3. doi:10.1136/jnnp.2008.158428

Pierce, M.C., Bertocci, G.E., Berger, R., Vogeley, E., 2002. Injury biomechanics for aiding in the diagnosis of abusive head trauma. *Neurosurg. Clin. N. Am.* 13, 155–168. doi:10.1016/S1042-3680(01)00006-7

Pooley, R.A., 2005. AAPM/RSNA physics tutorial for residents: fundamental physics of MR imaging. *Radiographics* 25, 1087–1099. doi:10.1148/rg.254055027

Porter, D. a., Heidemann, R.M., 2009. High resolution diffusion-weighted imaging using readout-segmented echo-planar imaging, parallel imaging and a two-dimensional navigator-based reacquisition. *Magn. Reson. Med.* 62, 468–475. doi:10.1002/mrm.22024

Potgieser, A.R.E., Wagemakers, M., Van Hulzen, A.L.J., De Jong, B.M., Hoving, E.W., Groen, R.J.M., 2014. The role of diffusion tensor imaging in brain tumor surgery: A review of the literature. *Clin. Neurol. Neurosurg.* 124, 51–58. doi:10.1016/j.clineuro.2014.06.009

Prabhu, S.S., Gasco, J., Tummala, S., Weinberg, J.S., Rao, G., 2011. Intraoperative magnetic resonance imaging-guided tractography with integrated monopolar subcortical functional mapping for resection of brain tumors. Clinical article. *J. Neurosurg.* 114, 719–726. doi:10.3171/2010.9.JNS10481

Preul, M.C., Feindel, W., 1991. Origins of Wilder Penfield's surgical technique.

- The role of the “Cushing ritual” and influences from the European experience. *J. Neurosurg.* 75, 812–820. doi:10.3171/jns.1991.75.5.0812
- Pruessner, J., Li, L., Series, W., Preussner, D., Collins, N., Kabani, S., Lupien, S., Evans, A., 2000. Volumetry of Hippocampus and Amygdala with High-resolution MRI and Three-dimensional Analysis Software: Minimizing the Discrepancies between Laboratories. *Cereb. Cortex* 10, 433–442. doi:10.1093/cercor/10.4.433
- Quigg, M., Bertram, E.H., Jackson, T., 1997. Longitudinal distribution of hippocampal atrophy in mesial temporal lobe epilepsy. *Epilepsy Res.* 27, 101–110.
- Radmanesh, A., Zamani, A. a, Whalen, S., Tie, Y., Suarez, R.O., Golby, A.J., 2015. Comparison of seeding methods for visualization of the corticospinal tracts using single tensor tractography. *Clin. Neurol. Neurosurg.* 129, 44–49. doi:10.1016/j.clineuro.2014.11.021
- Rajohan, V., Mohandas, E., 2007. The limbic system. *Indian J Psychiatry* 49, 132–139.
- Régis, J., Bartolomei, F., Rey, M., Genton, P., Dravet, C., Semah, F., Gastaut, J.-L.L., Chauvel, P., Peragut, J.-C.C., Régis, J., Bartolomei, F., Rey, M., Genton, P., Dravet, C., Semah, F., Gastaut, J.-L.L., Chauvel, P., Peragut, J.-C.C., 1999. Gamma knife surgery for mesial temporal lobe epilepsy. *Epilepsia* 40, 1551–

1556. doi:10.1111/j.0013-9580.2005.53904.x

Reid, M., 1978. Ultrasonic visualization of a cervical cord cystic astrocytoma. *AJR Am J Roentgenol* 131, 907–908.

Rennebaum, F., Kassubek, J., Pinkhardt, E., Hübers, A., Ludolph, A.C., Schocke, M., Fauser, S., 2016. Status epilepticus: Clinical characteristics and EEG patterns associated with and without MRI diffusion restriction in 69 patients. *Epilepsy Res.* 120, 55–64. doi:10.1016/j.eplepsyres.2015.12.004

Reuter, M., Tisdall, M.D., Qureshi, A., Buckner, R.L., van der Kouwe, A.J.W., Fischl, B., 2015. Head motion during MRI acquisition reduces gray matter volume and thickness estimates. *Neuroimage* 107, 107–115.  
doi:10.1016/j.neuroimage.2014.12.006

Riederer, F., Lanzenberger, R., Kaya, M., 2008. Network atrophy in temporal lobe epilepsy A voxel-based morphometry study. *Neurology* 419–425.

Roberts, D., Miga, M., Hartov, A., Eisner, S., Lemery, J., Kennedy, F., Paulsen, K., 1999. Intraoperatively updated neuroimaging using brain modeling and sparse data. *Neurosurgery* 45, 1199–1207.

Roberts, D.W., Strohbehm, J.W., Hatch, J.F., Murray, W., Kettenberger, H., 1986. A frameless stereotaxic integration of computerized tomographic imaging and the operating microscope. *J. Neurosurg.* 65, 545–549.  
doi:10.3171/jns.1986.65.4.0545

- Roberts, N., Puddephat, M., McNulty, V., 2000. The benefit of stereology for quantitative radiology. *Br. J. Radiol.* 73, 679–697.
- Robson, M., Anderson, A., Gore, J., 1997. Diffusion-weighted multiple shot echo planar imaging of humans without navigation. *Magn Reson Imaging* 38, 82–88.
- Rogers, B.P., Sheffield, J.M., Luksik, A.S., Heckers, S., 2012. Systematic Error in Hippocampal Volume Asymmetry Measurement is Minimal with a Manual Segmentation Protocol. *Front. Neurosci.* 6, 179.  
doi:10.3389/fnins.2012.00179
- Romano, A., D'Andrea, G., Calabria, L.F., Coppola, V., Espagnet, C.R., Pierallini, A., Ferrante, L., Fantozzi, L., Bozzao, A., 2011. Pre- and intraoperative tractographic evaluation of corticospinal tract shift. *Neurosurgery* 69, 696–704. doi:10.1227/NEU.0b013e31821a8555
- Rugg-Gunn, F., Boulby, P., Symms, M., Barker, G., Duncan, J., 2005. Whole-brain T2 mapping demonstrates occult abnormalities in focal epilepsy. *Neurology* 64, 318–325.
- Sagi, Y., Tavor, I., Hofstetter, S., Tzur-Moryosef, S., Blumenfeld-Katzir, T., Assaf, Y., 2012. Learning in the Fast Lane: New Insights into Neuroplasticity. *Neuron* 73, 1195–1203. doi:10.1016/j.neuron.2012.01.025
- Salama, G.R., Heier, L.A., Patel, P., Ramakrishna, R., Magge, R., Tsiouris, A.J., 2017.

Diffusion Weighted/Tensor Imaging, Functional MRI and Perfusion  
Weighted Imaging in Glioblastoma-Foundations and Future. *Front. Neurol.*  
8, 660. doi:10.3389/fneur.2017.00660

Salmenperä, T., Kälviäinen, R., Partanen, K., Pitkänen, a, 2001. Hippocampal and  
amygdaloid damage in partial epilepsy: a cross-sectional MRI study of 241  
patients. *Epilepsy Res.* 46, 69–82.

Salmenpera, T.M., Simister, R.J., Bartlett, P., Symms, M.R., Boulby, P.A., Free, S.L.,  
Barker, G.J., Duncan, J.S., 2006. High-resolution diffusion tensor imaging of  
the hippocampus in temporal lobe epilepsy. *Epilepsy Res.* 71, 102–106.  
doi:10.1016/j.eplepsyres.2006.05.020

Sandok, E.K., O'Brien, T.J., Jack, C.R., So, E.L., 2000. Significance of cerebellar  
atrophy in intractable temporal lobe epilepsy: A quantitative MRI study.  
*Epilepsia* 41, 1315–1320.

Sankar, T., Bernasconi, N., Kim, H., Bernasconi, A., 2008. Temporal lobe epilepsy:  
Differential pattern of damage in temporopolar cortex and white matter.  
*Hum. Brain Mapp.* 29, 931–944. doi:10.1002/hbm.20437

Sarioglu, F.C., Sahin, H., Pekcevik, Y., Sarioglu, O., Oztekin, O., 2017. Pediatric head  
trauma: an extensive review on imaging requisites and unique imaging  
findings. *Eur. J. Trauma Emerg. Surg.* 0, 0. doi:10.1007/s00068-017-0838-y

Sato, S., Iwasaki, M., Suzuki, H., Mugikura, S., Jin, K., Tominaga, T., Takase, K.,

- Takahashi, S., Nakasato, N., 2016. T2 relaxometry improves detection of non-sclerotic epileptogenic hippocampus. *Epilepsy Res.* 126, 1–9.  
doi:10.1016/j.eplepsyres.2016.06.001
- Scahill, R.I., Frost, C., Jemkins, R., Withwell, J.E., Rossor, M.N., Fox, N.C., 2003. A longitudinal study of brain volume changes in normal aging using serial registered magnetic resonance imaging. *Arch. Neurol.* 60, 989–994.  
doi:10.1001/archneur.60.7.989
- Scanlon, C., Mueller, S.G., Cheong, I., Hartig, M., Weiner, M.W., Laxer, K.D., 2013. Grey and white matter abnormalities in temporal lobe epilepsy with and without mesial temporal sclerosis. *J. Neurol.* 260, 2320–2329.  
doi:10.1007/s00415-013-6974-3
- Schaefer, P.W., Grant, P.E., Gonzalez, R.G., 2000. Diffusion-weighted MR Imaging of the Brain. *Radiology* 217, 331–345.  
doi:10.1148/radiology.217.2.r00nv24331
- Schnack, H.G., Van Haren, N.E.M., Brouwer, R.M., Van Baal, G.C.M., Picchioni, M., Weisbrod, M., Sauer, H., Cannon, T.D., Huttunen, M., Lepage, C., Collins, D.L., Evans, A., Murray, R.M., Kahn, R.S., Hulshoff Pol, H.E., 2010. Mapping reliability in multicenter MRI: Voxel-based morphometry and cortical thickness. *Hum. Brain Mapp.* 31, 1967–1982. doi:10.1002/hbm.20991
- Schoene-Bake, J.-C., Faber, J., Trautner, P., Kaaden, S., Tittgemeyer, M., Elger, C.E.,

- Weber, B., 2009. Widespread affections of large fiber tracts in postoperative temporal lobe epilepsy. *Neuroimage* 46, 569–76.  
doi:10.1016/j.neuroimage.2009.03.013
- Schuele, S.U., Lüders, H.O., 2008. Intractable epilepsy: management and therapeutic alternatives. *Lancet Neurol.* 7, 514–524. doi:10.1016/S1474-4422(08)70108-X
- Schwedemberg, T.H., 1957. Leukoencephalography following carbon monoxide asphyxia. *J Neuropathol Exp Neurol* 18, 597–608.
- Seidenberg, M., Kelly, K.G., Parrish, J., Geary, E., Dow, C., Rutecki, P., Hermann, B., 2005. Ipsilateral and contralateral MRI volumetric abnormalities in chronic unilateral temporal lobe epilepsy and their clinical correlates. *Epilepsia* 46, 420–430.
- Semah, F., Picot, M., Adam, C., Broglin, D., Arzimanoglou, A., Bazin, B., Cavalcanti, D., Baulac, M., 1998. Is the underlying cause of epilepsy a major prognostic factor for recurrence? *Neurology* 51, 1256–1262.
- Senft, C., Bink, A., Franz, K., Vatter, H., Gasser, T., Seifert, V., 2011. Intraoperative MRI guidance and extent of resection in glioma surgery: A randomised, controlled trial. *Lancet Oncol.* 12, 997–1003. doi:10.1016/S1470-2045(11)70196-6
- Senn, P., Lovblad, K., Zutter, D., Bassetti, C., Zeller, O., Donati, F., Schroth, G., 2003.

Changes on diffusion-weighted MRI with focal motor status epilepticus: case report. *Neuroradiology* 45, 246–249.

Serles, W., Li, L.M., Antel, S.B., Cendes, F., Gotman, J., Olivier, A., Andermann, F., Dubeau, F., Arnold, D.L., 2001. Time Course of Postoperative Recovery of N - Acetyl-Aspartate in Temporal Lobe Epilepsy 42, 190–197.

Shah, M.N., Leonard, J.R., Inder, G., Gao, F., Geske, M., Haydon, D.H., Omodon, M.E., Evans, J., Morales, D., Dacey, R.G., Smyth, M.D., Chicoine, M.R., Limbrick, D.D., 2012. Intraoperative magnetic resonance imaging to reduce the rate of early reoperation for lesion resection in pediatric neurosurgery. *J. Neurosurg. Pediatr.* 9, 259–64. doi:10.3171/2011.12.PEDS11227

Shahar, T., Rozovski, U., Marko, N.F., Tummala, S., Ziu, M., Weinberg, J.S., Rao, G., Kumar, V. a., Sawaya, R., Prabhu, S.S., 2014. Preoperative imaging to predict intraoperative changes in tumor-to-corticospinal tract distance: An analysis of 45 cases using high-field intraoperative magnetic resonance imaging. *Neurosurgery* 75, 23–30. doi:10.1227/NEU.0000000000000338

Shalit, M., Israeli, Y., Matz, S., Cohen, M., 1979. Intra-operative computerized axial tomography. *Surg. Neurol.* 11, 382–384.

Sheline, Y., Gado, M., Kraemer, H., 2003. Untreated depression and hippocampal volume loss. *Am. J. Psychiatry* 160, 1516–1518.

Sheline, Y.I., Wang, P.W., Gado, M.H., Csernansky, J.G., Vannier, M.W., 1996.

- Hippocampal atrophy in recurrent major depression. *Proc. Natl. Acad. Sci. U. S. A.* 93, 3908–3913. doi:10.1073/pnas.93.9.3908
- Shokouhi, M., Barnes, A., Suckling, J., Moorhead, T.W.J., Brennan, D., Job, D., Lymer, K., Dazzan, P., Reis Marques, T., MacKay, C., McKie, S., Williams, S.C.R., Lawrie, S.M., Deakin, B., Williams, S.R., Condon, B., 2011. Assessment of the impact of the scanner-related factors on brain morphometry analysis with Brainvisa. *BMC Med. Imaging* 11, 23. doi:10.1186/1471-2342-11-23
- Shrout, P.E., Fleiss, J.L., 1979. Intraclass Correlation: Uses in Assessing Rater Reliability. *Psychol. Bull.* 86, 420–428.
- Sindou, M., Guenot, M., Isnard, J., Ryvlin, P., Fischer, C., Mauguière, F., 2006. Temporo-mesial epilepsy surgery: Outcome and complications in 100 consecutive adult patients. *Acta Neurochir. (Wien)*. 148, 39–45. doi:10.1007/s00701-005-0644-x
- Sled, J.G., Zijdenbos, a P., Evans, a C., 1998. A nonparametric method for automatic correction of intensity nonuniformity in MRI data. *IEEE Trans. Med. Imaging* 17, 87–97. doi:10.1109/42.668698
- Soares, J., Marques, P., Alves, V., Sousa, N., 2013. A hitchhiker’s guide to diffusion tensor imaging. *Front. Neurosci.* 7, 1–14. doi:10.3389/fnins.2013.00031
- Sommer, W., 1980. Erkrankung des Ammonshorns als aetiologisches Moment der Epilepsie. *Arch Psychiatr* 10, 631–675.

- Spencer, D., Burchiel, K., 2012. Review Article Selective Amygdalohippocampectomy 2012. doi:10.1155/2012/382095
- Spencer, S., Berg, A., Vickrey, B., Sperling, M., Bazil, C., Shinnar, S., Langfitt, J., Walczak, T., Pacia, S., Surgery, and the M.S. of E., 2005. Multicenter Study of Epilepsy Surgery. Predicting long-term seizure outcome after resective epilepsy. *Neurology* 65, 912–918.
- Spencer, S., Huh, L., 2008. Outcomes of epilepsy surgery in adults and children. *Lancet Neurol.* 7, 525–537. doi:10.1016/S1474-4422(08)70109-1
- Spender, D., SS, S., Mattson, R., Williamson, P., Novelly, R., 1984. Access to the Posterior Medial Temporal Lobe Structures in the Surgical Treatment of Temporal Lobe Epilepsy 15, 667–671.
- Spetzler, R.F., Martin, N.A., 1986. A proposed grading system for arteriovenous malformations. *J. Neurosurg.* 65, 476–483. doi:10.3171/jns.1986.65.4.0476
- Spielmeyer, W., 1927. Die Pathogenese des epileptischen Krampfes. *Z Dtsch Ges Neurol Psychiatr* 109, 501–520.
- Steen, R.G., Hamer, R.M., Lieberman, J.A., 2007. Measuring brain volume by MR imaging: Impact of measurement precision and natural variation on sample size requirements. *Am. J. Neuroradiol.* 28, 1119–1125. doi:10.3174/ajnr.A0537
- Stefan, H., Hildebrandt, M., Kerling, F., Kasper, B.S., Hammen, T., Dorfler, A.,

- Weigel, D., Buchfelder, M., Blumcke, I., Pauli, E., 2009. Clinical prediction of postoperative seizure control: structural, functional findings and disease histories. *J. Neurol. Neurosurg. Psychiatry* 80, 196–200.  
doi:10.1136/jnnp.2008.151860
- Stejskal, E., Tanner, J., 1965. Spin diffusion measurements: spin echoes in the presence of a time-dependent field gradient. *J. Chem. Phys.* 42, 288.
- Suckling, J., Barnes, A., Job, D., Brennan, D., Lymer, K., Dazzan, P., Marques, T.R., Mackay, C., McKie, S., Williams, S.R., Williams, S.C.R., Deakin, B., Lawrie, S., 2012. The neuro/PsyGRID calibration experiment: Identifying sources of variance and bias in multicenter MRI studies. *Hum. Brain Mapp.* 33, 373–386. doi:10.1002/hbm.21210
- Suh, D.Y., Davis, P.C., Hopkins, K.L., Fajman, N.N., Mapstone, T.B., 2001. Nonaccidental Pediatric Head Injury: Diffusion-weighted Imaging Findings 49.
- Sutherland, G.R., Kaibara, T., Louw, D., Hoult, D.I., Tomanek, B., Saunders, J., 1999. A mobile high-field magnetic resonance system for neurosurgery. *J. Neurosurg.* 91, 804–813. doi:10.3171/jns.1999.91.5.0804
- Swenson, R., 2006. Chapter 9: Limbic system [WWW Document]. *Rev. Clin. Funct. Neurosci.* URL  
[http://www.dartmouth.edu/~rswenson/NeuroSci/chapter\\_9.html](http://www.dartmouth.edu/~rswenson/NeuroSci/chapter_9.html)

(accessed 3.28.18).

Sylvester, P.T., Evans, J.A., Zipfel, G.J., Chole, R.A., Uppaluri, R., Haughey, B.H., Getz,

A.E., Silverstein, J., Rich, K.M., Kim, A.H., Dacey, R.G., Chicoine, M.R., 2015.

Combined high-field intraoperative magnetic resonance imaging and

endoscopy increase extent of resection and progression-free survival for

pituitary adenomas. *Pituitary* 18, 72–85. doi:10.1007/s11102-014-0560-2

Szabo, K., Förster, A., Gass, A., 2014. Conventional and diffusion-weighted MRI of

the hippocampus. *Hippocampus Clin. Neurosci.* 34, 71–84.

doi:10.1159/000357925

Szabo, K., Poepel, A., Pohlmann-Eden, B., Hirsch, J., Back, T., Sedlaczek, O.,

Hennerici, M., Gass, A., 2005. Diffusion-weighted and perfusion MRI

demonstrates parenchymal changes in complex partial status epilepticus.

*Brain* 128, 1369–1376. doi:10.1093/brain/awh454

Takao, H., Hayashi, N., Ohtomo, K., 2011. Effect of scanner in longitudinal studies

of brain volume changes. *J. Magn. Reson. Imaging* 34, 438–444.

doi:10.1002/jmri.22636

Tanriverdi, T., Olivier, A., 2007. Cognitive changes after unilateral cortico-

amygdalo-hippocampectomy or unilateral selective-amyg-

dalohippocampectomy for mesial temporal lobe epilepsy. *Turk. Neurosurg.*

17, 91–99.

- Tanriverdi, T., Poulin, N., Olivier, A., 2008. Life 12 years after temporal lobe epilepsy surgery: A long-term, prospective clinical study. *Seizure* 17, 339–349. doi:10.1016/j.seizure.2007.11.003
- Tedrus, G.M.A.S., Pereira, R.B., Zoppi, M., 2017. Epilepsy, stigma, and family. *Epilepsy Behav.* 78, 265–268. doi:10.1016/j.yebeh.2017.08.007
- The Royal College of Radiologists, The Royal College of Paediatrics and Child Health, 2008. Standards for radiological investigations of suspected non-accidental injury [WWW Document]. URL [http://www.rcr.ac.uk/docs/radiology/pdf/RCPCH\\_RCR\\_final](http://www.rcr.ac.uk/docs/radiology/pdf/RCPCH_RCR_final) (accessed 2.20.18).
- Thivard, L., Lehericy, S., Krainik, A., Adam, C., Dormont, D., Chiras, J., Baulac, M., Dupont, S., 2005. Diffusion tensor imaging in medial temporal lobe epilepsy with hippocampal sclerosis. *Neuroimage* 28, 682–690. doi:10.1016/j.neuroimage.2005.06.045
- Thivard, L., Tanguy, M.L., Adam, C., Clemenceau, S., Dezamis, E., Lehericy, S., Dormont, D., Chiras, J., Baulac, M., Dupont, S., 2007. Postoperative recovery of hippocampal contralateral diffusivity in medial temporal lobe epilepsy. *Epilepsia* 48, 599–604. doi:10.1111/j.1528-1167.2006.00968.x
- Thom, M., 2014. Review: Hippocampal sclerosis in epilepsy: A neuropathology review. *Neuropathol. Appl. Neurobiol.* 40, 520–543. doi:10.1111/nan.12150

- Thom, M., Eriksson, S., Martinian, L., Caboclo, L.O., McEvoy, A.W., Duncan, J.S., Sisodiya, S.M., 2009. Temporal lobe sclerosis associated with hippocampal sclerosis in temporal lobe epilepsy: neuropathological features. *J. Neuropathol. Exp. Neurol.* 68, 928–938. doi:10.1097/NEN.0b013e3181b05d67
- Thomas, A.G., Koumellis, P., Dineen, R. a, 2011. The fornix in health and disease: an imaging review. *Radiographics* 31, 1107–21. doi:10.1148/rg.314105729
- Thurman, D.J., Logroscino, G., Beghi, E., Hauser, W.A., Hesdorffer, D.C., Newton, C.R., Scorza, F.A., Sander, J.W., Tomson, T., 2017. The burden of premature mortality of epilepsy in high-income countries: A systematic review from the Mortality Task Force of the International League Against Epilepsy. *Epilepsia* 58, 17–26. doi:10.1111/epi.13604
- Toga, A., Mazziotta, J., 2002. *Brain mapping: the methods*. Elsevier.
- Tournier, J.-D., Mori, S., Leemans, A., 2011. Diffusion tensor imaging and beyond. *Magn. Reson. Med.* 65, 1532–1556. doi:10.1002/mrm.22924
- Treiber, J.M., White, N.S., Steed, T.C., Bartsch, H., Holland, D., Farid, N., McDonald, C.R., Carter, B.S., Dale, A.M., Chen, C.C., 2016. Characterization and correction of geometric distortions in 814 Diffusion Weighted Images. *PLoS One* 11, 1–9. doi:10.1371/journal.pone.0152472
- Tuch, D.S., Reese, T.G., Wiegell, M.R., Makris, N., Belliveau, J.W., Van Wedeen, J.,

2002. High angular resolution diffusion imaging reveals intravoxel white matter fiber heterogeneity. *Magn. Reson. Med.* 48, 577–582.

doi:10.1002/mrm.10268

Urbach, H., Siebenhaar, G., Koenig, R., Oertzen, J., 2005. Limbic system abnormalities associated with Ammons horn sclerosis do not alter seizure outcome after amygdalohippocampectomy.

Vachon-Preseu, E., Roy, M., Martel, M.O., Caron, E., Marin, M.F., Chen, J., Albouy, G., Plante, I., Sullivan, M.J., Lupien, S.J., Rainville, P., 2013. The stress model of chronic pain: Evidence from basal cortisol and hippocampal structure and function in humans. *Brain* 136, 815–827. doi:10.1093/brain/aws371

Van Hecke, W., Leemans, A., D’Agostino, E., De Backer, S., Vandervliet, E., Parizel, P.M., Sijbers, J., 2007. Nonrigid coregistration of diffusion tensor images using a viscous fluid model and mutual information. *IEEE Trans. Med. Imaging* 26, 1598–1612. doi:10.1109/TMI.2007.906786

Van Paesschen, W., Sisodiya, S., Connelly, A., Duncan, J., Free, S., Raymond, A., Grunewald, R., Revesz, T., Shorvon, S., Fish, D., Stevens, J., Johnson, C., 2001. Quantitative hippocampal MRI and intractable temporal lobe epilepsy. *Neurology* 57, S5–S12.

Vargas, M.I., Delavelle, J., Kohler, R., Becker, C.D., Lovblad, K., 2009. Brain and spine MRI artifacts at 3 Tesla. *J. Neuroradiol.* 36, 74–81.

doi:10.1016/j.neurad.2008.08.001

Vazquez, E., Delgado, I., Sanchez-Montanez, A., Fabrega, A., Cano, P., Martin, N.,  
2014. Imaging abusive head trauma: why use both computed tomography  
and magnetic resonance imaging? *Pediatr. Radiol.* 44, 589–603.

doi:10.1007/s00247-014-3216-5

Veeramuthu, V., Narayanan, V., Kuo, T.L., Delano-Wood, L., Chinna, K., Bondi,  
M.W., Waran, V., Ganesan, D., Ramli, N., 2015. Diffusion Tensor Imaging  
Parameters in Mild Traumatic Brain Injury and Its Correlation with Early  
Neuropsychological Impairment: A Longitudinal Study. *J. Neurotrauma* 32,  
1497–1509. doi:10.1089/neu.2014.3750

Viergever, M.A., Maintz, J.B.A., Niessen, W.J., Noordmans, H.J., Pluim, J.P.W.,  
Stokking, R., Vincken, K.L., 2001. Registration, segmentation, and  
visualization of multimodal brain images. *Comput. Med. Imaging Graph.* 25,  
147–151. doi:10.1016/S0895-6111(00)00065-3

von Oertzen, J., Urbach, H., Jungbluth, S., Kurthen, M., Reuber, M., Fernandez, G.,  
Elger, C., 2002. Standard magnetic resonance imaging is inadequate for  
patients with refractory focal epilepsy. *J Neurol Neurosurg Psychiatry* 73,  
643–647.

Vos, S.B., Tax, C.M.W., Luijten, P.R., Ourselin, S., Leemans, A., Froeling, M., 2017.  
The importance of correcting for signal drift in diffusion MRI. *Magn. Reson.*

Med. 77, 285–299. doi:10.1002/mrm.26124

Wagner, F., Wimmer, W., Leidolt, L., Vischer, M., Weder, S., Wiest, R.,  
Mantokoudis, G., Caversaccio, M.D., 2015. Significant artifact reduction at  
1.5T and 3T MRI by the use of a cochlear implant with removable magnet:  
An experimental human cadaver study. *PLoS One* 10, 1–17.

doi:10.1371/journal.pone.0132483

Wakana, S., Caprihan, A., Panzenboeck, M.M., Fallon, J.H., Perry, M., Gollub, R.L.,  
Hua, K., Zhang, J., Jiang, H., Dubey, P., Blitz, A., van Zijl, P., Mori, S., 2007.  
Reproducibility of quantitative tractography methods applied to cerebral  
white matter. *Neuroimage* 36, 630–644.

doi:10.1016/j.neuroimage.2007.02.049

Walker, A., 1967. Temporal lobectomy. *J Neurosurg* 26, 642–649.

Wang, Y., Ma, X., Zhang, Z., Dai, E., Jeong, H.K., Xie, B., Yuan, C., Guo, H., 2018. A  
comparison of readout segmented EPI and interleaved EPI in high-  
resolution diffusion weighted imaging. *Magn. Reson. Imaging* 47, 39–47.

doi:10.1016/j.mri.2017.11.011

Wassermann, D., Makris, N., Rathi, Y., Shenton, M., Kikinis, R., Kubicki, M., Westin,  
C.F., 2016. The white matter query language: a novel approach for  
describing human white matter anatomy. *Brain Struct. Funct.* 221, 4705–

4721. doi:10.1007/s00429-015-1179-4

- Watson, C., Jack, C.R.J., Cendes, F., 1997. Volumetric magnetic resonance imaging: Clinical applications and contributions to the understanding of temporal lobe epilepsy. *Arch. Neurol.* 54, 1521–1531. doi:10.1088/0953-8984/13/49/305
- Wedeen, V.J., Wang, R.P., Schmahmann, J.D., Benner, T., Tseng, W.Y.I., Dai, G., Pandya, D.N., Hagmann, P., D’Arceuil, H., de Crespigny, A.J., 2008. Diffusion spectrum magnetic resonance imaging (DSI) tractography of crossing fibers. *Neuroimage* 41, 1267–1277. doi:10.1016/j.neuroimage.2008.03.036
- Wheatley, B., 2008. Selective Amygdalohippocampectomy: the trans-middle temporal gyrus approach 1–5. doi:10.3171
- Whitwell, J.L., Crum, W.R., Watt, H.C., Fox, N.C., 2001. Normalization of cerebral volumes by use of intracranial volume: Implications for longitudinal quantitative mr imaging. *Am. J. Neuroradiol.* 22, 1483–1489. doi:MultipleADFTLD-Converted #29; Thesis\_references-Converted #14; Used to be #970
- Wiebe, Samuel, Blume, M.D., Warren, Girvin, M.D., John, Eliasziw, P.D., Michael, Ph.D., Samuel, W., Warren, B., John, G., Michael, E., Wiebe, Samuel, Blume, M.D., Warren, Girvin, M.D., John, Eliasziw, P.D., Michael, Ph.D., Wiebe, S., Blume, W.T., Girvin, J.P., Eliasziw, M., 2001. A Randomized, Controlled Trial of Surgery for Temporal-Lobe Epilepsy. *N. Engl. J. Med.* 345, 1–8. doi:10.1097/00132586-200206000-00024

- Wieser, H., 2004. ILAE Commission Report. Mesial temporal lobe epilepsy with hippocampal sclerosis. *Epilepsia* 45, 695–714.
- Wieser, H.G., Blume, W.T., Fish, D., Goldensohn, E., Hufnagel, A., King, D., Sperling, M.R., Lüders, H., Pedley, T. a, 2001. ILAE Commission Report. Proposal for a new classification of outcome with respect to epileptic seizures following epilepsy surgery. *Epilepsia* 42, 282–6.  
doi:10.1227/NEU.0000000000000081
- Wieshmann, U., Clark, C., Symms, M., Barker, G., Birnie, K., Shorvon, S., 1999. Water diffusion in the human hippocampus in epilepsy. *Magn Reson Imaging* 17, 29–36.
- Wieshmann, U.C., Symms, M.R., Clark, C.A., Lemieux, L., Franconi, F., Parker, G.J.M., Barker, G.J., Shorvon, S.D., 1999. Wallerian degeneration in the optic radiation after temporal lobectomy demonstrated in vivo with diffusion tensor imaging. *Epilepsia* 40, 1155–1158. doi:10.1111/j.1528-1157.1999.tb00834.x
- Winston, G.P., 2012. The physical and biological basis of quantitative parameters derived from diffusion MRI. *Quant. Imaging Med. Surg.* 2, 254–65.  
doi:10.3978/j.issn.2223-4292.2012.12.05
- Winston, G.P., Daga, P., Stretton, J., Modat, M., Symms, M.R., McEvoy, A.W., Ourselin, S., Duncan, J.S., 2012. Optic radiation tractography and vision in

anterior temporal lobe resection. *Ann. Neurol.* 71, 334–341.

doi:10.1002/ana.22619

Winston, G.P., Stretton, J., Sidhu, M.K., Symms, M.R., Duncan, J.S., 2014.

Progressive white matter changes following anterior temporal lobe resection for epilepsy. *NeuroImage Clin.* 4, 190–200.

doi:10.1016/j.nicl.2013.12.004

Wisse, L., Daugherty, A., Olsen, R., Berron, D., Carr, V., Stark, C., Amaral, R.,

Amunts, K., Augustinack, J., Bender, A., Bernstein, J., Boccardi, M., Bocchetta, M., Burggren, A., Chakravarty, M., Chupin, M., Ekstrom, A., de Flores, R.,

Insausti, R., Kanel, P., Kedo, O., Kennedy, K., Kerchner, G., LaRocque, K., Liu,

X., Maass, A., Malykhin, N., Mueller, S., Ofen, N., Palombo, D., Parekh, M.,

Pluta, J., Pruessner, J., Raz, N., Rodrigue, K., Schoemaker, D., Shafer, A., Steve,

T., Suthana, N., Wang, L., Winterburn, J., Yassa, M., Yushkevich, P., la Joie, R.,

Group, the H.S., 2017. A harmonized segmentation protocol for

hippocampal and parahippocampal subregions: why do we need one and

what are the key goals? *Hippocampus* 27, 3–11. doi:10.1111/joms.12099

Woermann, F., Barker, G., Birnie, K., Meencke, H., Duncan, J., 1998. Regional

changes in hippocampal T2 relaxation and volume: a quantitative magnetic resonance imaging study of hippocampal sclerosis. *J Neurol Neurosurg Psychiatry* 65, 656–664.

Wolfsberger, S., Rössler, K., Regatschnig, R., Ungersböck, K., 2002. Anatomical

landmarks for image registration in frameless stereotactic neuronavigation.  
*Neurosurg. Rev.* 25, 68–72. doi:10.1007/s10143-001-0201-x

Wu, J.-S. (Shanghai M.C., XIU, G., Yan-Yan, S., Dong-Xiao, Z., Cheng-Jun, Y., Tian-Ming, Q., Jun-Feng, L., Jie, Z., Wei, Z., Ying, M., Liang-Fu, Z., 2014. 3.0-T Intraoperative Magnetic Resonance Imaging-Guided Resection in Cerebral Glioma Surgery: Interim Analysis of a Prospective, Randomized, Triple-Blind, Parallel-Controlled Trial. *Clin. Neurosurg.* 61, 145–154.

Wu, J., Mao, Y., Zhou, L., Tan, W., Hu, J., Song, Y., Hong, X., Du, G., 2007. Clinical evaluation and follow-up outcome of diffusion tensor imaging-based functional neuronavigation: a prospective, controlled study in patients with gliomas involving pyramidal tracts. *Neurosurgery* 61, 935–949.  
doi:10.1227/01.NEU.0000280087.99113.B0

Yang, J.Y., Beare, R., Seal, M.L., Harvey, A.S., Anderson, V.A., Maixner, W.J., 2017. A systematic evaluation of intraoperative white matter tract shift in pediatric epilepsy surgery using high-field MRI and probabilistic high angular resolution diffusion imaging tractography. *J Neurosurg Pediatr.* 19, 1–14.  
doi:10.3171/2016.11.PEDS16312.

Yasuda, C.L., Valise, C., Saúde, A.V., Pereira, A.R., Pereira, F.R., Ferreira Costa, A.L., Morita, M.E., Betting, L.E., Castellano, G., Mantovani Guerreiro, C.A., Tedeschi, H., de Oliveira, E., Cendes, F., 2010. Dynamic changes in white and gray matter volume are associated with outcome of surgical treatment in

temporal lobe epilepsy. *Neuroimage* 49, 71–9.

doi:10.1016/j.neuroimage.2009.08.014

Yogarajah, M., Focke, N.K., Bonelli, S.B., Thompson, P., Vollmar, C., McEvoy, A.W., Alexander, D.C., Symms, M.R., Koepp, M.J., Duncan, J.S., 2010. The structural plasticity of white matter networks following anterior temporal lobe resection. *Brain* 133, 2348–2364. doi:10.1093/brain/awq175

Yuce, I., Kantarci, M., Keles, P., Yesilyurt, H., Ogul, H., Yuce, H., Eren, S., 2016. Diffusion tensor imaging of the hippocampus in chronic cigarette smokers. *Eur. J. Radiol.* 85, 1538–1544. doi:10.1016/j.ejrad.2016.06.003

Yushkevich, P.A., Piven, J., Hazlett, H.C., Smith, R.G., Ho, S., Gee, J.C., Gerig, G., 2006. User-guided 3D active contour segmentation of anatomical structures: Significantly improved efficiency and reliability. *Neuroimage* 31, 1116–1128. doi:10.1016/j.neuroimage.2006.01.015

Zack, M.M., Kobau, R., 2017. National and State Estimates of the Numbers of Adults and Children with Active Epilepsy - United States, 2015. *MMWR. Morb. Mortal. Wkly. Rep.* 66, 821–825. doi:10.15585/mmwr.mm6631a1

Zhang, Y., Brady, M., Smith, S.M., 2001. Segmentation of Brain MR Images through a Hidden Markov Random Field Model and the Expectation Maximization Algorithm. *IEEE Trans. Med. Imaging* 20, 45–57.

Zhu, F.P., Wu, J.S., Song, Y.Y., Yao, C.J., Zhuang, D.X., Xu, G., Tang, W.J., Qin, Z.Y.,

Mao, Y., Zhou, L.F., 2012. Clinical application of motor pathway mapping using diffusion tensor imaging tractography and intraoperative direct subcortical stimulation in cerebral glioma surgery: A prospective cohort study. *Neurosurgery* 71, 1170–1183. doi:10.1227/NEU.0b013e318271bc61

Zimmerman, R.A., Bilaniuk, L.T., Farina, L., 2007. Non-accidental brain trauma in infants: diffusion imaging, contributions to understanding the injury process. *J. Neuroradiol.* 34, 109–114. doi:10.1016/j.neurad.2007.01.124